University of Stavanger

FACULTY OF SCIENCE AND TECHNOLOGY

Masters's Thesis

Study program/specialization: **Industrial Economics/ Petroleum Technology**	Autumn semester, 2023 Open
Author: **Jiwar Nori**	…… (Signature of author)
Program Coordinator: Supervisor(s): **Mesfin Belayneh**	
Title of master's thesis: ***Effects of Nanoparticles on the Neat Geopolymer: Experimental, Economic and Environmental Impact Studies***	
Credits: 30	
Keywords: Geopolymer Portland cement Fly ash Nanoparticles Potassium hydroxide Sodium hydroxide Sodium silicate Rheology UCS SEM EDS	Number of pages: .....65..... + Supplemental material/other: 80 Date/year 15/12/2023 Stavanger

ACKNOWLEDGEMENTS

I would like to express my deepest gratitude to professor **Mesfin Belayneh**, my academic supervisor, whose guidance, expertise, mentoring, and unwavering support were instrumental throughout my thesis work. His invaluable insights and encouragement significantly contributed to the successful completion of this thesis.

I extend my heartfelt appreciation to the generous senior engineer **Samdar Kakay** for his technical assistance and for instructing me in the use of the compressive strength testing apparatus.

Additionally, I would like to thank senior engineer **Espen Undheim** for assisting me with SEM and EDS analyses of my test samples.

I am profoundly thankful to my parents for their moral upbringing, unflagging encouragement, and unwavering support. Their belief in my capabilities has been a constant source of motivation.

Finally, I am deeply grateful to my wife, whose love, understanding, and patience have been my pillars of strength.

This thesis is a culmination of the collective support and encouragement from these remarkable individuals, and I am truly fortunate to have had them by my side throughout this journey.

ABSTRACT

In the oil and gas industry, cement is used for well construction and plug abandonment operations acting as a barrier element. According to NORSOK D-10, the well should be designed to control undesired flow from the reservoir to the surface. However, well integrity survey studies conducted on the North Sea production and injection wells have shown that about 11% of integrity failures are related to cement. The survey result indicated that the oil well cement does not satisfy the property requirements set by the NORSOK D-10 standard.

To ensure long-term integrity, the oil and gas industry is searching for alternative materials for plug and abandonment operations. Geopolymer is one of the alternatives in focus. Several investigators have conducted experimental studies on the geopolymers and the effect of nanoparticles on geopolymers. Results have shown the potential application of geopolymer as an alternative material to cement. However, extensive research should be performed to qualify geopolymer as a barrier element.

In this thesis, the effect of $CaCO_3$ and Al_2O_3 nanoparticles on neat geopolymer has been studied compared with G-class Portland cement. Furthermore, the economic and environmental aspects of these materials have been assessed.
Results showed that:

- After 1-day curing, cement is stronger than the geopolymers with and without nanoparticles. However, after 7 days of curing, the geopolymers showed a higher strength than the cement.
- In terms of environmental issues, geopolymers are environmentally friendly than the cement due to less CO_2 emission.
- In terms of economic evaluation, the reviewed analysis result showed that geopolymer concrete costs are over three times higher than cement based concrete. This suggests future research of developing a cost-effective geopolymer.

The results presented in this thesis are valid for the considered neat geopolymer, curing time, temperature, and pressure. Therefore, by changing curing conditions and the geopolymer's composition, one may achieve different results.

TABLE OF CONTENTS

LIST OF FIGURES

LIST OF TABLES

LIST OF ABBREVIATIONS

API = American Petroleum Institute

HSR = High Sulphate Resistant

I.R = Insoluble Residue

ISO = International Organization for Standardization

MSR = Moderate Sulphate Resistant

OPC = Ordinary Portland Cement

P&A = Plug and Abandonment

PSA = Petroleum Safety Authority

RPM = Revolution Per Minute

SEM = Scan Electron Microscope

EDS = dispersive X-ray spectroscopy

UCS = Uniaxial Compressive Strength

WCR = Water to Cement Ratio

Wt% = Weight percent

%bwoc = Percent by weight of cement

LIST OF SYMBOLS

A = cross-sectional area of specimen (mm^2)

F_{max} = force at time of failure (N)

G = Shear modulus (GPa)

K = Bulk modulus (GPa)

M = Modulus of Elasticity (GPa)

P_{max} = applied force at the moment the sample breaks (N)

Vp = Compressional wave velocity (km/s)

ρ = density (kg/m^3)

τ = Shear stress (Pa)

τ_c = Yield stress (Pa)

k = consistency index

n = flow index

μ_c = Viscosity (Pa.s)

γ = Shear rate (sec^{-1})

ΔM = change of mass

^oC = degrees Celsius

R_3 = Fann reading at 3 RPM

R_6 = Fann reading at 6 RPM

1 INTRODUCTION

This MSc thesis presents an experimental study of geopolymer and its economic evaluation along with environmental impacts. The experimental study part investigates the impact of nanoparticles ($CaCO_3/Al_2O_3$) and the mixture of sodium hydroxide (NaOH) and potassium hydroxide (KOH) on fly ash and sodium silicate based neat geopolymer. The geopolymer plugs have been characterized through destructive methods (UCS and SEM) and non-destructive methods (sonic, mass absorption, shrinkage, and rheology). On the other hand, the economic assessment deals with the cost and environmental evaluation of geopolymer compared with G-class cement.

1.1 Background

Portland cement is the prime material used as a well-barrier during well construction, production, and abandonment phases. The cementing job in well construction is divided into two operations: primary cementing and remedial cementing. Primary cementing involves the placement of cement around a casing and its main functions include providing zonal isolation to prevent fluid migration in the annulus, supporting the casing or liner string, and protecting the casing from corrosive formation fluids [1].

In case of primary cementing failure, the remedial cementing operation is carried out. These operations, such as squeeze cementing and plug cementing, are carried out to rectify issues that may have arisen during primary cementing. Plug cementing is typically performed when operators abandon a well due to its end of productive life [1].

In Figure 1.1, we can see an illustration of the process involved in placing cement and the final constructed well structure. Figure 1.2, on the other hand, demonstrates before and after application of cement in plug and abandonment (P&A) operations for a well. In this case, cement plugs are applied as primary, secondary, and surface plugs.

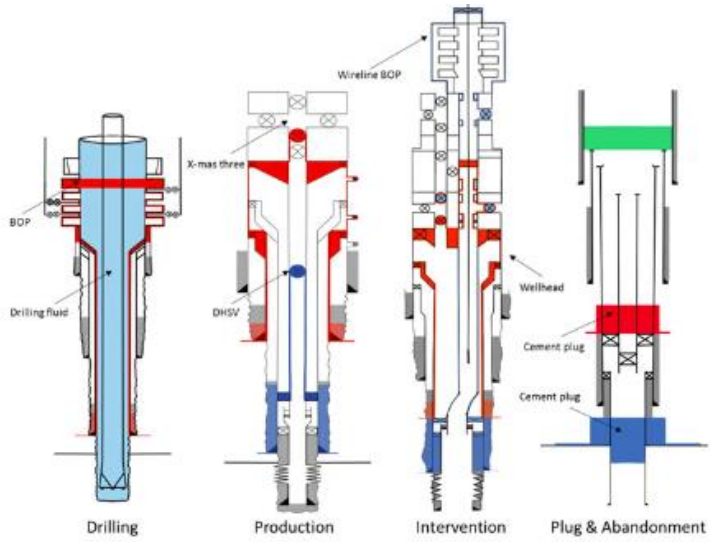

Figure 1.1 Process of Petroleum Well Cementing [2]

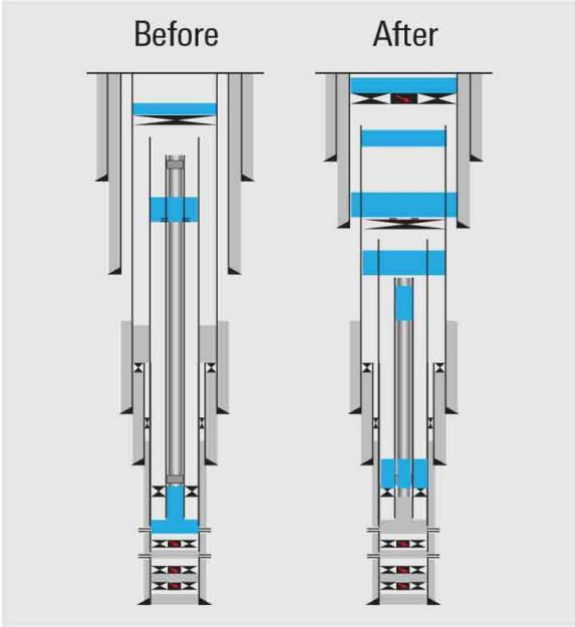

Figure 1.2 Application of Cement Plug (P&A) [3]

Ensuring the long-term integrity of a well primarily depends on the cement quality and good cementing job. However, in the long run, the permeability of cement will increase due to cracking, debonding, and shear failure mechanisms induced by pressure and temperature loading which leads to reservoir fluid leakage [4].

Figure 1.3 illustrates the potential pathways for reservoir fluids leakage to the surface. (1) between cement and exterior of the casing, (2) between cement and interior of the casing, (3) through cement, (4) through casing, (5) in cement fractures, (6) between cement and rock [5]. Mechanisms (1), (2), and (6) involve fluid transport through microannuli, where tiny gaps between the components become the preferred flow path.

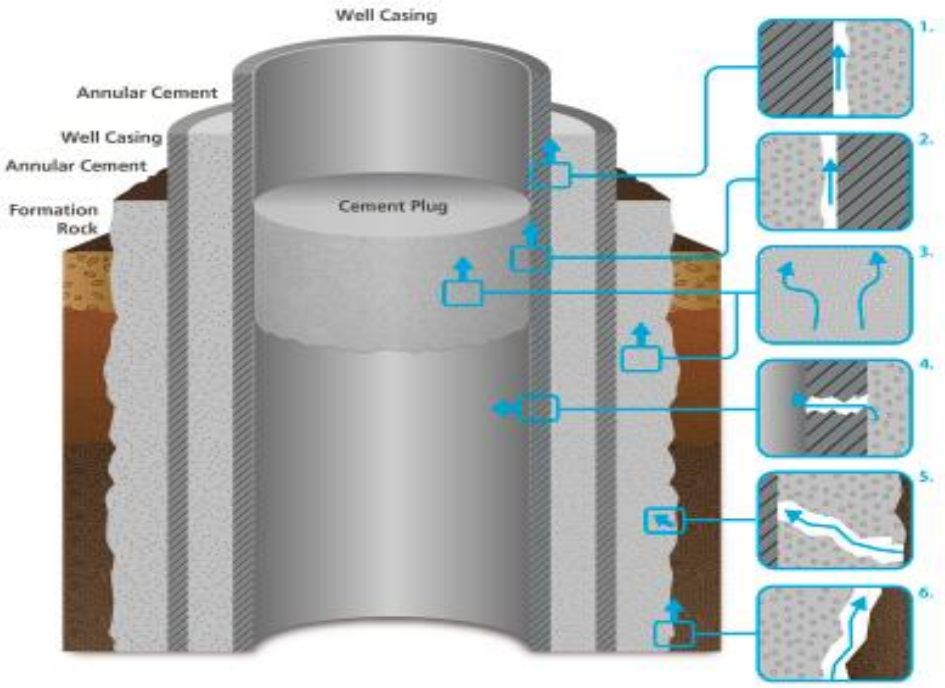

Figure 1.3 Potential Leakage Pathways [5]

For long-term structural integrity, NORSOK D-010 defined well integrity as the "*Application of technical, operational, and organizational solutions to reduce the risk level of undesired formation fluids leaks throughout the life cycle of a well*." [6]

Moreover, the NORSOK D-010 demands criteria for cement properties:

a) Be impermeable.
b) Have long-term integrity.
c) Be non-shrinking.
d) Be ductile – (non-brittle) – able to withstand mechanical loads/impact.
e) Have resistance to different chemicals/substances (H_2S, CO_2, and hydrocarbons).
f) Have wetting, to ensure bonding to steel.

However, well integrity surveys have revealed the presence of integrity problems in several wells. Norway's Petroleum Safety Authority (PSA) has conducted a well integrity survey on 71 wells, consisting of 31 production wells and 40 injection wells. The results depicted in Figure 1.4 show that cement recorded an 11% failure rate [7].

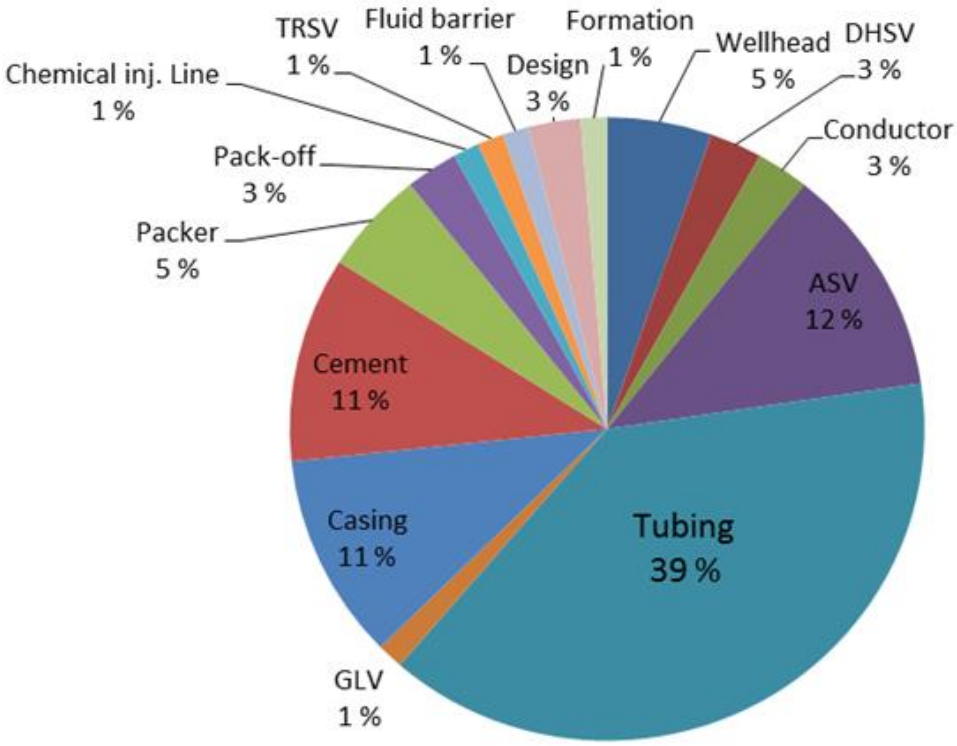

Figure 1.4 Barrier Element Failure [7]

As evident from the integrity survey, it becomes apparent that the existing cement falls short of meeting the NORSOK D-010 standards and carries a risk of failure. This suggests the need for enhancements in the well barrier systems.

Portland cement, which is the most used cement as well as barrier poses significant challenges due to its high energy consumption and resource requirements. Moreover, its production releases substantial amounts of harmful gases like SO_2, NO_x, and CO_2, contributing to environmental pollution. The production of each ton of cement results in the generation of approximately one ton of carbon dioxide, with the cement industry alone responsible for emitting around 7% of CO_2 gas. Hence, there is an urgent necessity to explore alternatives to Portland cement [8].

Over the past few years, geopolymers have emerged as a promising alternative to traditional cementitious materials due to their potential for reduced environmental impact and enhanced mechanical properties. Its advantageous properties include less requirement for energy consumption, emitting less CO_2, exhibiting high strength, shrinking less, exhibiting low permeability, fire, and chemical corrosion resistance as well as durability [9].

1.2 Problem Formulation

During well construction and plug and abandonment phases, cement is used to fill the annular spacing between the casing and plug the well to hinder any undesired leakage from the subsurface to the surface. According to the integrity surveys, there are recorded numerous integrity issues with the traditional cementitious materials. Although geopolymer has emerged as a promising alternative to these traditional cementitious materials it is not excluded from some issues. Unlike cement which hardens early due to the chemical process of hydration in the presence of water, setting is an issue for geopolymer. Furthermore, in the oil industry, time is of the essence and the time taken for the geopolymer to set and harden requires longer rig operating times. Drilling rigs can cost hundreds of thousands of dollars per day to operate, and any delay or downtime can result in significant financial losses. In recent years, the application of nanoparticles has shown a great effect on the improvement of conventional cement properties and performances, meanwhile, limited studies have been conducted on the influence of nanoparticles on geopolymer, but early findings indicate encouraging outcomes.

The research questions to be addressed are:

a) Provided that geopolymer is to be used for ***well construction***, what is the impact of nanoparticles on the early curing of the geopolymer as compared with the neat geopolymer and G-class cement?

b) Provided that geopolymer is to be used for ***the plug and abandonment*** operation, what is the impact of nanoparticles on the geopolymer as compared with the neat geopolymer and G-class cement?

c) What is the ***cost and environmental*** aspect of geopolymer as compared with G-class cement?

1.3 Scope and Objectives

The primary objective of the thesis is to deal with the research questions addressed in the problem formulation part. The activities are:

- Literature review on geopolymer and nanoparticles impact in the oil and gas industry.
- Conduct an experimental study on the effect of nanoparticles on neat geopolymer synthesized from the binding of fly ash and alkaline solution. The geopolymer plugs will be characterized with destructive and non-destructive tests.
- Finally, present the economic and environmental aspect of geopolymer.

1.4 Research Methods

Figure 1.5 displays an overview of the structure of the thesis work, which comprises four parts. The first part deals with a literature study on the geopolymer and nanoparticles application in the petroleum industry. The second part experimentally investigates the impact of nanoparticles, alkaline molar ratio, and alkaline mixture on the neat geopolymer based on the experimental destructive and non-destructive test datasets. The third part is the modelling part which will develop new empirical models. The fourth and final part will be the economic evaluation where the cost, effect, and environmental factors are being evaluated.

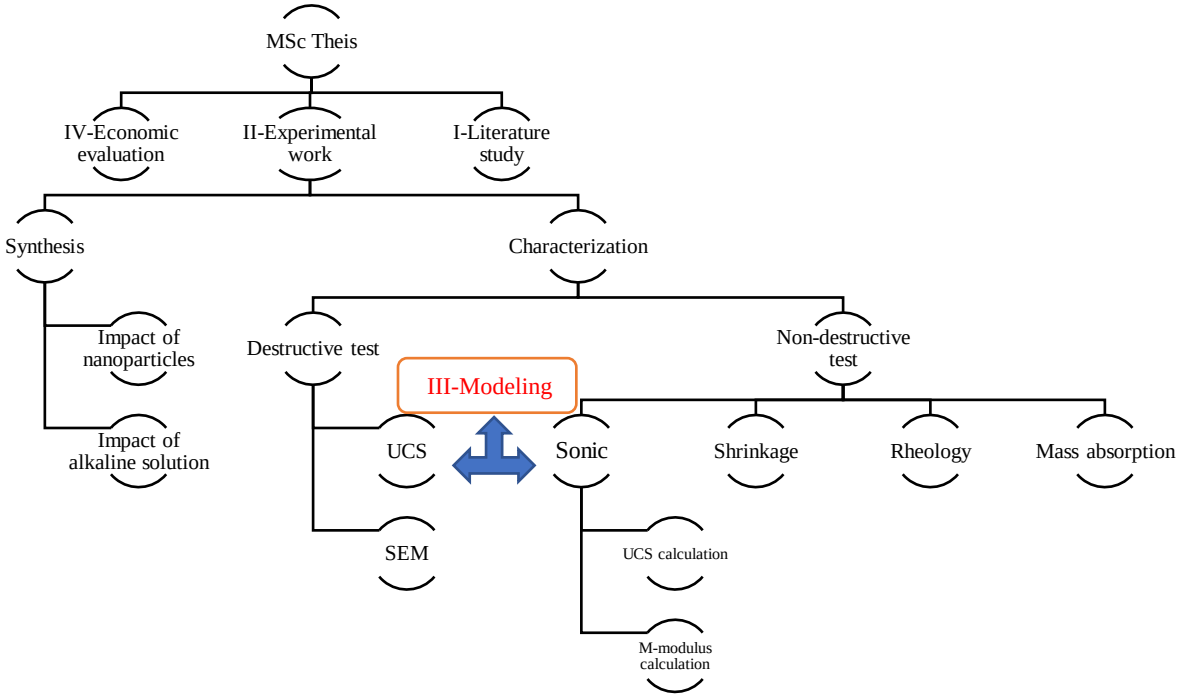

Figure 1.5 Research Methodology

2 LITERATURE STUDY

Chapter 2 presents a literature review of Portland cement, geopolymer, and the effect of nanoparticles on geopolymers.

2.1 Portland Cement

Portland cement is a hydraulic binding material composed of Portland cement clinker, with the addition of 0-5% limestone or granulated blast furnace slag, and a controlled quantity of gypsum. There are two types of Portland cement: type I named P·I, which contains no hybrid materials, and type II named P·II, where the Portland cement clinker can be mixed with less than 5% limestone or granulated blast furnace slag during the grinding process [10].

2.1.1 API Classification of Portland Cement

Ordinary Portland Cement (OPC) is widely utilized in the petroleum industry, meeting the standard physical and chemical properties specified by the American Petroleum Institute (API). These API standards ensure that Portland cement fulfills the required criteria.

Portland cement is categorized into eight API classes, denoted by the letters A to H, with three grades available: ordinary (O), moderate sulfate resistance (MSR), and high sulfate resistance (HSR). Presently, classes E and F, so-called retarded cements are infrequently used worldwide and have been removed from the latest edition of (API 10 A), which aligns with the International Organization for Standardization (ISO 10426-1) [4].
Table 2.1 presents the description of the API cement classes briefly.

Table 2.1 Brief Description of the API Classes [4]

Class A	**Used for situations where no special properties are required.**
Class B	Used for situations where moderate or high sulphate resistance is required.
Class C	Used for situations where high early strength development is required.
Classes D, E and F	Were intended for use in deeper wells, the number of faster-hydrating phases are reduced, and the grain size of the particles are increased. Because the technology has improved greatly since the retarders used in these classes were first made and are today outdated, these classes are rarely used today.
Classes G and H	These classes were developed after improvement of retarders and accelerators. They are used as a basic well cement.

2.1.2 Portland Cement´s Hydration Process

Portland cement is a hydraulic cement, which sets and hardens when cement reacts with water. The strength is obtained by a process known as hydration.

Portland cement consists of four primary compounds known as clinker minerals which are the following: C_3S, C_2S, C_3A, and C_4AF. The hydration of C_3S is often used as a model to understand the hydration process of Portland cement. The hydration of these individual clinker phases differs from the hydration of the multi-component system Portland cement.
The presence of individual clinker phases can influence one another's hydration behavior. For example, the presence of hydrating C_3S can lead to modifications in the hydration of C_3A [4].

Table 2.2 shows the composition of minerals of the major compounds.

Table 2.2 Mineralogical Composition of Portland Cement Clinker [4]

Shorthand form	Formula	Mineral name	Mass%
C_3S	$3CaO*SiO_2$	Alite	60-65
C_2S	$2CaO*SiO_2$	Belite	20-25
C_3A	$3CaO*Al_2O_3$	Aluminate	5-12
C_4AF	$4CaO*\ Al_2O_3*Fe_2O_3$	Ferrite	6-12

The two most crucial compounds contributing to the development of strength in Portland cement are C_3S and C_2S. Together, these silica-based compounds make up approximately 80-90 wt% of the cement. During the hydration process of Portland cement, a chemical reaction occurs, leading to the formation of calcium silicate hydrate and calcium hydroxide [4].

$$\mathbf{2C_3S \rightarrow C_3S_2H_3 + 3CH}$$

$$\mathbf{2C_2S + 4H \rightarrow C_3S_2H_3 + CH}$$

The hydration of both C_3S and C_2S results in the formation of a similar C-S-H phase. However, the hydration of C_3S plays a primary role in setting and early strength development, while the hydration of C_2S largely contributes to the final strength [4]. Figure 2.1 demonstrates the exothermic process of C_3S hydration, which undergoes through five distinct stages:

I. Preinduction period
II. Induction period
III. Acceleration period
IV. Deceleration Period
V. Diffusion period

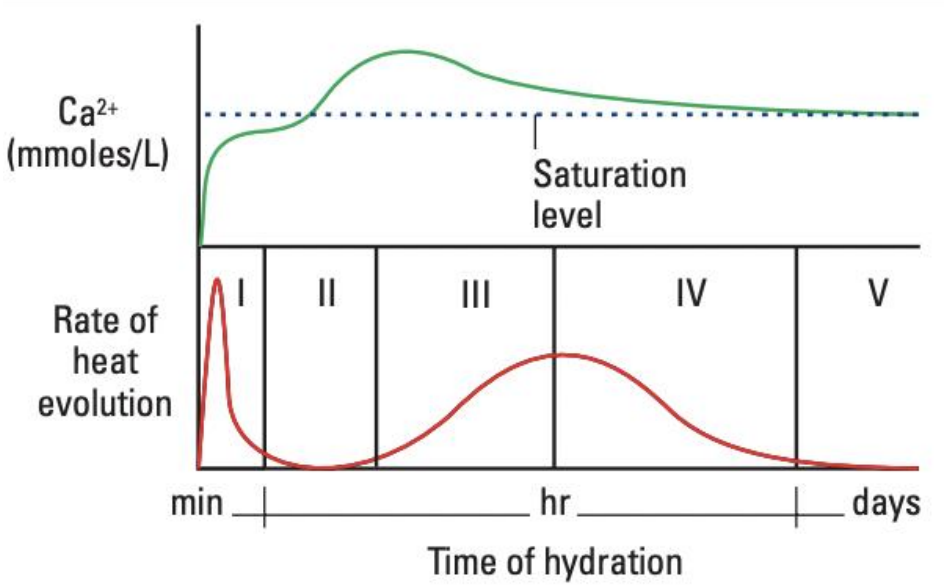

Figure 2.1 Schematic Representation of Changes Taking Place During Hydration of C_3S [4]

2.2 Geopolymer

Geopolymer synthesis involves the activation of aluminosilicate precursors with alkaline solutions, leading to the formation of a three-dimensional inorganic polymer network, resulting in the hardening of the geopolymer. This network exhibits cementitious properties, making geopolymers suitable for various applications in various industries [11].

Unlike conventional Portland cement, geopolymers do not rely on limestone-based clinker production, which is a major contributor to greenhouse gas emissions. Instead, they utilize industrial by-products like fly ash, slag, and natural pozzolans, thereby transforming waste materials into value-added construction products. Figure 2.2 illustrates the synthesis process of geopolymer.

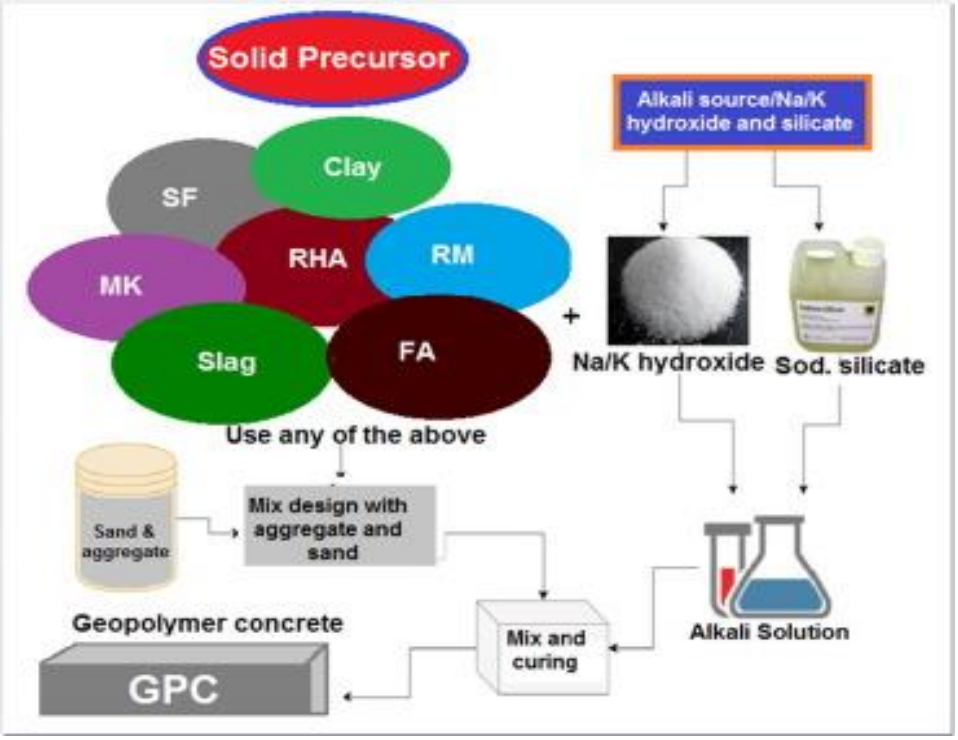

Figure 2.2 Synthesis of Geopolymer Cement [11]

2.3 Effect of Nanoparticles on Geopolymer

Several investigators have tested different types of nanoparticles on geopolymers. Results have shown that nanoparticles improve the mechanical, setting, viscosity, elasticity, fluid loss, microstructure, and petrophysical properties of geopolymers. In the following table, some of the selected research papers are reviewed with their main results summarized.

Table 2.3 Review of the Effect of Nanoparticles on Geopolymer [12-20]

Author [12-20]	Aluminosilicate material	Nanoparticles and Characterization	Key findings
Ibrahim et al. (2018) [12]	Natural pozzolan-based alkali-activated concrete	Nanoparticle: • Nano-silica (SiO_2) Tests: • Compressive strength • Setting time	Results: • 5% replacement of NP with nano-SiO_2 resulted in higher compressive strength and decreased the initial and final setting times
Alomayri (2019) [13]	Fly ash-based geopolymer pastes	Nanoparticle: • Nano-alumina (Al_2O_3) Tests:	Results: • Flexural strength, flexural modulus, fracture toughness, compressive strength, impact strength, microstructure, and hardness improved with the addition of nano alumina

		• Flexural strength • Flexural modulus • Fracture toughness • Compressive strength • Impact strength • Microstructure • Hardness • SEM	• The optimum amount of nano alumina is 2 wt% • SEM observations show microstructure of the geopolymer is more compact, with fewer pores, when the nanoparticle content is lower than 3 wt%
Chindaprasirt et al. (2019) [14]	Calcium fly ash-based geopolymer paste	Nanoparticles: • Nano-silica (SiO_2) • Nano-alumina (Al_2O_3) Tests: • Compressive strength • Setting time	Results: • SiO_2/Al_2O_3 ratios in the range of 3.20–3.70 resulted in products with the highest strengths • increasing 0.7 moles of Al_2O3 to the mix with (SiO_2/Al_2O_3 = 2.57) led to the fastest setting of less than 20 min
Alvi et al. (2020) [15]	Ground Granulated Blast Furnace Slag (GGBFS	Nanoparticles: • Nano-alumina Al_2O_3 • (MWCNT-OH) Tests: • Shear Stress • Fluid-loss test • Pumpability • Uniaxial compressive strength • Stress and strain curves • Tensile strength • Sonic strength • XRD • SEM	Results: • Nanomaterials significantly enhanced the pumping time of the neat geopolymer slurry • Nano-additives increase the thickening time to 3 hrs at 50C and 14.7 MPa • MWCNT-OH decreased fluid loss of the geopolymer • AL-0450 increased fluid loss of the geopolymer • AL-0450 and MWCNT-OH both increased the compressive strength of neat geopolymer from 2945 psi to 4154 psi and 4274 psi after 28 days • AL-0450 showed more increase in Young's modulus after 3 days • AL-0450 and MWCNT-OH-based mixtures slightly increase the ratio of UCS and E after 28 days • UCA results confirm that maximum strength development occurs at the early stages of curing • SEM analysis confirms dense and compact microstructure formation with the nanomaterials
Adak et al. (2014) [16]	Fly ash-based geopolymer mortar	Nanoparticle • Nano-silica (SiO_2) Tests: • compressive strength • Flexural strength • Permeability	Results: • Optimum strength at ambient temperature due to the addition of 6% of nano SiO_2 • The addition of 6% nano SiO_2 is optimum for better pore structure modification

		• Water absorption • FESEM • XRD	• Water absorption and RCPT shows appreciable improvement • Initial and final setting times were reduced significantly due to the addition of 4% of nano SiO_2
Phoo-ngernkham et al. (2014) [17]	High calcium fly ash-based geopolymer paste	Nanoparticles: • Nano-silica (SiO_2) • Nano-alumina (Al_2O_3) Tests: • XRD • SEM • Setting time • Compressive strength • Modulus of elasticity • Flexural strength • The shear bond strength between concrete substrate and geopolymer	Results: • Nano-SiO_2 as an additive to fly ash results in a decrease in the setting time • The addition of nano-Al_2O_3 results in only a slight reduction in setting time • Adding 1–2% nanoparticles could improve the compressive strength, flexural strength, and elastic modulus of geopolymer due to the formation of additional CASH or CSH, NASH gel in geopolymer matrix • The maximum compressive strength of geopolymer paste was achieved with 2% nano-silica and 1% nano alumina • Additions of both nano-SiO_2 and nano-Al_2O_3 enhance the shear bond strength between concrete substrate and geopolymer • SEM and XRD results showed microstructures of geopolymer pastes containing 1–2% nano-SiO_2 and nano-Al_2O_3 were enhanced with a denser matrix and increased reaction product
Gao et al. (2013) [18]	Metakaolin-based geopolymer paste	Nanoparticle: • Nano-silica (SiO_2) Tests: • Compressive strength • Setting time • SEM • MIP • FTIR analysis	Results: • When the amounts of 0%, 1%, 2%, and 3% NS were added, the compressive strength of geopolymers at 60 days were 43.7 MPa, 68.4 MPa, 59.5 MPa, and 49.2 MPa, respectively • The initial setting times of 0%,1%, 2%, and 3% NS samples at an S/L ratio of 0.97 were 315,295, 277, and 240 min, while their final setting times were 375, 360, 330, and 285 min, respectively • The FTIR spectrum of geo-polymer samples contained a distinct intensity band at 1300 to 900 cm^{-1} associated with the Si-O-T asymmetric vibration

			• MIP analysis showed that specimens added 1% NS were more compact
Rovnanik et al. (2016) [19]	Fly ash-based geopolymer paste	Nanoparticle: • MWCNT Tests: • Compressive strength • Modulus of elasticity • Fracture test • Acoustic emission activity • SEM	Results: • Application of MWCNTs up to 0.2% improves the mechanical properties as compressive strength and modulus of elasticity • The optimum amount of MWCNTs showing the best mechanical performance of the fly ash geopolymer is 0.15% • MWCNTs cause the fly ash geopolymer to be slightly less resistant to fracture • 0.05% of MWCNTs can dramatically reduce the formation of microcracks detected by the AE method during the hardening process.
Assaedi et al. (2020) [20]	Low calcium fly ash-based geopolymer paste	Nanoparticle: • Nano-$CaCO_3$ Tests: • Flexural • Compressive strength • Impact strength • Hardness • SEM	Results: • The mechanical properties of geopolymers were improved after the addition of 1–2 wt% $CaCO_3$ • Nanocomposites were found to be denser as compared to the control sample • Mechanical properties decrease when the contents of $CaCO_3$ particles increase higher than 2.0 wt% • The addition of nanoparticles up to 2.0 wt% led to a better bonding interface and good cohesion between the binder and different particles

From the literature study, we can observe that nanoparticles enhanced the mechanical, setting, viscosity, elasticity, fluid loss, microstructure, and petrophysical properties. The performance of the various nanoparticles depends on the concentrations used. There is limited research on the effect of nanoparticles on geopolymer, and the most used nanoparticle reported from the literature is SiO_2. However, Alexander [21] has used SiO_2 in water solution and its impact on his neat geopolymer was not significant. Therefore, in this thesis, due to the availability of $CaCO_3$ and Al_2O_3 nanoparticles in the laboratory, their impacts on Alexander's [21] neat geopolymer will be investigated.

3 EXPERIMENTAL WORK

Chapter 3 presents the different materials used and the methods that were followed in the synthesizing and characterization of geopolymer.

3.1 Materials

All the materials used have been provided by the University of Stavanger or its collaborating companies.

3.1.1 Water

The cement slurries were prepared using fresh water sourced from the laboratory's tap, with the assumption of its purity and freedom from any contamination. Furthermore, the predominant choice for water in cement slurries within oil and gas fields is typically freshwater, making the use of a nearby freshwater source a practical option.

3.1.2 Portland Class G Cement

The Portland G-class cement, which is widely used in oil well applications, was procured from Heidelberg Materials. As per API SPEC 10A/NS-EN ISO 10426-1 [22], cement is tested and have shown a higher sulfate resistance. The chemical composition and physical characteristics of the cement are provided in Tables 3.1 and 3.2.

Table 3.1 Physical Properties of Portland Cement [22]

Density (lb/gal)	Surface Area (m^2/kg)	Max. Consistency Bc	Thickening time Min
16	317	13	108

Table 3.2 Chemical Compositions of Portland Cement (*I.R = Insoluble residue) [22]

Cr(VI)	SO_3	C_3A	C_2S	$C_4AF+ 2C_3A$	Na_3O	MgO	I.R*	Loss on Ignition
0.00%	1.73%	1.7%	55.6%	15.2%	0.48%	1.43%	0.1%	0.79%

3.1.3 Geopolymer Components

Geopolymer slurry is formed by a process that involves the transformation of aluminosilicate materials into geopolymers by a reaction between aluminosilicate precursors and alkaline activators. The solid aluminosilicate precursor used in this thesis was fly ash while the alkaline activators were NaOH, KOH, and Na_2SiO_3.

3.1.3.1 Aluminosilicate Precursor (Fly Ash)

Figure 3.1 shows the low-calcium fly ash class F used in this thesis. The standard composition of fly ash can be found in Table 3.3. The fly ash utilized in this study was supplied by Heidelberg Materials. As indicated in the table, the primary constituents of fly ash are SiO_2 and Al_2O_3.

Table 3.3 Fly Ash Composition [22]

SiO_2	Al_2O_3	Fe_2O_2	CaO	MgO	SO_3	Na_2O & K_2O
54.90%	25.80%	6.90%	8.70%	1.80%	0.60%	0.60%

Figure 3.1 Fly Ash

3.1.3.2 Alkaline Solution

To initiate the geopolymerization process and create the binding slurry, the presence of an alkaline solution is imperative. The alkaline solution is formulated by combining alkaline activators sodium silicate (Na_2SiO_3) with (NaOH/KOH) in the ratio of 2.5.

3.1.3.2.1 Sodium Hydroxide 12 M (NaOH)

Sodium hydroxide (NaOH) is one of the most used alkaline activators in geopolymer synthesis which offers a high alkalinity. It was procured from VWR, Avantor® [23].

3.1.3.2.2 Potassium Hydroxide 12 M (KOH)

Potassium hydroxide (KOH) is another effective alkaline activator used in geopolymerization. It exhibits similar characteristics to NaOH, with the advantage of being less corrosive, making it suitable for certain applications. The product was purchased from Solberg Industri [24].

3.1.3.2.3 Sodium Silicate (Na_2SiO_3)

In this thesis, the sodium silicate (Na_2SiO_3) utilized was procured from PQ Corporation [25]. The solution contains 45-65% water content and maintains a molar ratio within the range of 1.6-2.6.

3.1.4 Description of Nanoparticles

To investigate the effect of nanoparticles on the geopolymer described in the previous sections, two types of nanoparticles are used in water solution namely, carbon carbonate ($CaCO_3$) nanoparticle solution and aluminium oxide (Al_2O_3) nanoparticle solution. The description of the nanoparticles will be presented below.

3.1.4.1 Calcium Carbonate Nanoparticle Solution (Nano-$CaCO_3$)

The calcium carbonate $CaCO_3$ used in this thesis was procured from U.S. Research Nanomaterials Inc. The particles have a size of 50 nm and are also dispersed in water which contains roughly 40% by weight of the particles [26].

3.1.4.2 Aluminium Oxide Nanoparticle Solution (Nano-Al_2O_3)

In this thesis, the aluminium oxide solution (Al_2O_3) used was procured from U.S. Research Nanomaterials Inc. The particles have a size of 30 nm and a purity of 99.99%. The particles are also dispersed in water which contains roughly 20% by weight of the particles [27].

3.2 Characterization Methods

The characterization methods of the geopolymer plug specimens are summarized in Figure 3.2. The first phase of testing is non-destructive tests, where the samples are characterized through ultrasonic, mass absorption, shrinkage, and rheology. The second phase is a mechanical destructive test with uniaxial compressive strength and SEM.

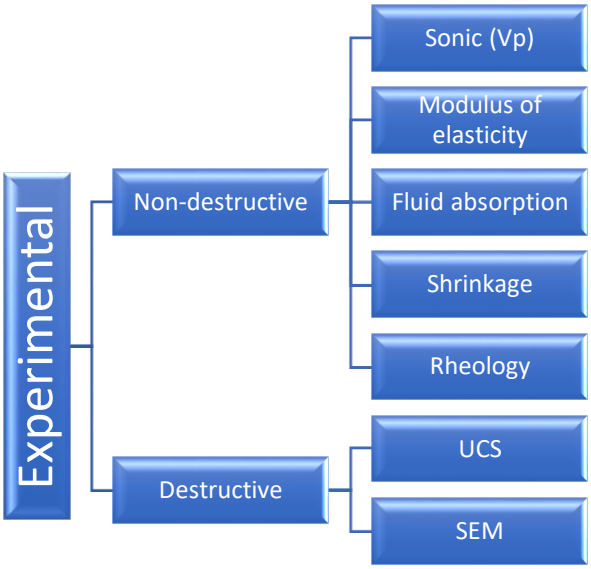

Figure 3.2 Scope of Experimental Work

3.2.1 Sonic Travel Time

Ultrasonic inspection is a non-destructive approach employed to assess a material's capability to propagate mechanical sonic waves through its structure. When a structure contains cracks, pores, entrapped air, or is inadequately cemented, the travel time of these waves is greater compared to well-compacted and robust materials. Figure 3.3 illustrates the CNS Farnell Pundit 7 device used to record the travel time of the ultrasonic pulses emitted through the specimens from the transmitter to the receiver. Before conducting tests, the measuring equipment is calibrated with a calibration plug having a travel time of 25.2 μs. It is crucial to ensure that the surface of the plugs, both at the bottom and the top, have close contact with the metallic surfaces of both the transmitter and receiver transducers.

As shown in Equation 3.1, the compressional wave velocity is calculated using the length of the plug specimen and the recorded travel time.

Equation 3.1

$$V_p = \frac{l}{t}$$

Where:

- V_p is the P-wave's velocity (m/s)
- l is the length of a plug (m)
- t is the P-wave's travel time through a plug (seconds)

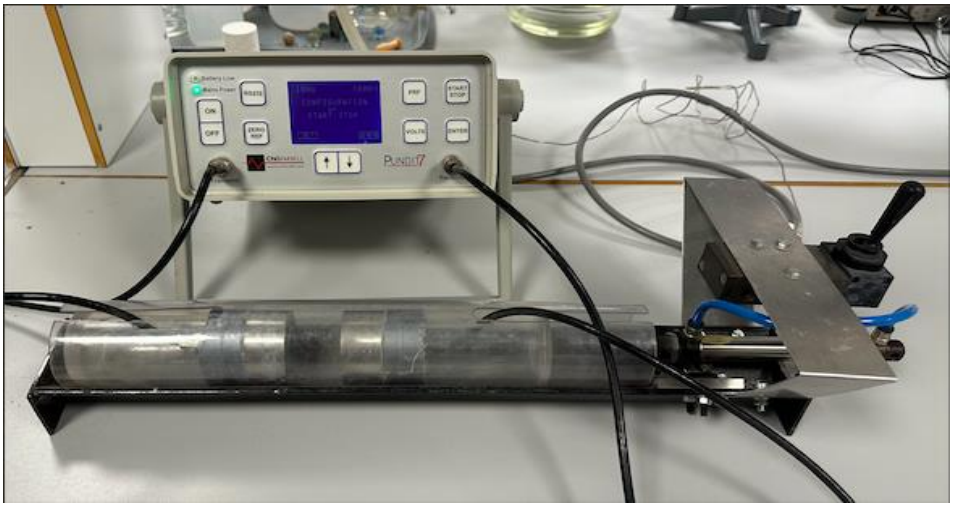

Figure 3.3 CNS Farnell Pundit 7 Device for Sonic Travel Time Measurement

3.2.2 Modulus of Elasticity

Elastic modulus is the measurement of a material's elasticity, indicating its resistance to being deformed elastically when stress is applied. The compressional wave velocity is related to the bulk and shear modulus [28].

Equation 3.2

$$v_p = \sqrt{\frac{K + \frac{4}{3}G}{\rho}}$$

The compressional wave velocity and the density of the plugs are measured during the non-destructive test. Derived from Equation 3.2, the modulus of elasticity is estimated in Equation 3.3 as:

Equation 3.3

$$M = K + \frac{4}{3} * G = V_p^2 * \rho * 10^{-9}$$

Where:

- $M = K + \frac{4}{3} * G$ = dynamic modulus of elasticity
- K = bulk modulus which is the measure of the material resistance for hydrostatic loading (GPa)
- G = shear modulus which is the measure of the material resistance for the shear loading (GPa)
- V_p = compressional wave velocity (m/s)
- ρ = density of plug (kg/m^3)

3.2.3 Mass Absorption

The plug's internal structure is characterized by assessing its porosity and permeability, which determine its fluid flow capacity. Nonetheless, due to the unavailability of measuring equipment in this thesis, we indirectly analyze the internal structure by examining mass absorption. We calculate the percentage change in mass absorbed after immersing the plugs in water, relative to their initial dry mass, as follows:

Equation 3.4

$$\Delta M = \frac{M_t - M_0}{M_0} * 100$$

Where:

- ΔM = the change of mass (%)
- M_0 = the mass before being immersed in water
- M_t = the mass of the plug after being taken out of the water

3.2.4 Shrinkage

Cement is expected to possess a non-shrinkage characteristic, as per NORSOK D10 standards. This requirement is essential because any shrinkage in the cement can potentially create a pathway for leakage between the casing and the cement. Shrinkage tests were conducted on the neat, nano-based geopolymers, and G-class cement to get a comparison between their shrinkage results. These slurries were poured into pipes and cured in an oven for several days. When taken out, water was added onto the top of the pipes and left to rest for 24 hours to check for any signs of water leakage as illustrated in Figure 3.4.

Figure 3.4 Test Setup for Shrinkage

3.2.5 Rheology

Rheology is the scientific discipline dedicated to examining the deformation characteristics of fluids under varying conditions. The behavior of a fluid is contingent upon the flow regime, determined by factors like velocity, viscosity, and geometry. Understanding the rheological characteristics of fluids used in drilling operations holds significant importance due to the extensive fluid transport involved. This is particularly crucial for substances like drilling fluid and cement, as high viscosity in cement can impede proper pumping and displacement by pumps [29].

Figure 3.5 illustrates the viscometer that was used to measure the viscosity of geopolymer and cement slurries. The measurements were taken at different rotational speeds, specifically at 300, 200, 100, 6, and 3 revolutions per minute (RPM). The Herschel-Bulkley model is a modified power law model. The model is a three-parameter and describes drilling fluids in a wellbore. The model reads as follows [29].

Equation 3.5

$$\tau = \tau_\gamma + k\gamma^n$$

The Herschel-Bulkley yield stress is calculated as:

Equation 3.6

$$\tau_\gamma = 1.067 * (2 * R_6 - R_3)$$

Where:

- τ = shear stress for Herschel-Bulkley model [lbf/100ft^2]
- τ_γ = yield stress [lbf/100ft^2]
- k = consistency index [lbf.s^n/100ft^2]

- n = flow index
- γ = shear rate [1/s]
- R_3 = Fann reading at 3 RPM
- R_6 = Fann reading at 6 RPM

Figure 3.5 Fann Viscometer

3.2.6 Compressive Strength (UCS)

Uniaxial compressive strength is the measure of a material's ability to withstand compressive forces until it eventually fractures. This is one of the traditional methods used in destructive testing to determine a material's compressive strength. However, it's worth noting that compressive strength can also be determined using non-destructive testing methods. Figure 3.6 illustrates the Zwick apparatus, which was utilized to run a series of tests. This apparatus is connected to the testXpert II software program, which records the compressive data. The initial position is adjusted by the specimen's height, after which the specimen is securely positioned and centered between the two loading plates for the crushing test. Before running the test, the force is calibrated to zero and then initiated. Throughout the testing process, an axial load is continuously applied to the plug until it crushes the specimen.

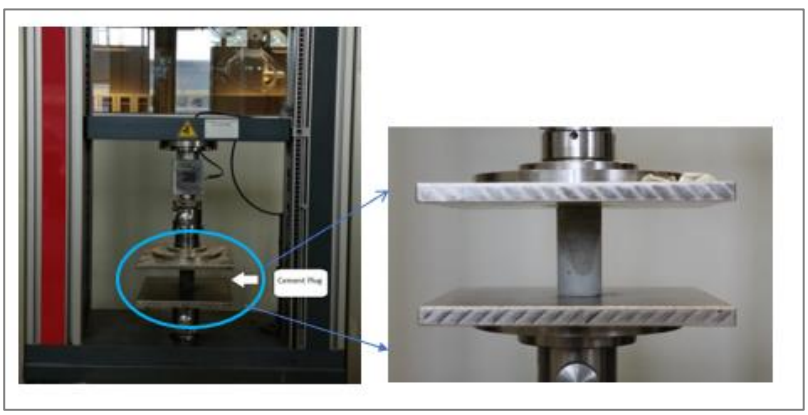

Figure 3.6 Zwick Z020 Apparatus for Destructive Compressive Testing

The uniaxial compressive strength (UCS) is calculated by dividing the force required to crush the specimens by the cross-sectional area of the specimens [30].

Equation 3.7

$$UCS = \frac{F_{max}}{A}$$

Where:

- UCS = Uniaxial compressive strength (MPa)
- F_{max} = Force at the time of failure (N)
- A = Cross-sectional area of the specimen (mm^2)

3.2.7 Scanning Electron Microscope (SEM)

In contrast to conventional optical microscopes that utilize light, SEM (Scanning Electron Microscope) utilizes electrons to generate images. SEM offers several advantages when compared to traditional microscopes, including a larger depth of field that enables it to focus on more of the specimen simultaneously. Additionally, it boasts higher resolution capabilities, allowing for significantly greater image magnification. One notable distinction is that SEM relies on electrons rather than lenses [31]. Following the UCS test, a thin and flat sample of the remains will be forwarded for SEM analysis. Employing SEM will offer valuable insights into the internal structure characterization of the geopolymer and furnish important data regarding the effect of the added nanoparticles. Figure 3.7 displays the SEM device.

Figure 3.7 JSM-IT800 SEM Device

3.2.8 Empirical UCS vs Vp Model

In the existing literature, various empirical models establish a connection between uniaxial compressive strength and compressional wave velocity. These models are typically derived from data related to specific rock materials and cement, which limits their applicability and predictive accuracy.

In Chapter 5 of this thesis, we will develop an empirical model based on the geopolymer dataset. We will then evaluate the predictive performance of our model in comparison to three existing empirical models: one based on shale rock (Horsrud, 2001) [32], another based on cement (Titlestad, 2021) [33], and last one based on geopolymer (Alexander, 2023) [21]. These models are represented as follows:

Horsrud's model: (Shale rock)

Equation 3.8

$$UCS = 0.77 \cdot V_p^{2.93}$$

Titlestad's model: (Cement)

Equation 3.9

$$UCS = 0.2191 \cdot V_p^{3.9503}$$

Alexander´s model: (Geopolymer)

Equation 3.10

$$UCS = 10.453 \cdot V_p^{1.1886}$$
$$R^2 = 0.6894$$

Where, Vp is in km/s and UCS is in MPa

3.3 Geopolymer Synthesis and Slurry Preparation

The neat geopolymer has been formulated by Alexander Høyvik [21] by using the 10 M NaOH blended with sodium silicate, fly ash, and extra water. Using Alexander's formulation, in this thesis, the neat geopolymer has been formulated by using 10 and 12 M NaOH blended with KOH. Then, the impact of nanoparticles on the neat geopolymer was evaluated both in the early (1-day) and the later (3 and 7-days) curing at 60°C.

Firstly, we begin with the precise weighing of all the chemicals and components. Then we mix sodium silicate with 12 M sodium hydroxide and 12 M potassium hydroxide. The mixture is manually stirred before being poured over the fly ash with water. It is then stirred again for a period until we see the slurry becoming thin. The resulting geopolymer slurry is subsequently molded into plastic molding cups. These cups, containing the slurries are directly placed in an oven. Rather than allowing the cups to rest in the open air, we promptly place them in the oven shown in Figure 3.8. This approach mirrors the operational reality in wellbore scenarios, where cement slurry is directly pumped into the well. By placing the samples in this accelerated curing process in the oven, we aim to simulate the conditions and time constraints encountered in wellbore operations. This approach allows us to create a more representative and practical testing environment for our geopolymer samples, aligning with the conditions they will encounter in the field. The samples are aged and tested at 1-day, 3-days, and 7-days in an oven with a temperature of 60°C. When taking the plugs out from the oven, the top of the plugs usually has uneven surfaces and irregularities due to free fluid, but the top layers weren't cut to be like the downhole cement. The plugs were just polished to get a uniform surface. For modeling purposes, the non-destructive tests are measured on the day when the samples are undergoing destructive tests. The experimental tests were designed based on three plugs for each batch of slurry. In the following section, an overview of the design background and their compositions are presented.

Figure 3.8 The Oven Used for Curing of Plugs

3.4 Experimental Test Designs

For this thesis, there were four test designs made. Consisting of test design #1: effect of NaOH molar concentration, test design #2: effect of NaOH-KOH alkaline solution mixture, test design #3: studying the effect of nanoparticles, and test design #4 to characterize neat G-class cement to evaluate the geopolymers early and later period curing behaviors.

3.4.1 Test Design #1 Effect of NaOH Molar Concentration

As mentioned in section 3.3, Alexander's neat geopolymer was based on 10 M NaOH. To study the effect of Molar concentration, in test designs #1, 10 M, and 12 M NaOH-based neat geopolymers were synthesized. The aim was to select the Molar concentration which gives a higher strength during the early curing period.

Table 3.4 Test Design 1

Plug (#)	Fly ash (g)	Water (g)	Sodium silicate (g)	NaOH (g)	# of samples
1	202	20	75	10	3
2	202	20	75	12	3

3.4.2 Test Design #2 Effect of 12 Molar NaOH-KOH Mix Concentration

Based on test design #1, results showed that the 12 M recorded higher strength of the geopolymer. Therefore, the rest of the designs were based on 12 M NaOH. The goal of the second test design is to study the impact of NaOH/KOH mixtures and to determine which concentration of either sodium hydroxide (NaOH) or potassium hydroxide (KOH) yields the most favorable results in terms of the geopolymer's properties.

A total of 5 geopolymer plugs were synthesized, and three samples were made of each plug #1-5 for statistical purposes. Table 3.5 shows the amount of fly ash, water, sodium silicate, NaOH, and KOH for test design #2.

By systematically varying the concentrations of NaOH and KOH while keeping other materials constant, we aim to identify the optimal combination that produces the desired properties in our neat geopolymer and use it in further investigations. These samples underwent a curing period of 3 days.

Table 3.5 Test Design 2

Plug (#)	Fly ash (g)	Water (g)	Sodium silicate (g)	12M NaOH (g)	12M KOH (g)	# of samples
1	202	20	75	30	0	3
2	202	20	75	20	10	3
3	202	20	75	15	15	3
4	202	20	75	10	20	3
5	202	20	75	00	30	3

3.4.3 Test Design #3 Effect of Nanoparticle Concentration

From test design #2, the best composition will be qualified as a neat geopolymer. To further achieve a better geopolymer performance, test design #3 was designed. The design idea here is to extend the experimental investigation by introducing and adding the nanoparticles, which are calcium carbonate ($CaCO_3$) and aluminum oxide (Al_2O_3), into the mixture of the optimal combination found in the previous table for our neat geopolymer.

For statistical analysis purposes, three samples were synthesized for each plug. As shown in Table 3.6, the concentrations used for each nanoparticle are 0.1 g and 0.2 g to study their impact on geopolymer properties. These samples were cured for 3 days and the plugs giving the best results from each nanoparticle are also tested for 7 days.

Table 3.6 Test Design 3

Plug (#)	Fly ash (g)	Water (g)	Sodium silicate (g)	12M NaOH (g)	12M KOH (g)	$CaCO_3$ NPs (g)	Al_2CO_3 NPs (g)	# of samples
1	202	20	75	15	15	0.1	-	3
2	202	20	75	15	15	0.2	-	3
3	202	20	75	15	15	-	0.1	3
4	202	20	75	15	15	-	0.2	3

3.4.4 Test Design #4 G-class Cement

G-class Portland cement is commonly used in oil wells both for well construction and for plug and abandonment. In addition to the geopolymer, the test design #4 was designed. The objective of this test design was for comparison with the geopolymers. The Portland cement

was mixed with a water/solid ratio of 0.44 as per API standards. These samples underwent a curing period of 1,3, and 7 days.

Table 3.7 Test Design 4

Plug (#)	Cement (g)	Water (g)	# of samples	Curing days
1	227.27	100	2	1
2	227.27	100	2	3
3	227.27	100	2	7

4 RESULTS AND DISCUSSION

This chapter presents the experimental test results obtained from the four test matrices. Both the destructive and non-destructive results of the nano-treated geopolymers are compared to the nano-free geopolymers and the neat G-class cement. The results presented in this chapter are the average values of the samples.

4.1 Effect of NaOH Molar Concentration

Alexander [21] used a 10 M NaOH-based geopolymer cured at 65°C. In addition, the curing process included 1-day exposure of the samples to air before putting them in the oven.

In this thesis, to overcome the possible solid sagging issues, it was decided to put the sample directly to the oven skipping exposure of the sample in the air as Alexander [21] did. The first study in this thesis was to determine the NaOH molar concentration that gives a higher strength and is to be used in the neat geopolymer. For this, two neat geopolymers were synthesized with 10 M and 12 M of NaOH molar concentration and the UCS of the samples were tested after 3 days in an oven at 60°C. Figure 4.1 shows that the UCS of the 10 M NaOH-based geopolymer recorded 13 MPa and the 12 M NaOH-based geopolymer had 18 MPa. From these results, the 12 M NaOH was selected for further neat geopolymer synthesis.

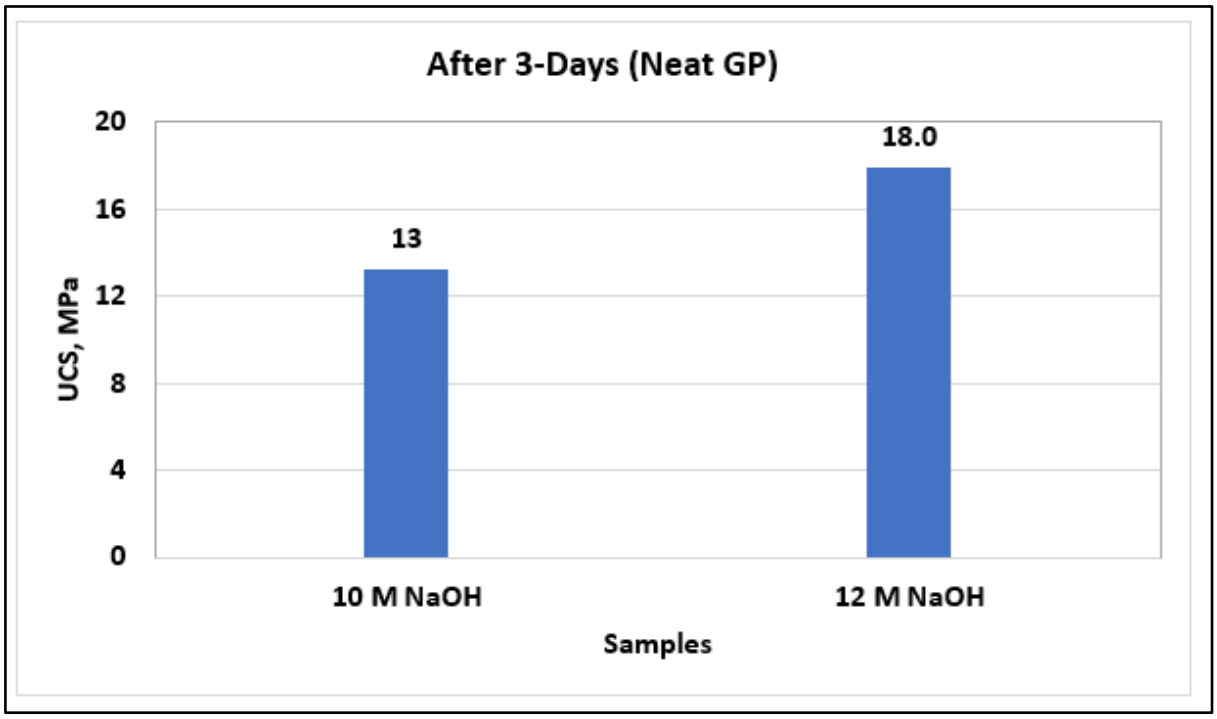

Figure 4.1 Effect of NaOH Molar Concentration

4.2 Effect of Single and Combined NaOH-KOH Solutions

In literature, both NaOH and KOH are used as alkaline activators in geopolymers. Based on test design #2, the study aimed to evaluate the single effect and the combined effects of the alkaline solution. Based on the results, the best alkaline solution will be selected to be blended with sodium silicate. Figure 4.2 shows the effect of NaOH/KOH solutions on the UCS of the neat geopolymer. Results after 7 days of curing at a temperature of 60°C, showed that the equal mix of NaOH and KOH gives the highest average UCS of 19 MPa. The neat NaOH gives the second highest average UCS of 18 MPa. The rest alkaline blending-based geopolymers showed lower UCSs. Therefore, based on the results, the [15 g NaOH/15 g KOH] mix concentration was selected to be used for the neat geopolymer synthesis.

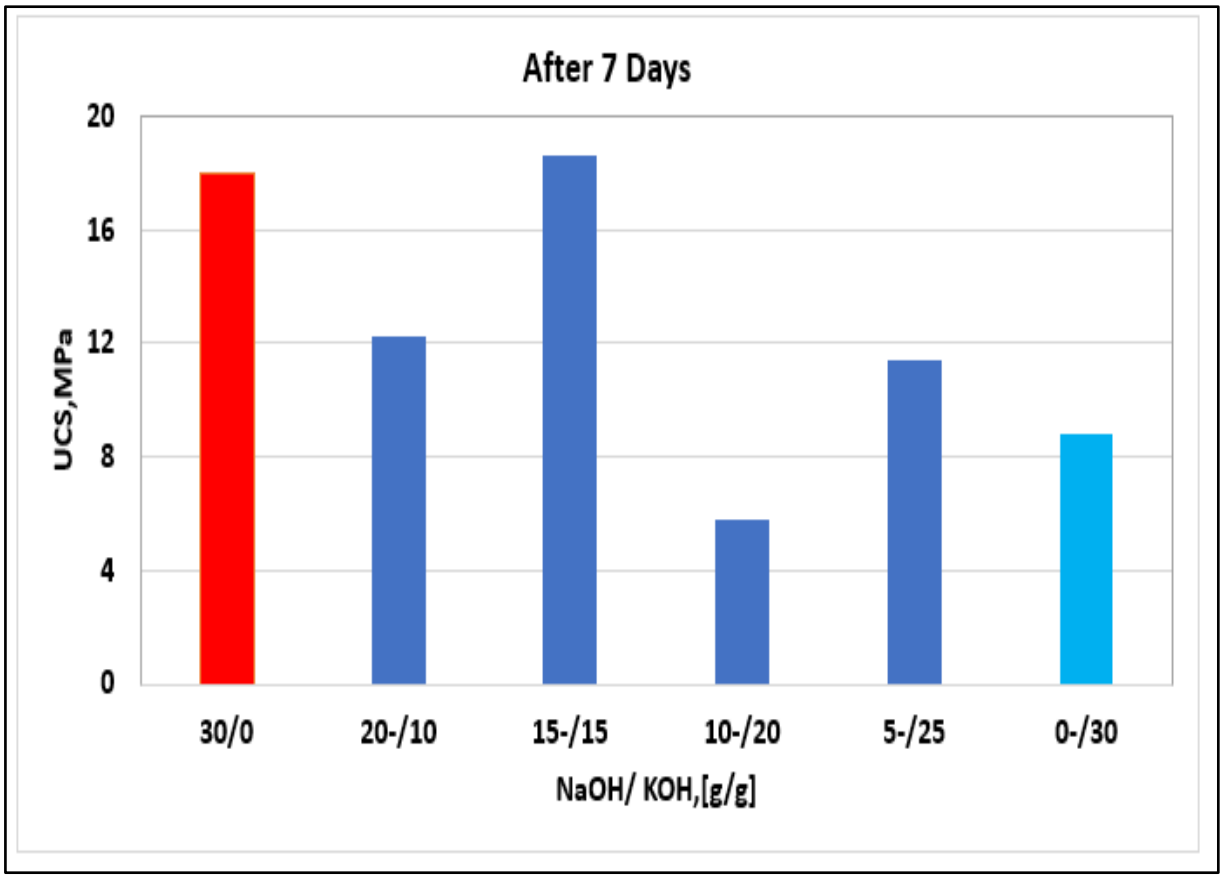

Figure 4.2 Effect of Single and Combined NaOH-KOH Solutions on the Uniaxial Compressive Strength of Geopolymers After 7 days

4.3 Effect of Nanoparticles

To study the impact of nanoparticles on the early setting of our neat geopolymer, we blended different concentrations of $CaCO_3$ and Al_2O_3 nanoparticles on the neat geopolymer. From the study, the best strength obtained from the $CaCO_3$ and Al_2O_3 were 0.1 g and 0.2 g, respectively. The selection of those concentrations was obtained after testing each of the nanoparticles at 0.1 g and 0.2 g, and then finding the best concentration for each nanoparticle. Furthermore, the investigations continued with the obtained concentrations at 1, 3, and 7 days, respectively.

4.3.1 Effect of Nanoparticles on the Uniaxial Compressive Strength After 1 Day

To study the impact of nanoparticles on the neat geopolymer´s early strength development, we conducted destructive and non-destructive tests after 1 day of curing at 60°C. The results are compared with the neat G-class cement. From Figure 4.3 we observe that nanoparticles indicated an impact on the UCS of the neat geopolymer. In the percentile, the addition of 0.1 g $CaCO_3$ and 0.2 g Al_2O_3 increased the strength of the neat geopolymer by 12.75% and 7.51%, respectively. On the other hand, the strength of the G-class cement has shown to be about 120.74% stronger than the neat geopolymer. This difference in early strength is due to the exothermic process of hydration when the cement reacts with water. The results show that the curing process of the geopolymer at the early stage is slower than the cementitious material. However, at higher pressure and temperature, one may achieve different curing development. The results shown here are valid at the atmospheric pressure and 60°C conditions.

If an industry is planning to use geopolymer for well construction purposes to fill annular spacing between the well and the casing or secondary cement job, this thesis author suggests performing extensive research to investigate the desired early development of geopolymer so that the possible undesired non-productive time will be minimized.

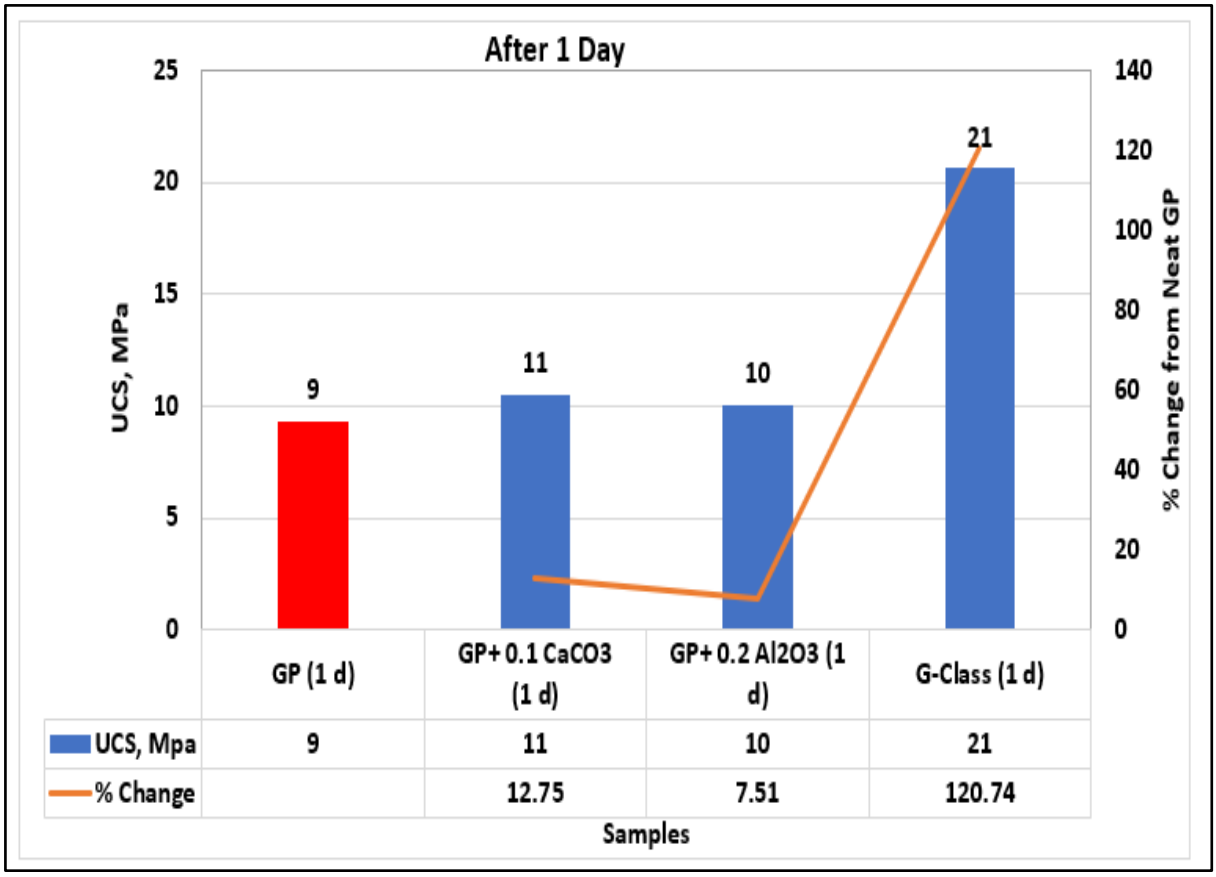

Figure 4.3 Effect of Nanoparticles on the Uniaxial Compressive Strength of Geopolymers After 1 Day

4.3.2 Effect of Nanoparticles on the Uniaxial Compressive Strength after 3 Days

Further, the impact of curing days is investigated to study the rate of strength development. The geopolymer and G-class cement samples have been cured for 3 days at 60°C at atmospheric pressure. Figure 4.4 displays uniaxial compressive test results. Compared with the 1-day strength, the 3-day strength development exhibited a significant increment. Quantitatively, results showed that $CaCO_3$ and Al_2O_3 nanoparticle additives increased the neat geopolymer strength by 25.35% and 34.02%, respectively. On the other hand, the G-class cement still exhibits the highest UCS and is 70.19% stronger than the neat geopolymer.

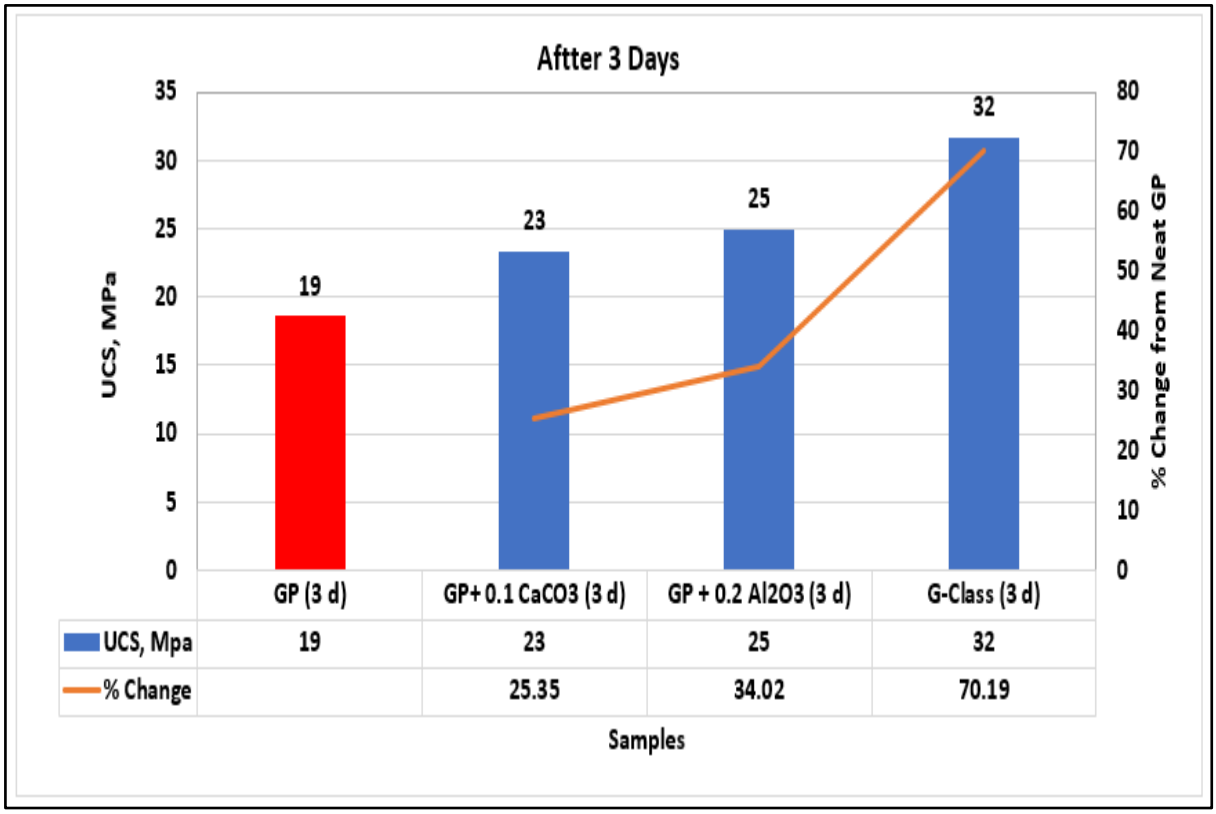

Figure 4.4 Effect of Nanoparticles on the Uniaxial Compressive Strength of Geopolymers After 3 Days

4.3.3 Effect of Nanoparticles on the Uniaxial Compressive Strength after 7 Days

Curing the geopolymer and G-class cement samples for 7 days, results as shown in Figure 4.5 indicate the continuous strength development in the geopolymer, but the temperature degrading effect on the G-class cement. After 1-day and 3-day curing, the G-class strength was significantly higher than the neat geopolymer. However, after 7 days of curing the neat geopolymer showed to be 2.83% stronger than the G-class cement. On the other hand, both the 0.1 g $CaCO_3$ and 0.2 g Al_2O_3 nanoparticle additives increased the UCS of the neat geopolymer by 17.96% and 9.10%, respectively. Due to the short research period, the long-term curing effect was not evaluated. It would have been interesting to investigate the impact of temperature on the samples over time. However, more research should be done to make a good conclusion.

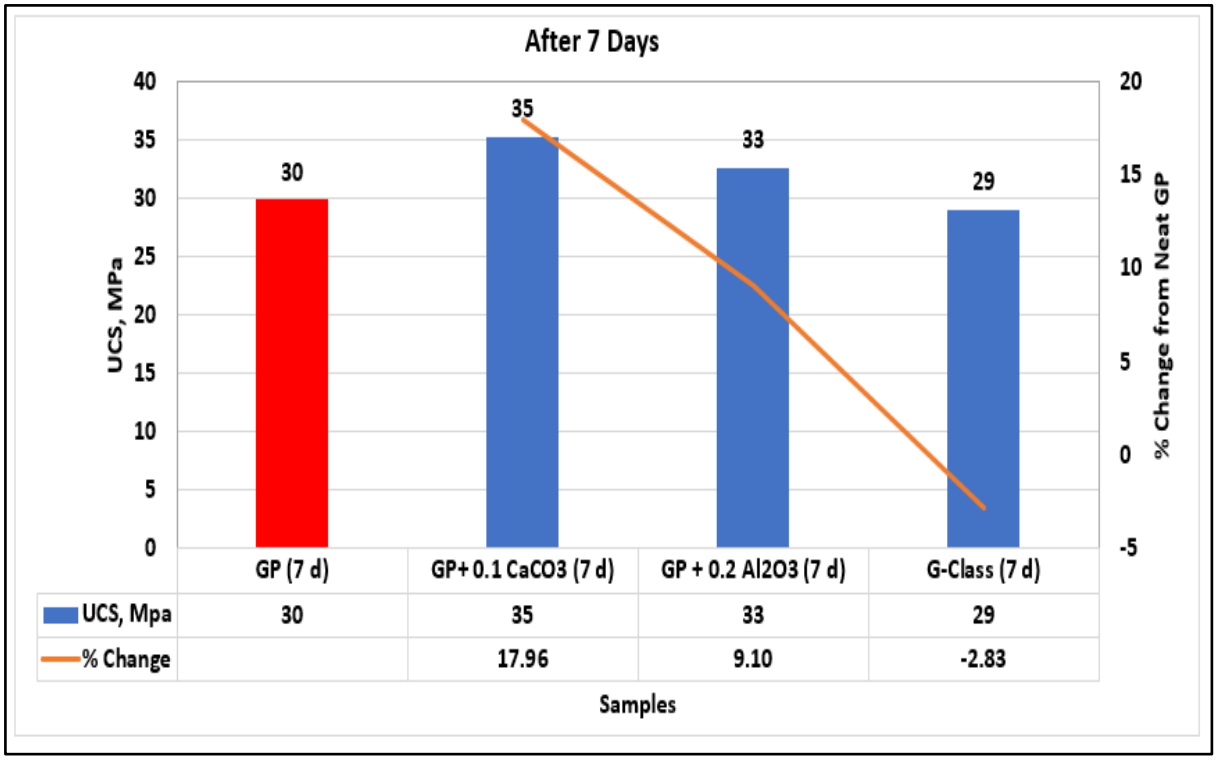

Figure 4.5 Effect of Nanoparticles on the Uniaxial Compressive Strength of Geopolymers After 7 Days

4.4 Effect of Nanoparticles on the Modulus of Elasticity After 1 and 7 Days

Before performing the destructive test, the non-destructive tests have been performed by measuring the sonic travel time, and mass of the samples. Based on the computed compressional wave velocity and the density of the plugs, the modulus of elasticity has been calculated by using Equation 3.3. Figure 4.6 displays the Modulus of elasticity (M) behaviors of the plugs. From the results, we can observe that G-class cement showed the highest M, while all the geopolymers have a similar M. The samples have very close density and velocity except for the G-class cement which has similar density to the geopolymers but a higher velocity. The reason could be that the concentration of the cement is higher than the concentration of fly ash in the geopolymer.

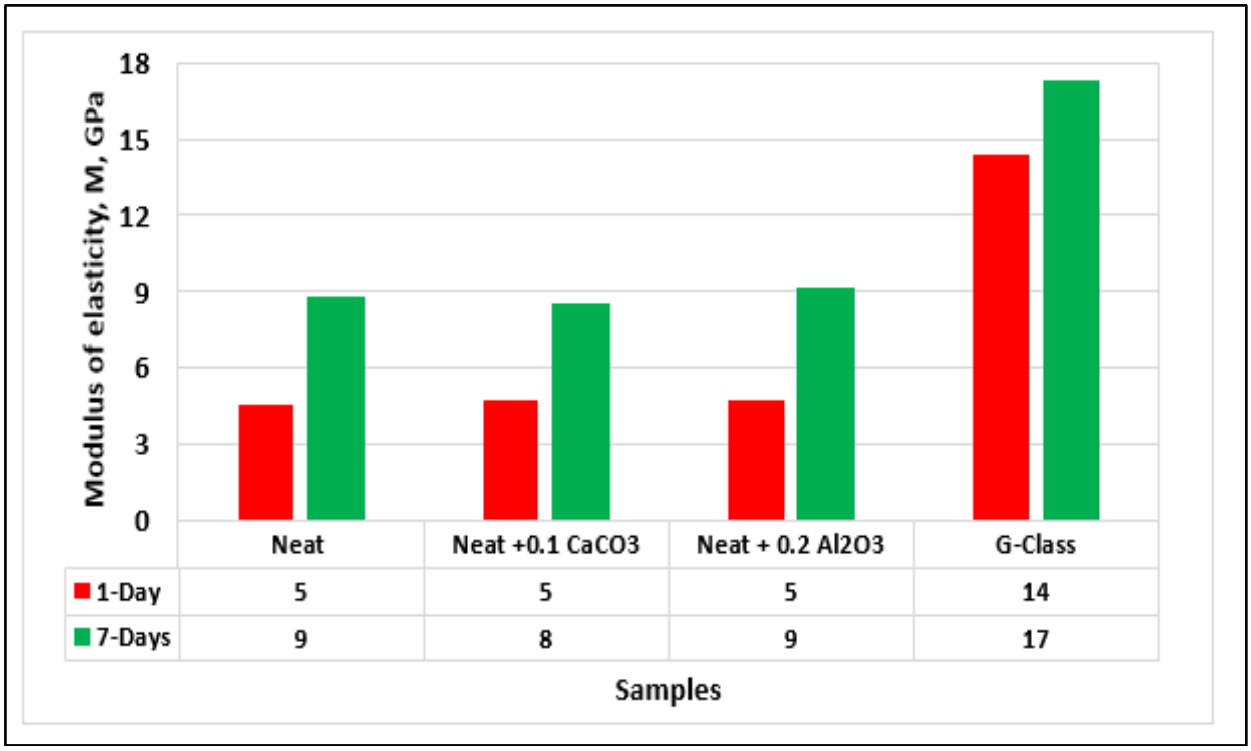

Figure 4.6 Effect of Nanoparticles on the Modulus of Elasticity After 1 and 7 Days

4.5 Effect of Nanoparticles on the Viscosity of GP

The pumpability and cement placement in the oil well, is one of the most considered properties in the petroleum industry. The flow of slurries in the wells is controlled by the viscosity which is the slurry's resistance to flow.

In this thesis, the viscometer responses of the best nanoparticle blended geopolymers along with the neat geopolymer and cement slurries have been measured.

Figure 4.7 presents the Fann viscometer measurement of the slurries at room temperature and pressure. It is observed that with the increase in shear rate, the shear stress of all the types of geopolymer systems behaves linearly, but the cement slurry shows a shear thinning behavior. Comparing the responses at very low shear rates, the shear stress of the cement is higher than the geopolymer responses and hence it requires more pressure to set into motion. The rheological parameters of the slurries were extracted by modeling the viscometer data with the Herschel-Bulkley model (Equation 3.5).

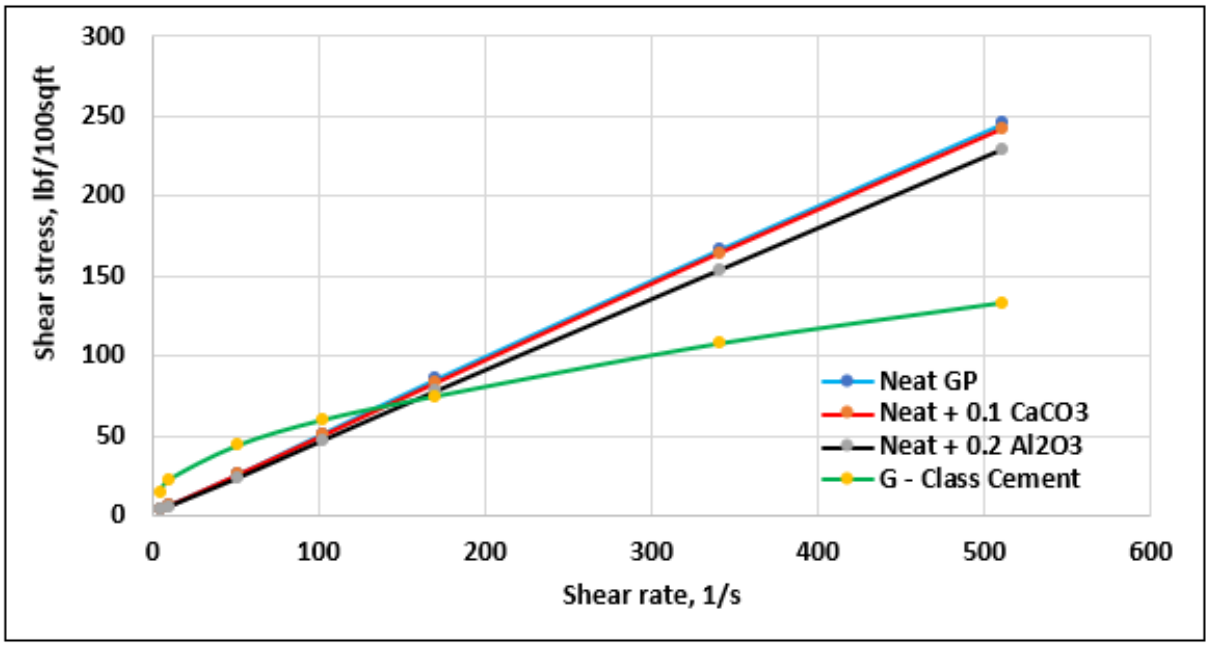

Figure 4.7 Viscometer Responses of the Neat GP, 0.1 g $CaCO_3$ GP, 0.2 g Al_2O_3 GP, and G-class Cement

Table 4.1 provides the calculated yield stress and plastic viscosity for the neat, nano-treated geopolymers, and the neat G-class cement. The geopolymers with and without nanoparticles have a very low and similar yield stress, which indicates that their resistance to flow is very low and doesn't need a high force applied to pump the slurry. On the other hand, cement has a high yield stress and needs a higher force applied to pump the cement in the wellbore.

Table 4.1 Viscosity Parameters

Rheological parameters	Cement	Neat GP	Neat GP+0.1g $CaCO_3$	Neat GP+0.2g Al_2O_3
k ($lbf.s^n/100ft^2$)	3.333	0.5367	0.5409	0.5367
N	0.5884	0.9814	0.9771	0.9814
τ_y ($lbf/100ft^2$)	7	1	1	1

4.6 Effect of Nanoparticles on the Water Absorption

To evaluate the porosity of the plugs indirectly, we used a water absorption test. Even though the test is not perfect, it allows us to get an indication on how the plugs absorb fluids at atmospheric pressure. After 4 days of curing in the oven and 18 hours in the air, the sample weight was recorded for another 7 days. The samples were weighed every day before

immersion in water. The fluid mass absorbed in the plugs is calculated based on the difference between the plug's mass before and after water absorption.

Due to the difference between the characteristics and the plug length of geopolymer and cement, the sample's mass absorption was normalized to get an equal start as shown in Figure 4.8. Furthermore, the normalized water absorption was transformed to the percentile water absorption as displayed in Figure 4.9. It is interesting to observe that the geopolymers had a much lower water absorption compared to G-class cement.

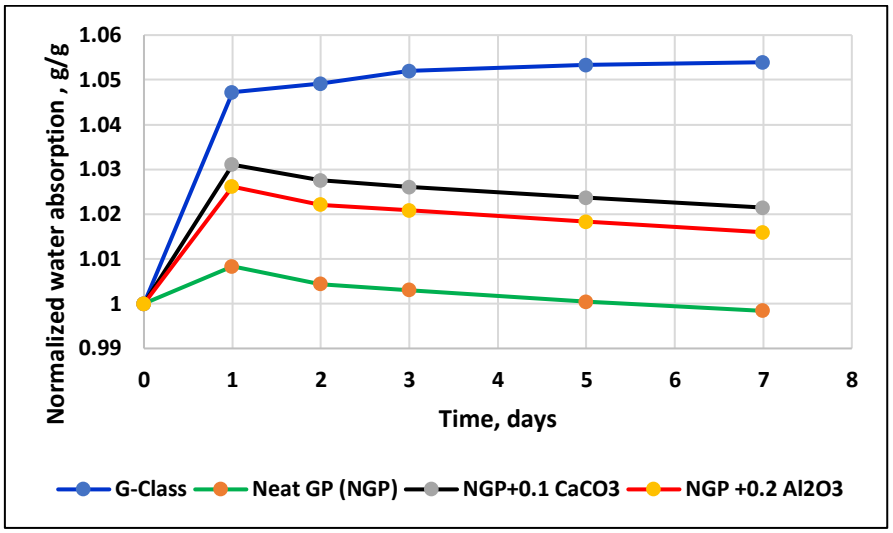

Figure 4.8 Normalized Mass of Water Absorption During Seven Days

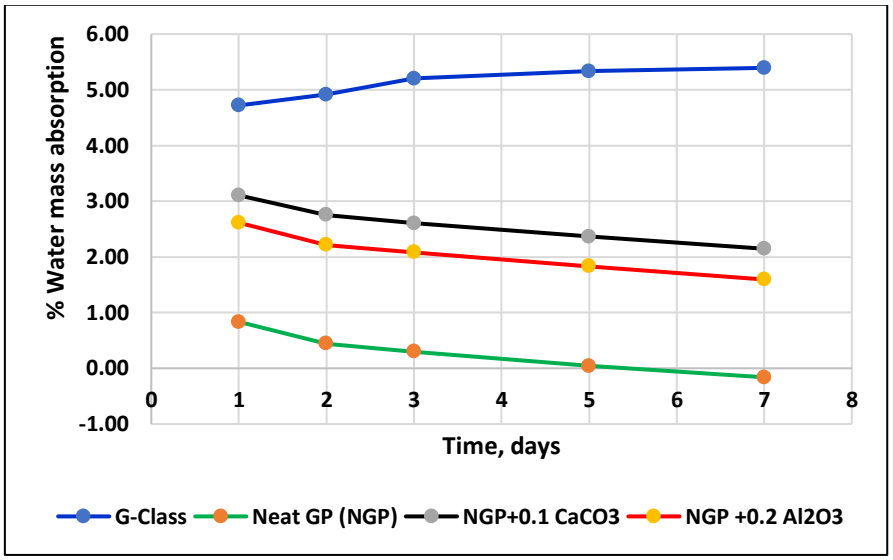

Figure 4.9 Water Mass Percentage of Water Absorption During Seven Days

4.7 Effect of Nanoparticles on Shrinkage

Figure 4.10 shows the temperature loading cycle on the geopolymer and cement samples. The first five days were the sample synthesis period at 60°C. The samples were then allowed to experience three room temperature and three 120°C cycles. Furthermore, the samples were placed at 120°C for five days. The reason for the considered temperature cycles is to evaluate the integrity of the samples after they have been exposed to harsh environmental conditions.

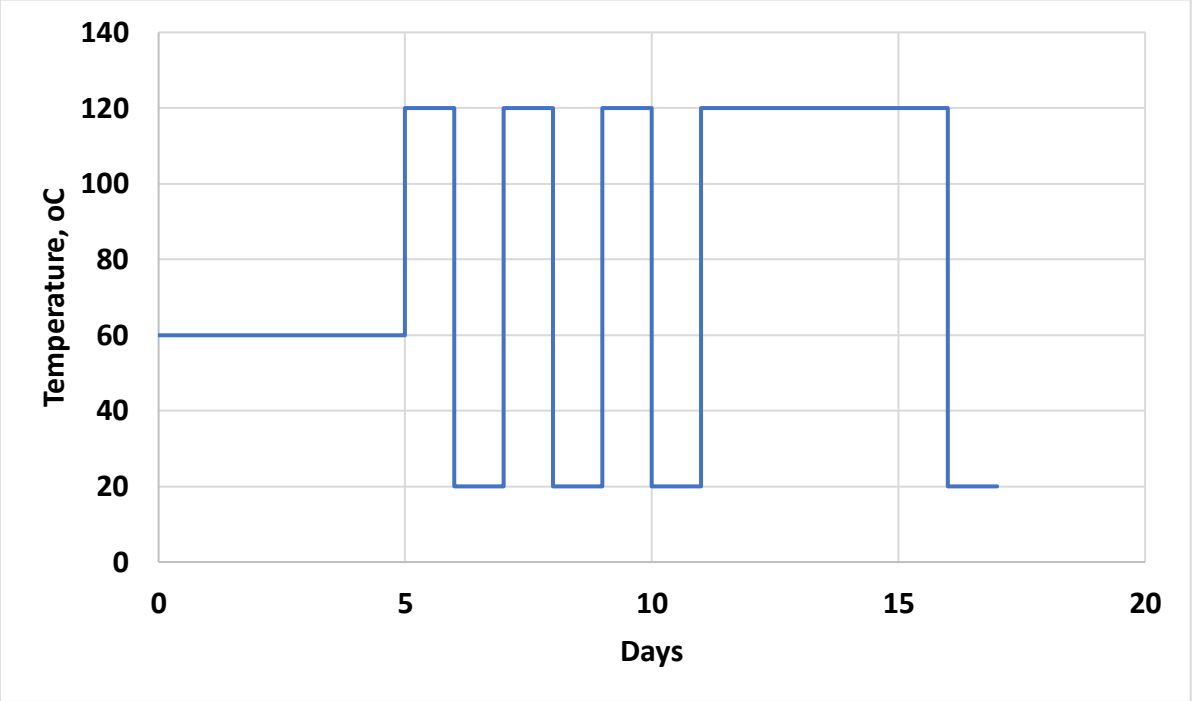

Figure 4.10 Temperature Loading Cycle on the Samples

After day 16, the samples were taken out of the oven and waited for some time until they lost the heat in the plugs. The pipes were filled with water on the top part of the samples for 24 hours. The water leakage was then measured. Figure 4.11 shows the measured result on day 17. As shown, the neat geopolymer exhibited almost no leakage. The addition of $CaCO_3$ and Al_2O_3 nanoparticle-based geopolymers shows a leakage of 1.02 g and 7.11 g, respectively. On the other hand, cement showed a higher leakage rate. The leakage could be through the plug-casing and the plugs as well. Even though the test is simple, the test was aimed to get an indication of the sample's responses to the temperature cycles.

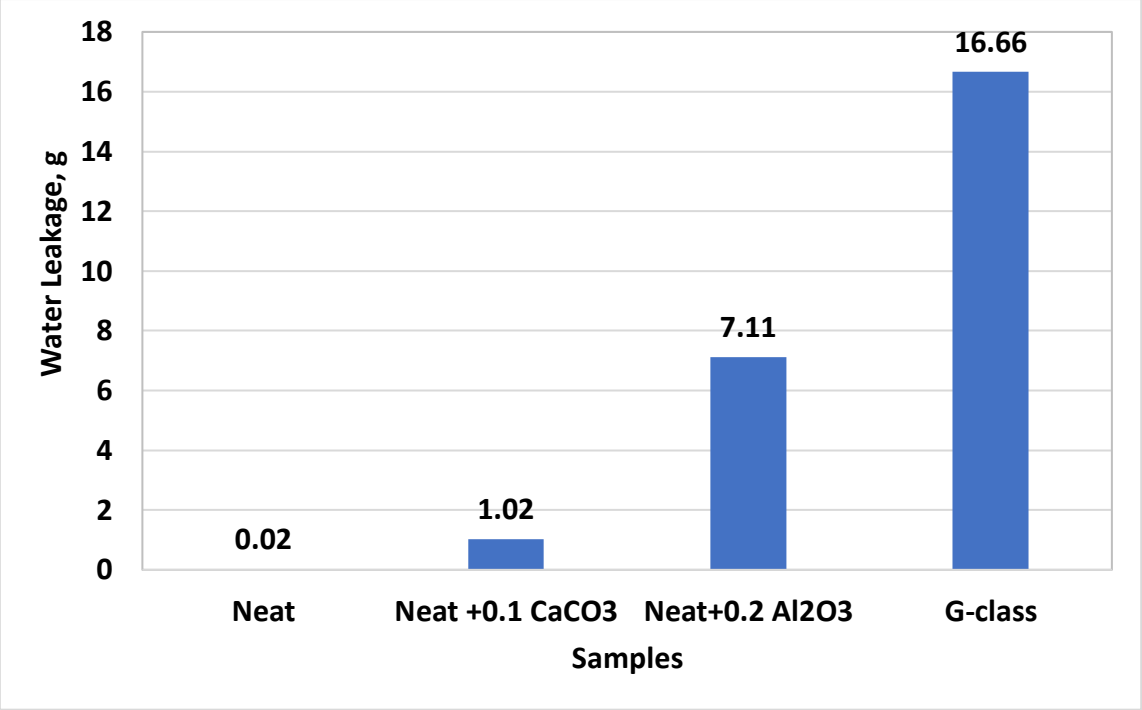

Figure 4.11 Water Leakage of the Samples

4.8 SEM and Element Analysis

To study the internal structure and the element analysis, in this section the Scan Electron Microscope (SEM) and Energy Dispersive X-ray Spectroscopy (EDS) analysis of the neat geopolymer and the nanoparticles ($CaCO_3$ and Al_2O_3) based geopolymers are presented. SEM pictures and EDS analyses have been performed at different selected localities and wider regions. For comparison purposes, SEM pictures have been taken from each sample and displayed in Figure 4.12, 4.13, and 4.14. One common feature among the samples is that the reaction process at the fly ash sphere begins with cracking and then formation of needle like structures. The samples also completely collapse and becomes into a set of needles. Several SEM pictures with different scaling have been taken and displayed in Appendix C.

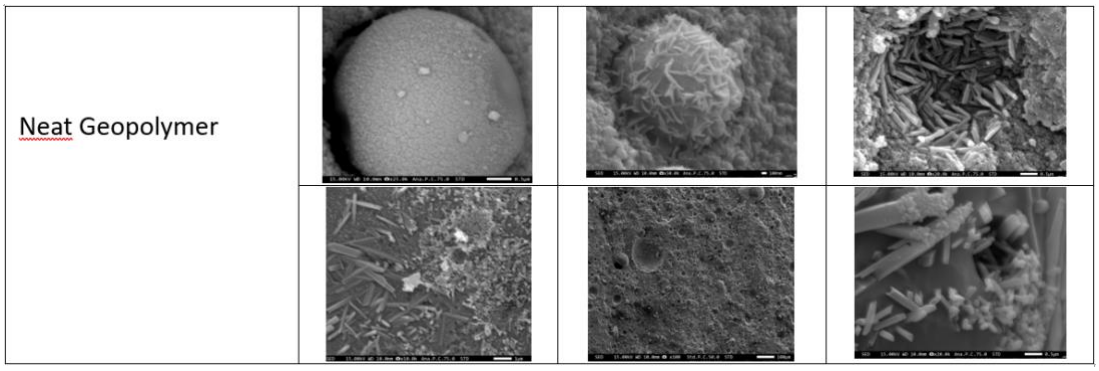

Figure 4.12 SEM Analysis of Nanoparticle Free-Neat Geopolymer

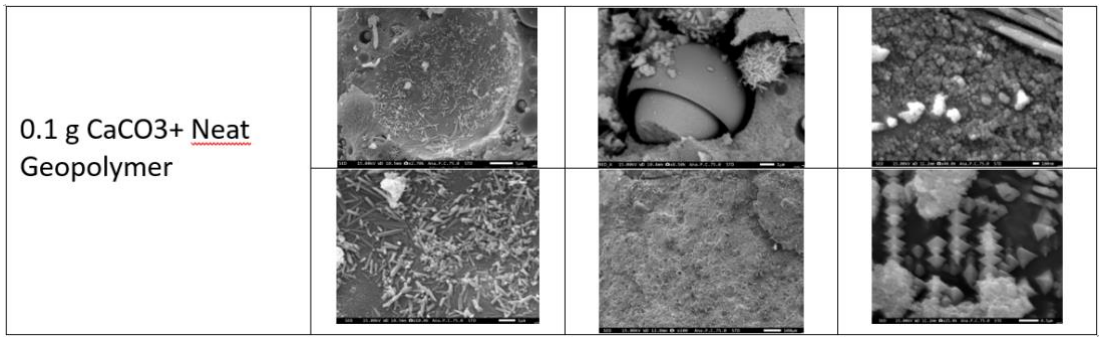

Figure 4.13 SEM Analysis of 0.1 g $CaCO_3$ Blended Geopolymer

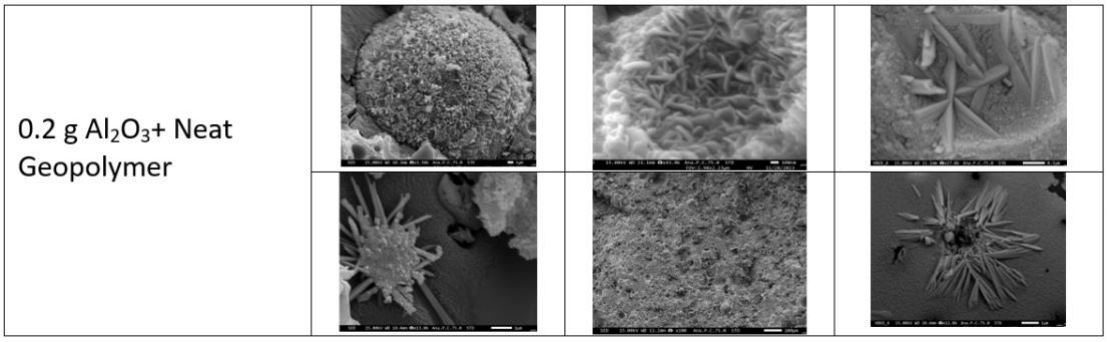

Figure 4.14 SEM Analysis of 0.2 g Al_2O_3 Blended Geopolymer

The element dispersion analysis of the samples was also further analyzed at the selected points. The selection at the fly ash sphere, where the geopolymer reaction performed. Figure 4.15 shows the spectrum analysis at the fly ash ball, at needle and other nearby zone. The element analysis spectrum 6, 7, and 8 showed that the O, Si, and Al are the main elements. Whereas the rest Fe, K, Na, and Mg showed less dominance with different concentration. However, Spectrum 8 shows that the analysis point is outside the fly ash sphere and the concentration of K exhibited higher value. The reason is that the K value was part of the KOH alkaline solution. Compared with the element analysis of the fly ash (Table 3.3), and alkaline activators (section 3.1.3.2.1 and section 3.1.3.2.2) and silicate (section 3.1.3.2.3), we can observe that no new elements have been created. Unfortunately, the EDS analysis except for the elements, it does not provide the possible creation of minerals through chemical reaction. Figure 4.16 also shows the EDS analysis of 0.1 g $CaCO_3$ blended Geopolymer. The dominant elements as shown in the spectrums 9, 10, and 11 are O, Si and Al, and Fe. Figure 4.17 displays the EDS analysis of 0.2 g Al_2O_3 blended Geopolymer. EDS showed that spectrums 16 and 17 exhibited a higher Si, O, Al. On the other hand, spectrum 18 showed Si, Fe and Al a higher concentration, with the less O. The overall analysis showed that the elements showed in the

EDS analyses are the one existing in the fly ash, sodium silicate and alkaline solutions (NaOH and KOH). Detailed EDS analyses are shown in Appendix C.

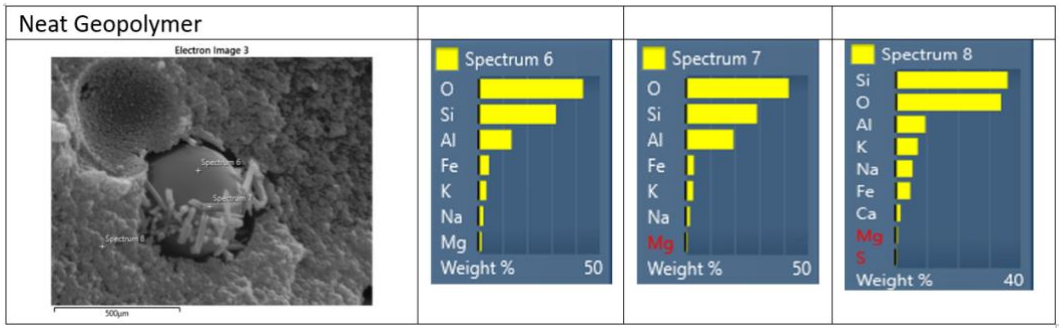

Figure 4.15 EDS Analysis of Nanoparticle Free-Neat Geopolymer

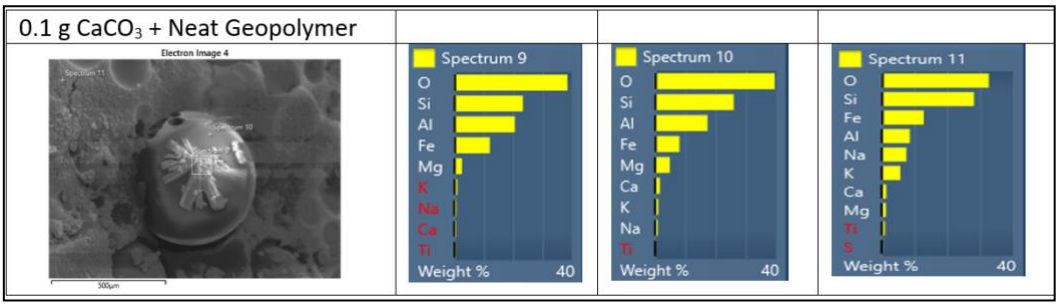

Figure 4.16 EDS Analysis of 0.1 g $CaCO_3$ Blended Geopolymer

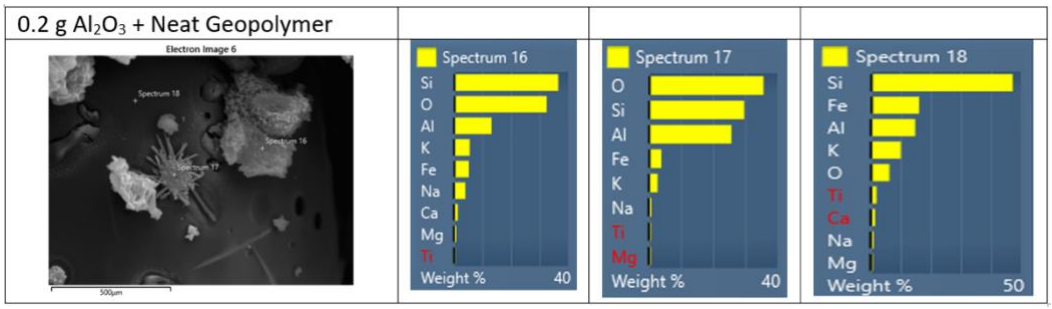

Figure 4.17 EDS Analysis of 0.2 g Al_2O_3 Blended Geopolymer

5 MODELLING AND TESTING

It is common practice to develop empirical models to estimate unmeasured parameters based on other measured parameters. In this thesis work, an empirical practical model has been developed by training destructive (UCS) data as the target and non-destructive (Vp) data as input.

The forthcoming section presents the development of a new model, model testing and comparison. The model prediction performance will be tested with datasets measured by Alexander [21]. The model prediction was also compared with the literature model derived based on rock, cement, and geopolymer listed in section 3.2.8.

5.1 Modelling

The average values of both the UCS and Vp of the plugs were used for the modeling. Before the execution of the destructive tests, the plug's velocity datasets were measured on the same day. The dataset considered from the modeling is the one measured after 7 days of curing.

To enhance the reliability of the model, outlier datasets were excluded. The source of the outlies was due to surface defects when preparing the samples, hence resulting in inaccurate measurements. These samples were removed as they were deemed unrepresentative.

Displaying the dataset as shown in Figure 5.1, the trend of the scattered datasets behaves as the power law model that fits the measurements with an R^2 of 0.923.

The formulated model reads:

Equation 5.1

$$UCS = 10^{-9}V_p^{3.1141}$$

Where, UCS is in MPa and Vp is in m/s.

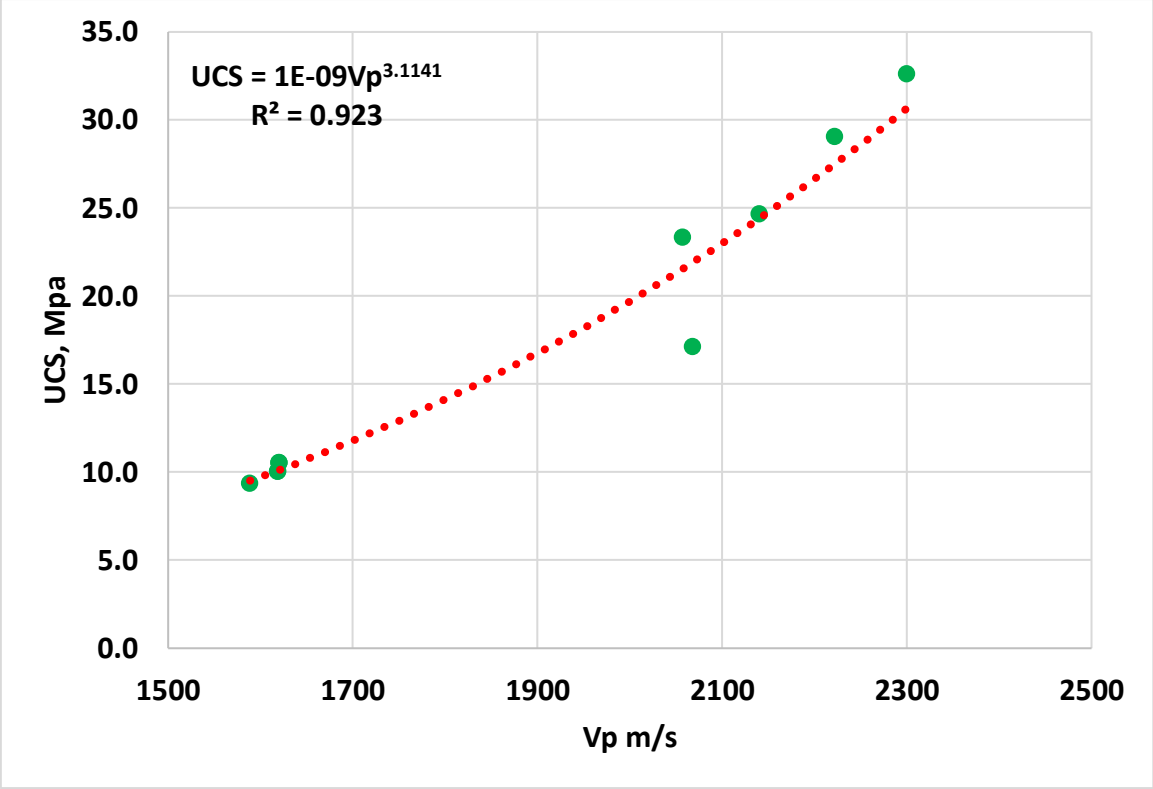

Figure 5.1 UCS vs Compressional Wave Velocity Modelling

5.2 Testing and Comparison

Alexander´s [21] geopolymer-measured data were used for the model evaluation. This thesis model (Equation 5.1) is compared with the shale rock-based Horsrud´s model [32], cement-based Hallvard Titlestad´s model [33], and Alexander´s geopolymer-based model [21].

Figure 5.2 displays the comparison of the model predictions. Results show that this thesis´s model captures the measured dataset at the predicting for the compressional wave velocity in the range between 2.142-2.389 km/s. The model prediction deviates from the measurement for velocity outside the listed range. The reason was that this thesis model has been developed for the compressional wave velocity up to 2.3 km/s as shown in Figure 5.1. On the other hand, Alexander's model manages to estimate the measured dataset outside the mentioned range since his model has been generated for a velocity higher than 2.3 km/s. This suggests that considering a wide velocity spectrum data that could be obtained from long curing days, one can generate a good model.

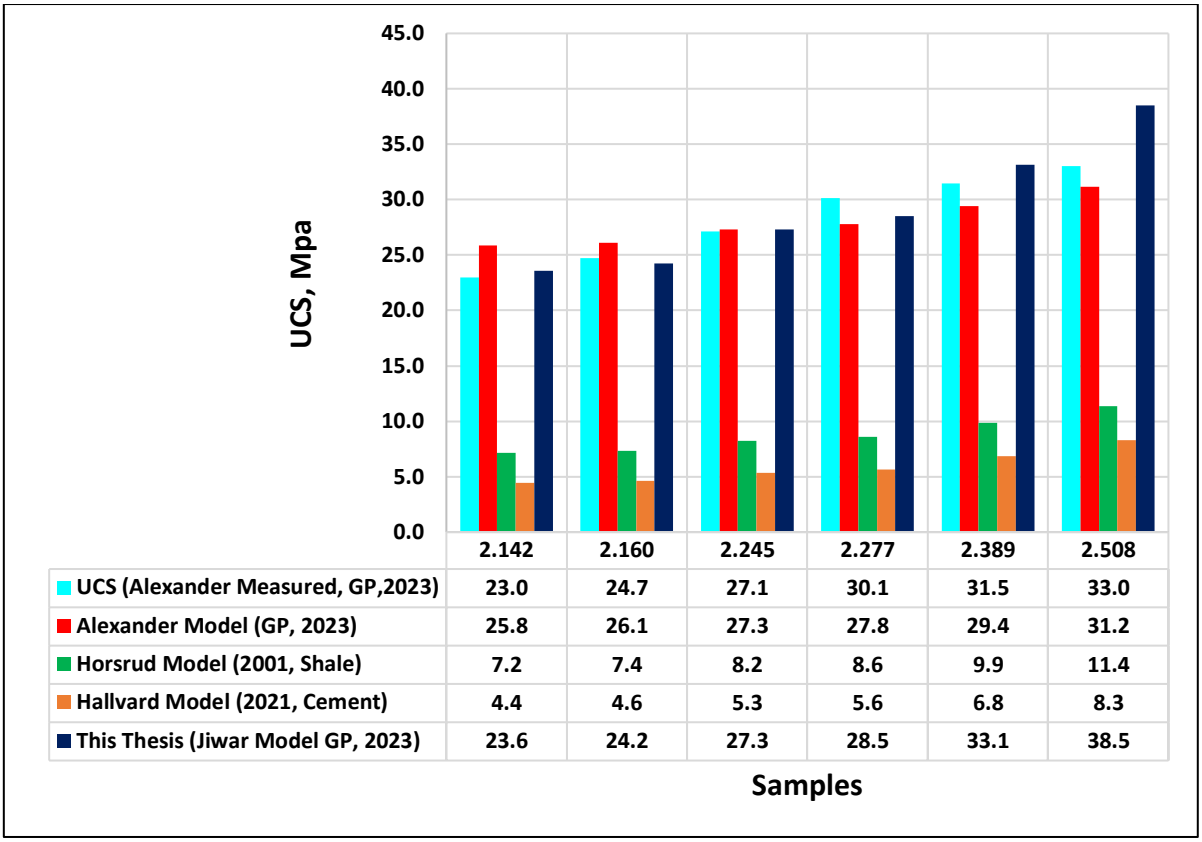

	2.142	2.160	2.245	2.277	2.389	2.508
UCS (Alexander Measured, GP,2023)	23.0	24.7	27.1	30.1	31.5	33.0
Alexander Model (GP, 2023)	25.8	26.1	27.3	27.8	29.4	31.2
Horsrud Model (2001, Shale)	7.2	7.4	8.2	8.6	9.9	11.4
Hallvard Model (2021, Cement)	4.4	4.6	5.3	5.6	6.8	8.3
This Thesis (Jiwar Model GP, 2023)	23.6	24.2	27.3	28.5	33.1	38.5

Figure 5.2 Comparison of This Thesis Model Prediction vs Literature

6 ECONOMIC AND ENVIRONMENTAL ASPECTS OF GEOPOLYMER

Geopolymers represent an innovative and environmentally friendly technology with significant economic implications within the oil and gas industry. In this chapter, we will delve into the economic aspects of geopolymers, exploring their potential to drive cost savings, enhance sustainability, and promote economic growth.

6.1 Environmental Impact of Geopolymer vs Cement

a) The by-product (CO_2) with Cement

Cement is one of the most widely used construction materials worldwide, but its manufacturing process is associated with a significant environmental concern due to the emission of carbon dioxide (CO_2), a potent greenhouse gas. The production of cement primarily involves the heating of limestone (calcium carbonate) to create clinker, which is then ground into a fine powder to produce the final product [34]. During this process, CO_2 is released in two main ways:

- **Decarbonization of Limestone:** The first major source of CO_2 emissions in cement manufacturing is the chemical reaction called decarbonization. When limestone is heated in a rotary kiln to temperatures of around 1450°C, it undergoes a thermal decomposition. This chemical reaction releases a substantial amount of CO_2 into the atmosphere, accounting for a significant portion of the carbon emissions associated with cement production. The thermal decomposition reaction is expressed as follows [34].

$CaCO_3$ (limestone) + heat → CaO (calcium oxide) + CO_2 (carbon dioxide)

- **Fossil Fuel Combustion:** The second major source of CO_2 emissions in cement manufacturing arises from the use of fossil fuels to heat the kilns. Typically, coal, petroleum coke, and natural gas are used as fuels in the cement industry. The combustion of these fuels produces additional CO_2 as a byproduct, contributing to the carbon footprint of cement production [35].

b) The by-product (CO_2) with geopolymer

Unlike cement, which relies on calcium-based chemistry, geopolymers are typically based on aluminosilicate materials and do not involve the high-temperature calcination of limestone. Carbon footprint analyses comparing geopolymer and Portland cement have shown that the reduction in CO_2 emissions achieved with geopolymer cement can vary, ranging from as high as 80% to as low as 9% [36]. Here's how geopolymers differ in terms of CO_2 production:

- **Low Carbon Emissions from Secondary Raw Materials:** Geopolymers can be produced from a variety of secondary raw materials, including fly ash, slag, metakaolin, calcined clays, zeolite, and natural volcanic ash. These materials often have lower embodied carbon and do not require the energy-intensive decarbonization process of limestone. Therefore, the initial carbon footprint associated with the raw materials in geopolymers is typically lower than that of cement.

- **Lower Energy Consumption:** The manufacturing process for geopolymers generally involves mixing the raw materials with an alkaline activator at moderate temperatures around 60-100°C, which is significantly lower than the temperatures required for cement clinker production. This lower energy requirement translates to reduced CO_2 emissions during the manufacturing process.

In summary, geopolymers represent a promising alternative to traditional cement in terms of reducing CO_2 emissions. Their production typically generates fewer emissions due to the absence of limestone calcination and the use of lower-temperature processes.

6.2 Improved Well Integrity

6.2.1 Low Permeability and Decreased Risk of Potential Leakage

Geopolymer materials create a robust barrier within the wellbore due to its low permeability. This characteristic is particularly beneficial in preventing fluid migration and gas leakage, further enhancing well integrity. The decreased risk of leakage not only enhances

environmental safety but also reduces the financial and operational risks. Geopolymer's ability to maintain a secure and impermeable wellbore significantly contributes to overall well integrity and cost reduction in oil and gas production operations.

6.2.2 Reduced Casing and Cementing Failures

Geopolymer was shown to have low shrinkage and high compressive strength [37]. This interprets a reduced risk of casing and cementing failures, which are common challenges in the oil and gas industry. Improved casing and cementing reliability directly contribute to enhanced well integrity.

6.2.3 Chemical Stability

Geopolymer, being highly resistant to chemical corrosion, significantly improves well integrity [38]. Traditional cementitious materials used in well construction can degrade over time due to the harsh chemical environment encountered in oil and gas reservoirs. Geopolymer, on the other hand, exhibits remarkable chemical stability, ensuring long-term well integrity.

6.2.4 Temperature and Pressure Resistance

Geopolymer materials can withstand high temperatures and pressures encountered in deep oil and gas reservoirs [39]. This resistance is crucial for maintaining well integrity over the lifespan of the well. Traditional materials may deteriorate or weaken under extreme conditions, leading to costly repairs or even well abandonment.

6.3 Reduced Operational Direct and Indirect Costs Required During the Production of Geopolymer

Geopolymers are typically composed of industrial waste materials like fly ash, slag, and other aluminosilicate sources. By utilizing these waste products as feedstocks, geopolymers reduce the demand for virgin raw materials, thereby lowering material costs. This

not only makes them cost-effective but also helps in waste management and reduces the environmental impact associated with disposal.

6.4 Cost-Benefit Analysis of Geopolymer Comparing with Cement

Given the environmental benefits associated with geopolymer over traditional cement, it is also essential to understand the cost implications of synthesizing neat geopolymer compared to traditional cement to identify the most economically viable one. Here we evaluate the average cost of the necessary materials for synthetization.

6.4.1 Estimation of Costs

The cost of implementing these types of cement is based on two primary components: direct costs (e.g., cost of materials and transportation) and indirect costs such as (e.g., industry standardization, curing time, and downtime hardening).

6.4.1.1 Indirect Costs

Limited standardization and slower curing time compared to Portland cement which results in a very big expense for each operative day waiting for the curing and downtime hardening. On the other hand, cement is a well-established and standardized material in the construction industry, including oil and gas wells, making it easier to procure and comply with regulations.

Geopolymers may not have as extensive industry standards as cement, potentially leading to challenges in procurement and regulatory compliance.

6.4.1.2 Direct Costs

Since we were not able to get the exact direct prices of the materials and didn't manufacture our geopolymer cement concretes. We have taken material costs from a case study at the University of North Carolina [36] and a dissertation at Wayne State University [40].

Table 6.1 and 6.2 shows two different cost analyses of geopolymer materials based on their geopolymer compositions.

Table 6.1 Cost of Constituent Materials in Geopolymer Cement Concrete and Portland Cement Concrete [36]

Material	Cost per 45,4 kg	Geopolymer cement concrete, 0.454 kg	Cost for 0.765 m^3 geopolymer cement concrete	Portland cement concrete, 0.454 kg	Cost for 0.765 m^3 precast Portland cement concrete
Sodium silicate	$42.00	125.758	$116.34	0	$0
Sodium hydroxide	$64.00	16.344	$23.04	0	$0
Fly ash	$1.13	357.298	$8.92	0	$0
Fine aggregate	$0.42	621.98	$5.79	567.5	$5.28
Coarse aggregate	$0.49	621.98	$6.73	817.2	$8.84
Water	$0.02	34.05	$0.02	118.04	$0.06
Portland cement	$5.64	0	$0	295.1	$36.69
Total	n/a	1777.41	$160.83	1797.84	$50.88

Table 6.2 The Breakdown of Material Prices [40]

Material	Price ($/ton)
Fly ash	50-80
Na_2SO_4	80-150
NaOH	280-490
Meta	380 - 600
SF	380 - 600
Sand	38 - 40
Portland cement	95-106

6.4.2 Comparison and Decision-Making

Environmentally, producing geopolymer will contribute to making a greener world and save the world by avoiding pollution caused by greenhouse gases. Furthermore, it saves a lot of energy usage compared to the traditional cements which is also an economical saving.

Economically, pumping the geopolymer into the wellbores and cementing it helps to improve and ensure long-term well integrity and durability, which is financially cost-saving and reduces financial and operational risks compared to traditional types of cement.

On the other hand, the estimation of total costs (direct cost + indirect cost) proves that geopolymer can cost up to 3 times more than cement costs when the same amount is produced. Moreover, it can also cause big financial losses due to its late strength development compared to Portland cement and downtime. In the oil and gas industry, early hardening is a crucial requirement to avoid longer rig operating times. Time plays a big role in the industry since the operation of the drilling rigs can cost the oil companies hundreds of thousands per dollar each day. To conclude, for the time being, traditional cement is still the preferable material in the industry economically and more research have to be conducted to develop a cost-effective geopolymer.

7 SUMMARY AND CONCLUSION

Cement is commonly used for oil well construction and plug and abandonment operations. Since cement does not completely satisfy the requirements stated by the NORSOK D-010 [6], the oil industry is searching for a new alternative material that replaces cement. For this, the geopolymer is one of the candidates, which is currently in the research phase.
In this thesis work, based on Alexander's [21] neat geopolymer, the impact of nanoparticles has been evaluated. Moreover, compared with the Portland G-class cement, the economic aspect of geopolymer along with the environmental issues have been analyzed.

As shown in Table 7.1, the 12 M NaOH-based neat geopolymer was shown 38.46% stronger than the 10 M NaOH-based neat geopolymer. The impact of nanoparticles has been tested on the 12 M-based neat geopolymer and the results are provided in Table 7.2.

Table 7.1 Effect of NaOH Molar Concentration on Alexander's [21] Neat Geopolymer

Geopolymer (GP)	NaOH molar concentration	Curing days	Neat GP UCS, MPa	% Change of 12 M With Respect to 10 M Neat GP
Neat GP	10 M	3	13	
	12 M		18	+38.46%

Table 7.2 Effect of Nanoparticles on Neat Geopolymer Compared with G-class Cement

Geopolymer(GP) And Cement	NaOH/KOH molar concentration	Curing age, days	Best Nanopaticles dosage, g	Neat GP UCS, MPa	GP with Nanoparticle And Cement, UCS, MPa	% Change With Respect to Neat GP
Neat GP	12 M	1	-	9		
		3		19		
		7		30		
GP with $CaCO_3$ NP	12 M	1	0.1 g		11	+12.75
		3			23	+25.35
		7			35	+17.96
GP with Al_2O_3 NP	12 M	1	0.2 g		10	+7.51
		3			25	+34.02
		7			33	+9.10
G-Class cement	-	1	-		21	+120.74
		3			32	+70.19
		7			29	-2.83

The main finding in this thesis work is summarized as follows:

Strength development after 1 day:

- An early development study was conducted to evaluate the application of geopolymer for well construction. That is to answer research question 1 addressed in section 1.2. Results show that after 1 day of strength analysis, the addition of 0.1 g $CaCO_3$ and 0.2 g Al_2O_3 increased the uniaxial compressive strength of the neat geopolymer by 12.75% and 7.51%, respectively.
- However, the G-class cement is about 120.7% stronger than the neat geopolymer.

Strength development after 3 days:

- The strength development after 3 days of curing results showed that the addition of 0.1 g $CaCO_3$ and 0.2 g Al_2O_3 increased the uniaxial compressive strength of neat geopolymer by 23.35% and 34.02%, respectively.
- However, the G-class cement is about 70.2 % stronger than the neat geopolymer.

Strength development after 7 days:

- The strength development after 7 days of curing results showed that the addition of 0.1 g $CaCO_3$ and 0.2 g Al_2O_3 increased the uniaxial compressive strength of neat geopolymer by 17.96 % and 9.10%, respectively.
- However, the G-class cement showed thermal degradation and reduced the strength by 2.83% as compared to the neat geopolymer.

Results showed that the geopolymer with an extended curing period (7 days) is stronger than the G-class cement. Moreover, the addition of nanoparticles enhances the mechanical properties of the neat geopolymer.

Empirical UCS-Vp model:

- The empirical model developed in this thesis predicted the geopolymer data measured by Alexander [21] for the compressional wave velocity between 2.142-2.389 km/s. Compared with literature models derived based on rock and cement, the models did not estimate the geopolymer dataset. It is also observed that the geopolymer-based

empirical model developed by Alexander [21] predicts the dataset even outside the mentioned velocity range.

SEM and Element Analysis:

- In the comparison of the neat geopolymer with the nano-based geopolymers, the SEM pictures showed similar polymerization processes and unreacted fly ashes. Moreover, the element analysis also shows extra elements in the nano-based geopolymers as compared with the neat geopolymer. However, the picture did not show very special phenomena that distinguish among the samples.

Environmental Aspect Analysis:

- The comparison between the environmental aspects of cement and geopolymers highlights the latter as a promising and eco-friendly alternative. Geopolymers, by leveraging aluminosilicate materials and avoiding the high-temperature processes of limestone calcination, demonstrate a substantial reduction in CO_2 emissions. The use of secondary raw materials with lower embodied carbon and lower energy consumption during manufacturing contributes to the overall environmental benefits of geopolymers.
- While the reduction in CO_2 emissions with geopolymers varies, ranging from 80% to 9% in comparison to Portland cement, the consistent trend has a positive impact on environmental sustainability. The findings underscore the potential of geopolymers to play a crucial role in the industry's efforts to minimize its carbon footprint. Further research and development in geopolymers hold the key to advancing sustainable practices and promoting a greener and more environmentally responsible future.

Economic Analysis:

- In weighing the economic viability of geopolymer against traditional cement, certain advantages emerge, such as reduced material costs through the use of industrial waste. However, challenges in terms of limited standardization, slower curing time, and higher overall costs, particularly in the oil and gas industry, suggest that, for the time being, traditional cement remains the more economically preferable option. Despite the environmental benefits of geopolymers, their delayed strength development and associated downtime pose significant economic hurdles, emphasizing the need for

further advancements in technology and industry standardization for widespread economic adoption.

Finally, this thesis concludes that the results and analyses presented are valid for the considered experimental sample mixtures and curing temperature and pressure conditions. Changing the chemical composition and temperature/pressure conditions, we may achieve different results.

Although, the results clearly show the potential application of nanoparticle and geopolymer blended systems that could be used as an alternative for G-class cement. The reasons are due to their performance, cost-effectiveness, and being environment friendly.

REFERENCES

[1] Watts, D. (2018, January 15). Cementing operations. In SPE PetroWiki. https://petrowiki.spe.org/index.php?title=Cementing_operations&oldid=53699

[2] Mukhtarov, A. (2022). Extraction of geothermal energy resources associated with abandoned oil and gas wells: benefits and limits (Master's thesis). Politecnico di Torino.

[3] Schlumberger. (2016, January 18). CoilTOOLS Tools and Solutions Enable Gulf of Mexico Operator to Efficiently Reabandon High-Risk Well. Case Study. Retrieved from https://www.slb.com/resource-library/case-study/ct/coiltools-reabandon-gom-cs

[4] Nelson, E.B., & Guillot, D. (Eds.). (2006). Well Cementing (2nd ed.). Schlumberger.

[5] Bennett, T. (2016). Well Cement Integrity and Cementing Practices. The University of Adelaide, Australia.

[6] Standards Norway. (2021). NORSOK D-010 Well integrity in drilling and well drilling operations, rev 5.

[7] Vignes, B., Safety, P., & Aadnoy, B.S. (2008). Well-Integrity Issues Offshore Norway. IADC/SPE Drilling Conference, Orlando, 4-6 March 2008, 91-119. doi:10.2118/112535-MS

[8] Singh, N. B., Saxena, S. K., Kumar, M., & Rai, S. (2019). Geopolymer cement: Synthesis, Characterization, Properties, and Applications. Materials Today: Proceedings, 15(3), 364-370. doi:10.1016/j.matpr.2019.04.095

[9] Cong, P., & Cheng, Y. (2021). Advances in geopolymer materials: A comprehensive review. Journal of Traffic and Transportation Engineering (English Edition), 8(3), 283-314. https://doi.org/10.1016/j.jtte.2021.03.004

[10] Editor-in-Chief: Haimei Zhang (Ed.). (2011). Building Materials in Civil Engineering. Woodhead Publishing. ISBN 978-1-84569-956-7 (online).

[11] Singh, N.B., & Middendorf, B. (2020). Geopolymers as an alternative to Portland cement: An overview. Construction and Building Materials, 237, 117455. doi:10.1016/j.conbuildmat.2019.117455

[12] Ibrahim, M., Johari, M.A.M., Maslehuddin, M., & Rahman, M.K. (2018). Influence of nano-SiO2 on the strength and microstructure of natural pozzolan-based alkali-activated concrete. Construction and Building Materials, 173, 573-585. doi:10.1016/j.conbuildmat.2018.04.051

[13] Alomayri, T. (2019). Experimental study of the microstructural and mechanical properties of geopolymer paste with nanomaterial (Al2O3). Journal of Building Engineering, 25, 100788. doi:10.1016/j.jobe.2019.100788

[14] Chindaprasirt, P., De Silva, P., Sagoe-Crentsil, K., & Hanjitsuwan, S. (2012). Effect of SiO2 and Al2O3 on the setting and hardening of high-calcium fly ash-based geopolymer systems. Journal of Materials Science, 47(11), 4876–4883. doi:10.1007/s10853-012-6353-y

[15] Alvi, M.A.A., Khalifeh, M., & Agonafir, M.B. (2020). Effect of nanoparticles on properties of geopolymers designed for well cementing applications. Journal of Petroleum Science and Engineering, 191, 107128. doi:10.1016/j.petrol.2020.107128

[16] Adak, D., Sarkar, M., & Mandal, S. (2014). Effect of nano-silica on strength and durability of fly ash-based geopolymer mortar. Construction and Building Materials, 70, 453-459. doi:10.1016/j.conbuildmat.2014.07.093

[17] Phoo-ngernkham, T., Chindaprasirt, P., Sata, V., Hanjitsuwan, S., & Hatanaka, S. (2014). The effect of adding nano-SiO2 and nano-Al2O3 on properties of high calcium fly ash geopolymer cured at ambient temperature. Materials & Design, 55, 58-65. doi:10.1016/j.matdes.2013.09.049

[18] Gao, K., Lin, K.-L., Wang, D., Shiu, H.-S., Hwang, C.-L., & Cheng, T.-W. (2013). Effects of Nano-SiO2 on Setting Time and Compressive Strength of Alkali-activated Metakaolin-based Geopolymer. The Open Civil Engineering Journal, 7, 84-92. doi:10.2174/1874149501307010084

[19] Rovnaník, P., Šimonová, H., Topolář, L., Schmid, P., & Keršner, Z. (2016). Effect of Carbon Nanotubes on the Mechanical Fracture Properties of Fly Ash Geopolymer. Procedia Engineering, 151, 321-328. doi:10.1016/j.proeng.2016.07.360

[20] Assaedi, H., Alomayri, T., Kaze, C.R., Jindal, B.B., Subaer, S., Shaikh, F., & Alraddadi, S. (2020). Characterization and properties of geopolymer nanocomposites with different contents of nano-CaCO3. Construction and Building Materials, 252, 119137. doi:10.1016/j.conbuildmat.2020.119137

[21] Høyvik, A. (2023). Effect of SiO2 nanoparticle and Quartz microparticle on the newly formulated geopolymer: Experimental and Modelling Studies. Bachelor's Thesis, University of Stavanger

[22] Heidelberg Materials. (n.d.). Retrieved from https://www.sement.heidelbergmaterials.no/no

[23] Merck. (n.d.). Natriumhydroksid 50 - 52% in water, colorless liquid for ion chromatography. VWR, Avantor®. Retrieved from https://no.vwr.com/store/product/25257332/natriumhydroksid-50-52-in-water-colourless-liquid-for-ion-chromatography#order

[24] Solberg Industri. (n.d.). Homepage. Retrieved from https://www.solbergindustri.no/en

[25] PQ Corporation. (n.d.). Products. Retrieved from https://www.pqcorp.com/products/

[26] US Research Nanomaterials, Inc. (n.d.). Precipitated Calcium Carbonate Nanoparticles / Precipitated CaCO3 Nanopowder, 50nm, 40wt%, Water Dispersion. Houston, TX, USA. Retrieved from https://www.us-nano.com/inc/sdetail/34324

[27] US Research Nanomaterials, Inc. (n.d.). Aluminum Oxide Al2O3 Nanopowder / Nanoparticles Water Dispersion (Alpha, 20wt%, 30nm). Houston, TX, USA. Retrieved from https://www.us-nano.com/inc/sdetail/623

[28] Fjær, E., Holt, R.M., Horsrud, P., Raaen, A.M., & Risnes, R.†. (2008). Petroleum Related Rock Mechanics (2nd ed.). Elsevier.

[29] Rehm, B. (2012). Flow Drilling: Underbalance Drilling with Liquid Single-Phase Systems. In Underbalanced Drilling: Limits and Extremes (pp. 39-108). Elsevier. https://doi.org/10.1016/B978-1-933762-05-0.50009-7

[30] Mohamad, J.D., Abang Hasbollah, D.Z., Mohd Taib, A., Md Dan, M.F., Jusoh, S.N., & Mat Said, K.N. (2022). Correlation between Uniaxial Compressive Strength and Point Load Strength of Penang Island Granites. In GEOTROPIKA & ICHITRA 2021, IOP Conf. Series: Earth and Environmental Science, 971, 012025. IOP Publishing. doi:10.1088/1755-1315/971/1/012025

[31] NanoScience Instruments. (n.d.). Scanning Electron Microscopy. Retrieved from https://www.nanoscience.com/techniques/scanning-electron-microscopy

[32] Horsrud, P. (2001, June 01). Estimating Mechanical Properties of Shale From Empirical Correlations. SPE Drill & Compl, 16(02), 68–73. https://doi.org/10.2118/56017-PA

[33] Titlestad, H. (2021). Effect of nano-SiO2, nano-Al2O3, MWCNT and FA on properties of Portland G-class cement (Master's thesis). University of Stavanger.

[34] Gibbs, M. J., Soyka, P., Conneely, D., & Kruger, D. (n.d.). CO2 Emissions from Cement Production. Good Practice Guidance and Uncertainty Management in National Greenhouse Gas Inventories. ICF Incorporated. Retrieved from https://www.ipcc-nggip.iges.or.jp/public/gp/bgp/3_1_Cement_Production.pdf

[35] Ishak, S. A., & Hashim, H. (2015). Low carbon measures for cement plant – a review. Journal of Cleaner Production, 103, 260-274. https://doi.org/10.1016/j.jclepro.2014.11.003

[36] Tempest, B., Snell, C., Gentry, T., Trejo, M., & Isherwood, K. (2015). Manufacture of full-scale geopolymer cement concrete components: A case study to highlight opportunities and challenges. PCI Journal, November–December 2015.

[37] Deb, P. S., Nath, P., & Sarker, P. K. (2015). Drying Shrinkage of Slag Blended Fly Ash Geopolymer Concrete Cured at Room Temperature. Procedia Engineering, 125, 594-600. https://doi.org/10.1016/j.proeng.2015.11.066

[38] Cong, P., & Cheng, Y. (2021). Advances in geopolymer materials: A comprehensive review. Journal of Traffic and Transportation Engineering (English Edition), 8(3), 283-314. https://doi.org/10.1016/j.jtte.2021.03.004

[39] Paiva, M. D. M., Silva, E. C. C. M., Melo, D. M. A., Martinelli, A. E., & Schneider, J. F. (2018). A geopolymer cementing system for oil wells subject to steam injection. Journal of Petroleum Science and Engineering, 169, 748-759. https://doi.org/10.1016/j.petrol.2018.06.022

[40] Shwekat, K. (2015). Benefit-Cost Analysis of Using Class F Fly Ash-Based Green Cement in Masonry Units. (Doctoral dissertation). Wayne State University, Detroit, Michigan.

APPENDIX A: FORCE VS DEFORMATION TEST

Test batch for compressive strength of NaOH-KOH concentration on neat GP 3 days:

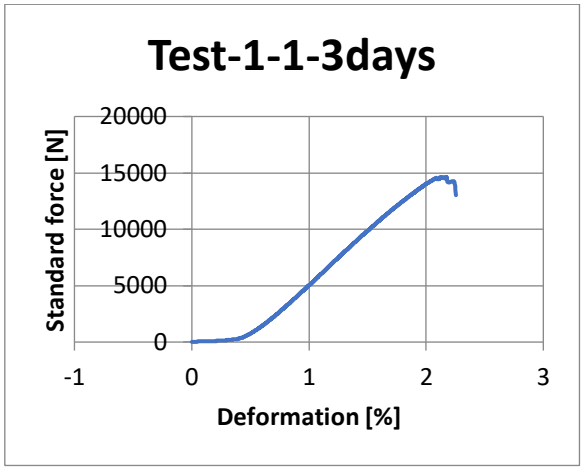

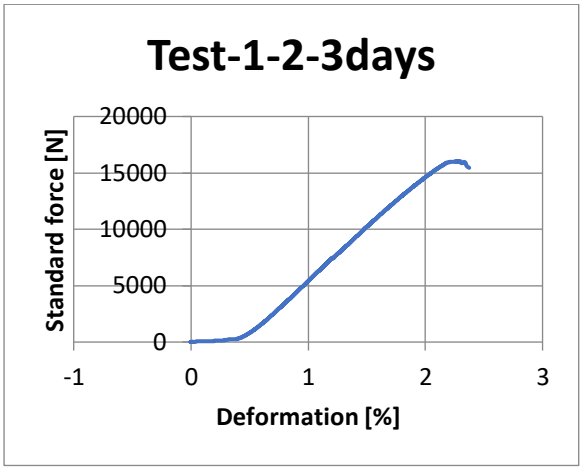

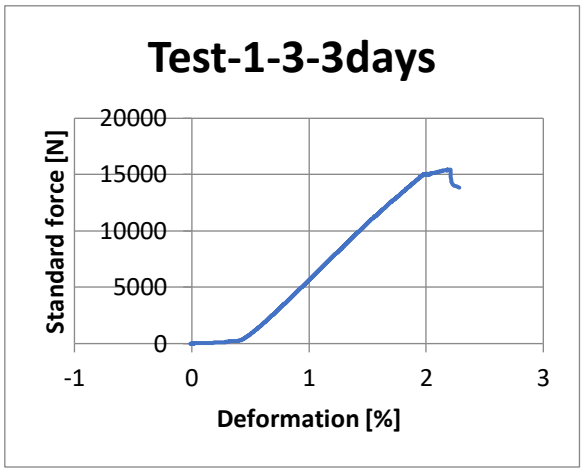

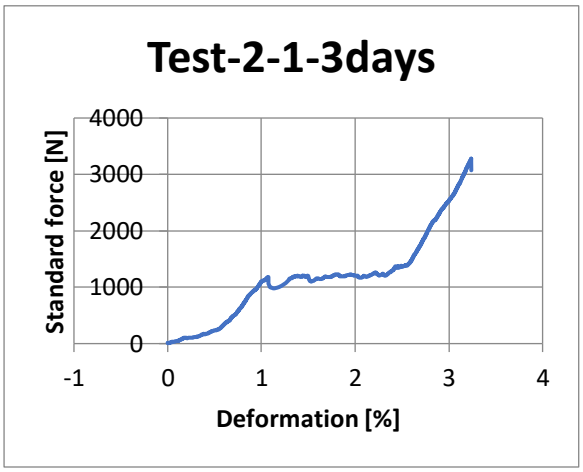

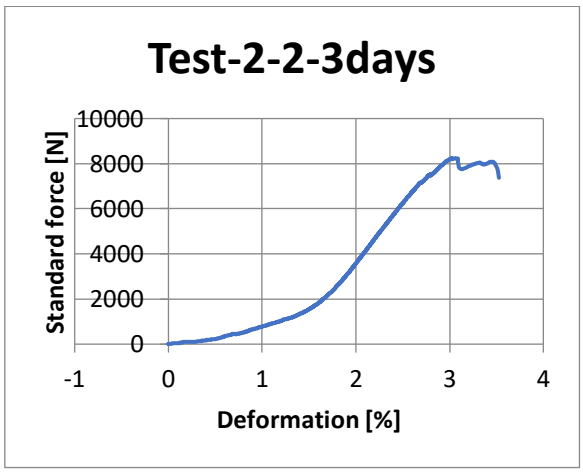

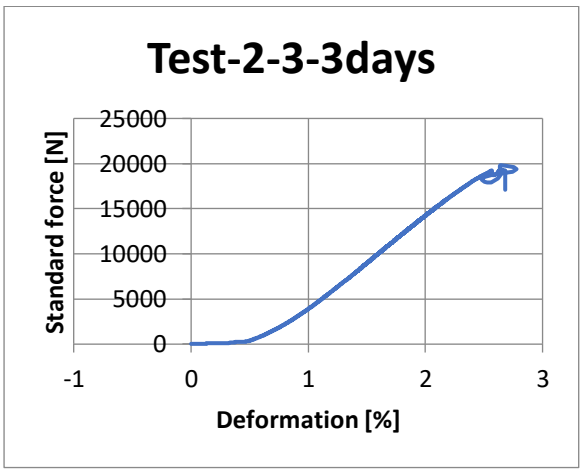

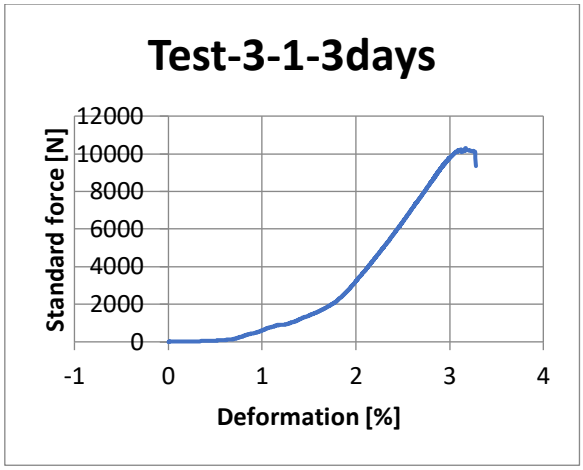
Test-3-1-3days
Standard force [N]
12000
10000
8000
6000
4000
2000
0
-1
0
1
2
3
4
Deformation [%]

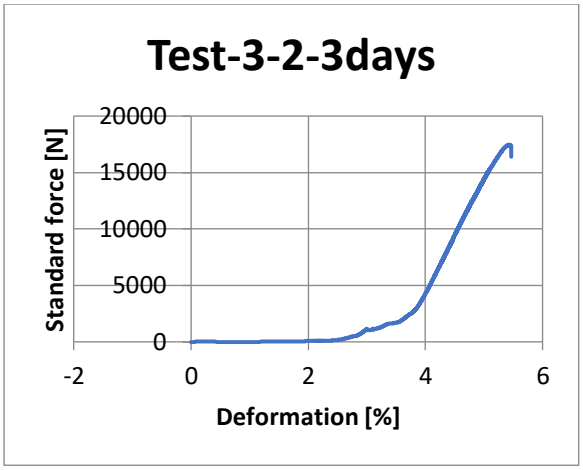
Test-3-2-3days
Standard force [N]
20000
15000
10000
5000
0
-2
0
2
4
6
Deformation [%]

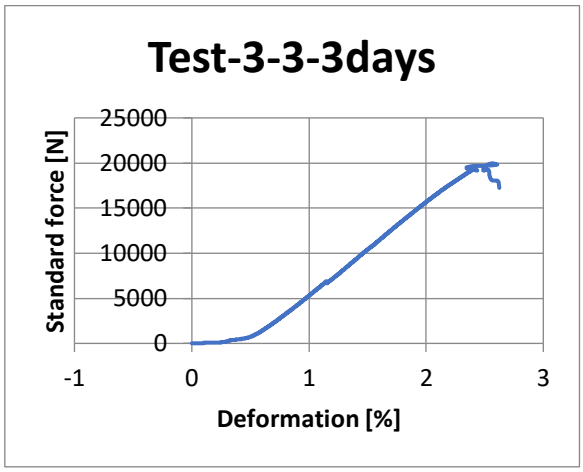
Test-3-3-3days
Standard force [N]
25000
20000
15000
10000
5000
0
-1
0
1
2
3
Deformation [%]

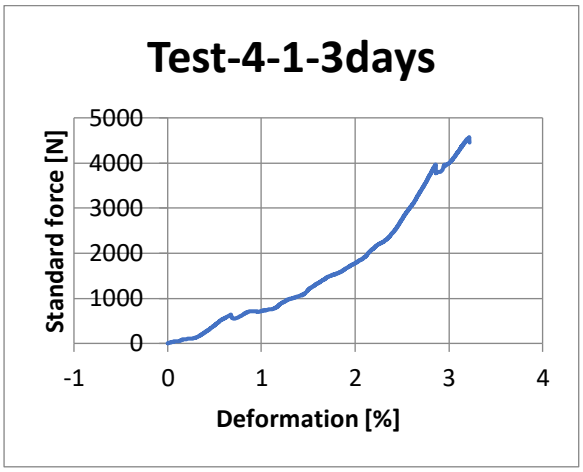
Test-4-1-3days
Standard force [N]
5000
4000
3000
2000
1000
0
-1
0
1
2
3
4
Deformation [%]

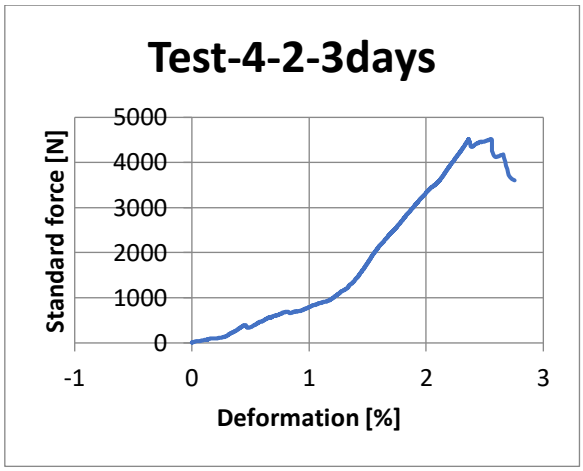
Test-4-2-3days
Standard force [N]
5000
4000
3000
2000
1000
0
-1
0
1
2
3
Deformation [%]

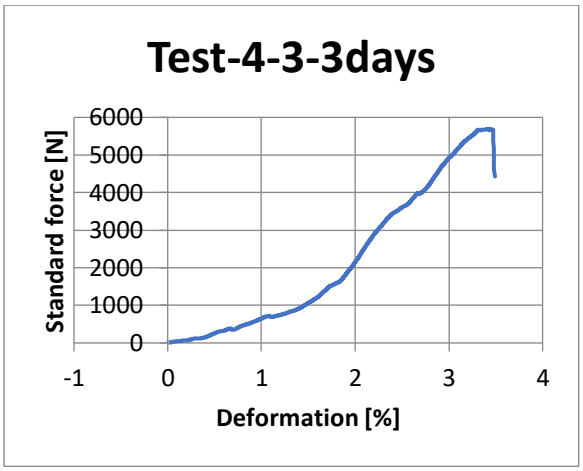
Test-4-3-3days
Standard force [N]
6000
5000
4000
3000
2000
1000
0
-1
0
1
2
3
4
Deformation [%]

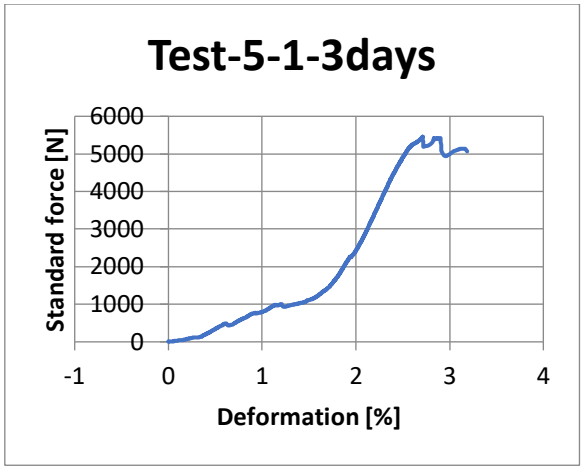
Test-5-1-3days
Standard force [N]
6000
5000
4000
3000
2000
1000
0
-1
0
1
2
3
4
Deformation [%]

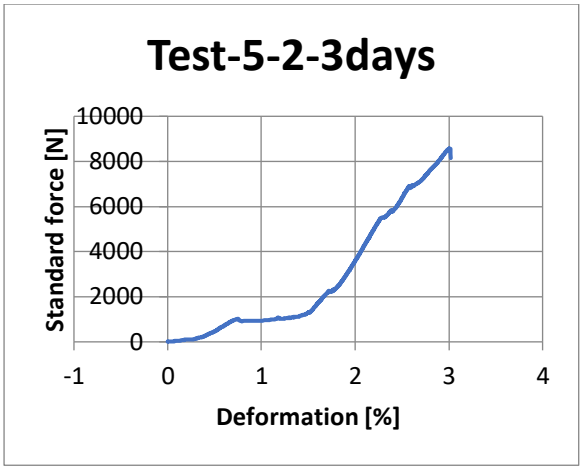
Test-5-2-3days
Standard force [N]
10000
8000
6000
4000
2000
0
-1
0
1
2
3
4
Deformation [%]

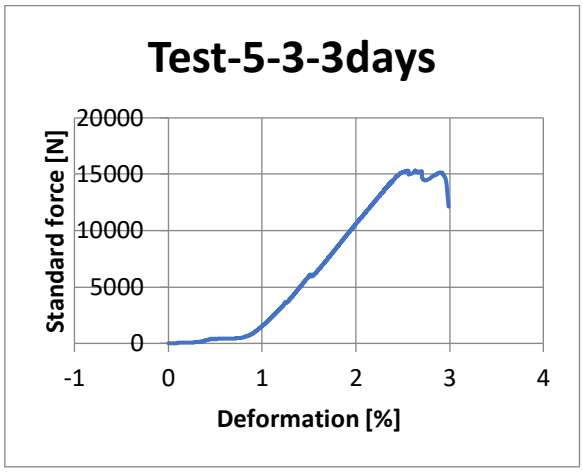
Test-5-3-3days
Standard force [N]
20000
15000
10000
5000
0
-1
0
1
2
3
4
Deformation [%]

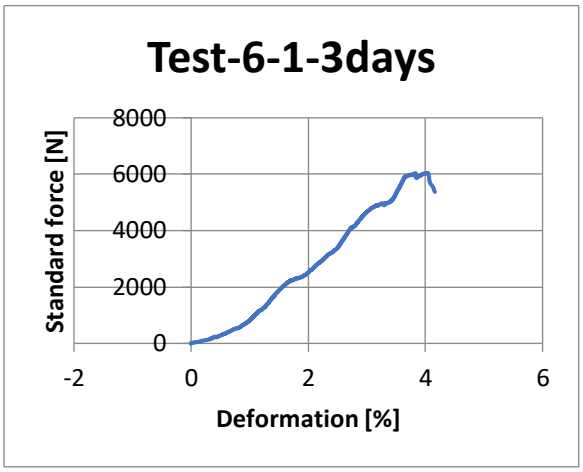
Test-6-1-3days
Standard force [N]
8000
6000
4000
2000
0
-2
0
2
4
6
Deformation [%]

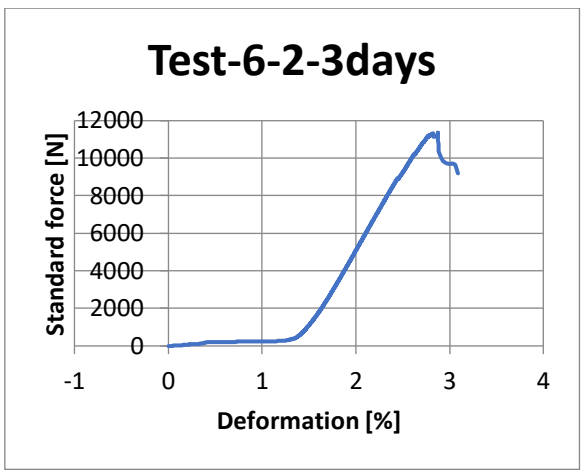
Test-6-2-3days
Standard force [N]
12000
10000
8000
6000
4000
2000
0
-1
0
1
2
3
4
Deformation [%]

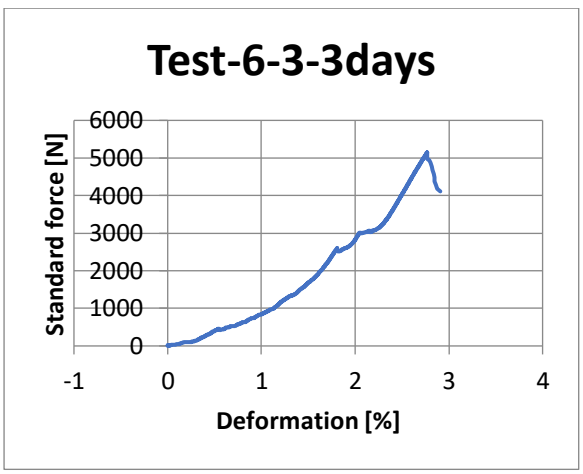
Test-6-3-3days
Standard force [N]
6000
5000
4000
3000
2000
1000
0
-1
0
1
2
3
4
Deformation [%]

Test batch for compressive strength on neat GP 1 and 7 days:

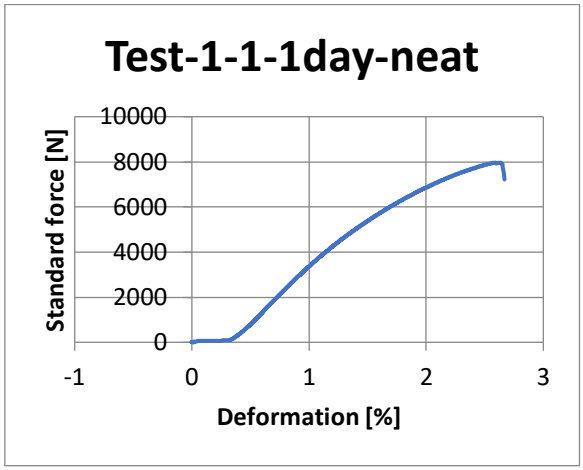

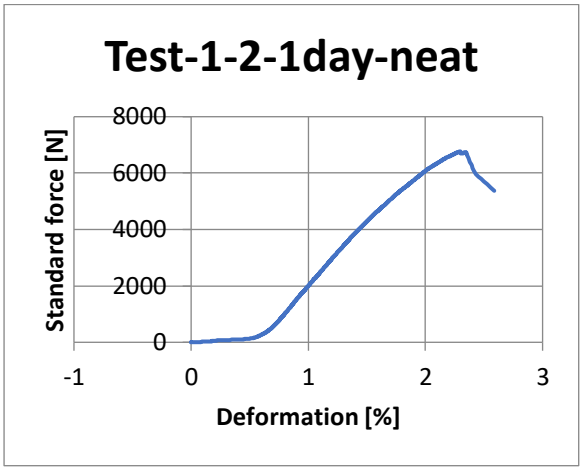

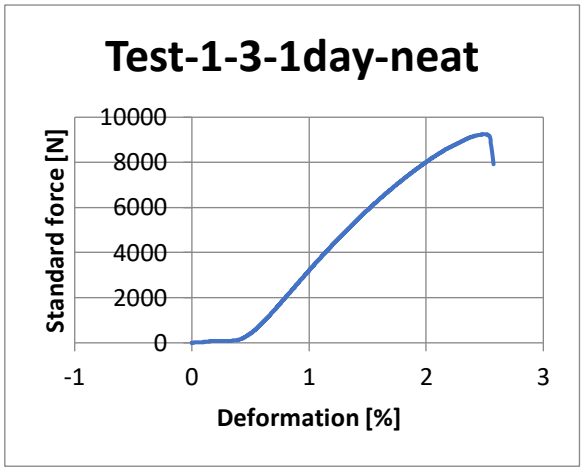

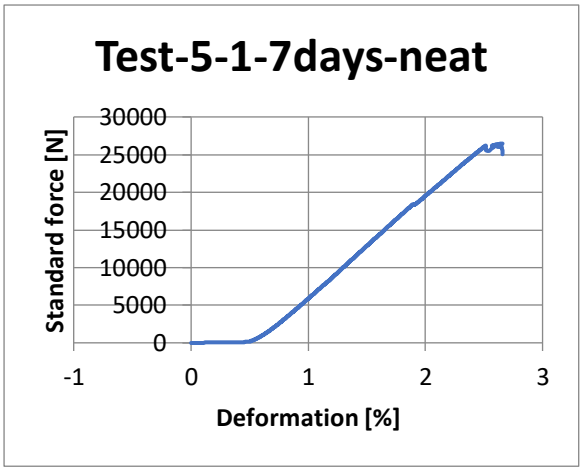

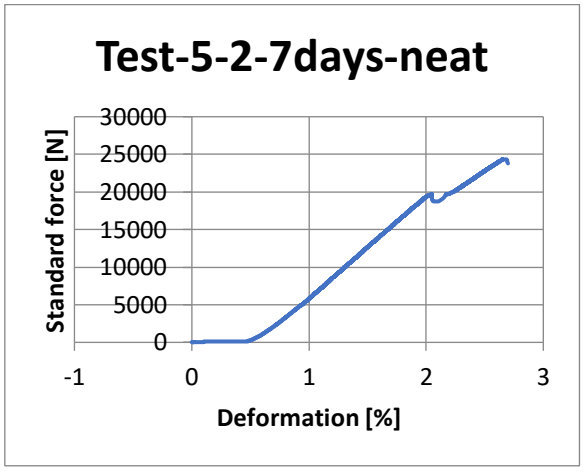

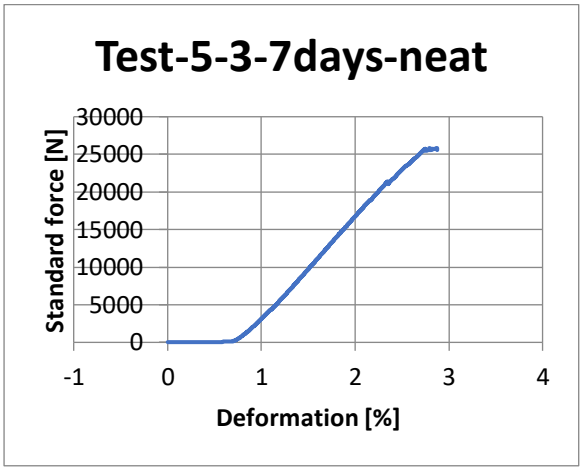

Test batch for compressive strength on GP + nanoparticles 1 day:

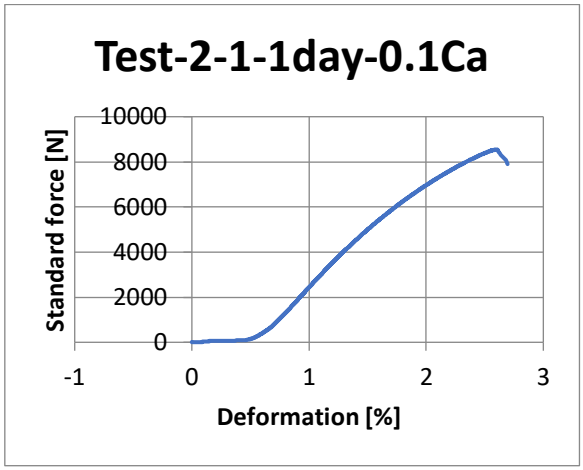

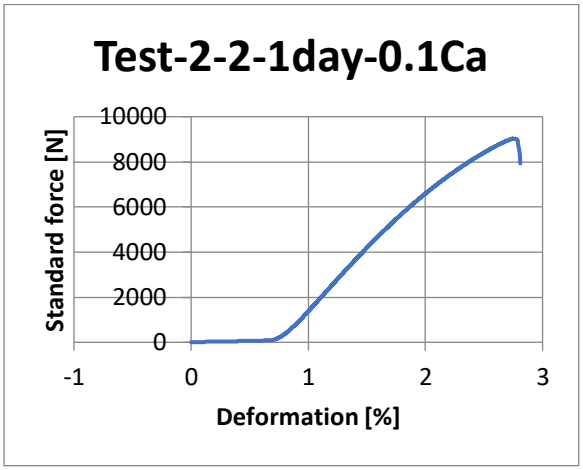

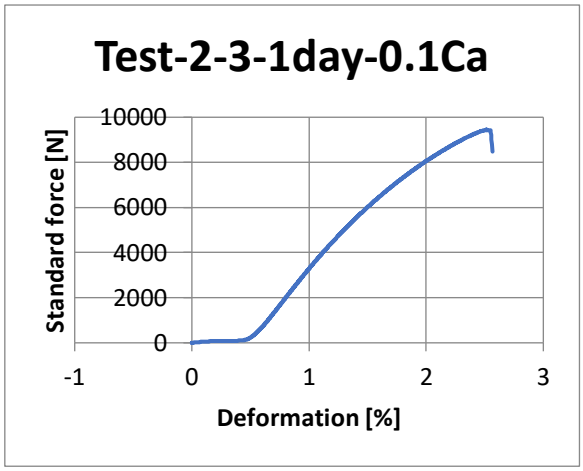

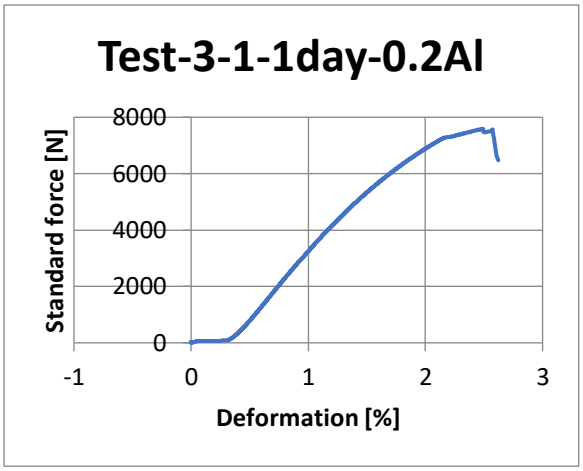

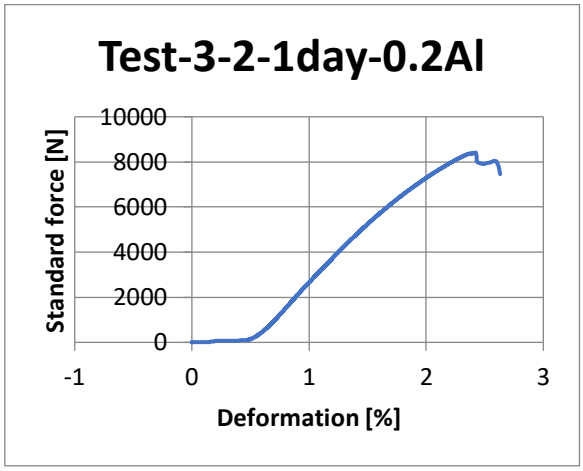

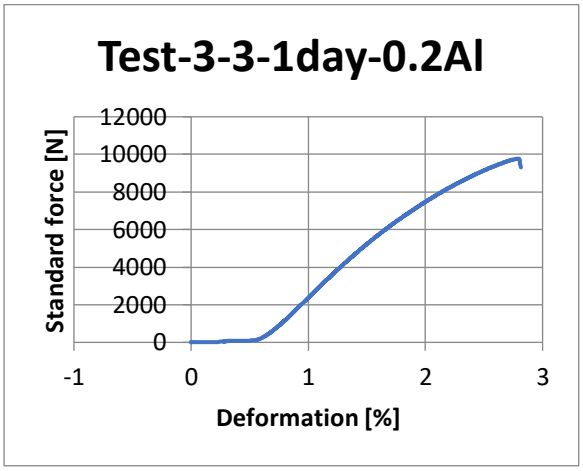

Test batch for compressive strength on GP + $CaCO_3$ nanoparticles 3 days:

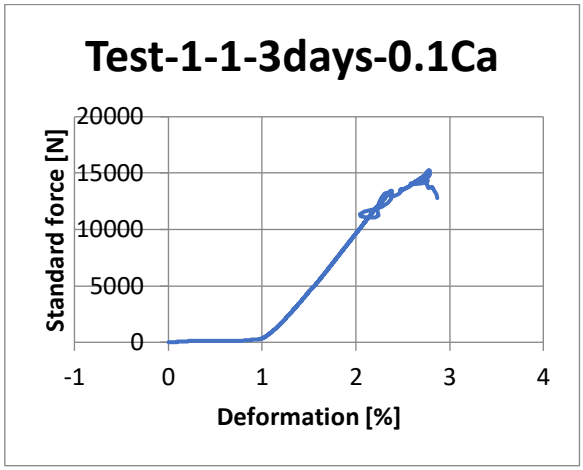

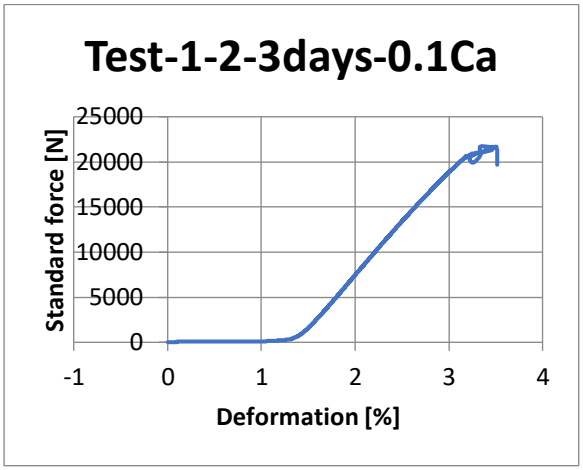

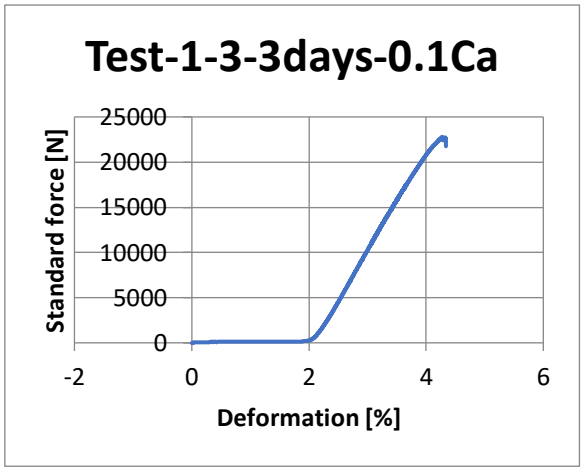

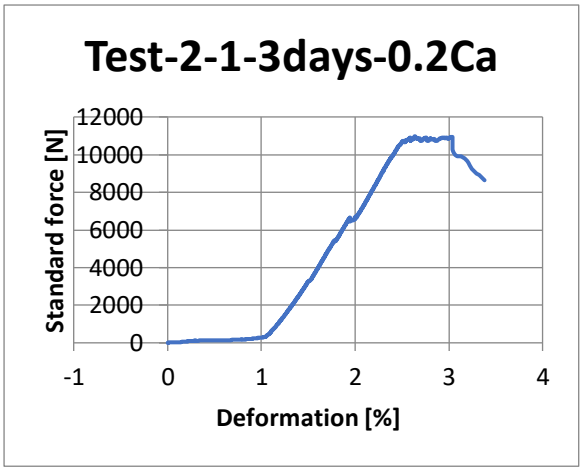

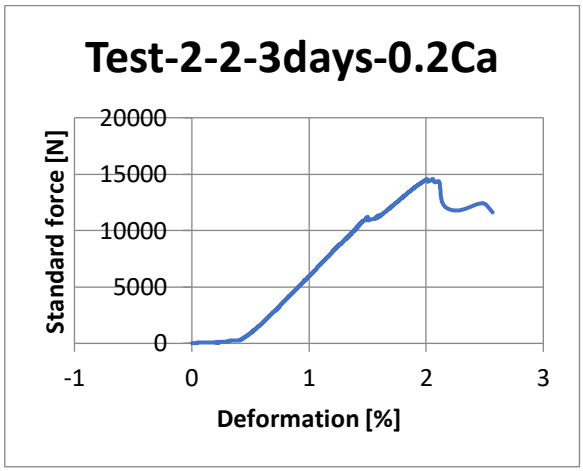

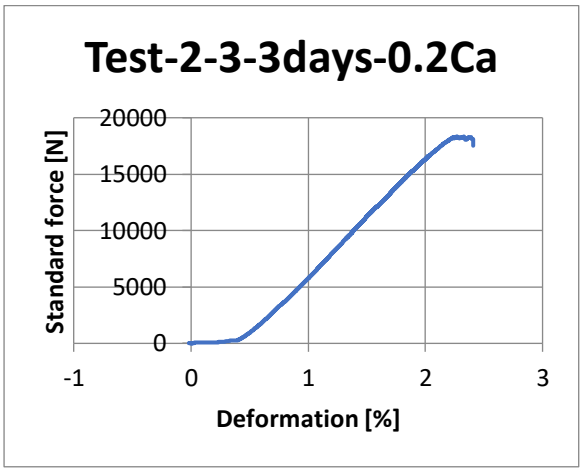

Test batch for compressive strength on GP + Al_2O_3 nanoparticles 3 days:

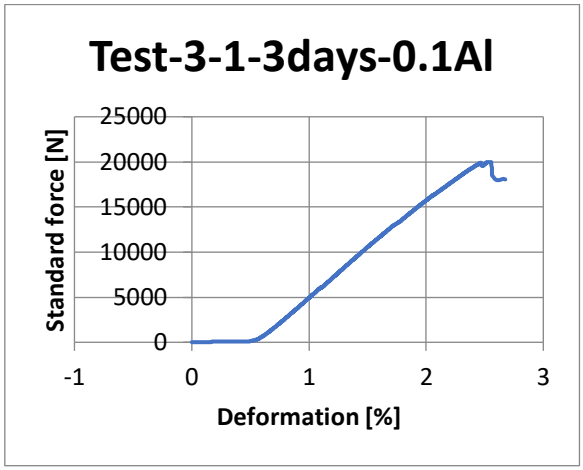

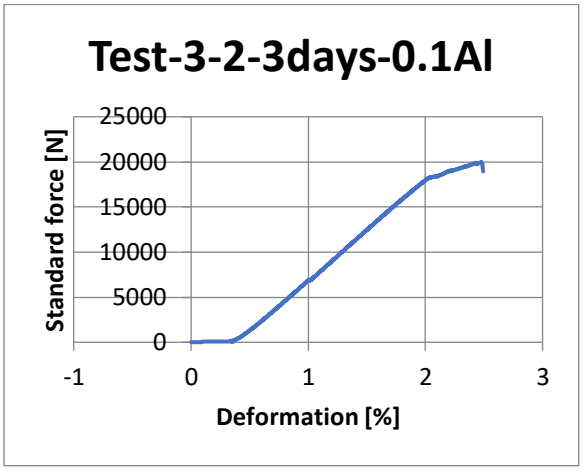

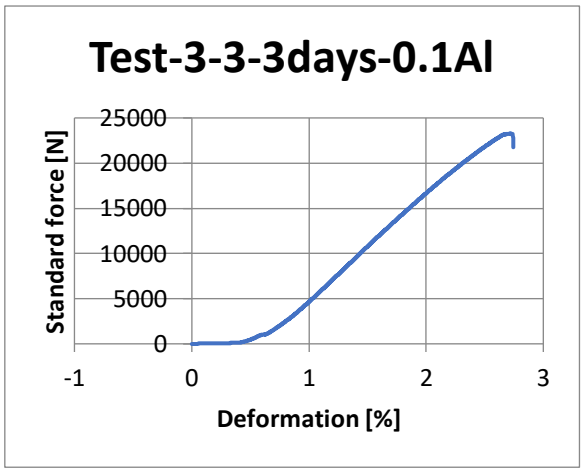

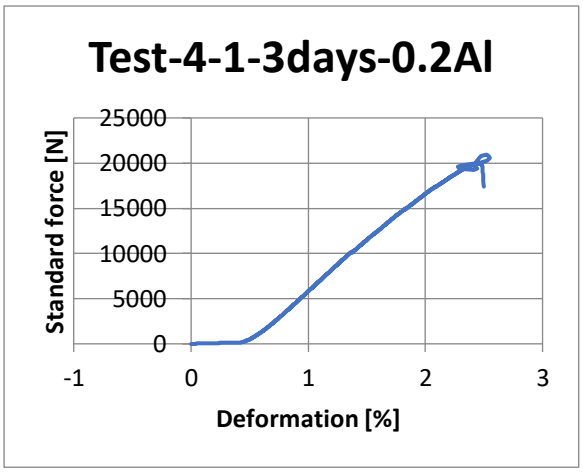

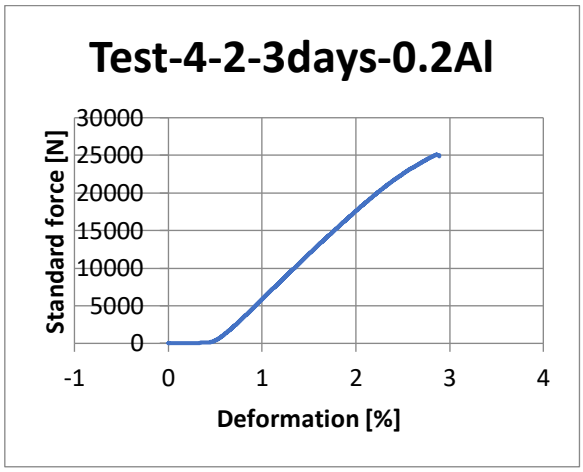

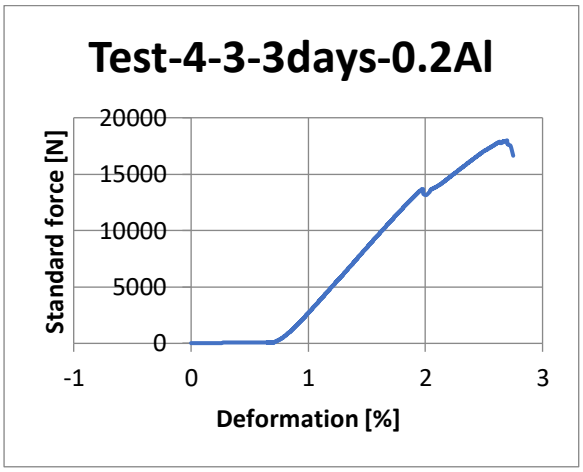

Test batch for compressive strength on GP + nanoparticles 7 days:

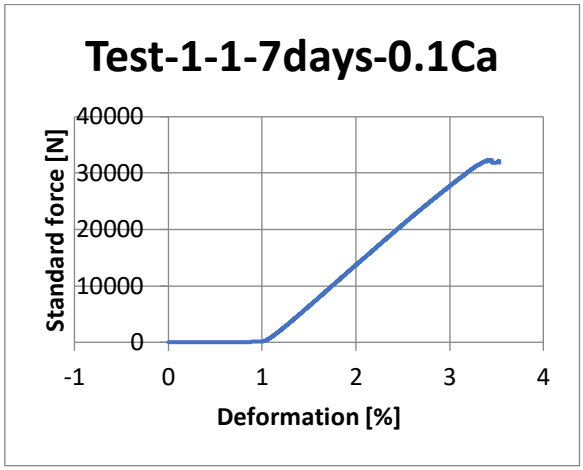

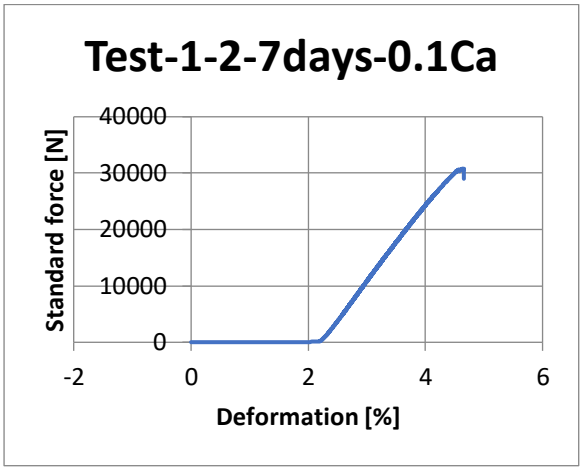

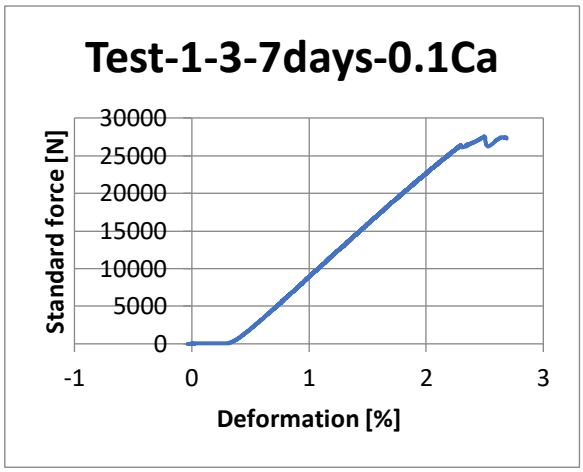

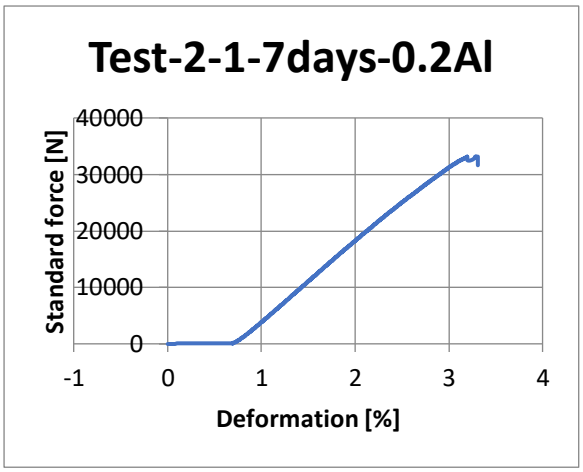

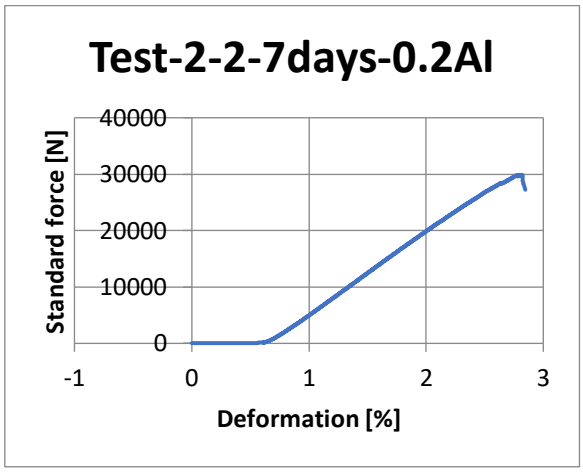

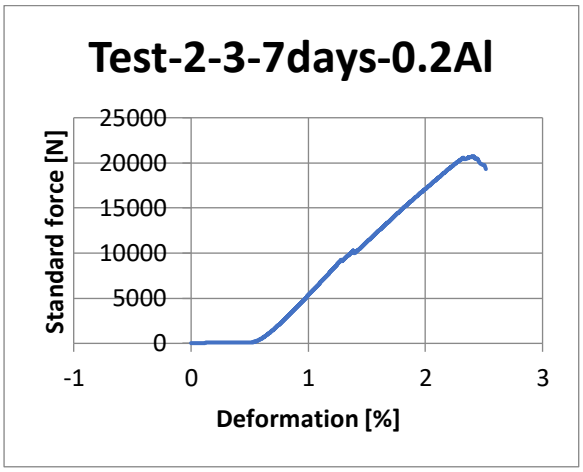

Test batch for compressive strength on G-class cement 1, 3, and 7 days:

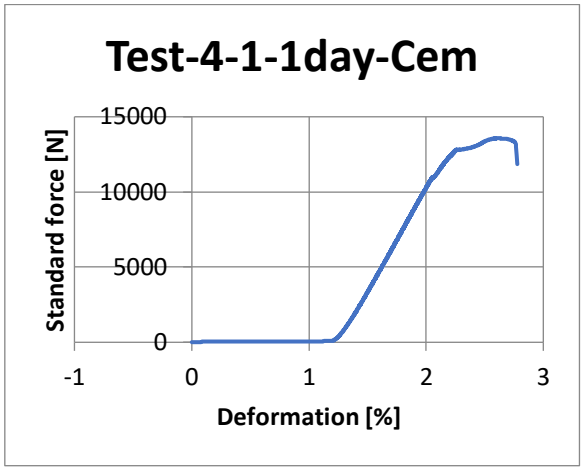

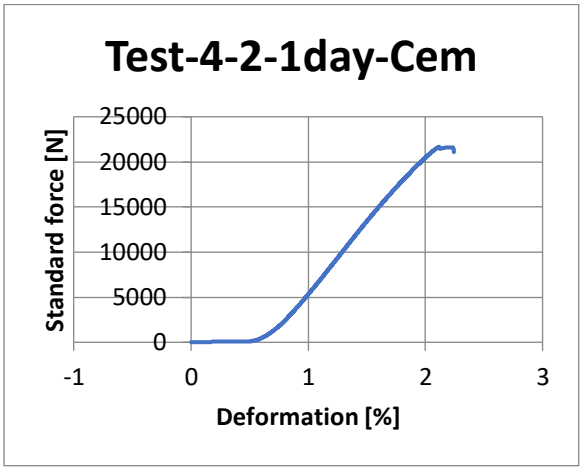

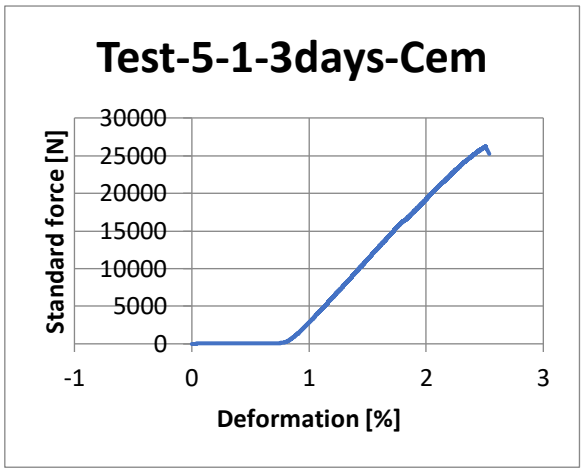

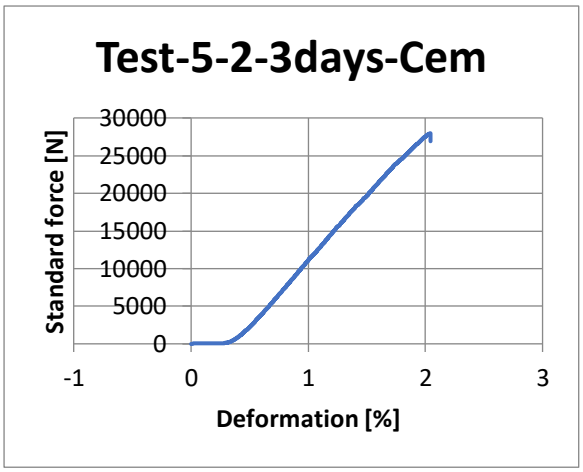

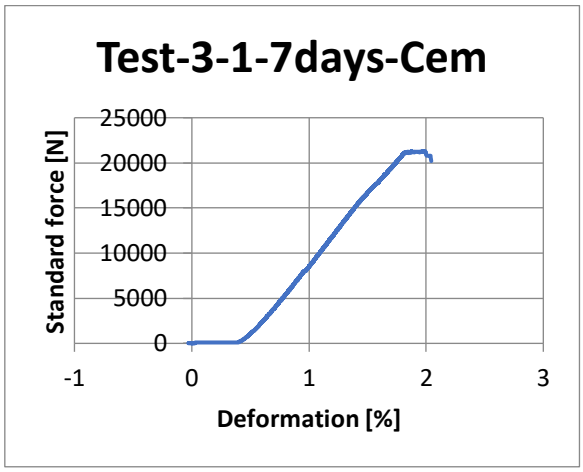

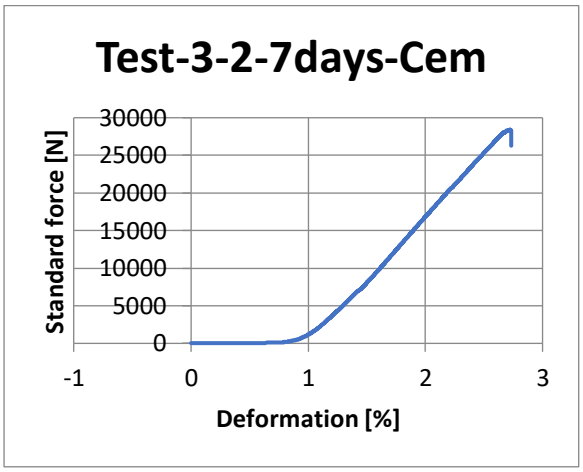

APPENDIX B: NON-DESTRUCTIVE MEASUREMENTS

Test batch for non-destructive 1-day samples:

Plug #	Mass, g	OD, mm	Length, mm	Volume, m^3	Density, kg/m^3	Sonic, µs	Velocity, m/s	(M), GPa
Neat GP 1-1	93.3	33	60	5.13179E-05	1818	36.3	1653	5.0
Neat GP 1-2	92	33	60	5.13179E-05	1793	38.2	1571	4.4
Neat GP 1-3	92.5	33	60	5.13179E-05	1802	38.9	1542	4.3
GP+$CaCO_3$ 2-1	91.1	33	60	5.13179E-05	1775	36.5	1644	4.8
GP+$CaCO_3$ 2-2	91.9	33	60	5.13179E-05	1791	37.7	1592	4.5
GP+$CaCO_3$ 2-3	93.4	33	60	5.13179E-05	1820	36.9	1626	4.8
GP+Al_2O_3 3-1	93.1	33	60	5.13179E-05	1814	37	1622	4.8
GP+Al_2O_3 3-2	95.56	33	61	5.21732E-05	1832	37	1649	5.0
GP+Al_2O_3 3-3	92.03	33	60	5.13179E-05	1793	37.8	1587	4.5
G-class 4-1	102.3	33	66	5.64497E-05	1812	23.2	2845	14.7
G-class 4-2	102.95	33	66	5.64497E-05	1824	23.8	2773	14.0

Test batch for non-destructive 3-days samples:

Plug #	Mass, g	OD, mm	Length, mm	Volume, m^3	Density, kg/m^3	Sonic, µs	Velocity, m/s	(M), GPa
0.1 $CaCO_3$ 1-1	92.1	33	61	5.21732E-05	1765	30.1	2027	7.3
0.1 $CaCO_3$ 1-2	91.8	33	60	5.13179E-05	1789	29.6	2027	7.4
0.1 $CaCO_3$ 1-3	91.99	33	60	5.13179E-05	1793	28.3	2120	8.1
0.2 $CaCO_3$ 2-1	91	33	60	5.13179E-05	1773	30.7	1954	6.8
0.2 $CaCO_3$ 2-2	93.29	33	61	5.21732E-05	1788	29.6	2061	7.6
0.2 $CaCO_3$ 2-3	94.6	33	62	5.30285E-05	1784	29.9	2074	7.7
0.1 Al_2O_3 3-1	90.98	33	60	5.13179E-05	1773	28.7	2091	7.7
0.1 Al_2O_3 3-2	92.65	33	61	5.21732E-05	1776	29.5	2068	7.6
0.1 Al_2O_3 3-3	92.92	33	60	5.13179E-05	1811	26.5	2264	9.3
0.2 Al_2O_3 4-1	93.55	33	61	5.21732E-05	1793	29.1	2096	7.9
0.2 Al_2O_3 4-2	92.32	33	61	5.21732E-05	1769	30.2	2020	7.2
0.2 Al_2O_3 4-3	90	33	60	5.13179E-05	1754	30.2	1987	6.9

Test batch for non-destructive 7-days samples:

Plug #	Mass, g	OD, mm	Length, mm	Volume, m^3	Density, kg/m^3	Sonic, μs	Velocity, m/s	(M), GPa
Neat GP 5-1	90.52	33	60	5.13179E-05	1764	25.9	2317	9.5
Neat GP 5-2	90.45	33	61.5	5.26009E-05	1720	28.2	2181	8.2
Neat GP 5-3	89.91	33	61	5.21732E-05	1723	27.3	2234	8.6
GP+$CaCO_3$ 1-1	90.75	33	61	5.21732E-05	1739	26.6	2293	9.1
GP+$CaCO_3$ 1-2	90.09	33	61.5	5.26009E-05	1713	28.1	2189	8.2
GP+$CaCO_3$ 1-3	90.21	33	62	5.30285E-05	1701	28.4	2183	8.1
GP+Al_2O_3 2-1	86.1	33	60	5.13179E-05	1678	27.3	2198	8.1
GP+Al_2O_3 2-2	90	33	61	5.21732E-05	1725	25.4	2402	9.9
GP+Al_2O_3 2-3	92.26	33	61	5.21732E-05	1768	26.5	2302	9.4
G-class 3-1	97.92	33	66	5.64497E-05	1735	21.4	3084	16.5
G-class 3-2	97.53	33	65	5.55944E-05	1754	20.3	3202	18.0

APPENDIX C: SEM images

Geopolymer with 0.1 g $CaCO_3$

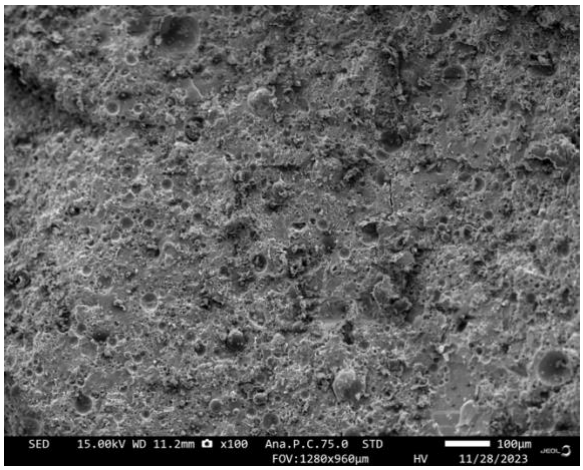

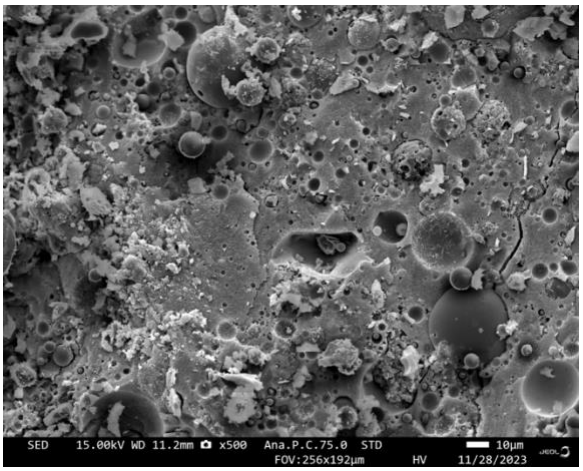

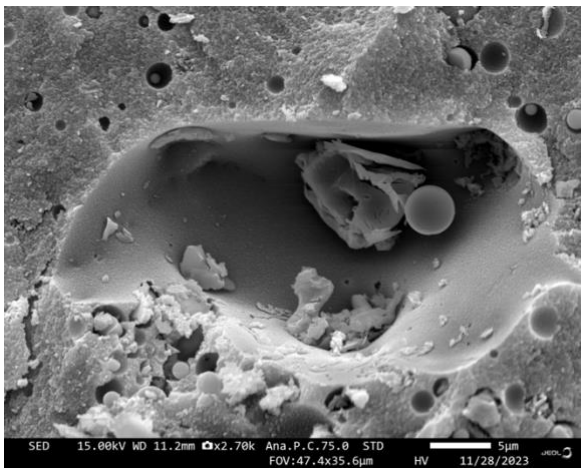

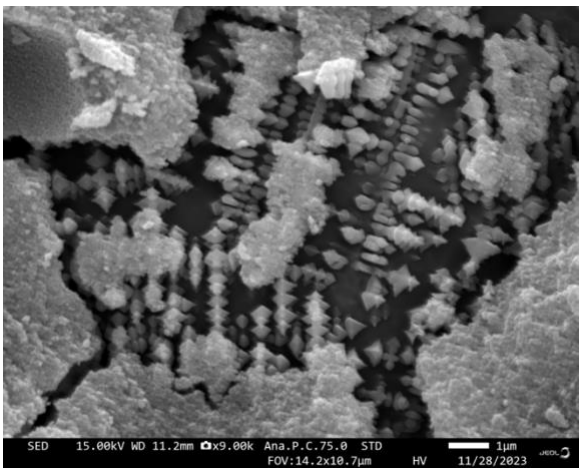

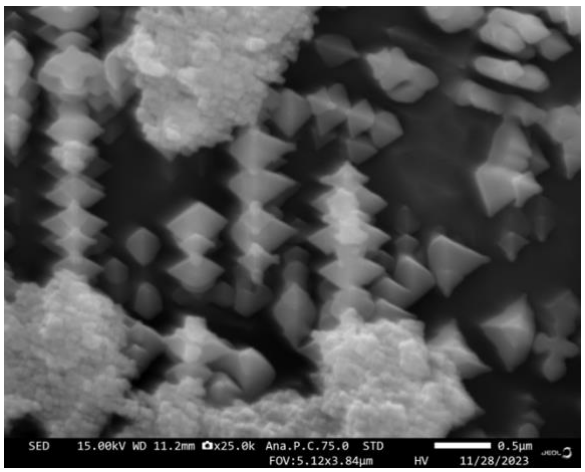

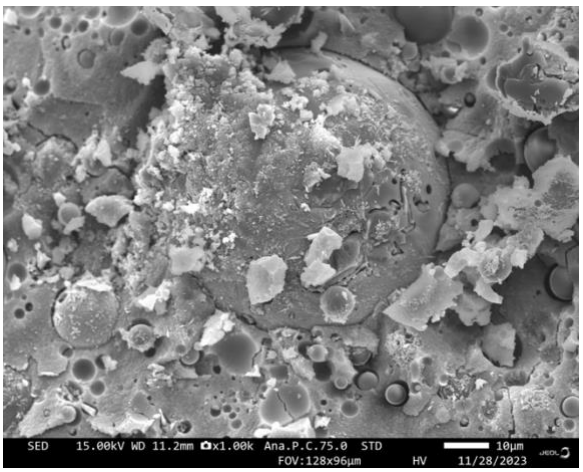

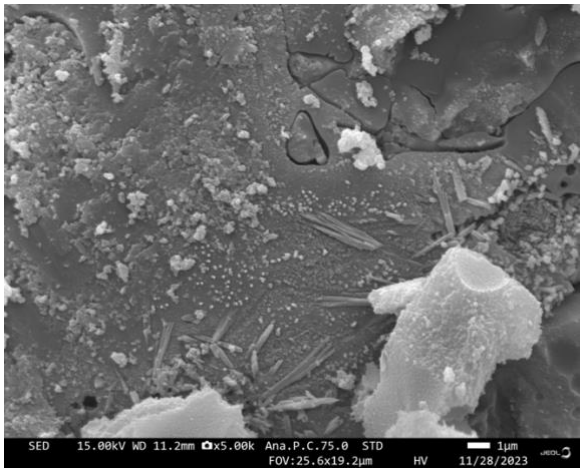
SED 15.00kV WD 11.2mm x5.00k Ana.P.C.75.0 STD
FOV:25.6x19.2µm HV 11/28/2023
1µm


SED 15.00kV WD 11.2mm x20.0k Ana.P.C.75.0 STD
FOV:6.40x4.80µm HV 11/28/2023
0.5µm

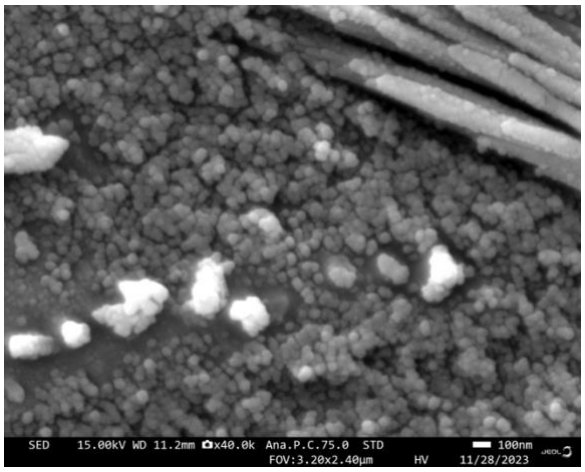
SED 15.00kV WD 11.2mm x40.0k Ana.P.C.75.0 STD
FOV:3.20x2.40µm HV 11/28/2023
100nm

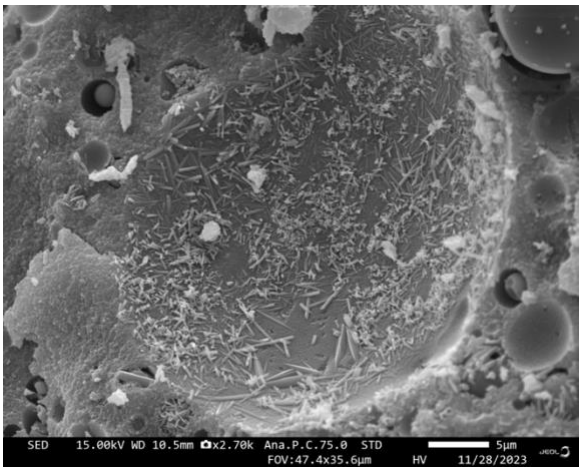
SED 15.00kV WD 10.5mm x2.70k Ana.P.C.75.0 STD
FOV:47.4x35.6µm HV 11/28/2023
5µm

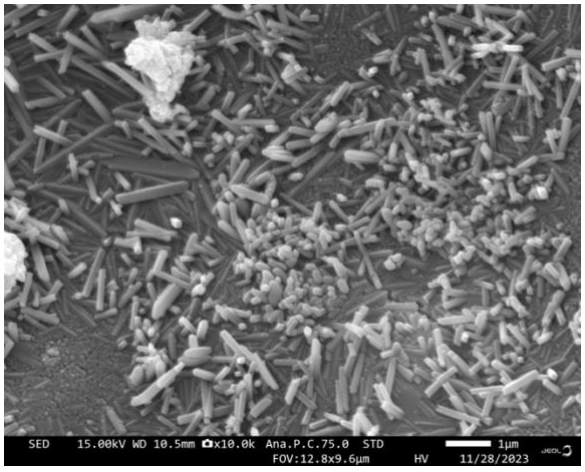
SED 15.00kV WD 10.5mm x10.0k Ana.P.C.75.0 STD
FOV:12.8x9.6µm HV 11/28/2023
1µm

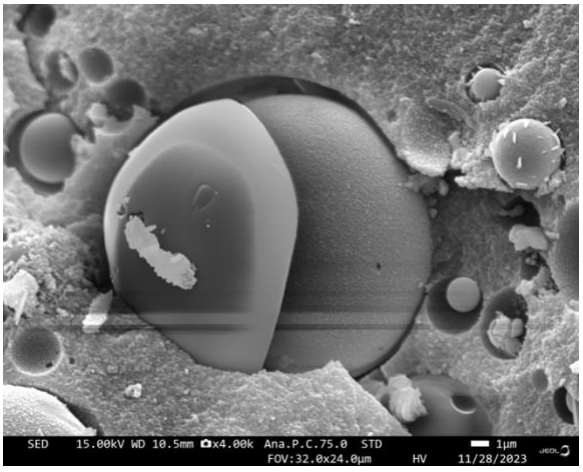
SED 15.00kV WD 10.5mm x4.00k Ana.P.C.75.0 STD
FOV:32.0x24.0µm HV 11/28/2023
1µm

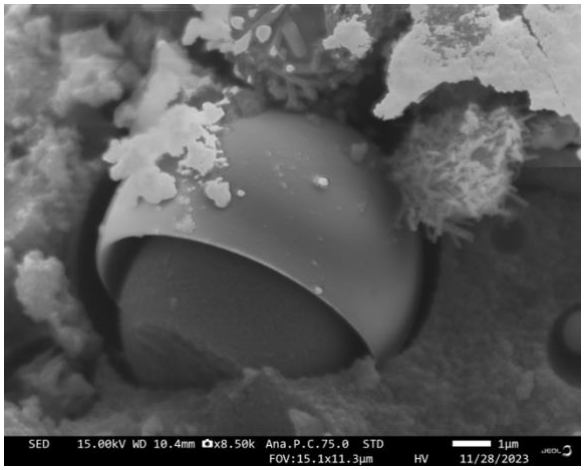
SED 15.00kV WD 10.4mm x8.50k Ana.P.C.75.0 STD
FOV:15.1x11.3µm HV 11/28/2023
1µm

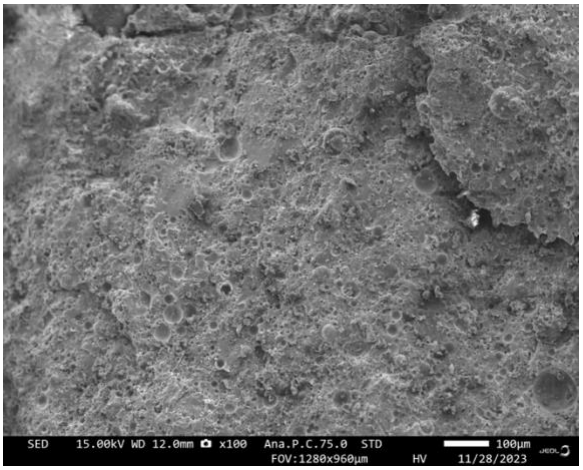
SED 15.00kV WD 12.0mm x100 Ana.P.C.75.0 STD
FOV:1280x960µm HV 11/28/2023
100µm

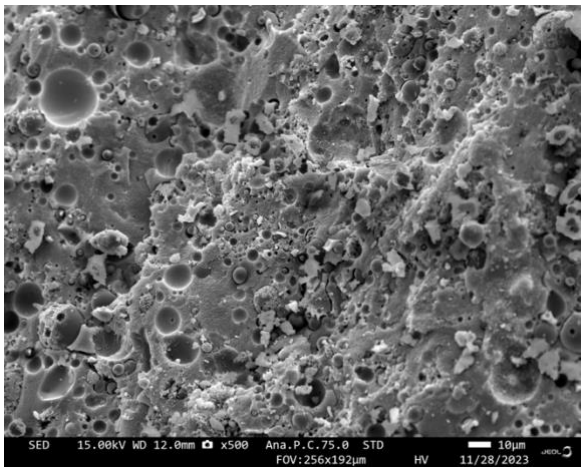
SED 15.00kV WD 12.0mm x500 Ana.P.C.75.0 STD
FOV:256x192µm HV 11/28/2023
10µm

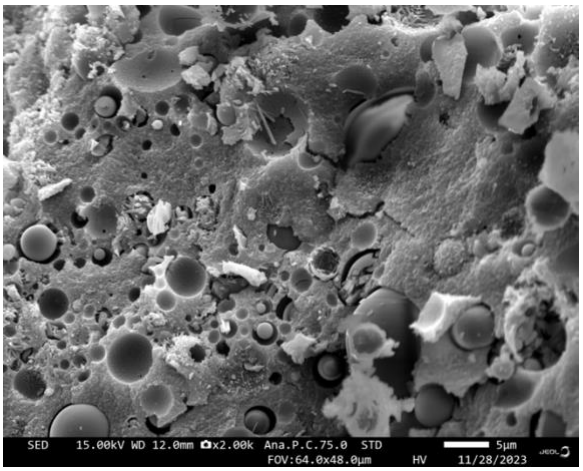
SED 15.00kV WD 12.0mm x2.00k Ana.P.C.75.0 STD
FOV:64.0x48.0µm HV 11/28/2023
5µm

Geopolymer with 0.2 g Al_2O_3

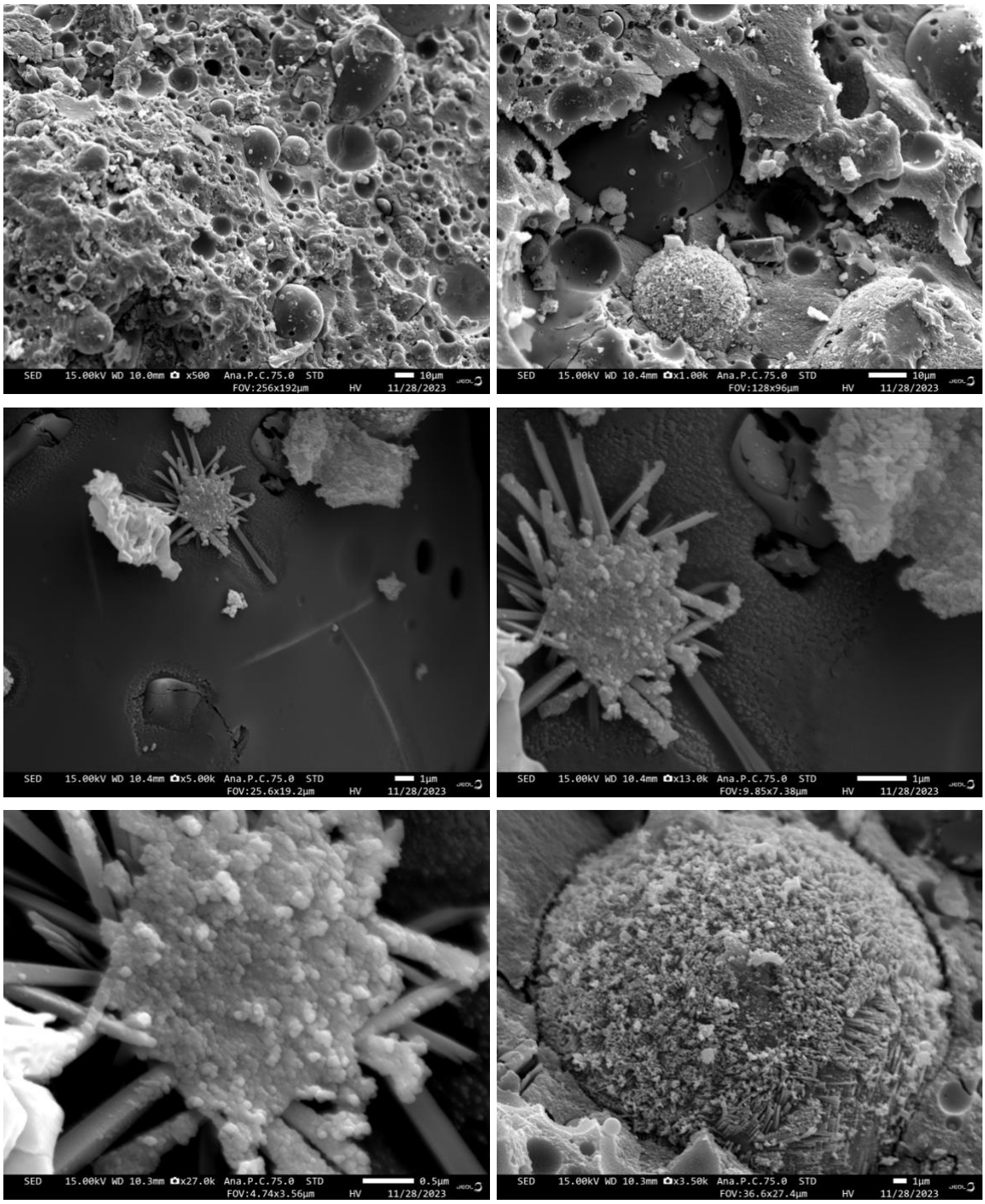

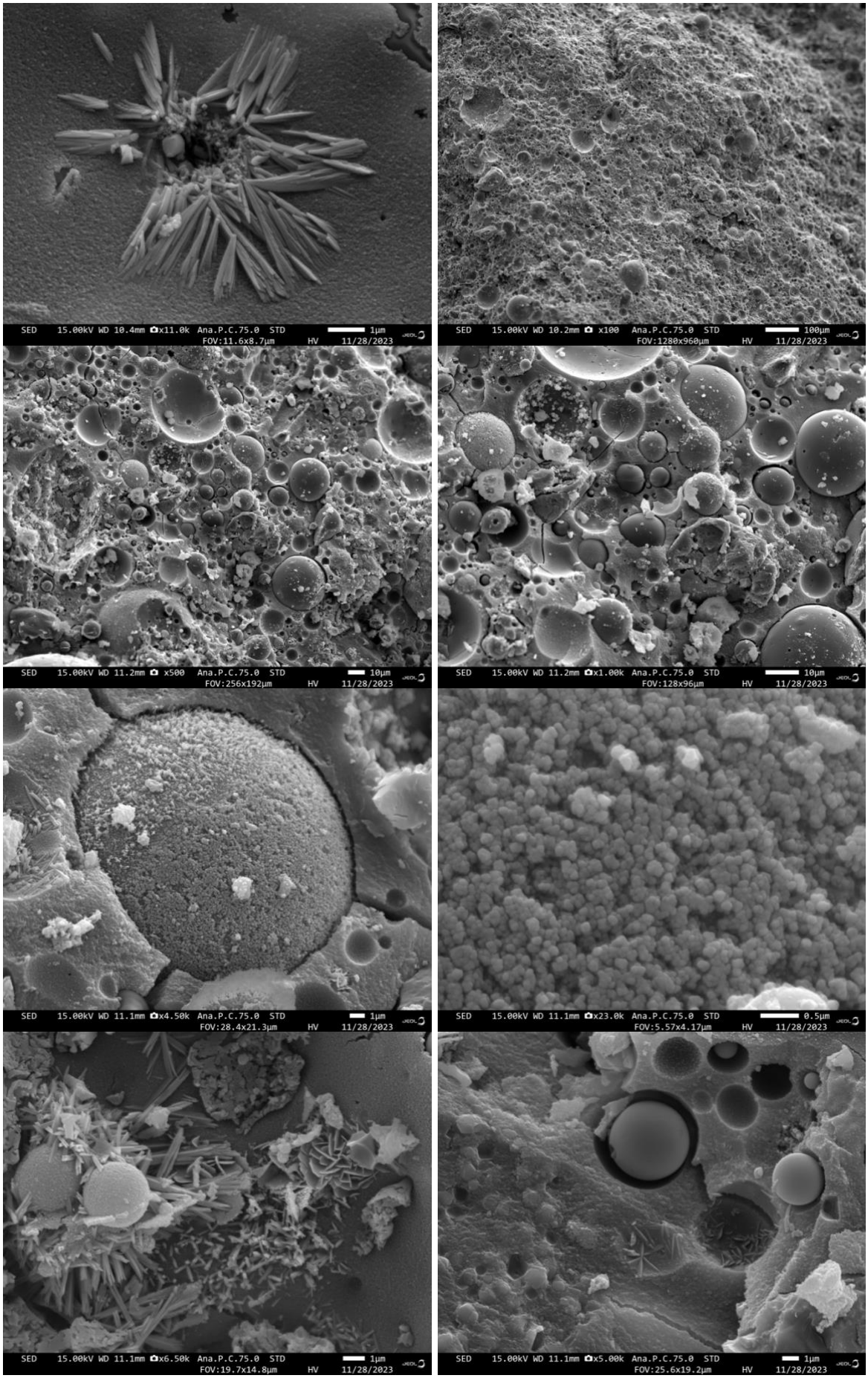
SED 15.00kV WD 10.4mm x11.0k Ana.P.C.75.0 STD 1µm
FOV:11.6x8.7µm HV 11/28/2023
SED 15.00kV WD 10.2mm x100 Ana.P.C.75.0 STD 100µm
FOV:1280x960µm HV 11/28/2023
SED 15.00kV WD 11.2mm x500 Ana.P.C.75.0 STD 10µm
FOV:256x192µm HV 11/28/2023
SED 15.00kV WD 11.2mm x1.00k Ana.P.C.75.0 STD 10µm
FOV:128x96µm HV 11/28/2023
SED 15.00kV WD 11.1mm x4.50k Ana.P.C.75.0 STD 1µm
FOV:28.4x21.3µm HV 11/28/2023
SED 15.00kV WD 11.1mm x23.0k Ana.P.C.75.0 STD 0.5µm
FOV:5.57x4.17µm HV 11/28/2023
SED 15.00kV WD 11.1mm x6.50k Ana.P.C.75.0 STD 1µm
FOV:19.7x14.8µm HV 11/28/2023
SED 15.00kV WD 11.1mm x5.00k Ana.P.C.75.0 STD 1µm
FOV:25.6x19.2µm HV 11/28/2023

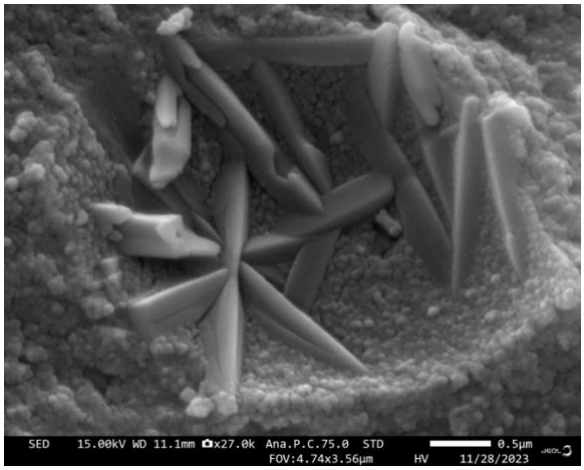
SED 15.00kV WD 11.1mm x27.0k Ana.P.C.75.0 STD 0.5µm
FOV:4.74x3.56µm HV 11/28/2023

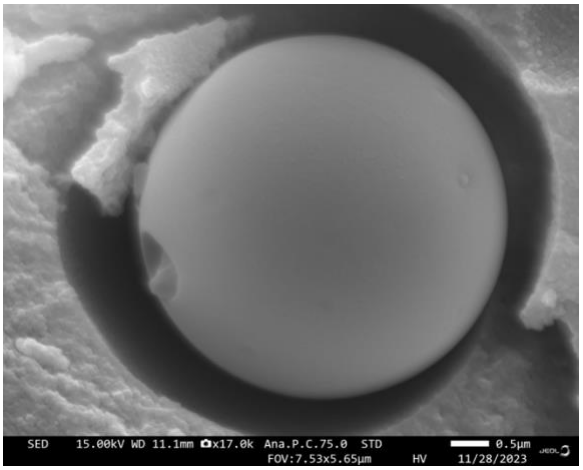
SED 15.00kV WD 11.1mm x17.0k Ana.P.C.75.0 STD 0.5µm
FOV:7.53x5.65µm HV 11/28/2023

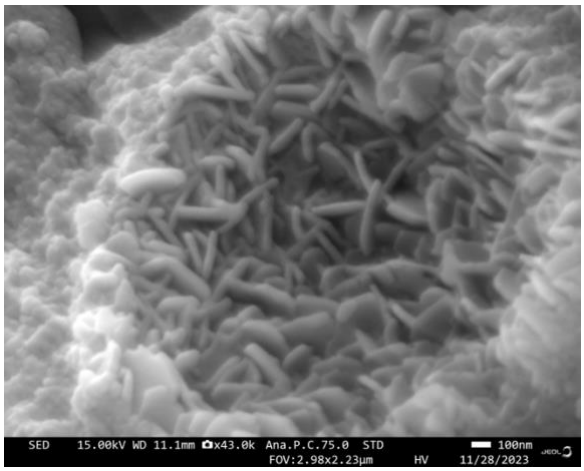
SED 15.00kV WD 11.1mm x43.0k Ana.P.C.75.0 STD 100nm
FOV:2.98x2.23µm HV 11/28/2023

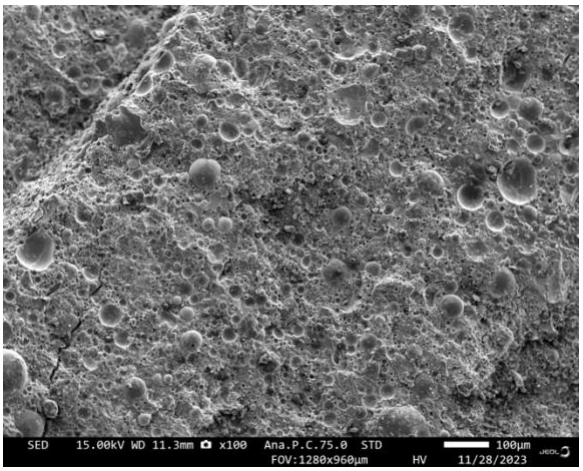
SED 15.00kV WD 11.3mm x100 Ana.P.C.75.0 STD 100µm
FOV:1280x960µm HV 11/28/2023

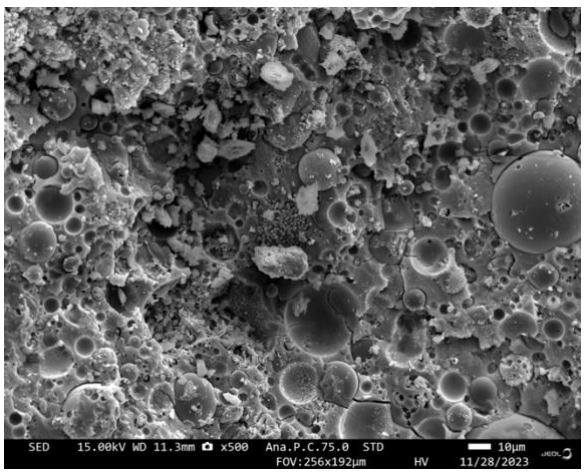
SED 15.00kV WD 11.3mm x500 Ana.P.C.75.0 STD 10µm
FOV:256x192µm HV 11/28/2023


SED 15.00kV WD 11.3mm x2.00k Ana.P.C.75.0 STD 5µm
FOV:64.0x48.0µm HV 11/28/2023

Neat geopolymer

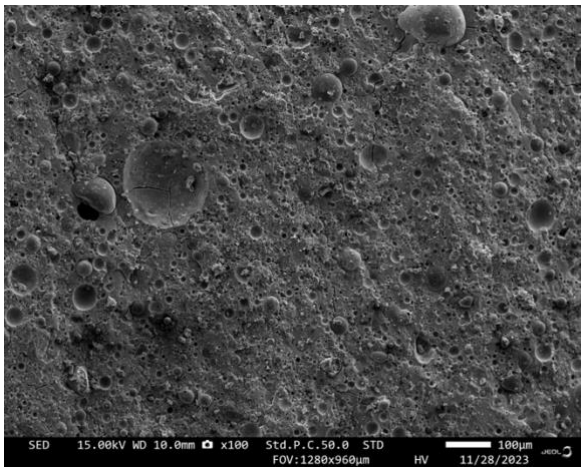

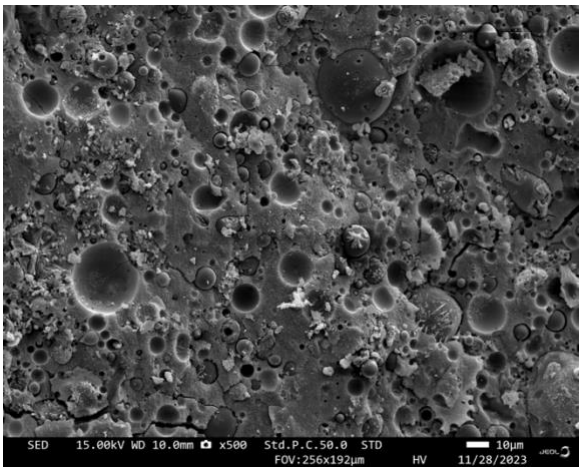

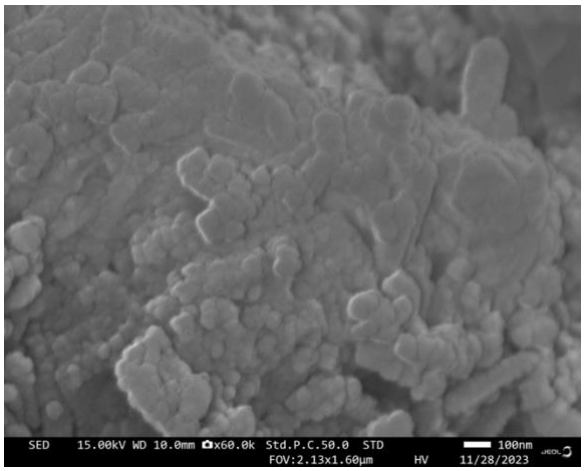

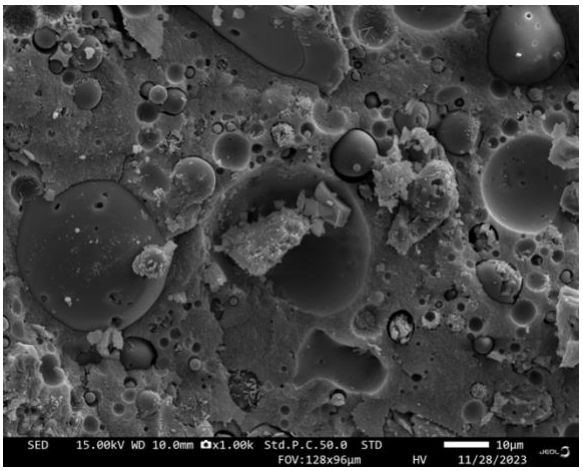

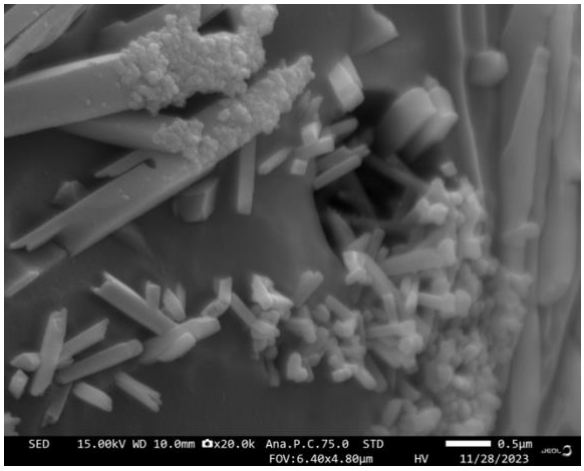

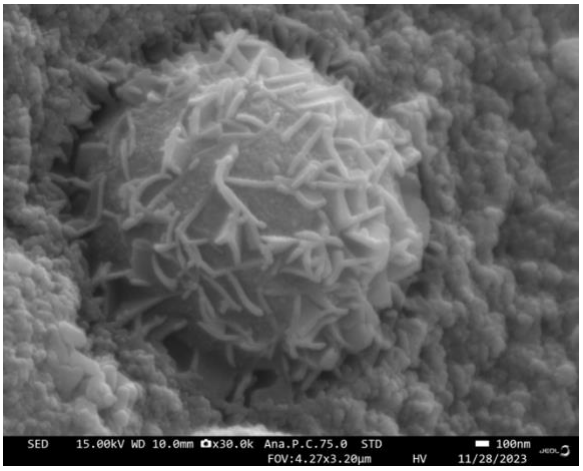

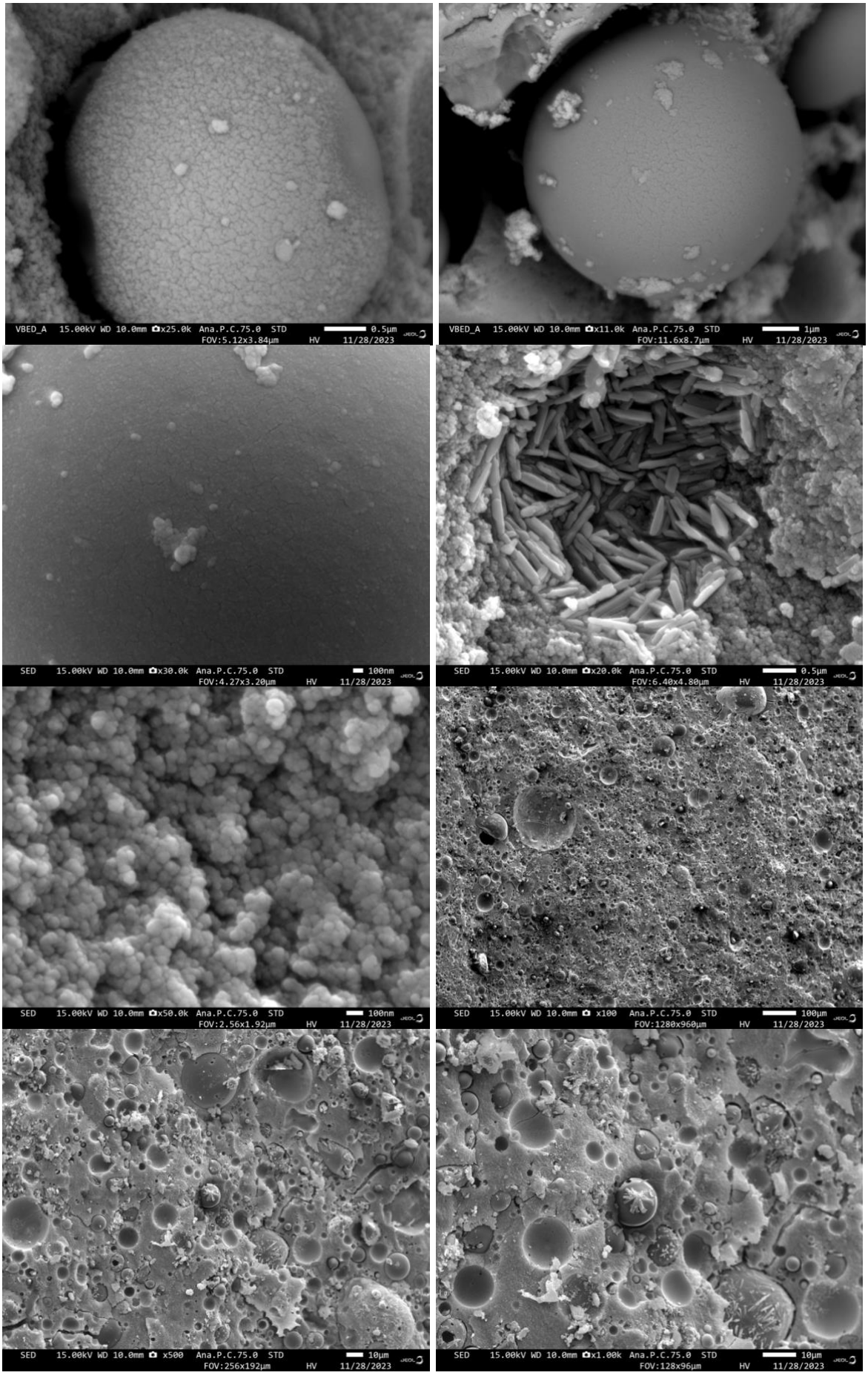
VBED_A 15.00kV WD 10.0mm x25.0k Ana.P.C.75.0 STD 0.5µm
FOV:5.12x3.84µm HV 11/28/2023
VBED_A 15.00kV WD 10.0mm x11.0k Ana.P.C.75.0 STD 1µm
FOV:11.6x8.7µm HV 11/28/2023
SED 15.00kV WD 10.0mm x30.0k Ana.P.C.75.0 STD 100nm
FOV:4.27x3.20µm HV 11/28/2023
SED 15.00kV WD 10.0mm x20.0k Ana.P.C.75.0 STD 0.5µm
FOV:6.40x4.80µm HV 11/28/2023
SED 15.00kV WD 10.0mm x50.0k Ana.P.C.75.0 STD 100nm
FOV:2.56x1.92µm HV 11/28/2023
SED 15.00kV WD 10.0mm x100 Ana.P.C.75.0 STD 100µm
FOV:1280x960µm HV 11/28/2023
SED 15.00kV WD 10.0mm x500 Ana.P.C.75.0 STD 10µm
FOV:256x192µm HV 11/28/2023
SED 15.00kV WD 10.0mm x1.00k Ana.P.C.75.0 STD 10µm
FOV:128x96µm HV 11/28/2023

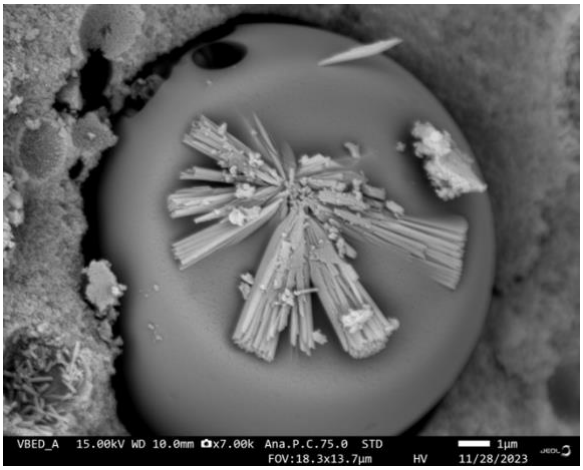
VBED_A 15.00kV WD 10.0mm x7.00k Ana.P.C.75.0 STD
FOV:18.3x13.7µm HV 11/28/2023
1µm

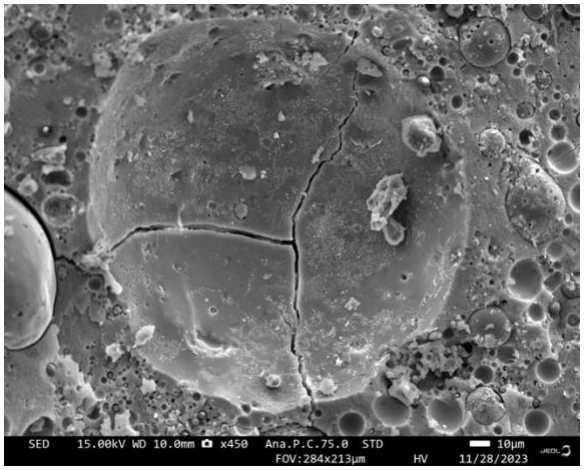
SED 15.00kV WD 10.0mm x450 Ana.P.C.75.0 STD
FOV:284x213µm HV 11/28/2023
10µm

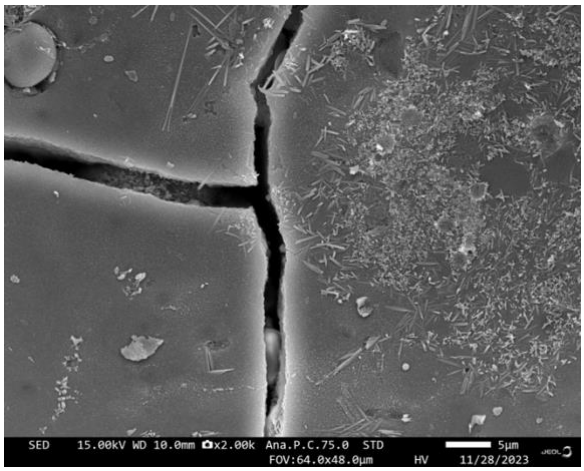
SED 15.00kV WD 10.0mm x2.00k Ana.P.C.75.0 STD
FOV:64.0x48.0µm HV 11/28/2023
5µm

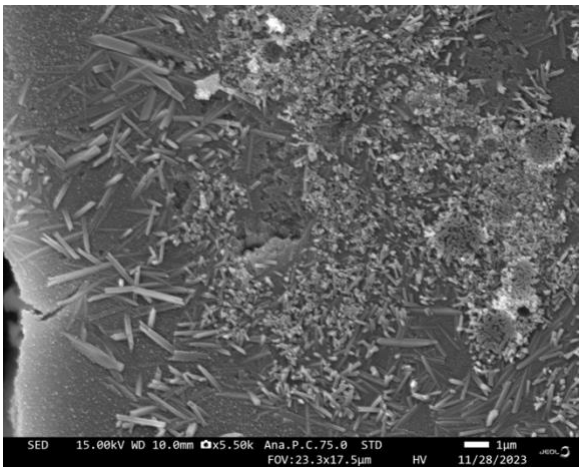
SED 15.00kV WD 10.0mm x5.50k Ana.P.C.75.0 STD
FOV:23.3x17.5µm HV 11/28/2023
1µm


VBED_A 15.00kV WD 10.0mm x10.0k Ana.P.C.75.0 STD
FOV:12.8x9.6µm HV 11/28/2023
1µm

Geopolymer with 0.1 g $CaCO_3$

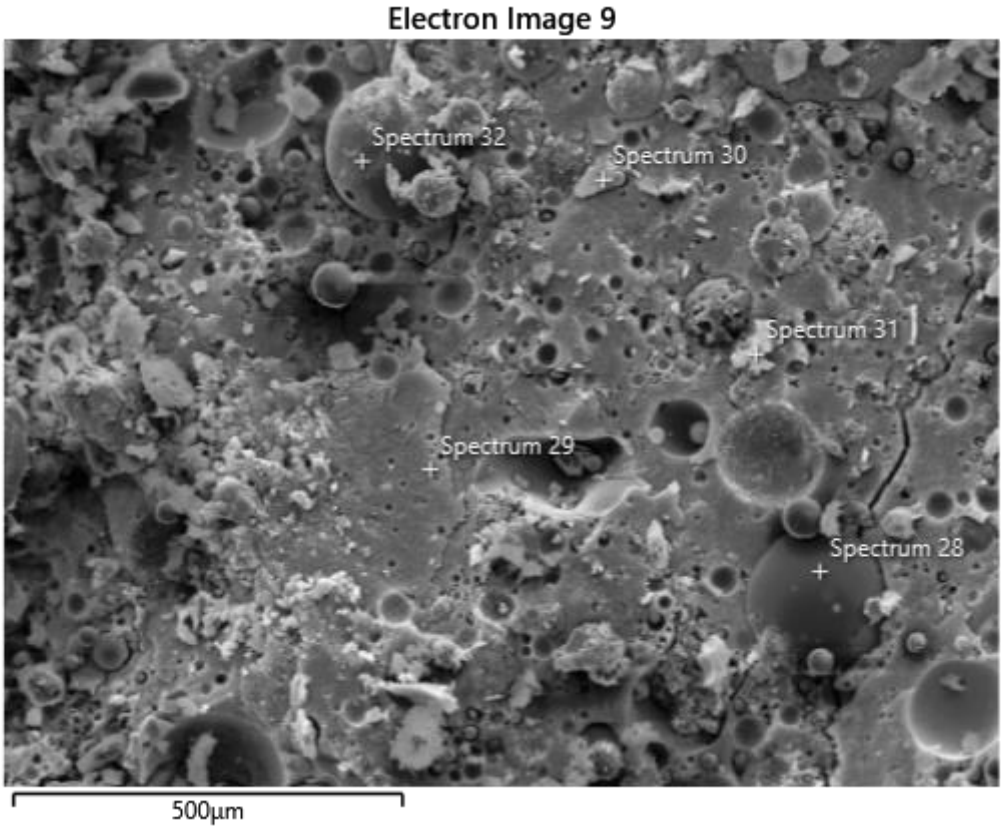

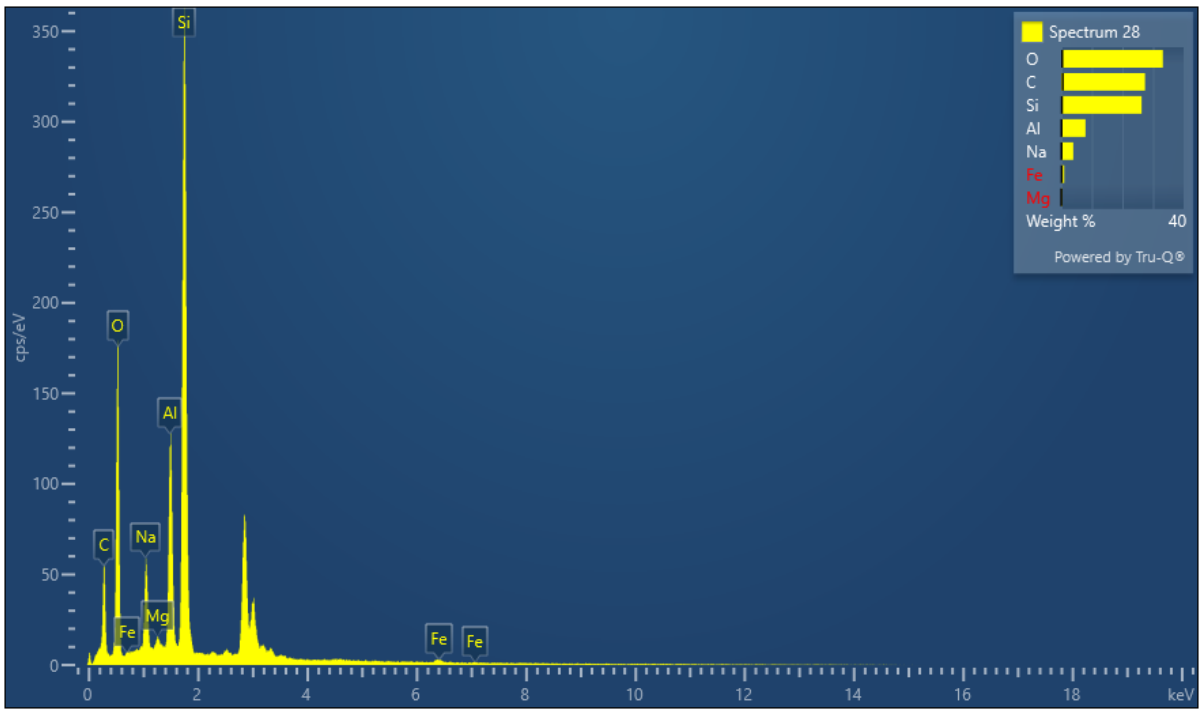

Spectrum 28									
Element	Signal Type	Line	Apparent Concentration	k Ratio	Wt%	Wt% Sigma	Standard Name	Factory Standard	Standardization Date
C	EDS	K series	1.54	0.01542	27.38	0.50	C Vit	Yes	
O	EDS	K series	10.27	0.03456	33.19	0.32	SiO2	Yes	
Na	EDS	K series	1.77	0.00747	3.90	0.09	Albite	Yes	
Mg	EDS	K series	0.13	0.00086	0.36	0.05	MgO	Yes	
Al	EDS	K series	2.98	0.02144	7.93	0.10	Al2O3	Yes	
Si	EDS	K series	9.31	0.07379	26.27	0.23	SiO2	Yes	
Fe	EDS	K series	0.29	0.00288	0.97	0.13	Fe	Yes	
Total					100.00				

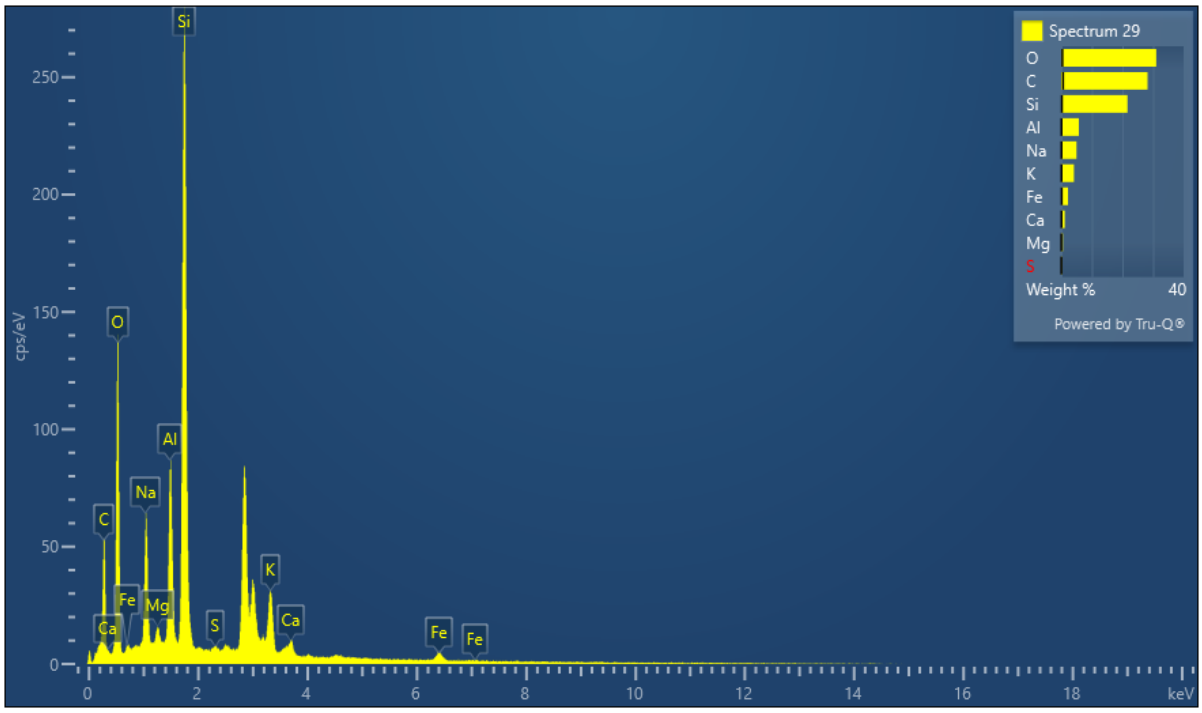

Spectrum 29									
Element	Signal Type	Line	Apparent Concentration	k Ratio	Wt%	Wt% Sigma	Standard Name	Factory Standard	Standardization Date
C	EDS	K series	1.71	0.01715	28.23	0.59	C Vit	Yes	
O	EDS	K series	8.05	0.02708	31.01	0.35	SiO2	Yes	
Na	EDS	K series	2.04	0.00859	5.01	0.10	Albite	Yes	
Mg	EDS	K series	0.17	0.00115	0.55	0.05	MgO	Yes	
Al	EDS	K series	1.95	0.01403	5.76	0.09	Al2O3	Yes	
Si	EDS	K series	7.17	0.05680	21.63	0.22	SiO2	Yes	
S	EDS	K series	0.08	0.00065	0.25	0.05	FeS2	Yes	
K	EDS	K series	1.42	0.01205	4.17	0.10	KBr	Yes	
Ca	EDS	K series	0.39	0.00348	1.18	0.07	Wollastonite	Yes	
Fe	EDS	K series	0.61	0.00610	2.21	0.16	Fe	Yes	
Total					100.00				

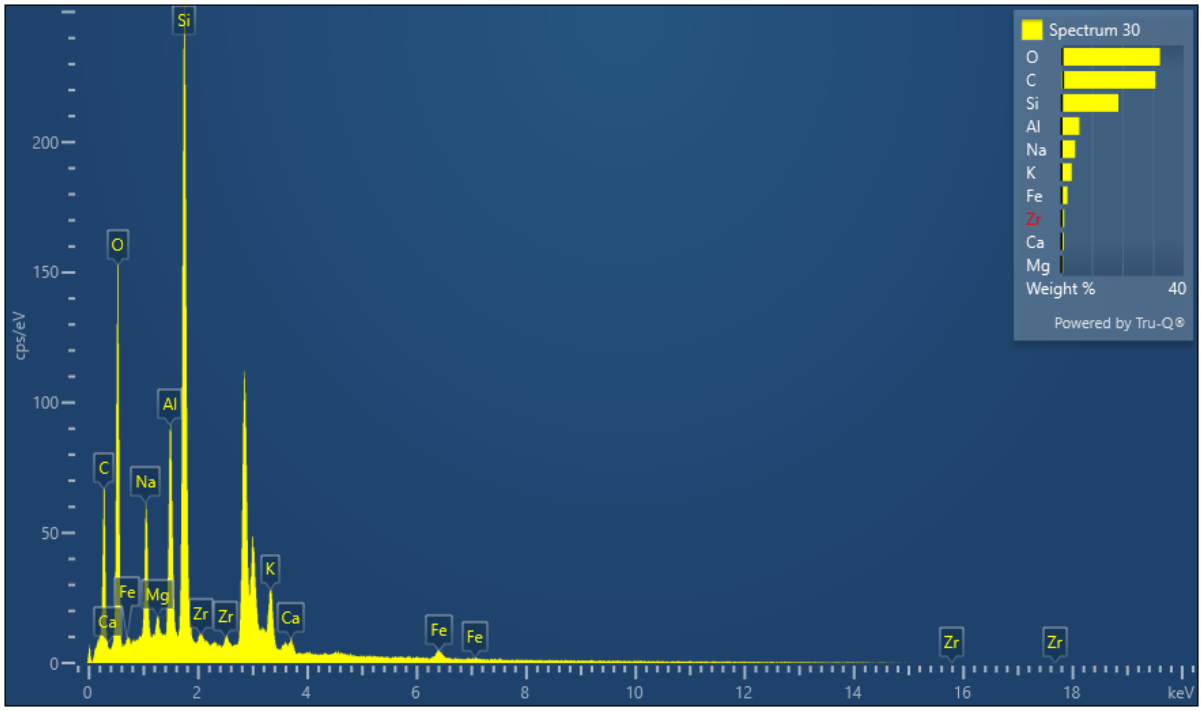

Spectrum 30									
Element	Signal Type	Line	Apparent Concentration	k Ratio	Wt%	Wt% Sigma	Standard Name	Factory Standard	Standardization Date
C	EDS	K series	2.11	0.02105	30.78	0.59	C Vit	Yes	
O	EDS	K series	8.77	0.02951	32.28	0.37	SiO2	Yes	
Na	EDS	K series	1.90	0.00803	4.55	0.10	Albite	Yes	
Mg	EDS	K series	0.18	0.00122	0.56	0.05	MgO	Yes	
Al	EDS	K series	2.09	0.01503	5.95	0.10	Al2O3	Yes	
Si	EDS	K series	6.40	0.05075	18.65	0.21	SiO2	Yes	
K	EDS	K series	1.21	0.01027	3.41	0.10	KBr	Yes	
Ca	EDS	K series	0.29	0.00261	0.84	0.07	Wollastonite	Yes	

Fe	EDS	K series	0.58	0.00578	2.01	0.16	Fe	Yes	
Zr	EDS	L series	0.23	0.00229	0.97	0.17	Zr	Yes	
Total					100.00				

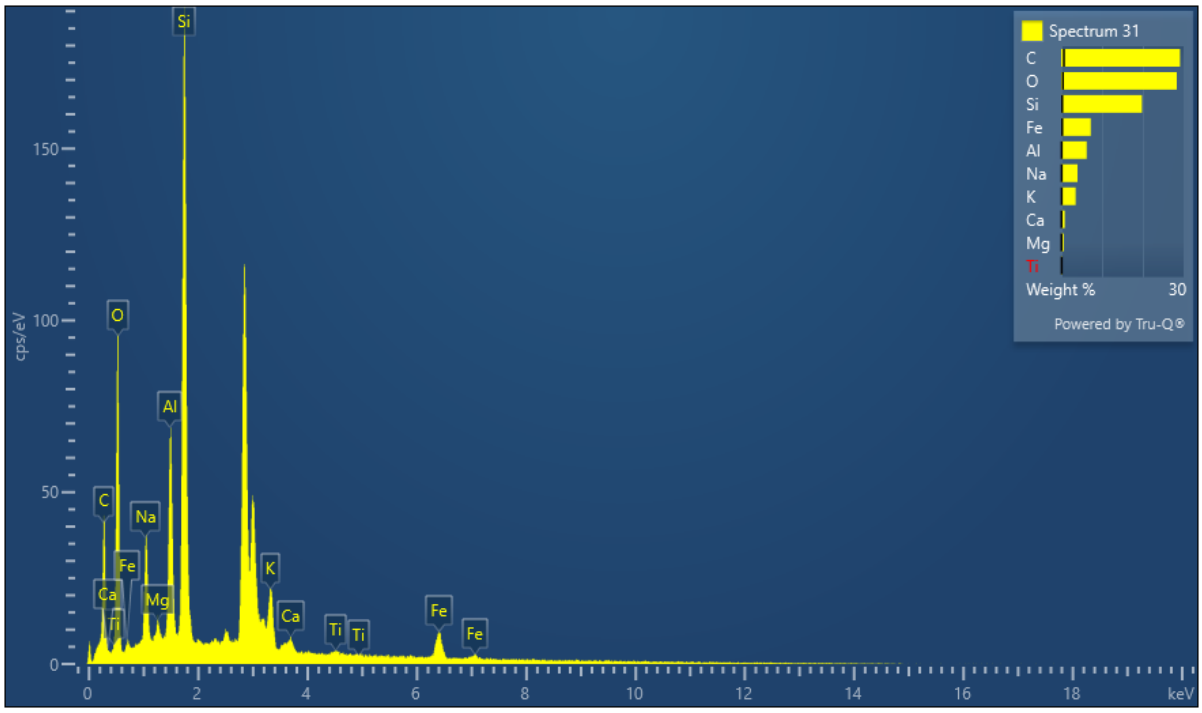

Spectrum 31									
Element	Signal Type	Line	Apparent Concentration	k Ratio	Wt%	Wt% Sigma	Standard Name	Factory Standard	Standardization Date
C	EDS	K series	1.37	0.01368	29.11	0.64	C Vit	Yes	
O	EDS	K series	5.57	0.01874	28.31	0.39	SiO2	Yes	
Na	EDS	K series	1.13	0.00476	4.01	0.10	Albite	Yes	
Mg	EDS	K series	0.14	0.00091	0.60	0.06	MgO	Yes	
Al	EDS	K series	1.53	0.01097	6.23	0.11	Al2O3	Yes	

Si	EDS	K series	4.77	0.03777	19.78	0.24	SiO2	Yes	
K	EDS	K series	0.90	0.00760	3.51	0.11	KBr	Yes	
Ca	EDS	K series	0.22	0.00194	0.87	0.08	Wollastonite	Yes	
Ti	EDS	K series	0.07	0.00068	0.33	0.10	Ti	Yes	
Fe	EDS	K series	1.50	0.01500	7.25	0.25	Fe	Yes	
Total					100.00				

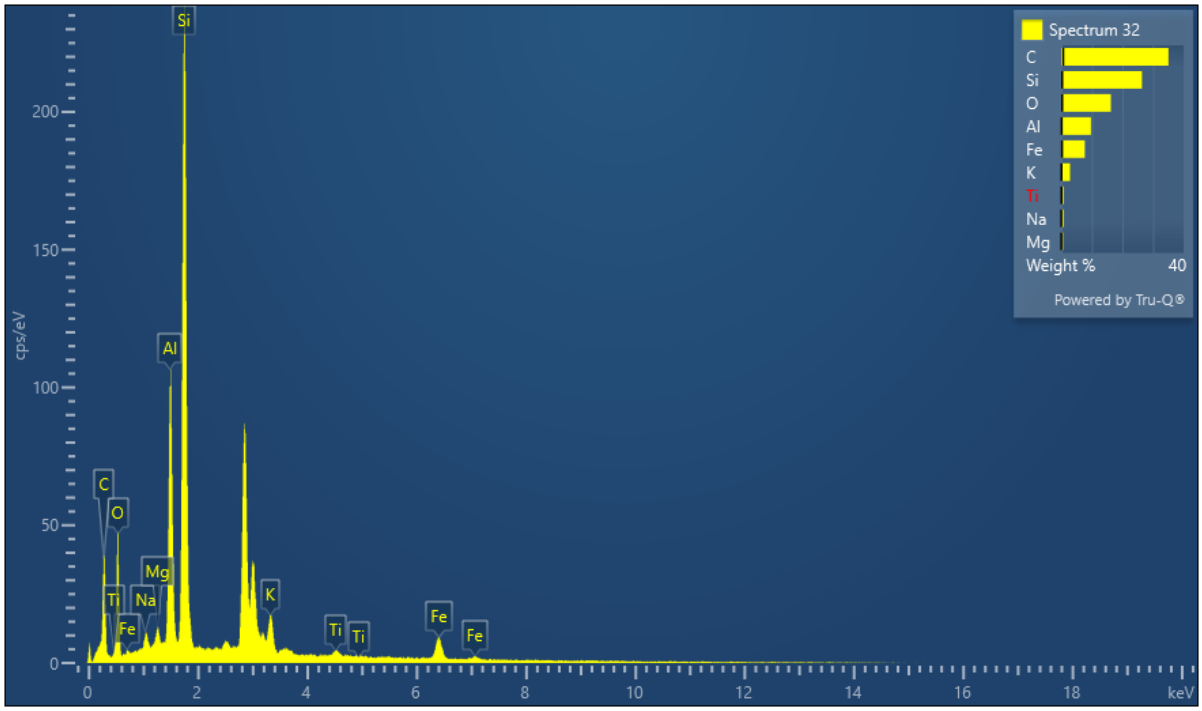

Spectrum 32									
Element	Signal Type	Line	Apparent Concentration	k Ratio	Wt%	Wt% Sigma	Standard Name	Factory Standard	Standardization Date
C	EDS	K series	1.31	0.01313	35.03	0.65	C Vit	Yes	
O	EDS	K series	2.63	0.00885	16.21	0.30	SiO2	Yes	
Na	EDS	K series	0.21	0.00090	0.74	0.06	Albite	Yes	

Mg	EDS	K series	0.15	0.00099	0.62	0.05	MgO	Yes	
Al	EDS	K series	2.46	0.01763	9.71	0.14	Al2O3	Yes	
Si	EDS	K series	6.16	0.04880	26.36	0.31	SiO2	Yes	
K	EDS	K series	0.69	0.00581	2.85	0.10	KBr	Yes	
Ti	EDS	K series	0.16	0.00156	0.78	0.10	Ti	Yes	
Fe	EDS	K series	1.53	0.01526	7.71	0.24	Fe	Yes	
Total					100.00				

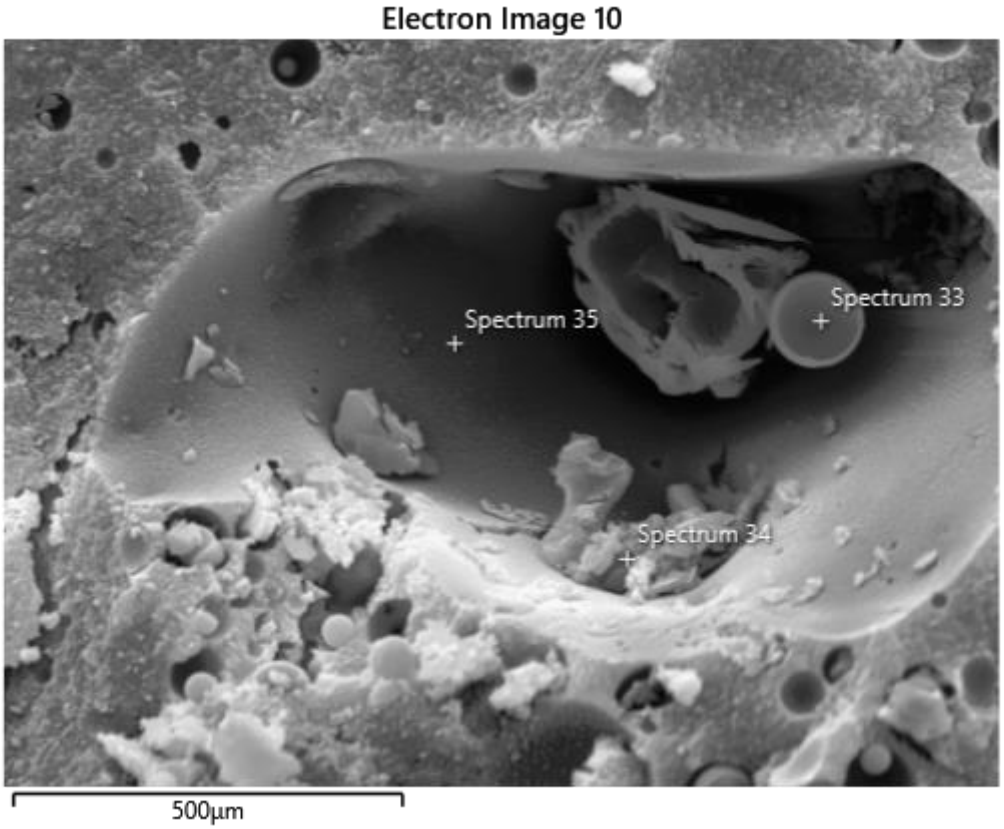

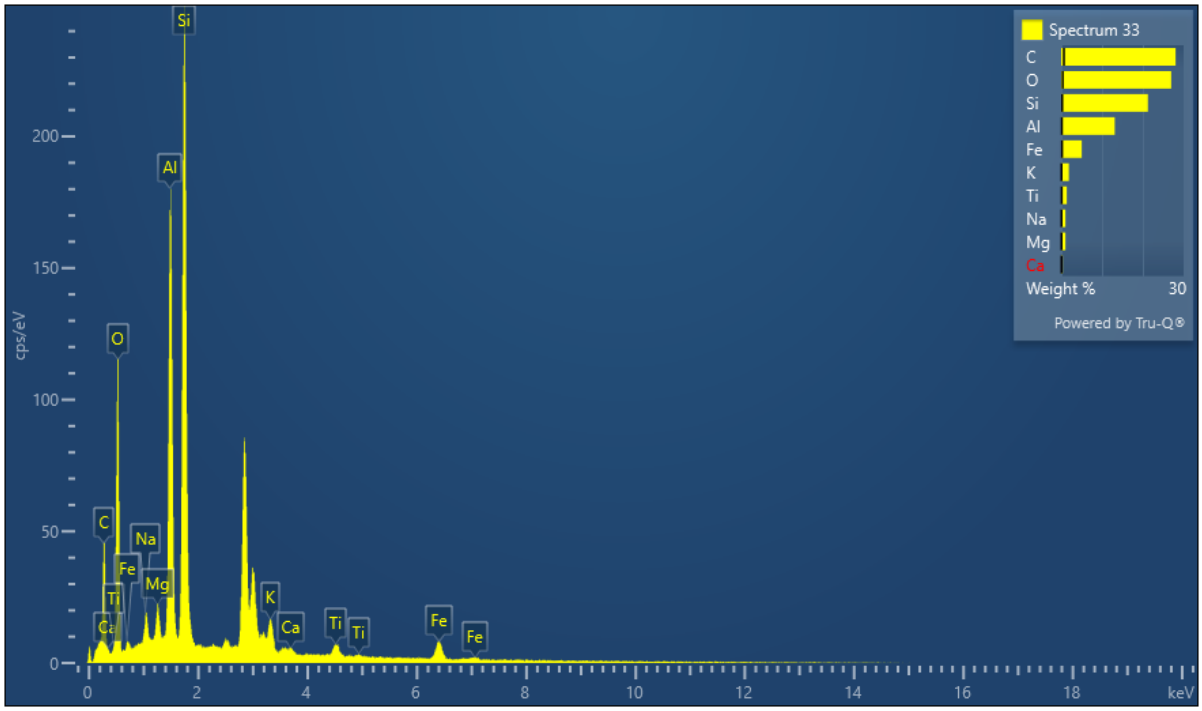

Spectrum 33									
Element	Signal Type	Line	Apparent Concentration	k Ratio	Wt%	Wt% Sigma	Standard Name	Factory Standard	Standardization Date
C	EDS	K series	1.46	0.01455	28.05	0.64	C Vit	Yes	
O	EDS	K series	6.64	0.02235	26.95	0.35	SiO2	Yes	
Na	EDS	K series	0.40	0.00167	1.04	0.06	Albite	Yes	
Mg	EDS	K series	0.32	0.00215	1.03	0.06	MgO	Yes	
Al	EDS	K series	4.32	0.03100	13.10	0.16	Al2O3	Yes	
Si	EDS	K series	6.29	0.04985	21.23	0.24	SiO2	Yes	
K	EDS	K series	0.60	0.00507	1.87	0.08	KBr	Yes	
Ca	EDS	K series	0.11	0.00101	0.36	0.06	Wollastonite	Yes	

Ti	EDS	K series	0.36	0.00359	1.36	0.10	Ti	Yes	
Fe	EDS	K series	1.32	0.01320	5.03	0.19	Fe	Yes	
Total					100.00				

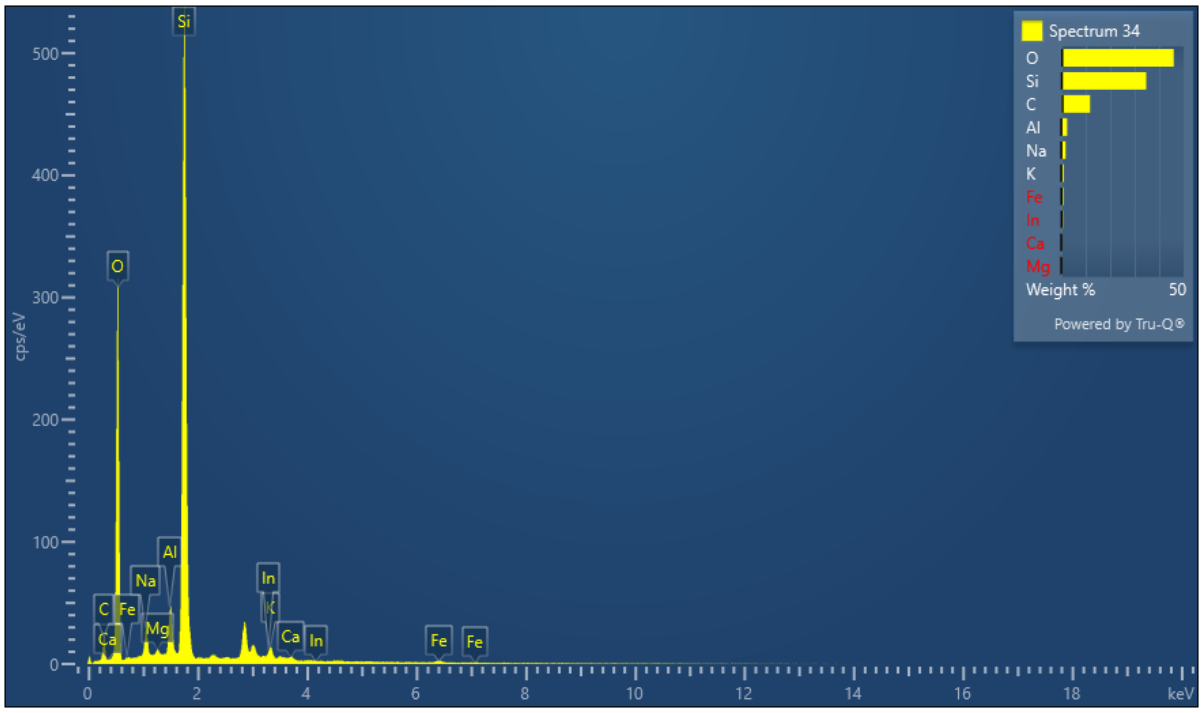

Spectrum 34									
Element	Signal Type	Line	Apparent Concentration	k Ratio	Wt%	Wt% Sigma	Standard Name	Factory Standard	Standardization Date
C	EDS	K series	0.64	0.00641	11.79	0.56	C Vit	Yes	
O	EDS	K series	18.37	0.06181	45.95	0.37	SiO2	Yes	
Na	EDS	K series	0.80	0.00336	1.78	0.06	Albite	Yes	
Mg	EDS	K series	0.11	0.00072	0.29	0.04	MgO	Yes	
Al	EDS	K series	0.96	0.00689	2.41	0.06	Al2O3	Yes	

Si	EDS	K series	13.85	0.10976	34.69	0.28	SiO2	Yes	
K	EDS	K series	0.40	0.00337	1.03	0.08	KBr	Yes	
Ca	EDS	K series	0.16	0.00141	0.41	0.06	Wollastonite	Yes	
Fe	EDS	K series	0.29	0.00290	0.91	0.12	Fe	Yes	
In	EDS	L series	0.23	0.00206	0.73	0.18	InAs	Yes	
Total					100.00				

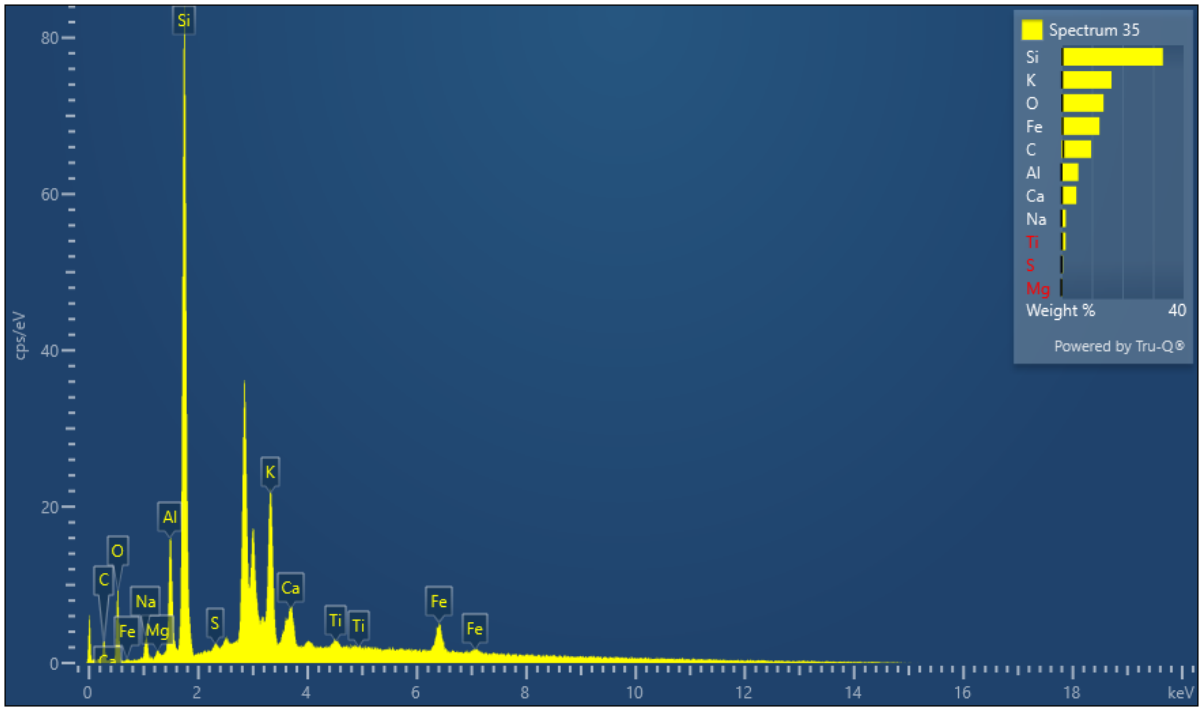

Spectrum 35									
Element	Signal Type	Line	Apparent Concentration	k Ratio	Wt%	Wt% Sigma	Standard Name	Factory Standard	Standardization Date
C	EDS	K series	0.09	0.00087	9.77	0.68	C Vit	Yes	
O	EDS	K series	0.54	0.00180	13.80	0.34	SiO2	Yes	

Na	EDS	K series	0.10	0.00044	1.47	0.08	Albite	Yes	
Mg	EDS	K series	0.02	0.00014	0.36	0.05	MgO	Yes	
Al	EDS	K series	0.37	0.00263	5.60	0.12	Al2O3	Yes	
Si	EDS	K series	2.15	0.01701	33.20	0.38	SiO2	Yes	
S	EDS	K series	0.03	0.00027	0.56	0.08	FeS2	Yes	
K	EDS	K series	1.09	0.00926	16.42	0.26	KBr	Yes	
Ca	EDS	K series	0.31	0.00274	4.91	0.19	Wollastonite	Yes	
Ti	EDS	K series	0.08	0.00076	1.42	0.20	Ti	Yes	
Fe	EDS	K series	0.69	0.00687	12.50	0.43	Fe	Yes	
Total					100.00				

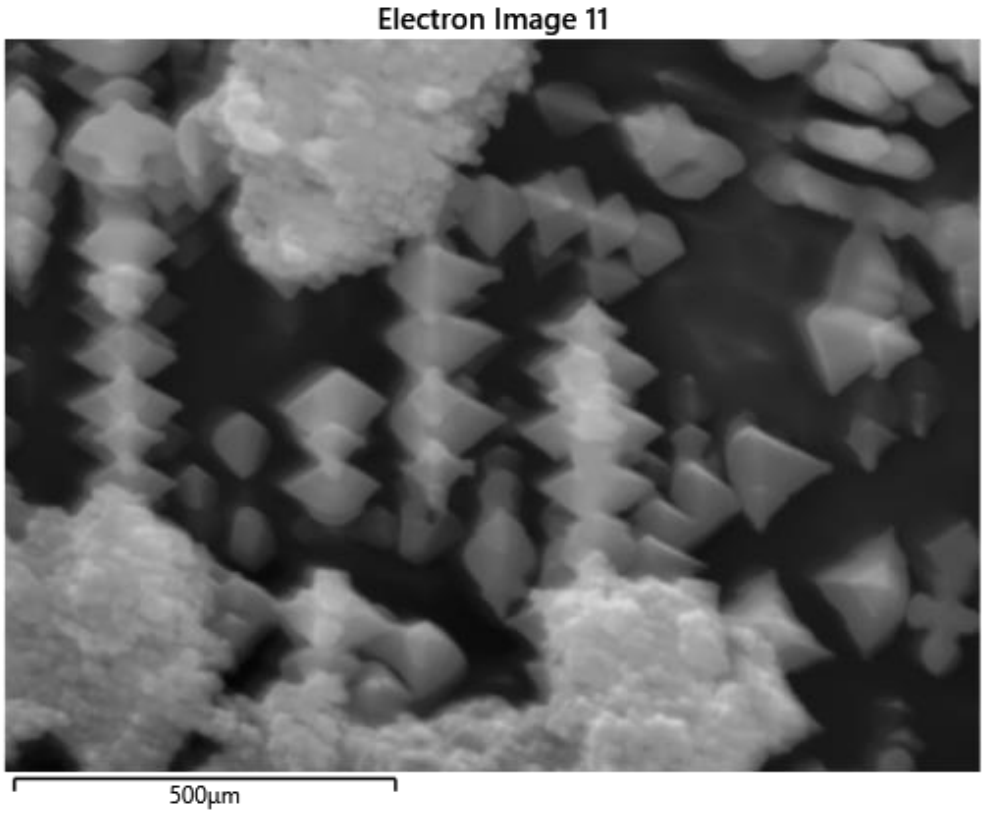

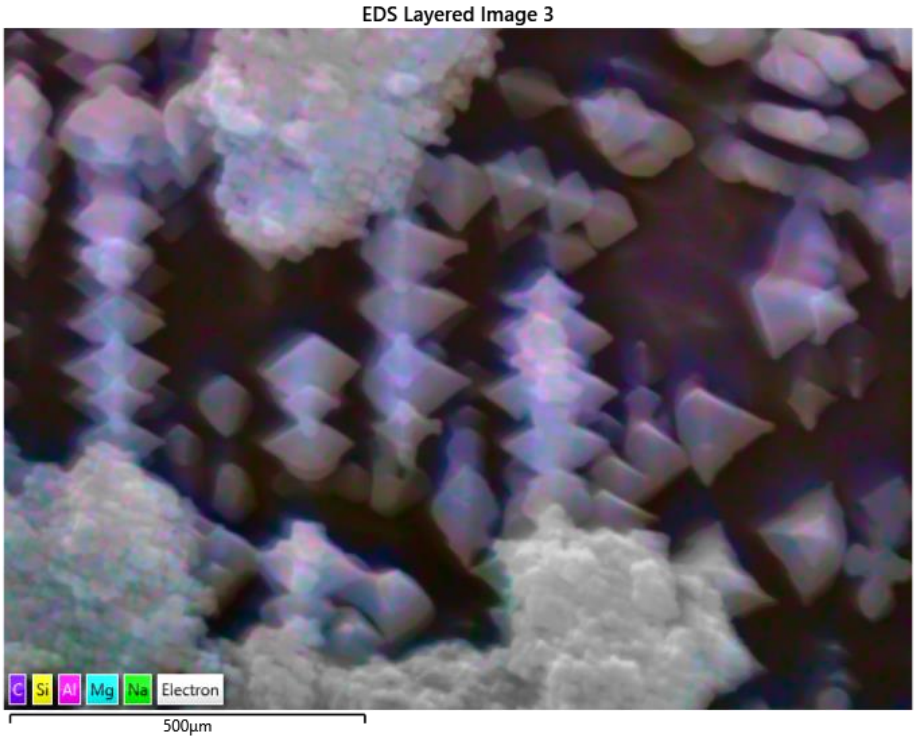
EDS Layered Image 3
C
Si
Al
Mg
Na
Electron
500µm

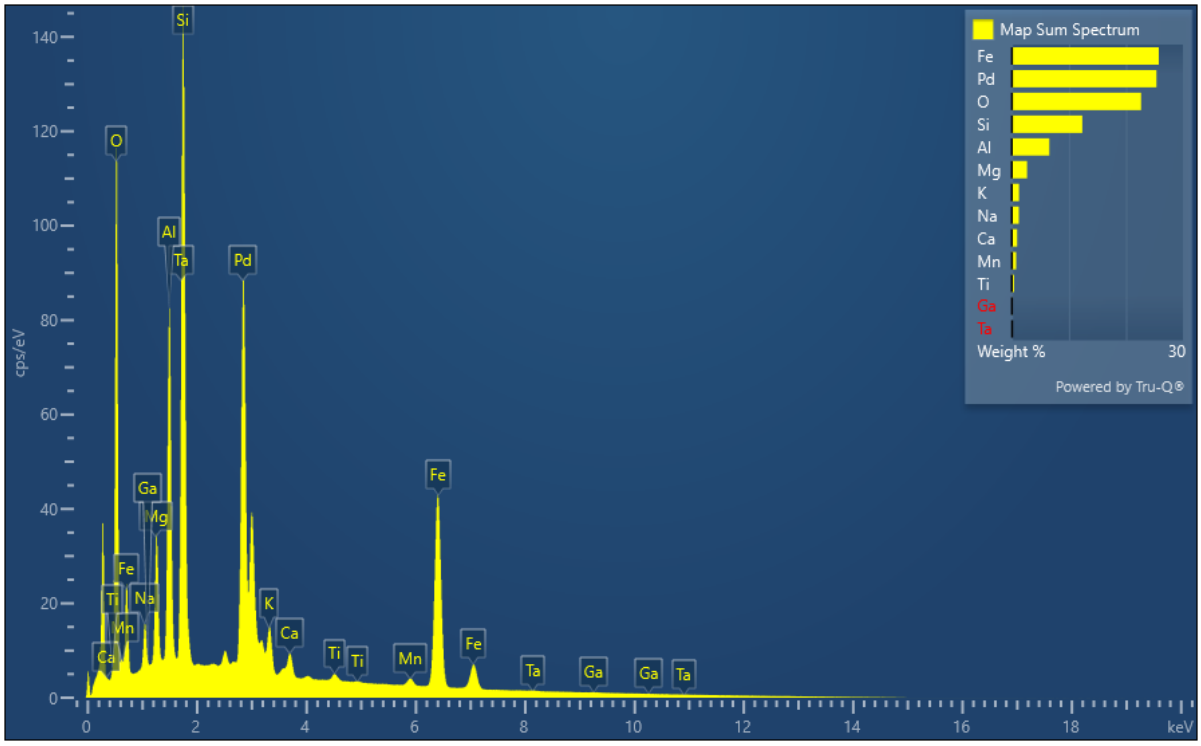
Map Sum Spectrum
Fe
Pd
O
Si
Al
Mg
K
Na
Ca
Mn
Ti
Ga
Ta
Weight %
30
Powered by Tru-Q®
cps/eV
keV
Si
O
Al
Ta
Pd
Ga
Mg
Fe
Ti
Na
Mn
Ca
K
Ca
Ti
Ti
Mn
Fe
Ta
Ga
Ga
Ta

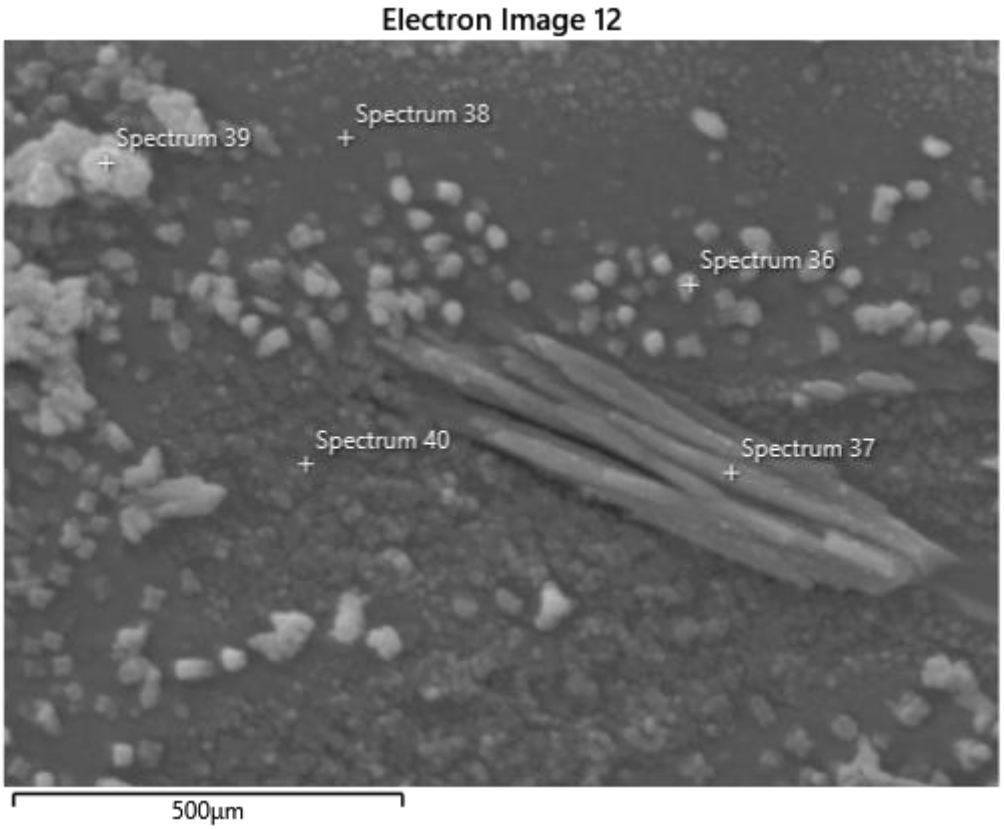

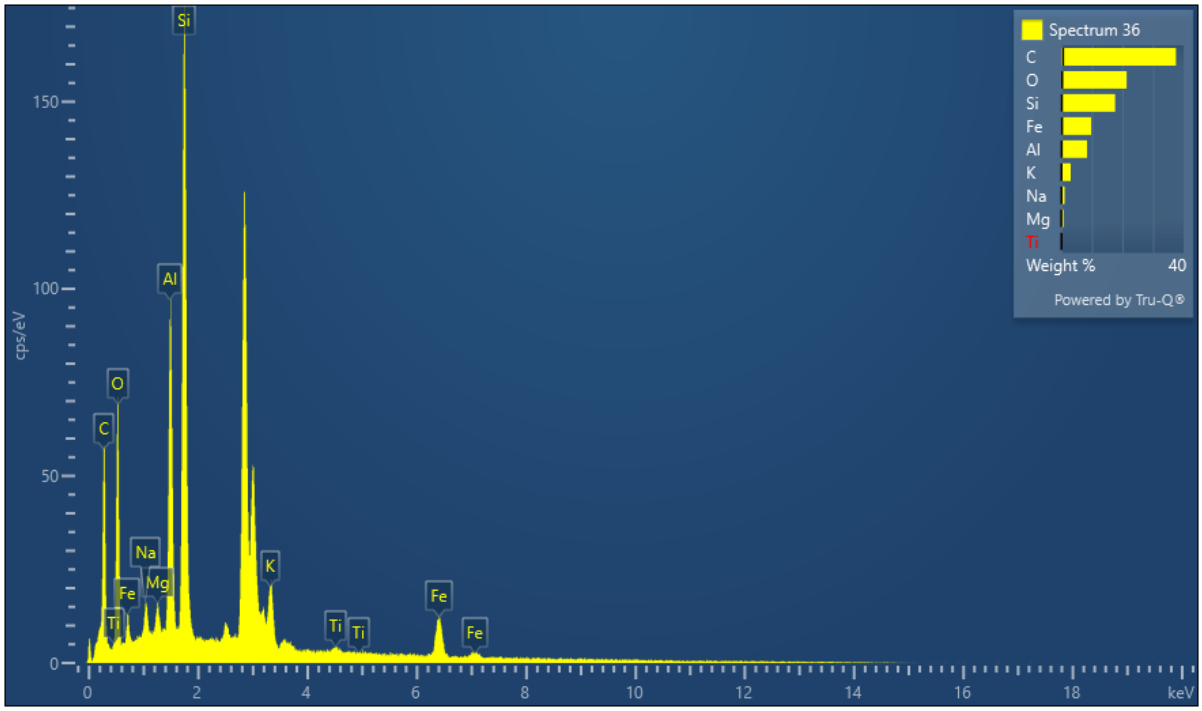

Spectrum 36									
Element	Signal Type	Line	Apparent Concentration	k Ratio	Wt%	Wt% Sigma	Standard Name	Factory Standard	Standardization Date

C	EDS	K series	1.94	0.01936	37.47	0.59	C Vit	Yes	
O	EDS	K series	4.00	0.01348	21.38	0.34	SiO2	Yes	
Na	EDS	K series	0.32	0.00133	1.08	0.08	Albite	Yes	
Mg	EDS	K series	0.19	0.00124	0.76	0.06	MgO	Yes	
Al	EDS	K series	2.21	0.01585	8.44	0.13	Al2O3	Yes	
Si	EDS	K series	4.39	0.03476	17.61	0.22	SiO2	Yes	
K	EDS	K series	0.82	0.00693	3.07	0.11	KBr	Yes	
Ti	EDS	K series	0.10	0.00096	0.44	0.10	Ti	Yes	
Fe	EDS	K series	2.10	0.02098	9.74	0.26	Fe	Yes	
Total					100.00				

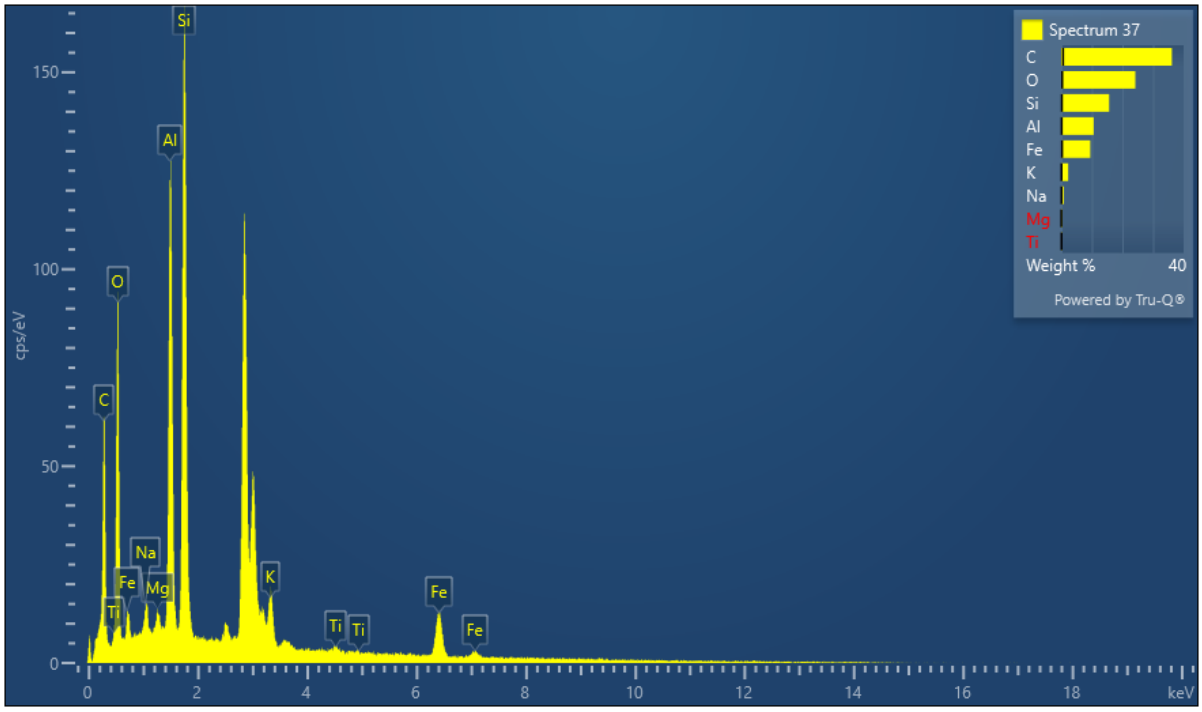

Spectrum 37									
Element	Signal Type	Line	Apparent Concentration	k Ratio	Wt%	Wt% Sigma	Standard Name	Factory Standard	Standardization Date
C	EDS	K series	2.05	0.02048	36.14	0.57	C Vit	Yes	
O	EDS	K series	5.17	0.01741	24.21	0.34	SiO2	Yes	
Na	EDS	K series	0.26	0.00111	0.83	0.07	Albite	Yes	
Mg	EDS	K series	0.11	0.00074	0.42	0.05	MgO	Yes	
Al	EDS	K series	3.01	0.02165	10.59	0.14	Al2O3	Yes	
Si	EDS	K series	4.16	0.03297	15.67	0.19	SiO2	Yes	
K	EDS	K series	0.66	0.00559	2.28	0.09	KBr	Yes	
Ti	EDS	K series	0.08	0.00085	0.36	0.09	Ti	Yes	
Fe	EDS	K series	2.23	0.02226	9.50	0.25	Fe	Yes	
Total					100.00				

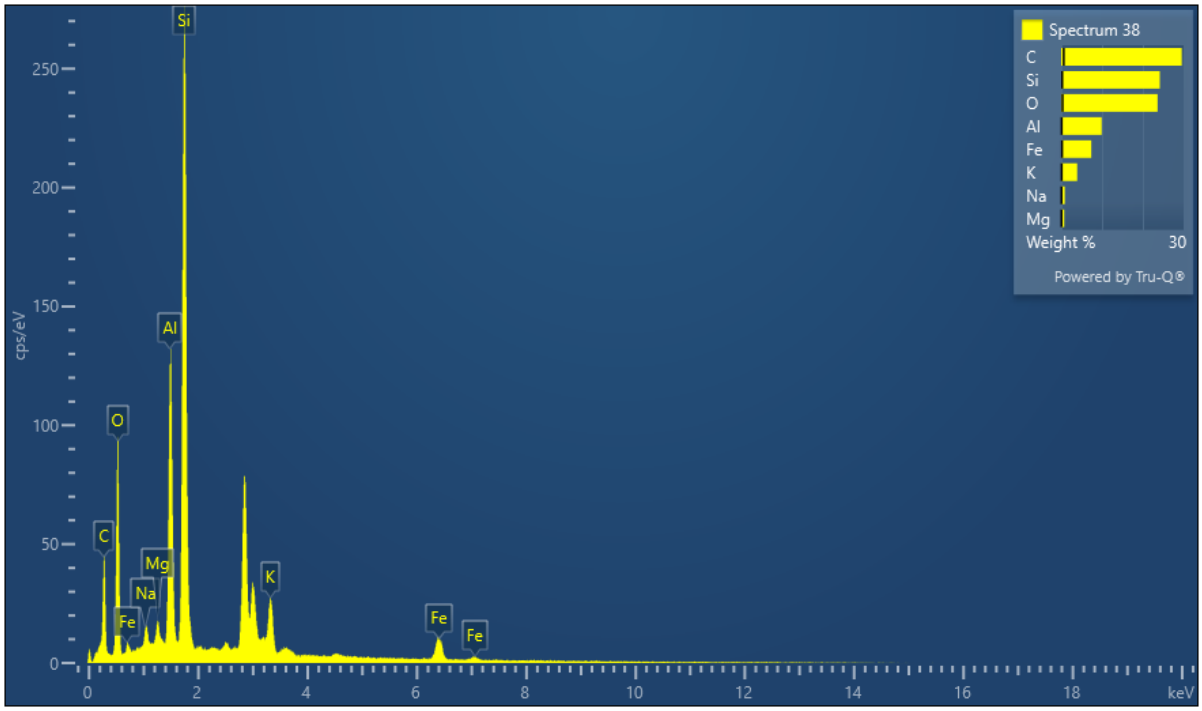

Spectrum 38									
Element	Signal Type	Line	Apparent Concentration	k Ratio	Wt%	Wt% Sigma	Standard Name	Factory Standard	Standardization Date
C	EDS	K series	1.46	0.01462	29.55	0.59	C Vit	Yes	
O	EDS	K series	5.42	0.01824	23.60	0.31	SiO2	Yes	
Na	EDS	K series	0.31	0.00130	0.86	0.06	Albite	Yes	
Mg	EDS	K series	0.22	0.00143	0.72	0.05	MgO	Yes	
Al	EDS	K series	3.13	0.02245	9.90	0.13	Al2O3	Yes	
Si	EDS	K series	7.09	0.05618	24.14	0.25	SiO2	Yes	
K	EDS	K series	1.20	0.01016	3.89	0.10	KBr	Yes	
Fe	EDS	K series	1.86	0.01857	7.35	0.21	Fe	Yes	
Total					100.00				

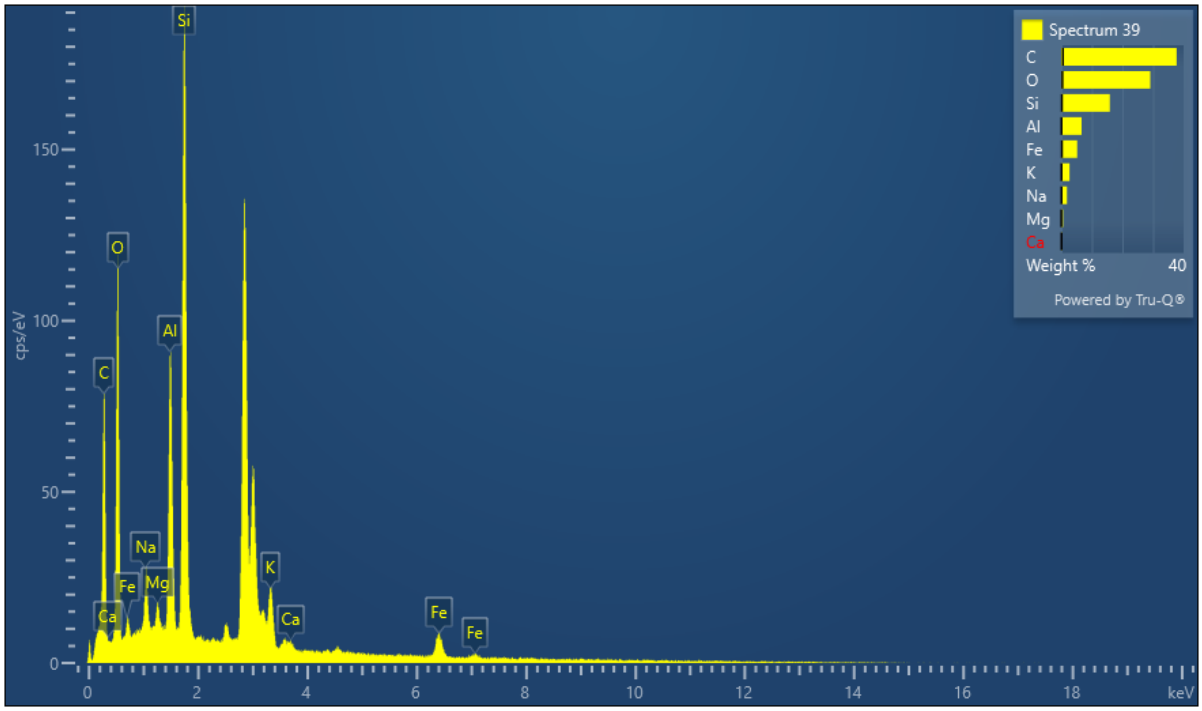

Spectrum 39									
Element	Signal Type	Line	Apparent Concentration	k Ratio	Wt%	Wt% Sigma	Standard Name	Factory Standard	Standardization Date
C	EDS	K series	2.55	0.02552	37.69	0.57	C Vit	Yes	
O	EDS	K series	6.72	0.02260	29.11	0.37	SiO2	Yes	
Na	EDS	K series	0.65	0.00276	1.86	0.08	Albite	Yes	
Mg	EDS	K series	0.17	0.00113	0.58	0.06	MgO	Yes	
Al	EDS	K series	2.06	0.01481	6.63	0.11	Al2O3	Yes	
Si	EDS	K series	4.78	0.03784	15.88	0.19	SiO2	Yes	
K	EDS	K series	0.85	0.00724	2.71	0.10	KBr	Yes	
Ca	EDS	K series	0.10	0.00093	0.34	0.07	Wollastonite	Yes	

Fe	EDS	K series	1.31	0.01313	5.19	0.21	Fe	Yes	
Total					100.00				

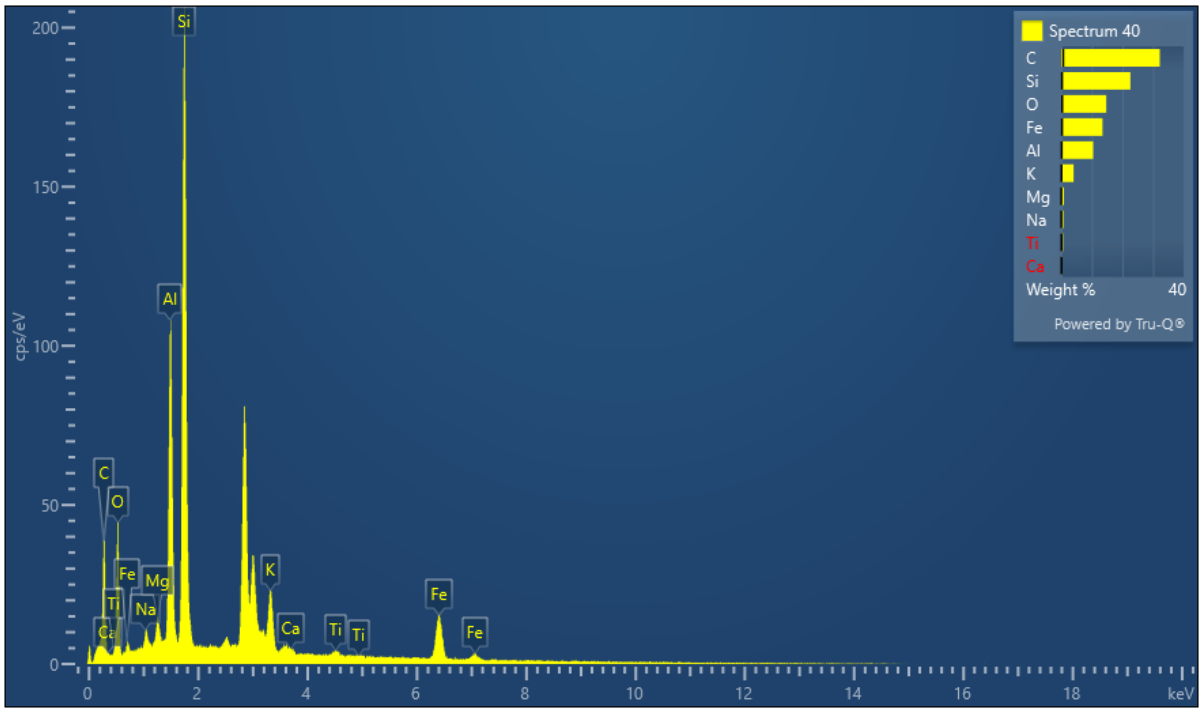

Spectrum 40									
Element	Signal Type	Line	Apparent Concentration	k Ratio	Wt%	Wt% Sigma	Standard Name	Factory Standard	Standardization Date
C	EDS	K series	1.29	0.01290	32.21	0.64	C Vit	Yes	
O	EDS	K series	2.51	0.00843	14.69	0.30	SiO2	Yes	
Na	EDS	K series	0.19	0.00079	0.69	0.06	Albite	Yes	
Mg	EDS	K series	0.20	0.00131	0.86	0.06	MgO	Yes	
Al	EDS	K series	2.55	0.01832	10.43	0.15	Al2O3	Yes	
Si	EDS	K series	5.17	0.04099	22.58	0.26	SiO2	Yes	

K	EDS	K series	1.00	0.00849	4.05	0.11	KBr	Yes	
Ca	EDS	K series	0.10	0.00093	0.43	0.07	Wollastonite	Yes	
Ti	EDS	K series	0.12	0.00121	0.59	0.10	Ti	Yes	
Fe	EDS	K series	2.74	0.02737	13.48	0.28	Fe	Yes	
Total					100.00				

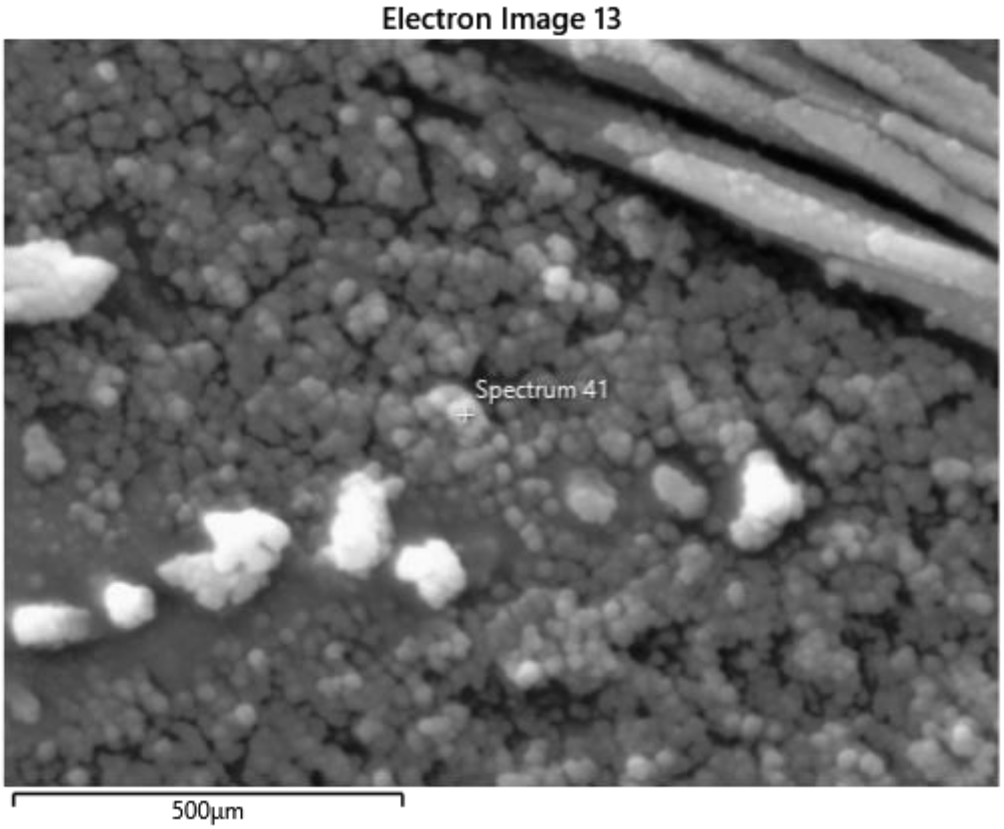

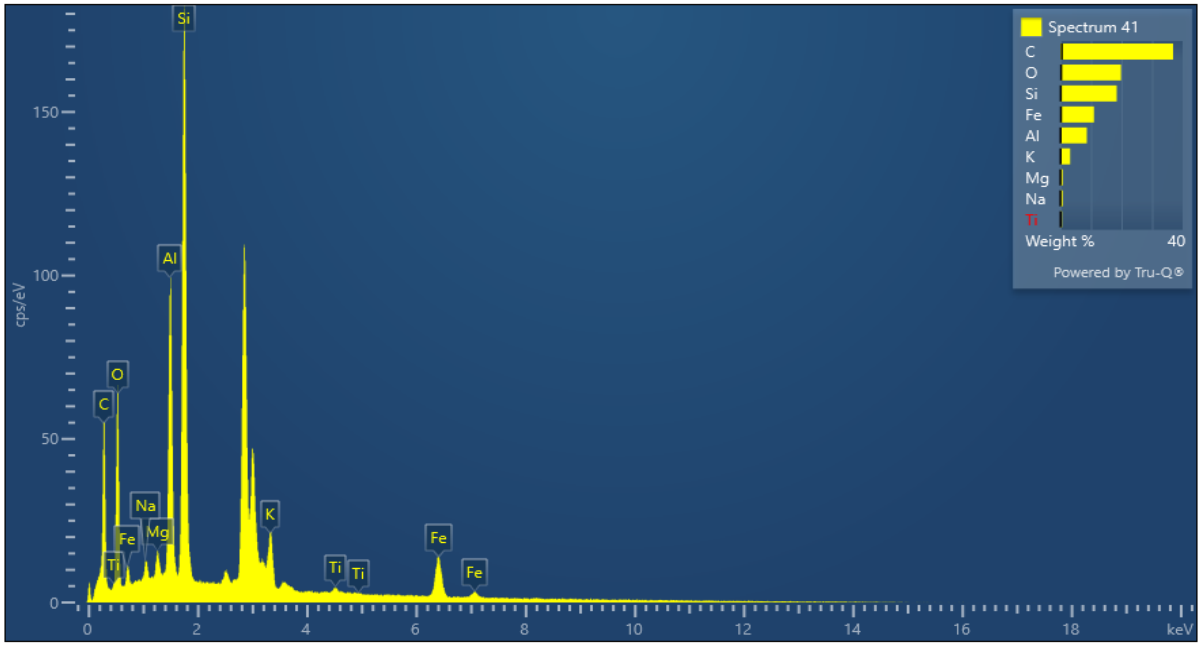

Spectrum 41									
Element	Signal Type	Line	Apparent Concentration	k Ratio	Wt%	Wt% Sigma	Standard Name	Factory Standard	Standardization Date
C	EDS	K series	1.87	0.01867	36.88	0.46	C Vit	Yes	
O	EDS	K series	3.72	0.01251	19.80	0.25	SiO2	Yes	
Na	EDS	K series	0.22	0.00091	0.74	0.05	Albite	Yes	
Mg	EDS	K series	0.19	0.00128	0.78	0.05	MgO	Yes	
Al	EDS	K series	2.28	0.01641	8.67	0.10	Al2O3	Yes	
Si	EDS	K series	4.62	0.03660	18.41	0.17	SiO2	Yes	
K	EDS	K series	0.86	0.00733	3.22	0.08	KBr	Yes	
Ti	EDS	K series	0.11	0.00114	0.52	0.07	Ti	Yes	
Fe	EDS	K series	2.39	0.02392	10.98	0.21	Fe	Yes	
Total					100.00				

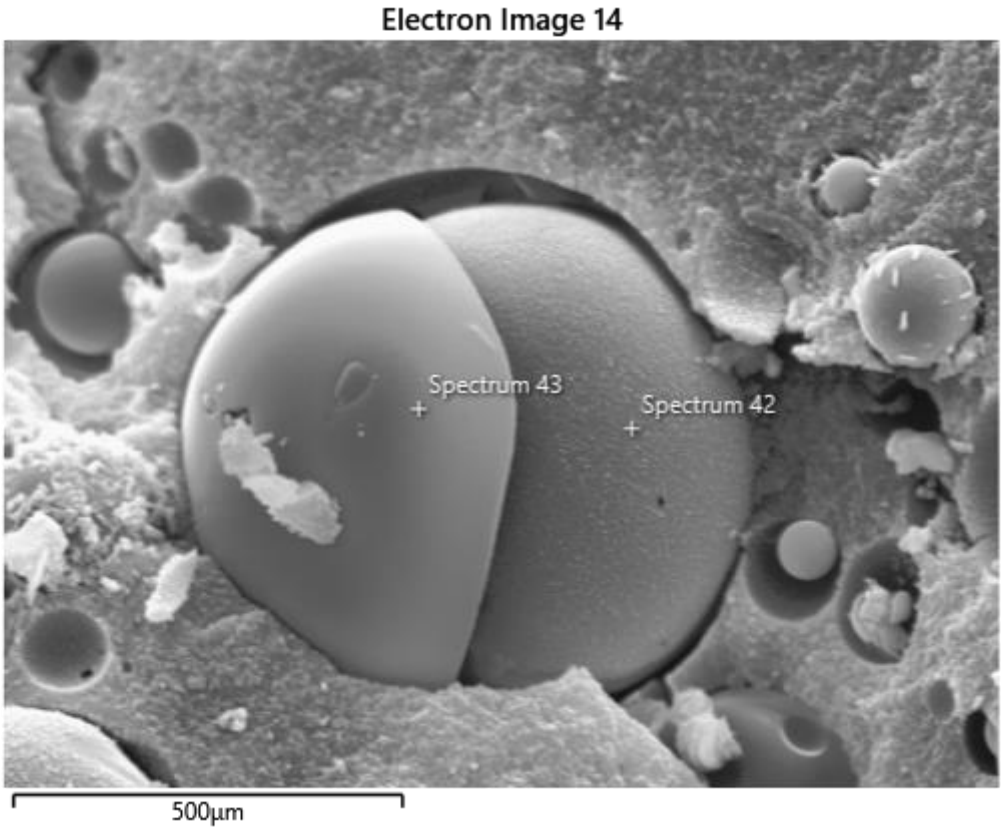
Electron Image 14
Spectrum 43
Spectrum 42
500µm

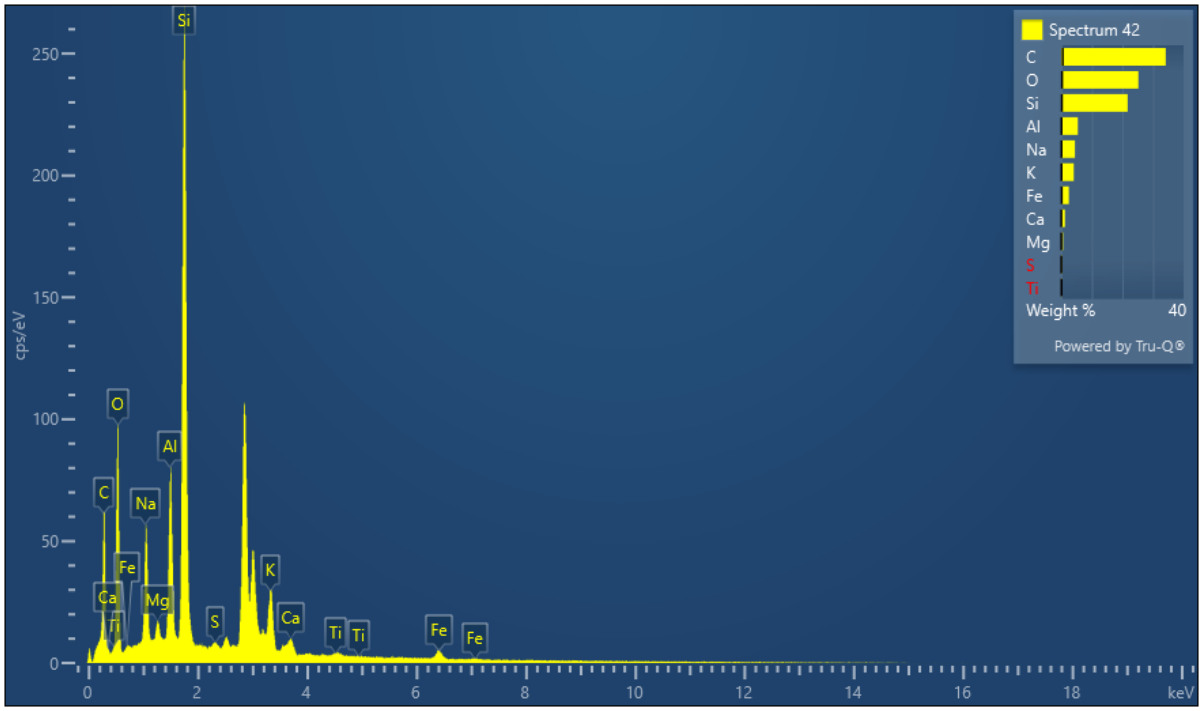
Spectrum 42
C
O
Si
Al
Na
K
Fe
Ca
Mg
S
Ti
Weight %
40
Powered by Tru-Q®
cps/eV
keV

Spectrum 42									
Element	Signal Type	Line	Apparent Concentration	k Ratio	Wt%	Wt% Sigma	Standard Name	Factory Standard	Standardization Date
C	EDS	K series	2.00	0.01997	34.14	0.47	C Vit	Yes	
O	EDS	K series	5.56	0.01870	25.22	0.29	SiO2	Yes	
Na	EDS	K series	1.74	0.00735	4.46	0.08	Albite	Yes	
Mg	EDS	K series	0.19	0.00126	0.62	0.04	MgO	Yes	
Al	EDS	K series	1.75	0.01259	5.41	0.07	Al2O3	Yes	
Si	EDS	K series	6.85	0.05432	21.70	0.19	SiO2	Yes	
S	EDS	K series	0.10	0.00082	0.33	0.04	FeS2	Yes	
K	EDS	K series	1.32	0.01122	4.12	0.08	KBr	Yes	
Ca	EDS	K series	0.38	0.00339	1.21	0.06	Wollastonite	Yes	
Ti	EDS	K series	0.08	0.00079	0.30	0.07	Ti	Yes	
Fe	EDS	K series	0.65	0.00646	2.49	0.13	Fe	Yes	
Total					100.00				

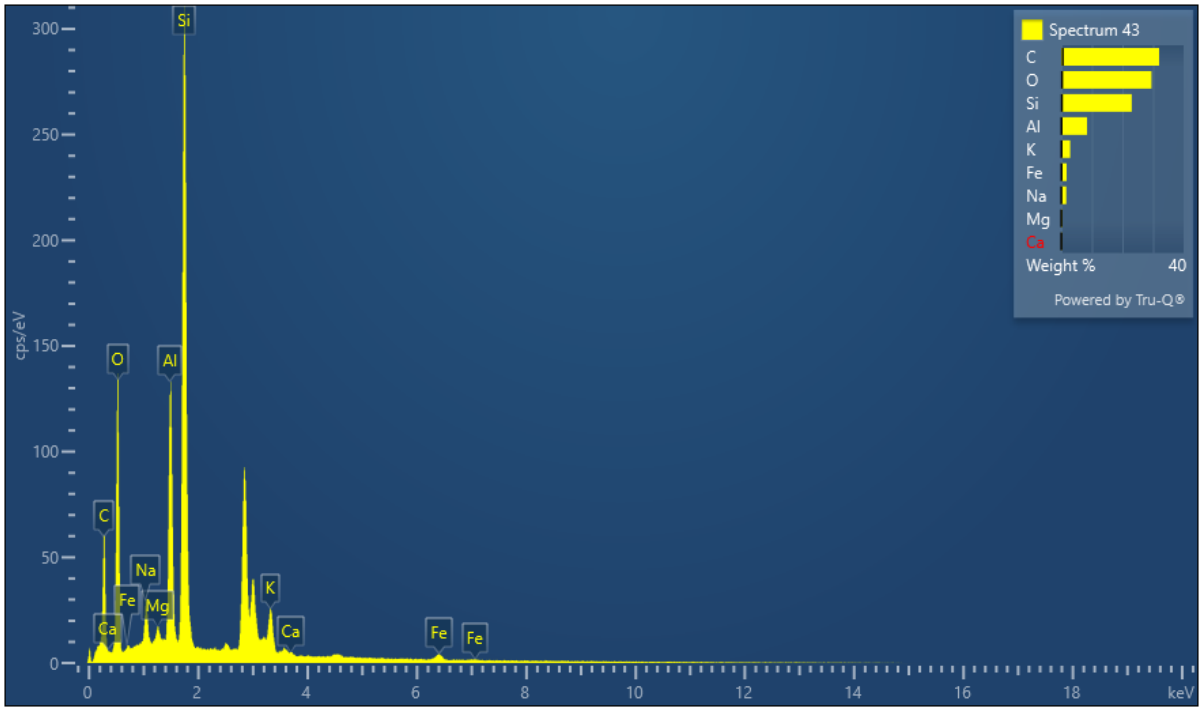

Spectrum 43									
Element	Signal Type	Line	Apparent Concentration	k Ratio	Wt%	Wt% Sigma	Standard Name	Factory Standard	Standardization Date
C	EDS	K series	1.96	0.01960	31.99	0.47	C Vit	Yes	
O	EDS	K series	7.85	0.02640	29.50	0.28	SiO2	Yes	
Na	EDS	K series	0.73	0.00307	1.67	0.05	Albite	Yes	
Mg	EDS	K series	0.16	0.00106	0.45	0.04	MgO	Yes	
Al	EDS	K series	3.14	0.02258	8.45	0.09	Al2O3	Yes	
Si	EDS	K series	8.00	0.06343	23.02	0.19	SiO2	Yes	
K	EDS	K series	1.05	0.00887	2.95	0.07	KBr	Yes	
Ca	EDS	K series	0.07	0.00064	0.21	0.05	Wollastonite	Yes	

Fe	EDS	K series	0.51	0.00509	1.76	0.12	Fe	Yes	
Total					100.00				

Geopolymer with 0.2 g Al_2O_3

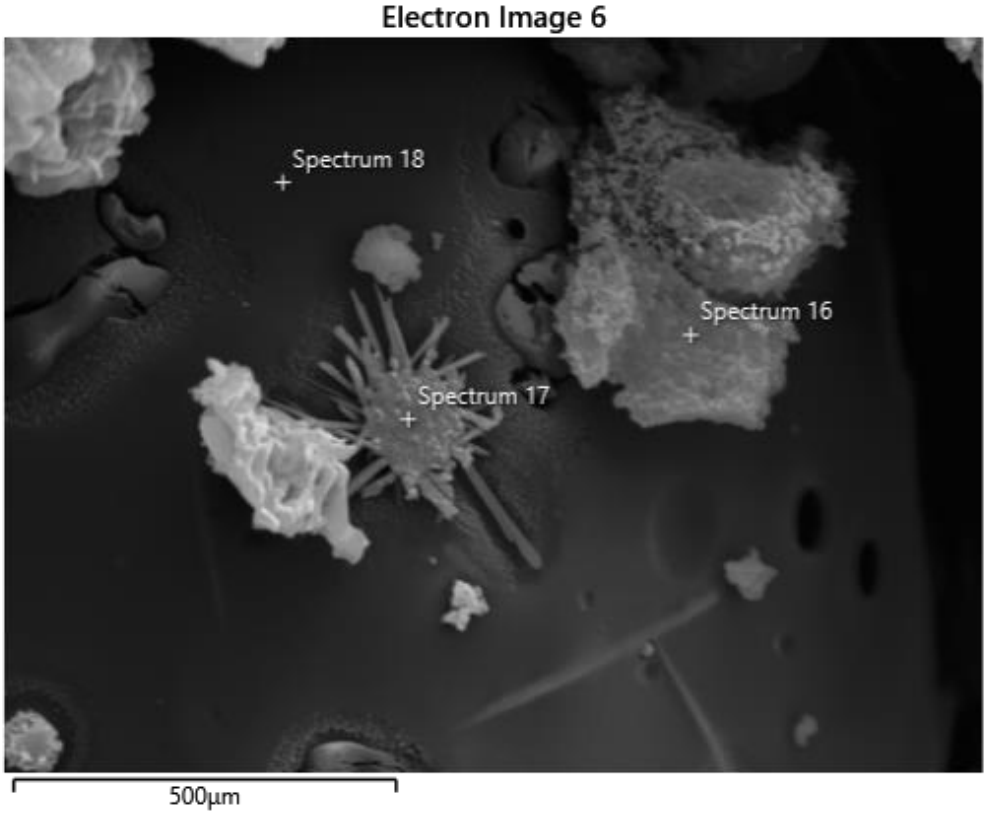

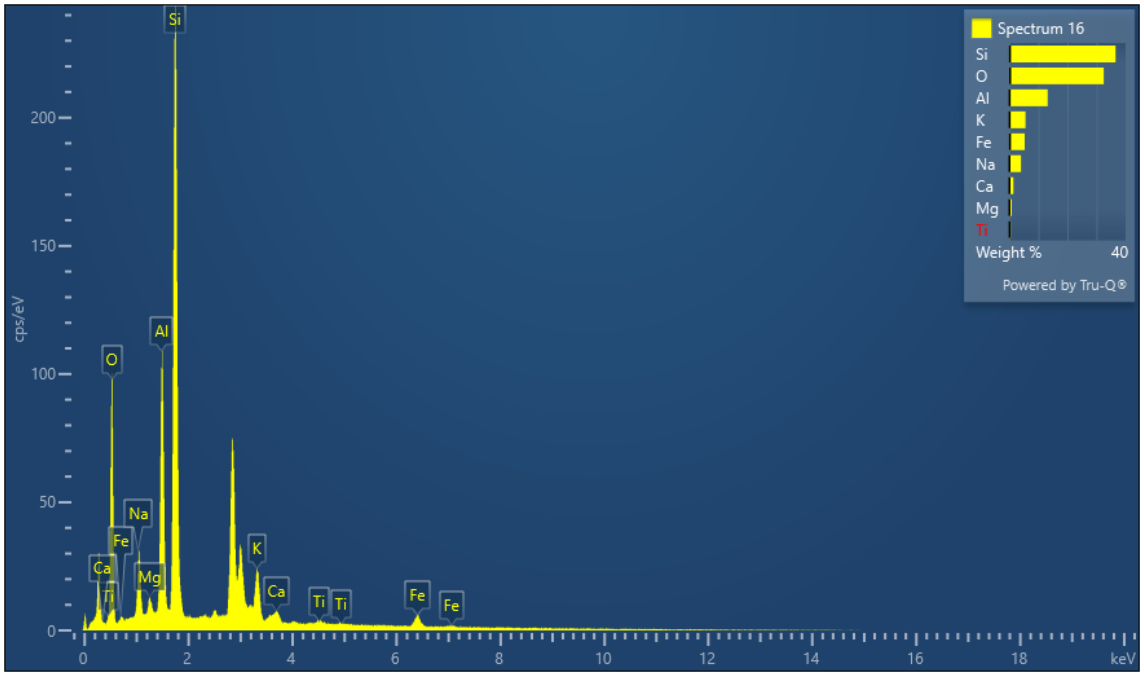

Spectrum 16

Element	Signal Type	Line	Apparent Concentration	k Ratio	Wt%	Wt% Sigma	Standard Name	Factory Standard	Standardization Date
O	EDS	K series	5.73	0.01928	32.46	0.32	SiO2	Yes	
Na	EDS	K series	0.92	0.00388	4.06	0.11	Albite	Yes	
Mg	EDS	K series	0.16	0.00105	0.88	0.07	MgO	Yes	
Al	EDS	K series	2.54	0.01826	13.23	0.15	Al2O3	Yes	
Si	EDS	K series	6.37	0.05048	36.52	0.26	SiO2	Yes	
K	EDS	K series	1.04	0.00882	5.61	0.14	KBr	Yes	
Ca	EDS	K series	0.26	0.00232	1.42	0.11	Wollastonite	Yes	
Ti	EDS	K series	0.08	0.00081	0.52	0.13	Ti	Yes	
Fe	EDS	K series	0.84	0.00836	5.29	0.26	Fe	Yes	

Total					100.00				

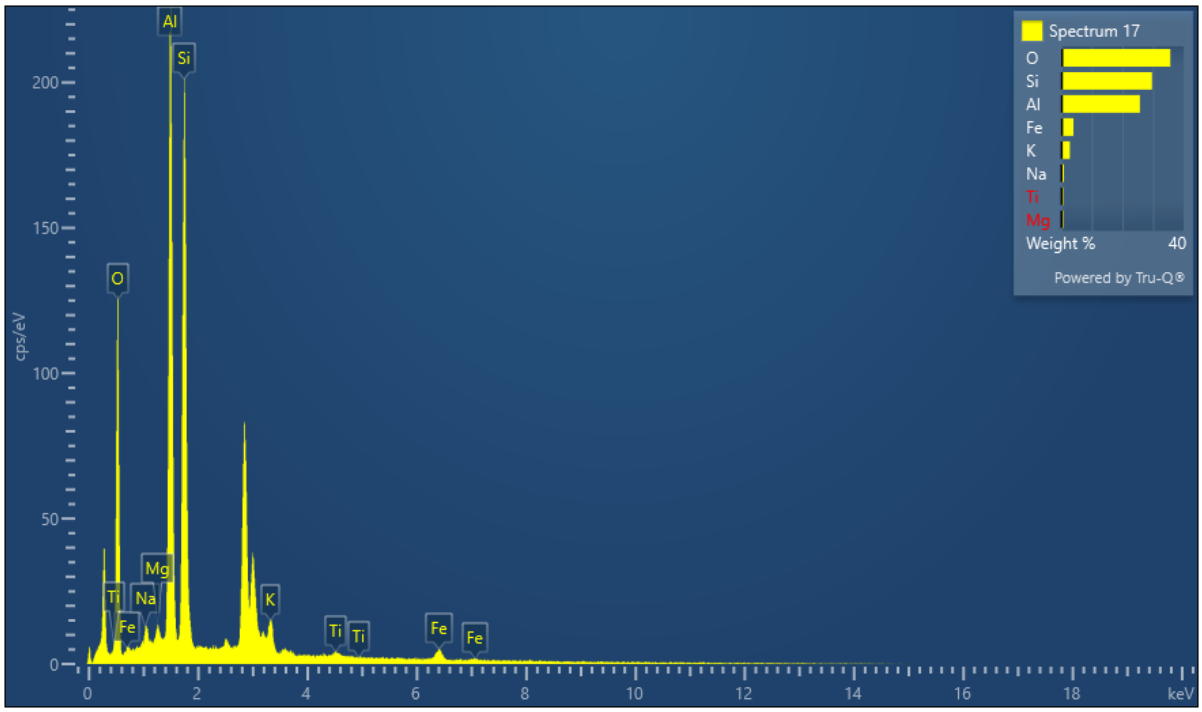

Spectrum 17

Element	Signal Type	Line	Apparent Concentration	k Ratio	Wt%	Wt% Sigma	Standard Name	Factory Standard	Standardization Date
O	EDS	K series	7.53	0.02533	35.64	0.29	SiO2	Yes	
Na	EDS	K series	0.22	0.00092	0.89	0.08	Albite	Yes	
Mg	EDS	K series	0.13	0.00088	0.65	0.07	MgO	Yes	
Al	EDS	K series	5.50	0.03951	25.68	0.20	Al2O3	Yes	
Si	EDS	K series	5.03	0.03986	29.67	0.23	SiO2	Yes	
K	EDS	K series	0.55	0.00466	2.80	0.12	KBr	Yes	
Ti	EDS	K series	0.11	0.00114	0.69	0.13	Ti	Yes	
Fe	EDS	K series	0.67	0.00670	3.99	0.25	Fe	Yes	

Total					100.00				

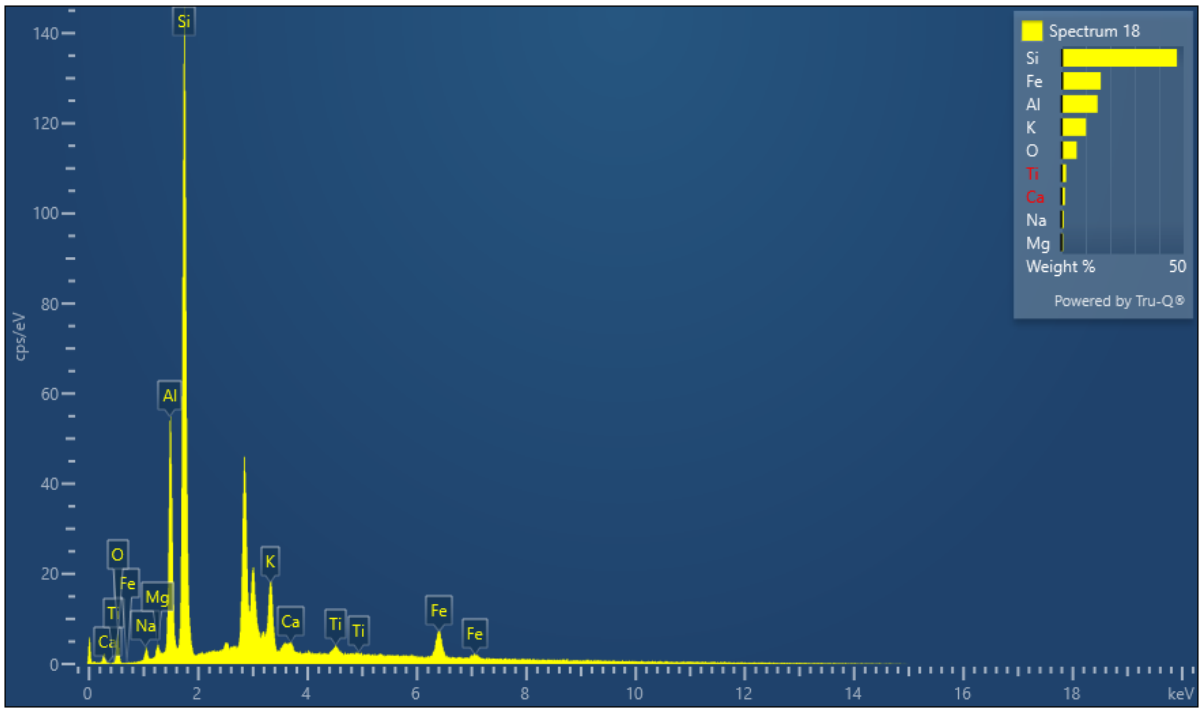

Spectrum 18

Element	Signal Type	Line	Apparent Concentration	k Ratio	Wt%	Wt% Sigma	Standard Name	Factory Standard	Standardization Date
O	EDS	K series	0.37	0.00126	6.32	0.23	SiO2	Yes	
Na	EDS	K series	0.10	0.00041	0.99	0.07	Albite	Yes	
Mg	EDS	K series	0.06	0.00042	0.76	0.06	MgO	Yes	
Al	EDS	K series	1.31	0.00941	14.85	0.18	Al2O3	Yes	
Si	EDS	K series	3.72	0.02945	47.27	0.35	SiO2	Yes	
K	EDS	K series	0.84	0.00712	10.13	0.21	KBr	Yes	
Ca	EDS	K series	0.12	0.00110	1.52	0.15	Wollastonite	Yes	

Ti	EDS	K series	0.14	0.00140	1.99	0.20	Ti	Yes	
Fe	EDS	K series	1.17	0.01171	16.18	0.41	Fe	Yes	
Total					100.00				

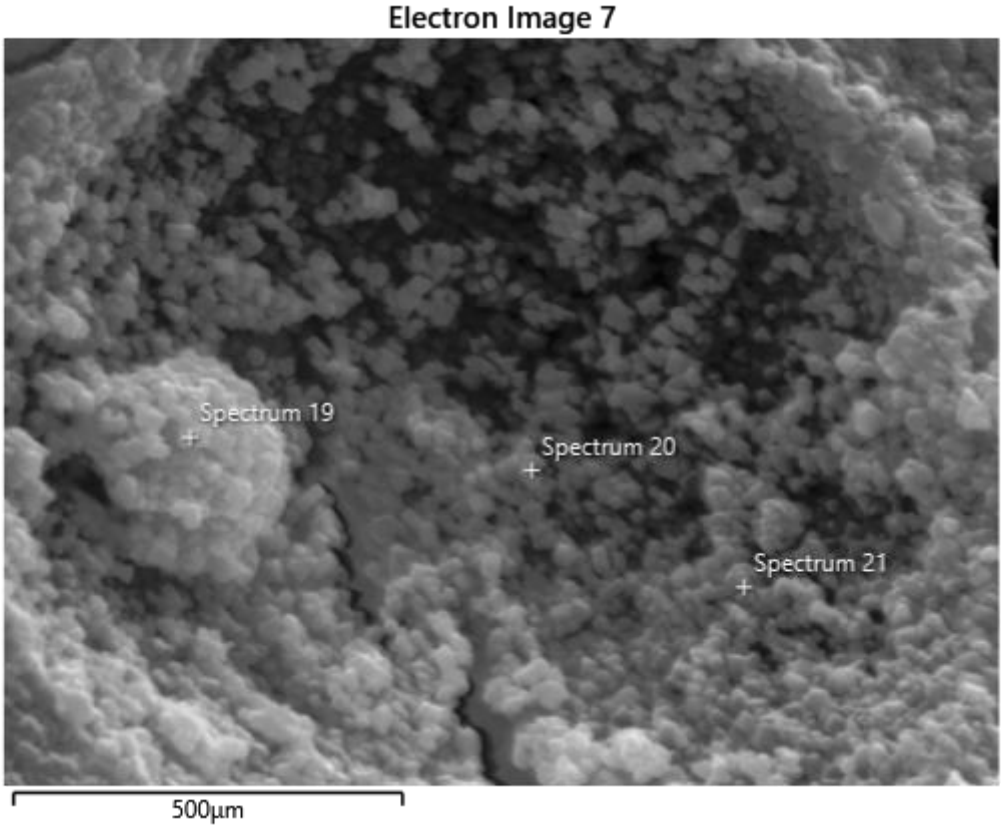

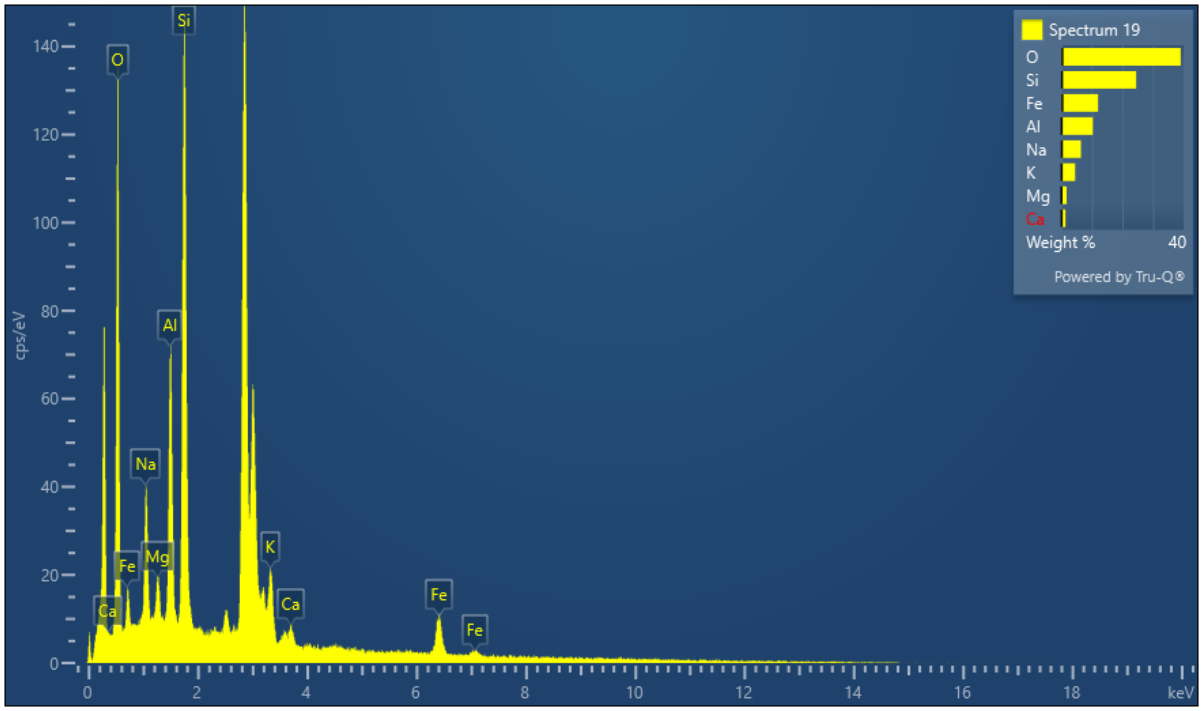

Spectrum 19

Element	Signal Type	Line	Apparent Concentration	k Ratio	Wt%	Wt% Sigma	Standard Name	Factory Standard	Standardization Date
O	EDS	K series	7.61	0.02561	39.06	0.36	SiO2	Yes	
Na	EDS	K series	1.12	0.00474	6.41	0.18	Albite	Yes	
Mg	EDS	K series	0.25	0.00164	1.76	0.12	MgO	Yes	
Al	EDS	K series	1.59	0.01142	10.34	0.17	Al2O3	Yes	
Si	EDS	K series	3.66	0.02904	24.51	0.25	SiO2	Yes	
K	EDS	K series	0.77	0.00654	4.51	0.17	KBr	Yes	
Ca	EDS	K series	0.23	0.00207	1.38	0.14	Wollastonite	Yes	
Fe	EDS	K series	1.72	0.01720	12.03	0.37	Fe	Yes	
Total					100.00				

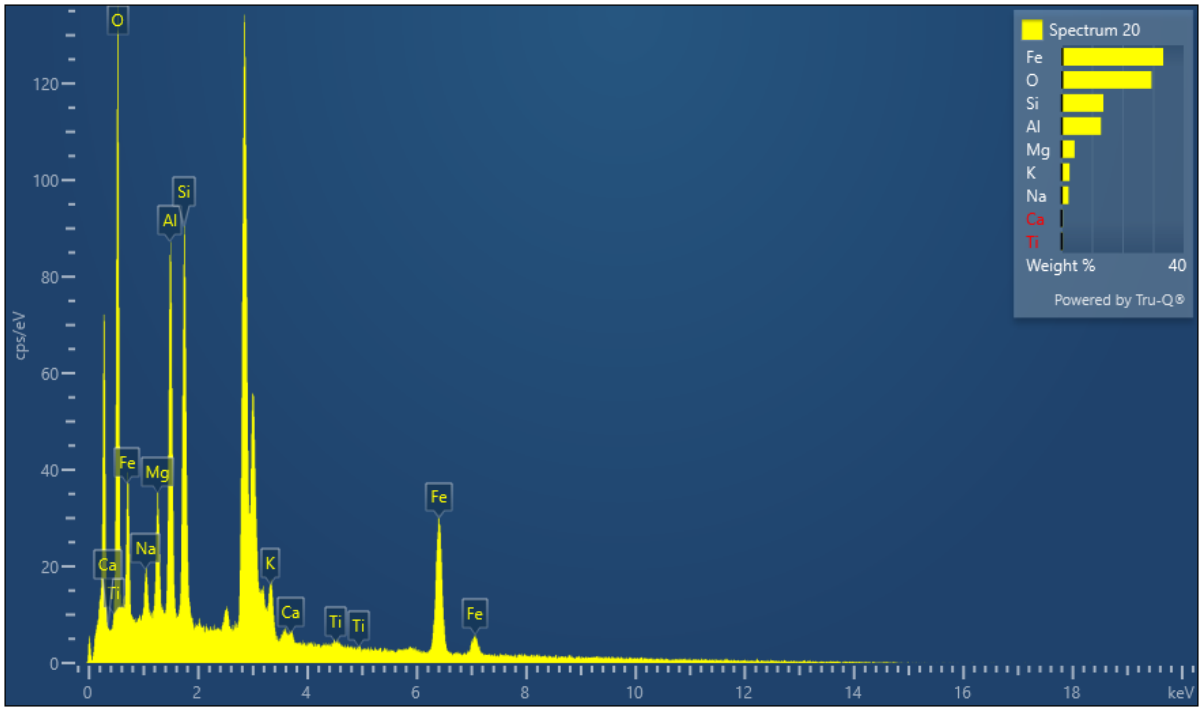

Spectrum 20

Element	Signal Type	Line	Apparent Concentration	k Ratio	Wt%	Wt% Sigma	Standard Name	Factory Standard	Standardization Date
O	EDS	K series	7.45	0.02508	29.46	0.34	SiO2	Yes	
Na	EDS	K series	0.37	0.00156	2.35	0.16	Albite	Yes	
Mg	EDS	K series	0.62	0.00409	4.39	0.14	MgO	Yes	
Al	EDS	K series	1.99	0.01431	12.97	0.19	Al2O3	Yes	
Si	EDS	K series	2.10	0.01667	13.79	0.19	SiO2	Yes	
K	EDS	K series	0.54	0.00461	2.73	0.14	KBr	Yes	
Ca	EDS	K series	0.10	0.00089	0.50	0.11	Wollastonite	Yes	
Ti	EDS	K series	0.08	0.00085	0.50	0.14	Ti	Yes	

Fe	EDS	K series	5.57	0.05567	33.30	0.40	Fe	Yes	
Total					100.00				

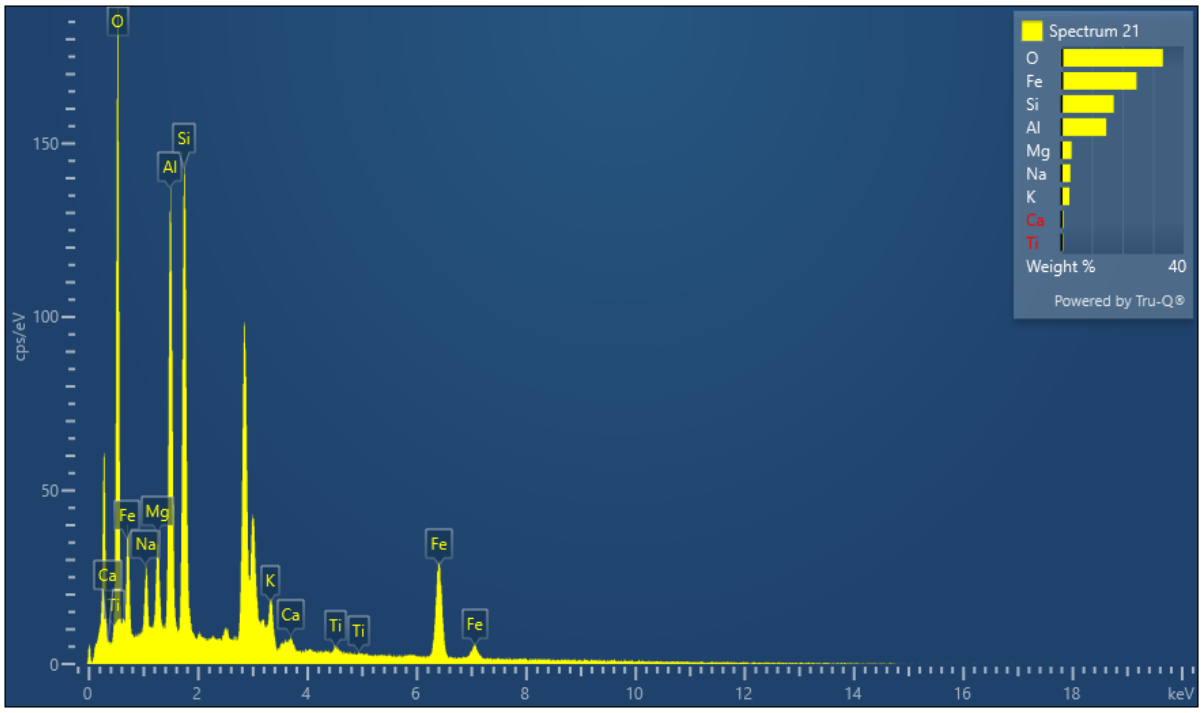

Spectrum 21

Element	Signal Type	Line	Apparent Concentration	k Ratio	Wt%	Wt% Sigma	Standard Name	Factory Standard	Standardization Date
O	EDS	K series	10.73	0.03610	33.20	0.29	SiO2	Yes	
Na	EDS	K series	0.69	0.00290	2.97	0.12	Albite	Yes	
Mg	EDS	K series	0.68	0.00449	3.37	0.11	MgO	Yes	
Al	EDS	K series	3.22	0.02310	14.73	0.16	Al2O3	Yes	
Si	EDS	K series	3.58	0.02839	17.16	0.18	SiO2	Yes	
K	EDS	K series	0.69	0.00585	2.63	0.11	KBr	Yes	

Ca	EDS	K series	0.19	0.00168	0.72	0.09	Wollastonite	Yes	
Ti	EDS	K series	0.14	0.00138	0.62	0.11	Ti	Yes	
Fe	EDS	K series	5.43	0.05430	24.60	0.32	Fe	Yes	
Total					100.00				

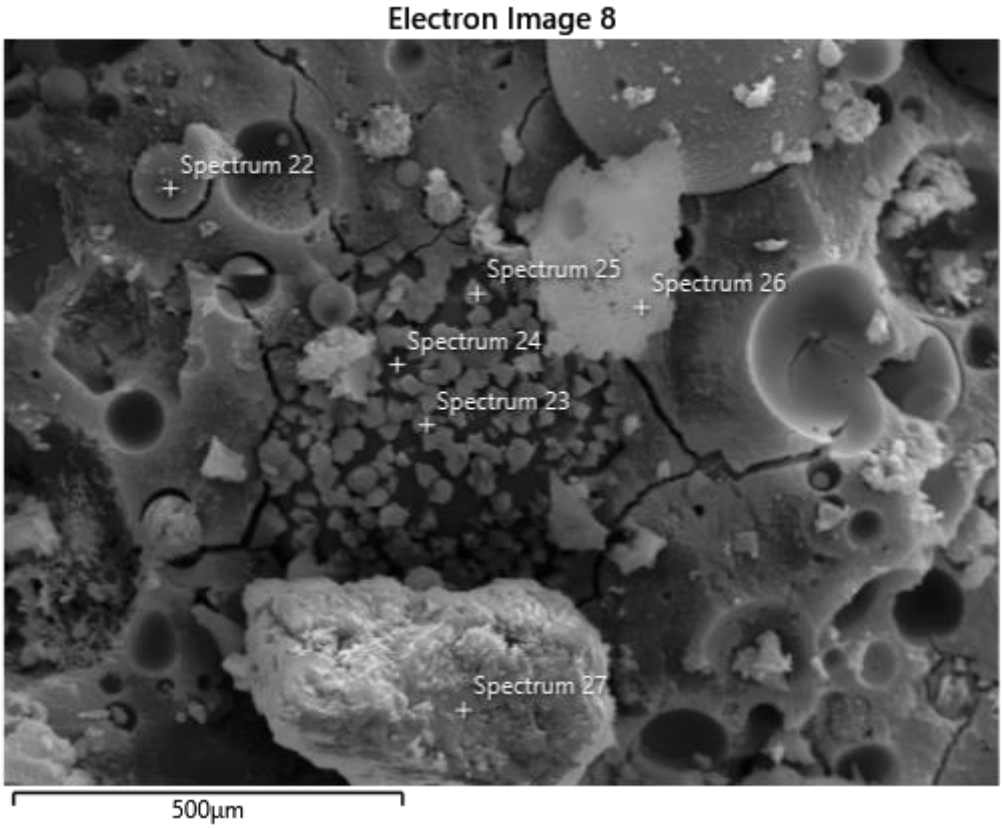

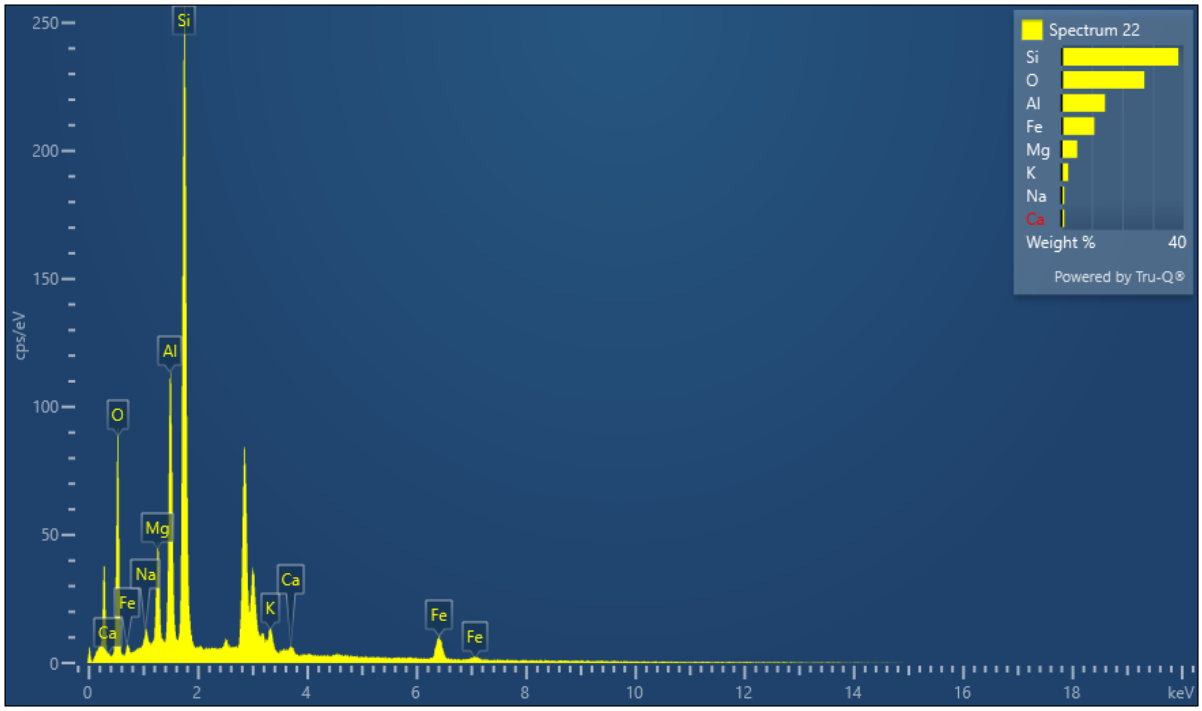

Spectrum 22

Element	Signal Type	Line	Apparent Concentration	k Ratio	Wt%	Wt% Sigma	Standard Name	Factory Standard	Standardization Date
O	EDS	K series	5.23	0.01759	27.13	0.28	SiO2	Yes	
Na	EDS	K series	0.22	0.00095	1.01	0.09	Albite	Yes	
Mg	EDS	K series	0.97	0.00646	5.21	0.11	MgO	Yes	
Al	EDS	K series	2.68	0.01924	14.30	0.16	Al2O3	Yes	
Si	EDS	K series	6.53	0.05172	38.27	0.26	SiO2	Yes	
K	EDS	K series	0.42	0.00360	2.27	0.13	KBr	Yes	
Ca	EDS	K series	0.18	0.00165	0.99	0.10	Wollastonite	Yes	
Fe	EDS	K series	1.74	0.01743	10.82	0.30	Fe	Yes	
Total					100.00				

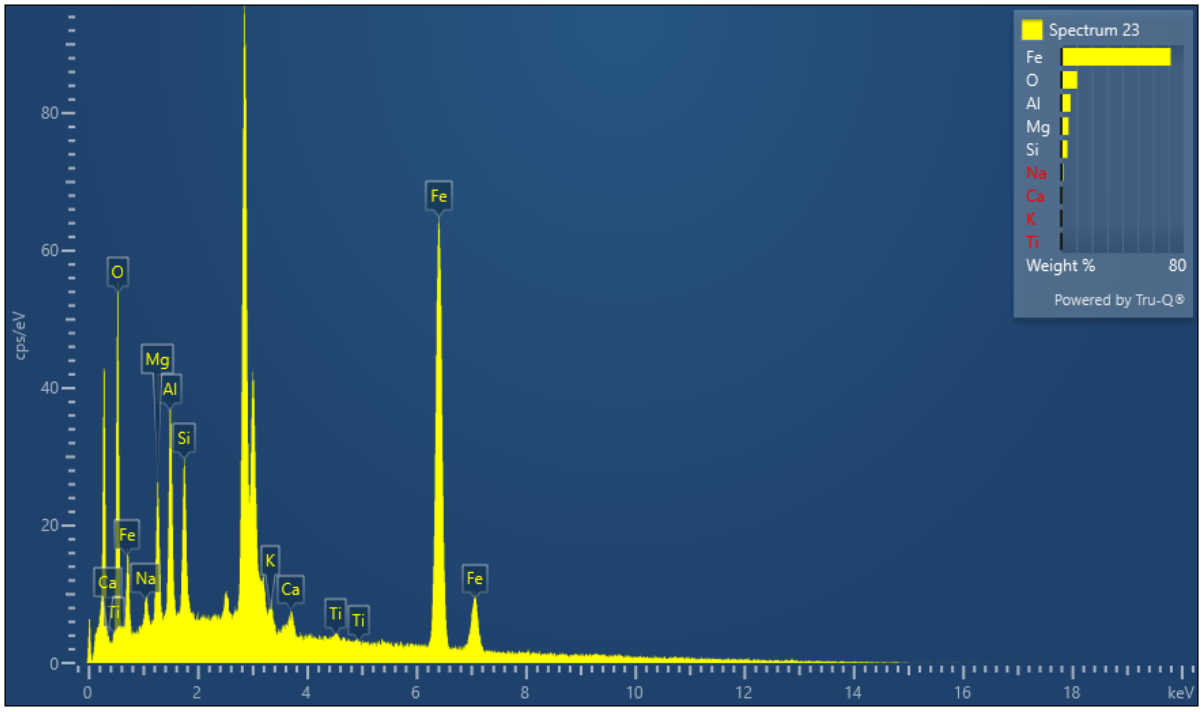

Spectrum 23

Element	Signal Type	Line	Apparent Concentration	k Ratio	Wt%	Wt% Sigma	Standard Name	Factory Standard	Standardization Date
O	EDS	K series	3.01	0.01013	10.40	0.19	SiO2	Yes	
Na	EDS	K series	0.15	0.00063	1.33	0.14	Albite	Yes	
Mg	EDS	K series	0.51	0.00338	4.75	0.14	MgO	Yes	
Al	EDS	K series	0.76	0.00547	6.09	0.13	Al2O3	Yes	
Si	EDS	K series	0.58	0.00458	4.11	0.11	SiO2	Yes	
K	EDS	K series	0.11	0.00092	0.52	0.09	KBr	Yes	
Ca	EDS	K series	0.18	0.00163	0.87	0.09	Wollastonite	Yes	
Ti	EDS	K series	0.07	0.00066	0.36	0.11	Ti	Yes	

Fe	EDS	K series	12.55	0.12551	71.55	0.32	Fe	Yes	
Total					100.00				

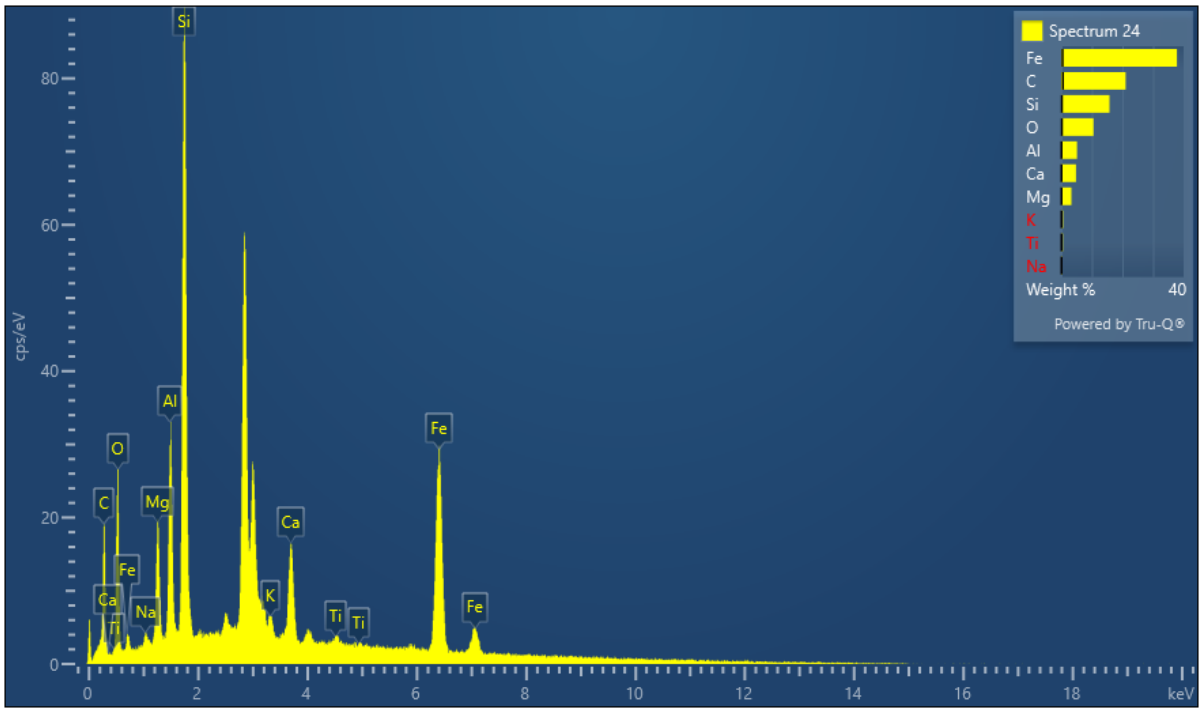

Spectrum 24

Element	Signal Type	Line	Apparent Concentration	k Ratio	Wt%	Wt% Sigma	Standard Name	Factory Standard	Standardization Date
C	EDS	K series	0.64	0.00637	21.04	0.56	C Vit	Yes	
O	EDS	K series	1.50	0.00504	10.54	0.22	SiO2	Yes	
Na	EDS	K series	0.05	0.00022	0.39	0.07	Albite	Yes	
Mg	EDS	K series	0.41	0.00275	3.33	0.09	MgO	Yes	
Al	EDS	K series	0.71	0.00510	5.17	0.10	Al2O3	Yes	
Si	EDS	K series	2.29	0.01813	15.75	0.18	SiO2	Yes	

K	EDS	K series	0.11	0.00091	0.61	0.08	KBr	Yes	
Ca	EDS	K series	0.84	0.00750	4.79	0.12	Wollastonite	Yes	
Ti	EDS	K series	0.08	0.00083	0.56	0.11	Ti	Yes	
Fe	EDS	K series	5.48	0.05481	37.82	0.40	Fe	Yes	
Total					100.00				

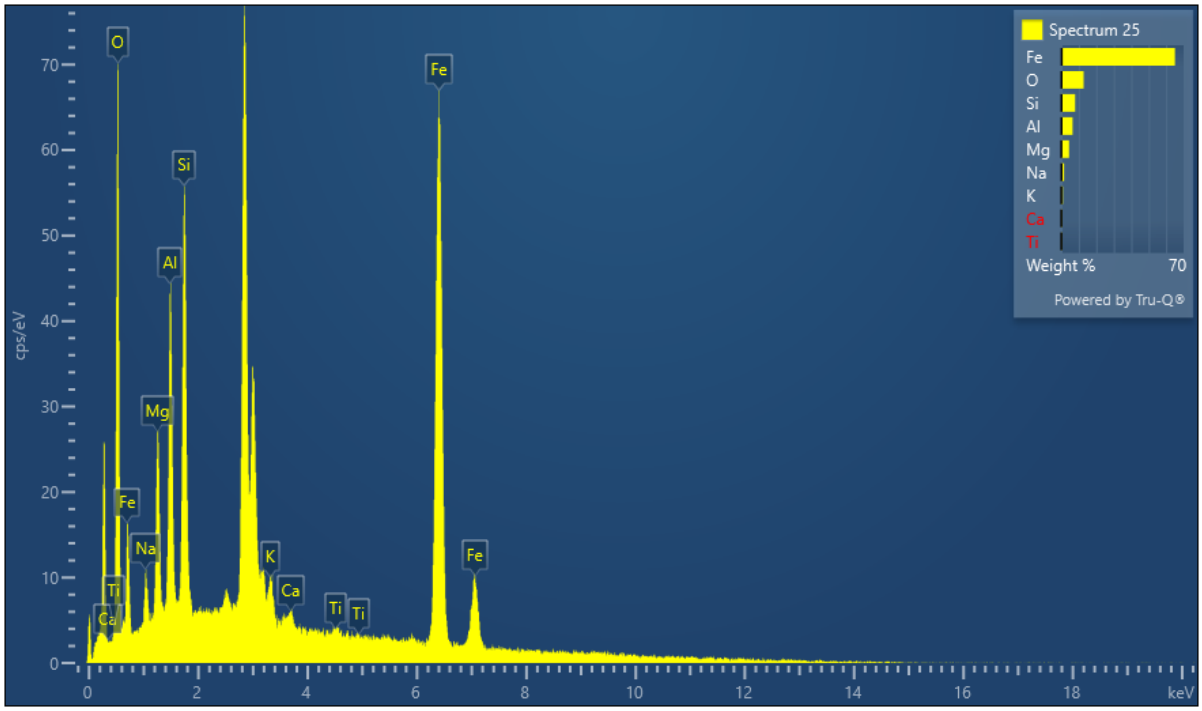

Spectrum 25

Element	Signal Type	Line	Apparent Concentration	k Ratio	Wt%	Wt% Sigma	Standard Name	Factory Standard	Standardization Date
O	EDS	K series	4.01	0.01349	12.85	0.18	SiO2	Yes	
Na	EDS	K series	0.21	0.00090	1.63	0.12	Albite	Yes	
Mg	EDS	K series	0.55	0.00365	4.41	0.12	MgO	Yes	

Al	EDS	K series	0.93	0.00671	6.47	0.12	Al2O3	Yes	
Si	EDS	K series	1.28	0.01011	7.97	0.13	SiO2	Yes	
K	EDS	K series	0.22	0.00182	0.94	0.09	KBr	Yes	
Ca	EDS	K series	0.10	0.00085	0.42	0.08	Wollastonite	Yes	
Ti	EDS	K series	0.06	0.00064	0.32	0.10	Ti	Yes	
Fe	EDS	K series	12.54	0.12539	64.99	0.29	Fe	Yes	
Total					100.00				

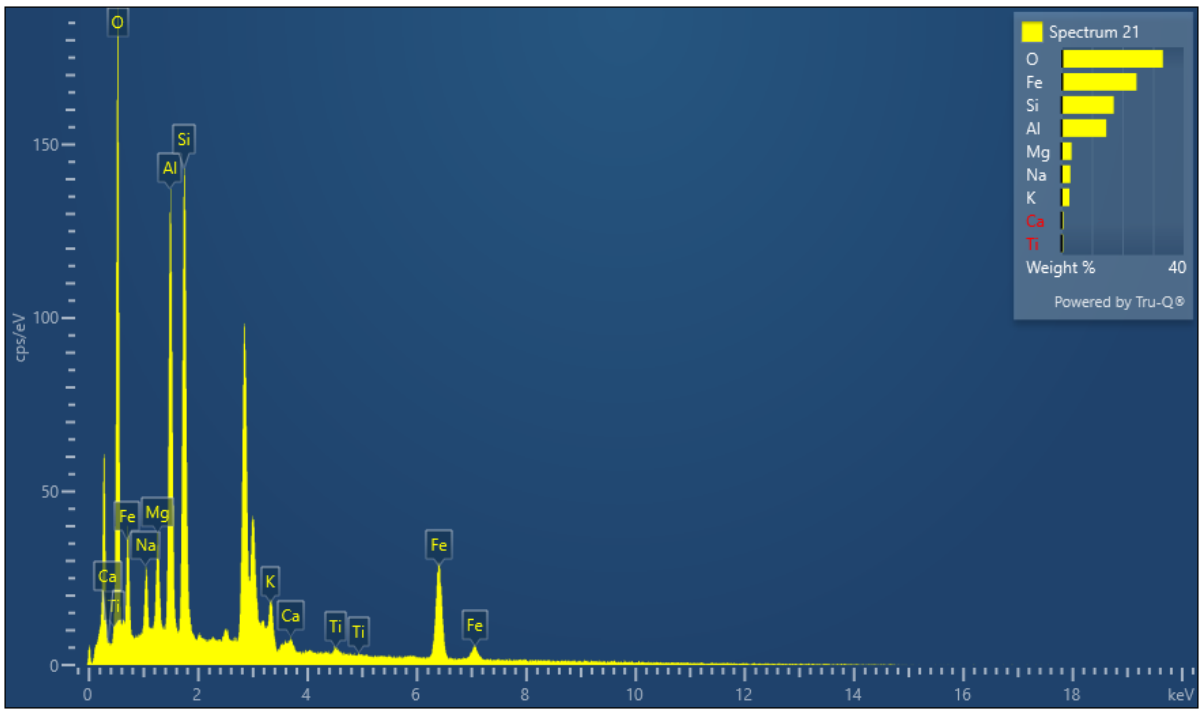

Spectrum 21

Element	Signal Type	Line	Apparent Concentration	k Ratio	Wt%	Wt% Sigma	Standard Name	Factory Standard	Standardization Date
O	EDS	K series	10.73	0.03610	33.20	0.29	SiO2	Yes	

Na	EDS	K series	0.69	0.00290	2.97	0.12	Albite	Yes	
Mg	EDS	K series	0.68	0.00449	3.37	0.11	MgO	Yes	
Al	EDS	K series	3.22	0.02310	14.73	0.16	Al2O3	Yes	
Si	EDS	K series	3.58	0.02839	17.16	0.18	SiO2	Yes	
K	EDS	K series	0.69	0.00585	2.63	0.11	KBr	Yes	
Ca	EDS	K series	0.19	0.00168	0.72	0.09	Wollastonite	Yes	
Ti	EDS	K series	0.14	0.00138	0.62	0.11	Ti	Yes	
Fe	EDS	K series	5.43	0.05430	24.60	0.32	Fe	Yes	
Total					100.00				

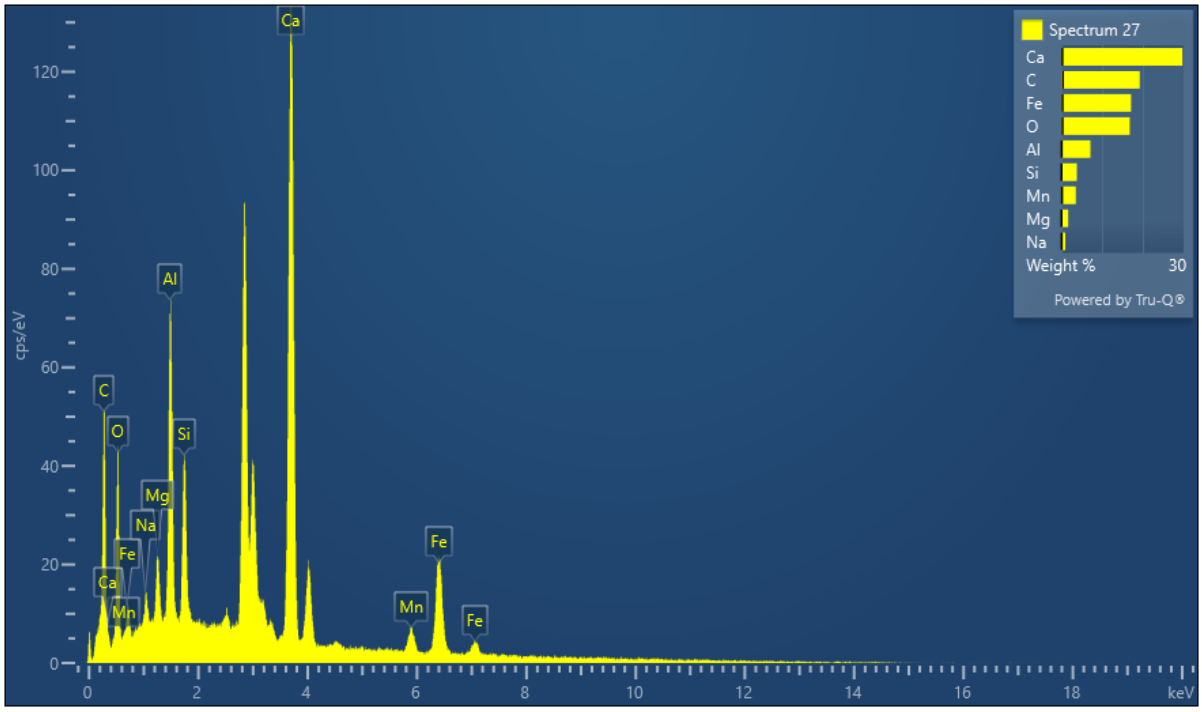

Spectrum 27

Element	Signal Type	Line	Apparent Concentration	k Ratio	Wt%	Wt% Sigma	Standard Name	Factory Standard	Standardization Date
C	EDS	K series	1.43	0.01434	19.24	0.42	C Vit	Yes	
O	EDS	K series	2.36	0.00794	16.77	0.32	SiO2	Yes	
Na	EDS	K series	0.22	0.00095	0.98	0.09	Albite	Yes	
Mg	EDS	K series	0.35	0.00229	1.68	0.08	MgO	Yes	
Al	EDS	K series	1.64	0.01175	7.15	0.12	Al2O3	Yes	
Si	EDS	K series	0.89	0.00708	3.81	0.09	SiO2	Yes	
Ca	EDS	K series	8.32	0.07435	29.70	0.27	Wollastonite	Yes	
Mn	EDS	K series	0.78	0.00776	3.57	0.19	Mn	Yes	
Fe	EDS	K series	3.81	0.03806	17.12	0.30	Fe	Yes	
Total					100.00				

Neat Geopolymer

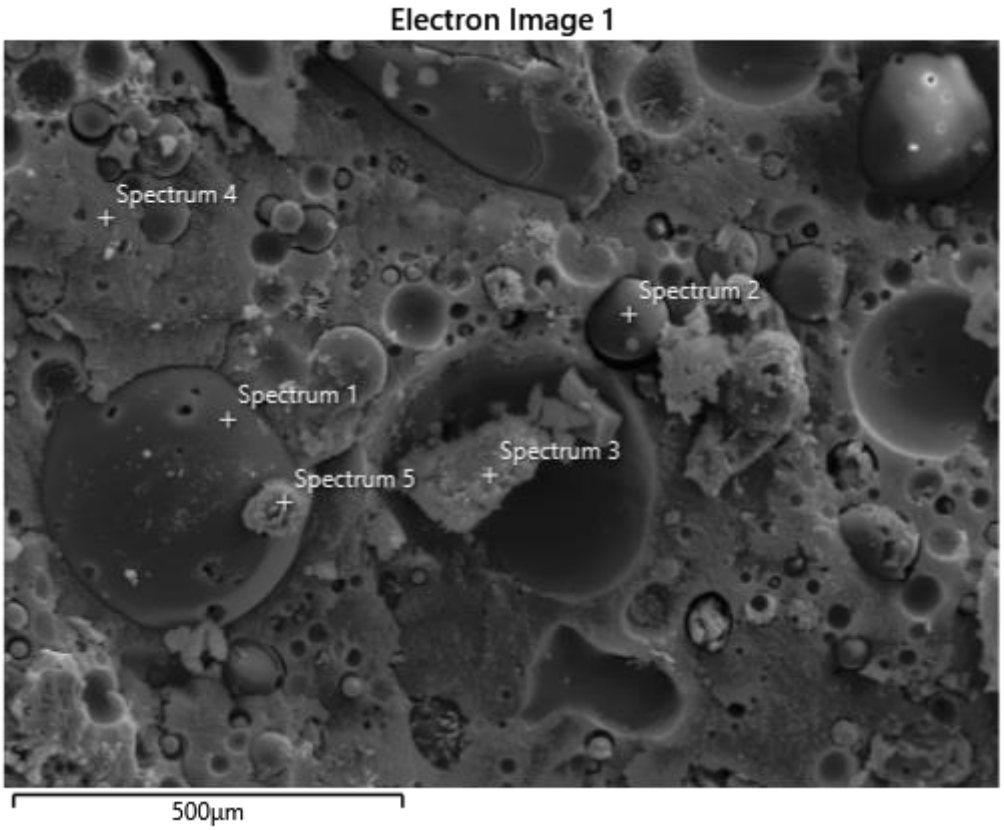

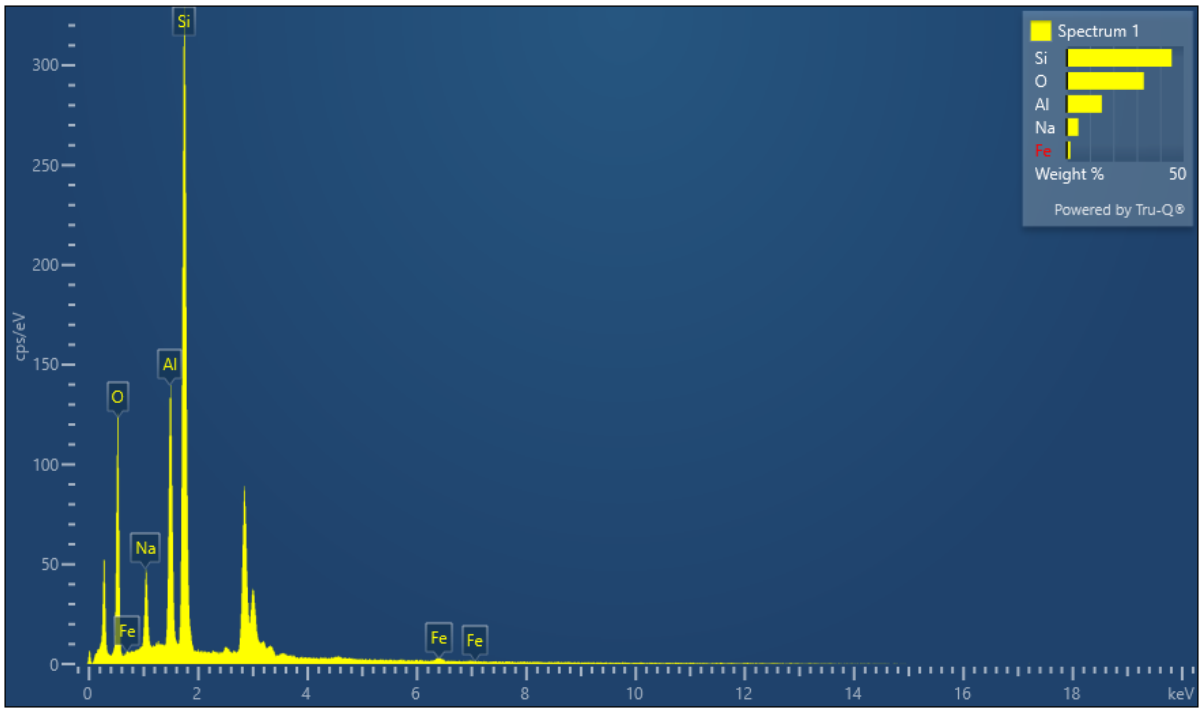

Spectrum 1									
Element	Signal Type	Line	Apparent Concentration	k Ratio	Wt%	Wt% Sigma	Standard Name	Factory Standard	Standardization Date
O	EDS	K series	7.06	0.02376	33.03	0.29	SiO2	Yes	
Na	EDS	K series	1.39	0.00588	5.17	0.12	Albite	Yes	
Al	EDS	K series	3.28	0.02357	15.13	0.16	Al2O3	Yes	
Si	EDS	K series	8.48	0.06717	44.91	0.27	SiO2	Yes	
Fe	EDS	K series	0.29	0.00294	1.76	0.23	Fe	Yes	
Total					100.00				

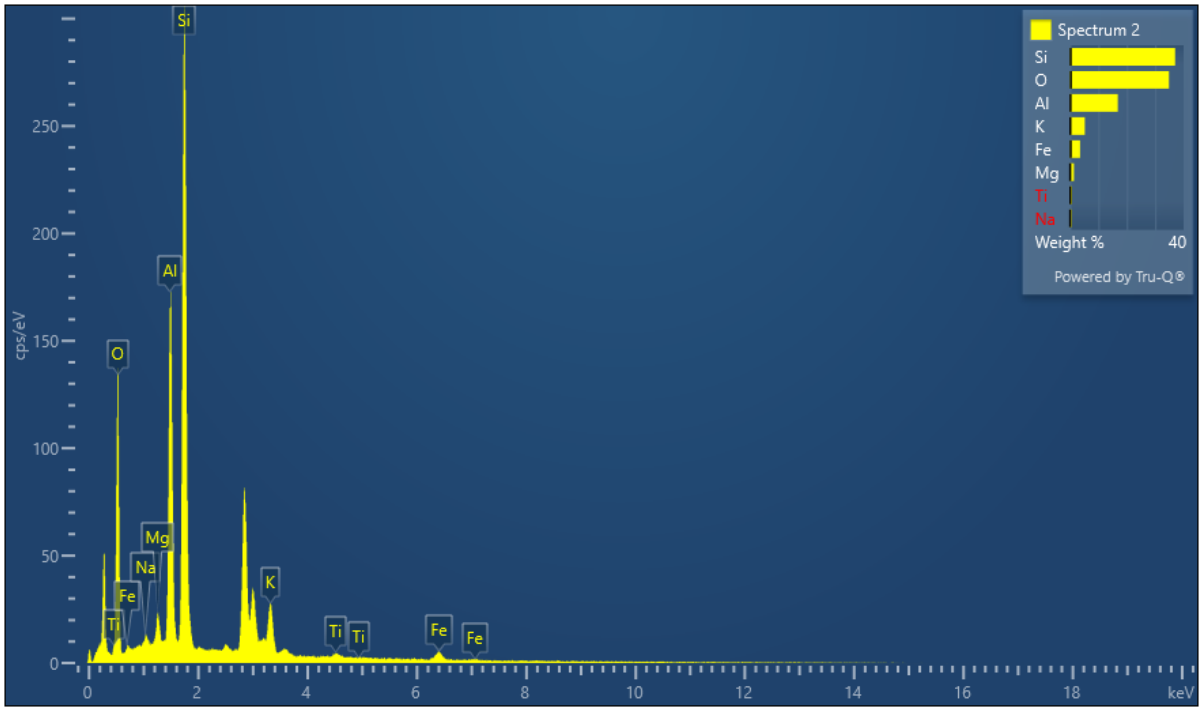

Spectrum 2									
Element	Signal Type	Line	Apparent Concentration	k Ratio	Wt%	Wt% Sigma	Standard Name	Factory Standard	Standardization Date
O	EDS	K series	7.80	0.02623	34.86	0.30	SiO2	Yes	

Na	EDS	K series	0.16	0.00067	0.56	0.08	Albite	Yes	
Mg	EDS	K series	0.33	0.00220	1.40	0.08	MgO	Yes	
Al	EDS	K series	4.13	0.02968	16.84	0.16	Al2O3	Yes	
Si	EDS	K series	7.83	0.06207	36.98	0.25	SiO2	Yes	
K	EDS	K series	1.18	0.00997	5.21	0.14	KBr	Yes	
Ti	EDS	K series	0.12	0.00125	0.66	0.12	Ti	Yes	
Fe	EDS	K series	0.68	0.00676	3.50	0.23	Fe	Yes	
Total					100.00				

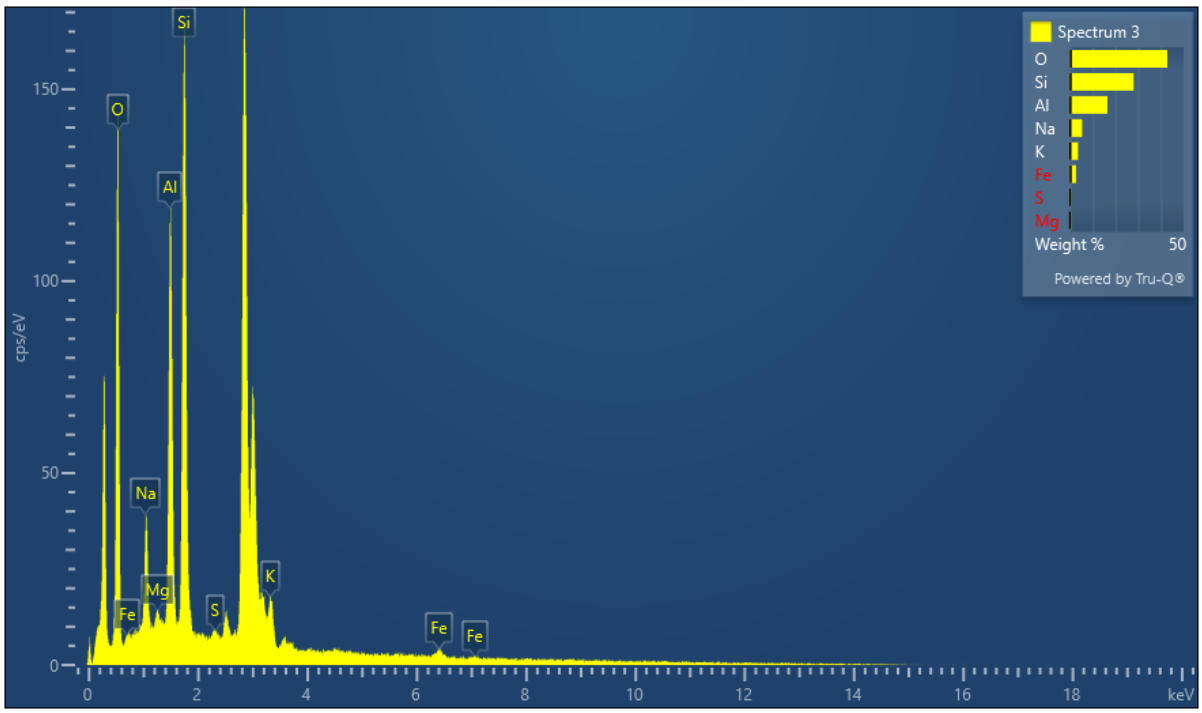

Spectrum 3

Element	Signal Type	Line	Apparent Concentration	k Ratio	Wt%	Wt% Sigma	Standard Name	Factory Standard	Standardization Date
O	EDS	K series	8.24	0.02771	42.79	0.36	SiO2	Yes	

Na	EDS	K series	1.06	0.00447	5.31	0.16	Albite	Yes	
Mg	EDS	K series	0.09	0.00058	0.56	0.11	MgO	Yes	
Al	EDS	K series	2.76	0.01981	16.44	0.20	Al2O3	Yes	
Si	EDS	K series	4.15	0.03287	27.99	0.27	SiO2	Yes	
S	EDS	K series	0.11	0.00092	0.77	0.12	FeS2	Yes	
K	EDS	K series	0.58	0.00492	3.52	0.18	KBr	Yes	
Fe	EDS	K series	0.36	0.00364	2.62	0.33	Fe	Yes	
Total					100.00				

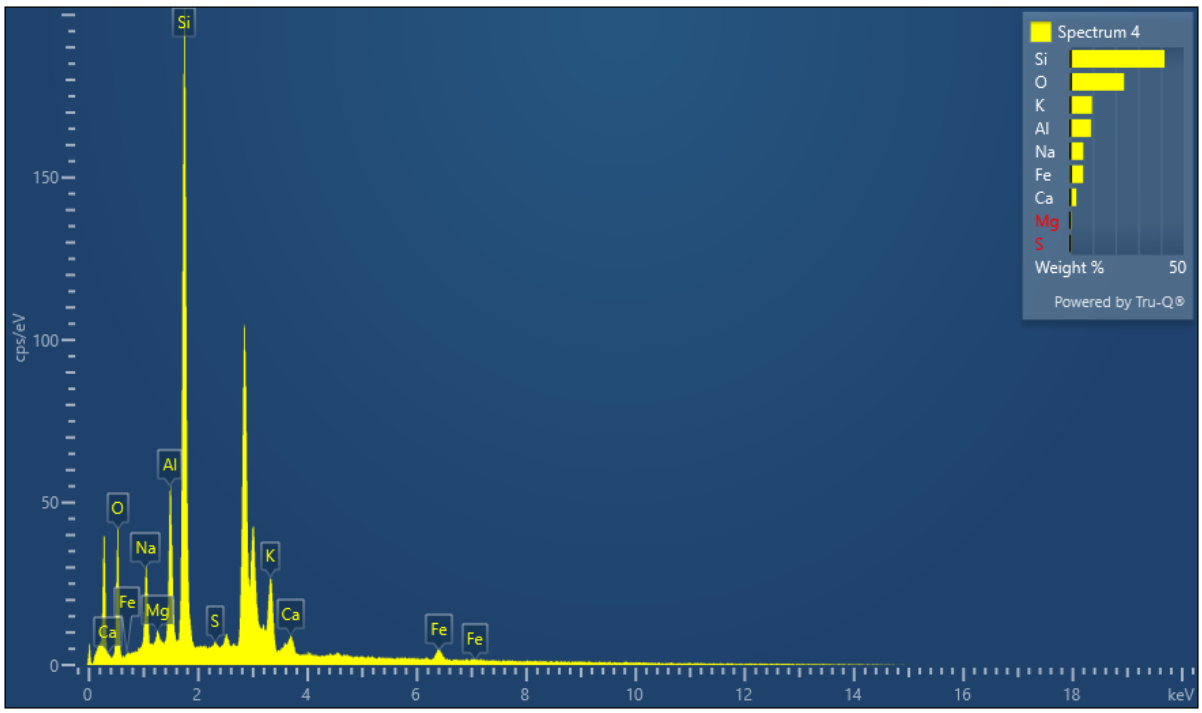

Spectrum 4

Element	Signal Type	Line	Apparent Concentration	k Ratio	Wt%	Wt% Sigma	Standard Name	Factory Standard	Standardization Date

O	EDS	K series	2.36	0.00795	23.78	0.36	SiO2	Yes	
Na	EDS	K series	0.91	0.00384	5.81	0.15	Albite	Yes	
Mg	EDS	K series	0.09	0.00061	0.76	0.10	MgO	Yes	
Al	EDS	K series	1.19	0.00853	9.19	0.16	Al2O3	Yes	
Si	EDS	K series	5.08	0.04025	41.59	0.33	SiO2	Yes	
S	EDS	K series	0.07	0.00059	0.68	0.12	FeS2	Yes	
K	EDS	K series	1.20	0.01013	9.61	0.21	KBr	Yes	
Ca	EDS	K series	0.34	0.00300	2.79	0.17	Wollastonite	Yes	
Fe	EDS	K series	0.61	0.00614	5.79	0.35	Fe	Yes	
Total					100.00				

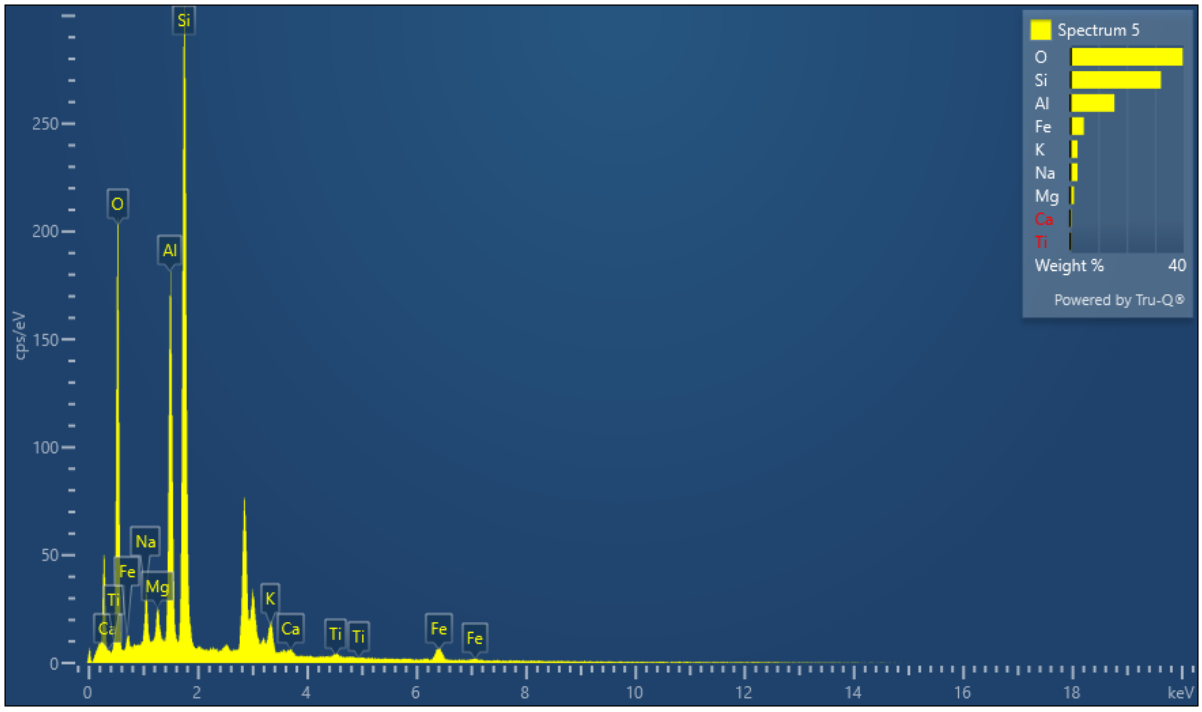

Spectrum 5									
Element	Signal Type	Line	Apparent Concentration	k Ratio	Wt%	Wt% Sigma	Standard Name	Factory Standard	Standardization Date
O	EDS	K series	11.83	0.03981	39.71	0.28	SiO2	Yes	
Na	EDS	K series	0.83	0.00351	2.62	0.09	Albite	Yes	
Mg	EDS	K series	0.36	0.00241	1.40	0.07	MgO	Yes	
Al	EDS	K series	4.29	0.03081	15.65	0.15	Al2O3	Yes	
Si	EDS	K series	7.80	0.06183	32.03	0.22	SiO2	Yes	
K	EDS	K series	0.70	0.00594	2.62	0.11	KBr	Yes	
Ca	EDS	K series	0.17	0.00148	0.63	0.08	Wollastonite	Yes	
Ti	EDS	K series	0.11	0.00110	0.49	0.10	Ti	Yes	
Fe	EDS	K series	1.10	0.01099	4.85	0.22	Fe	Yes	
Total					100.00				

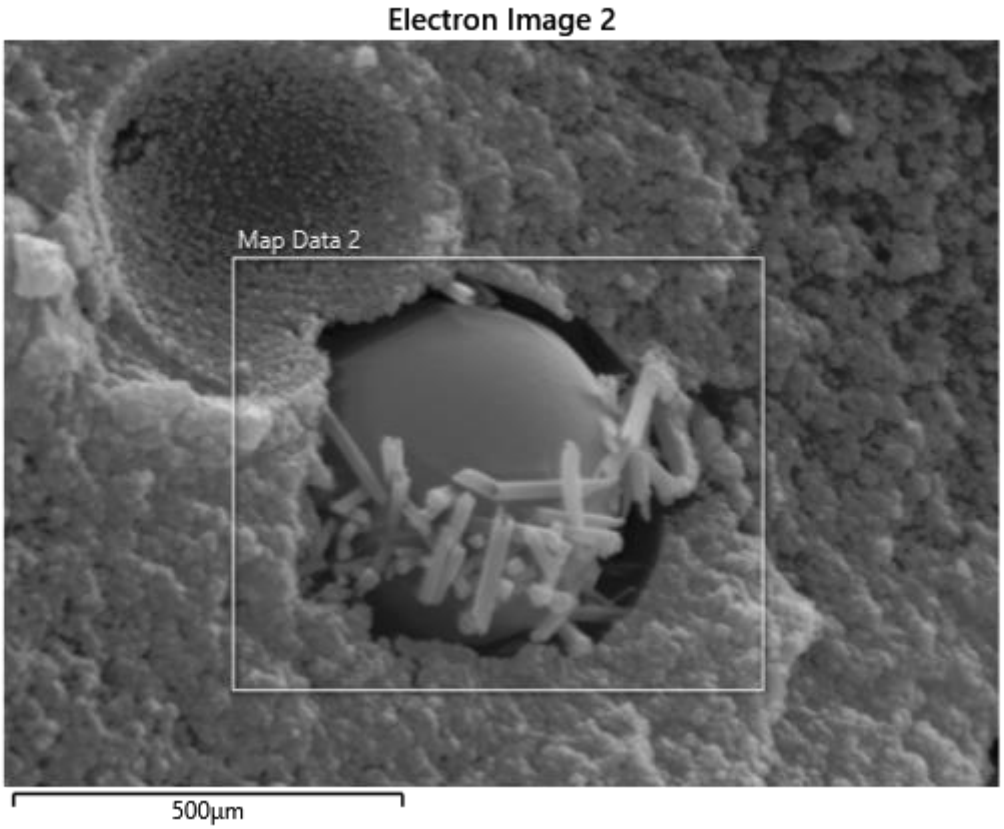
Electron Image 2
Map Data 2
500µm

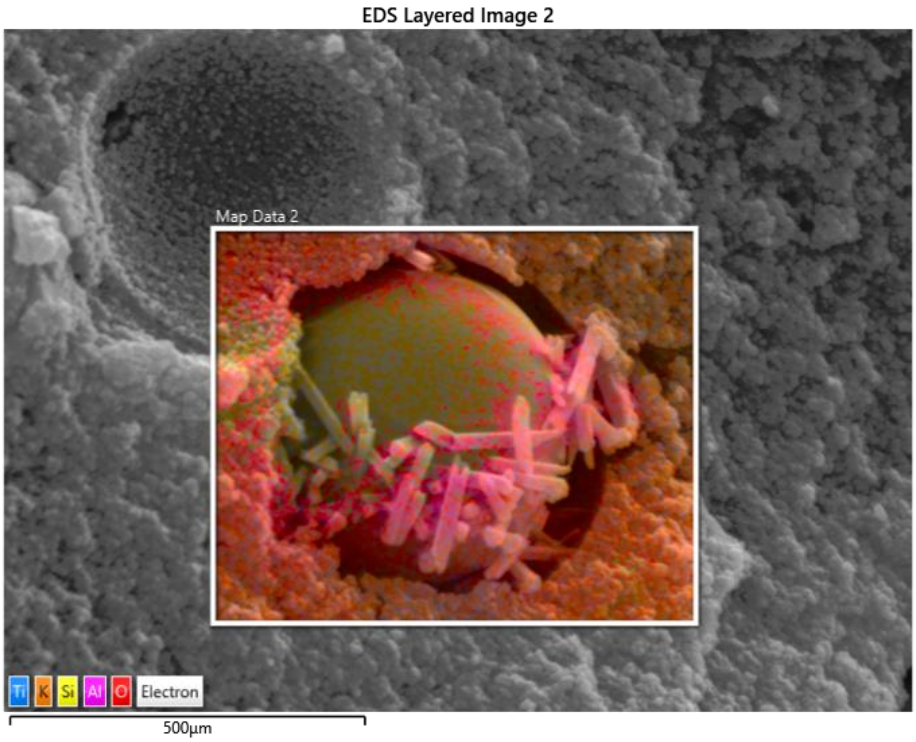
EDS Layered Image 2
Map Data 2
Ti
K
Si
Al
O
Electron
500µm

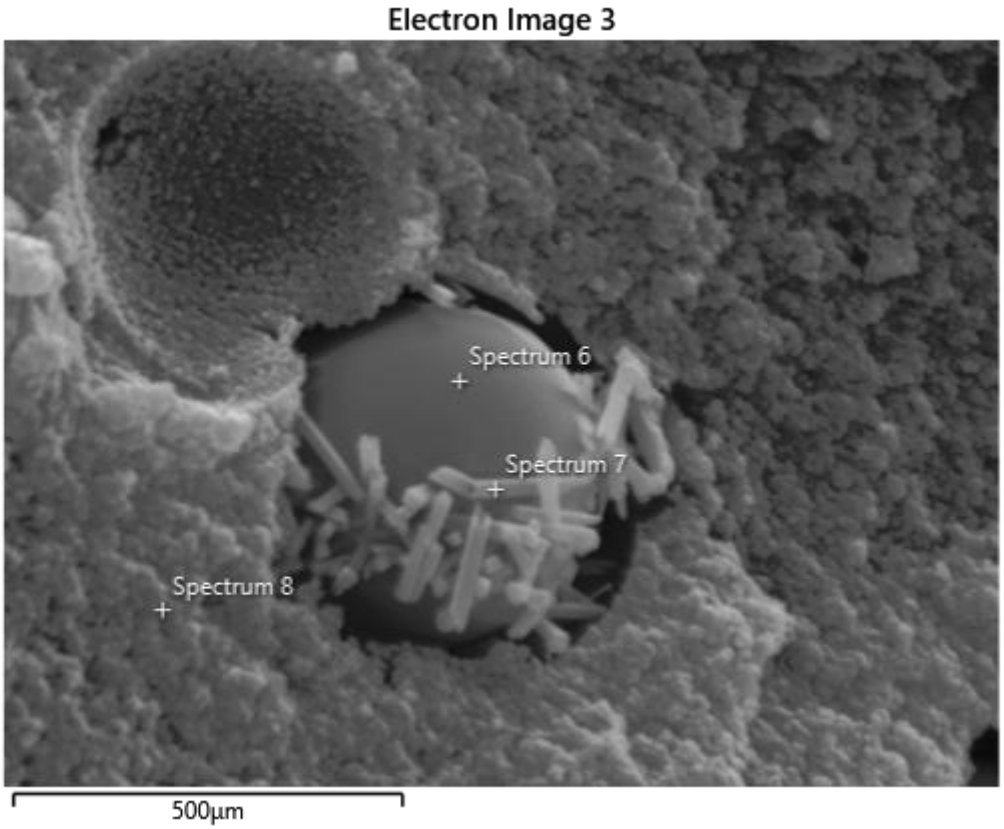
Electron Image 3
Spectrum 6
Spectrum 7
Spectrum 8
500µm

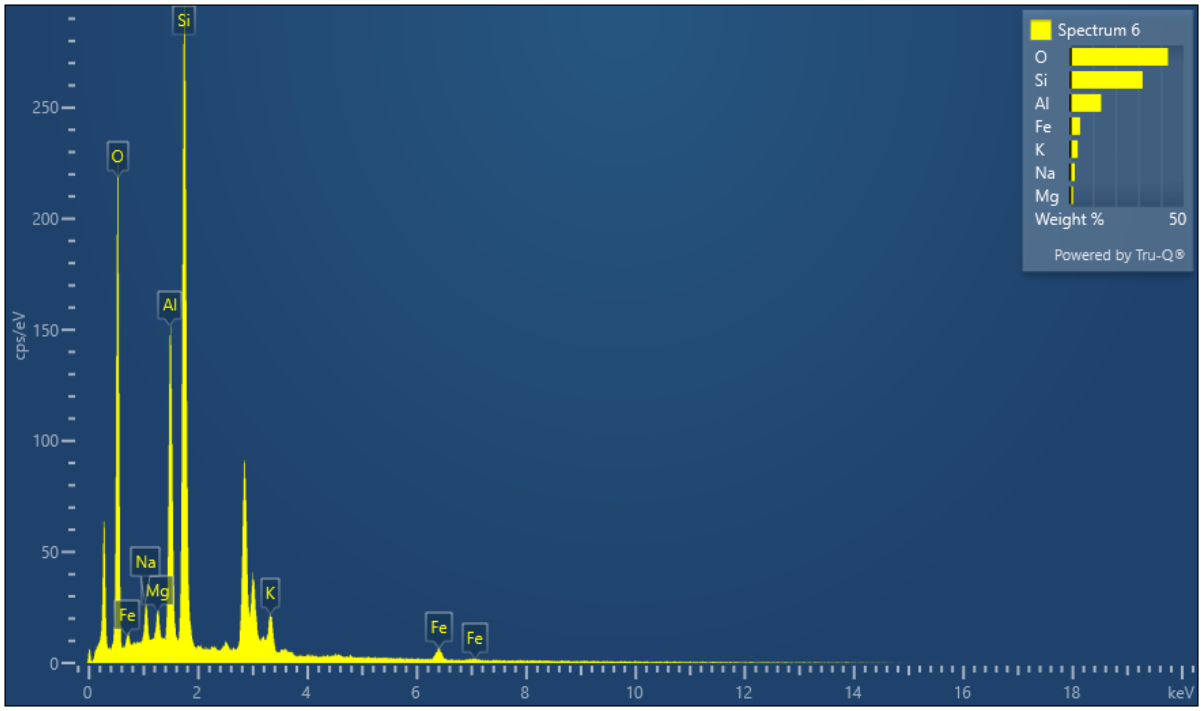
Spectrum 6
O
Si
Al
Fe
K
Na
Mg
Weight %
50
Powered by Tru-Q®
cps/eV
250
200
150
100
50
0
Si
O
Al
Na
Mg
Fe
K
Fe
Fe
0
2
4
6
8
10
12
14
16
18
keV

Spectrum 6

Element	Signal Type	Line	Apparent Concentration	k Ratio	Wt%	Wt% Sigma	Standard Name	Factory Standard	Standardization Date
O	EDS	K series	12.86	0.04327	43.12	0.28	SiO2	Yes	
Na	EDS	K series	0.63	0.00267	2.11	0.10	Albite	Yes	
Mg	EDS	K series	0.33	0.00217	1.32	0.08	MgO	Yes	
Al	EDS	K series	3.59	0.02579	13.71	0.14	Al2O3	Yes	
Si	EDS	K series	7.58	0.06006	31.96	0.22	SiO2	Yes	
K	EDS	K series	0.86	0.00729	3.36	0.12	KBr	Yes	
Fe	EDS	K series	0.96	0.00959	4.43	0.22	Fe	Yes	
Total					100.00				

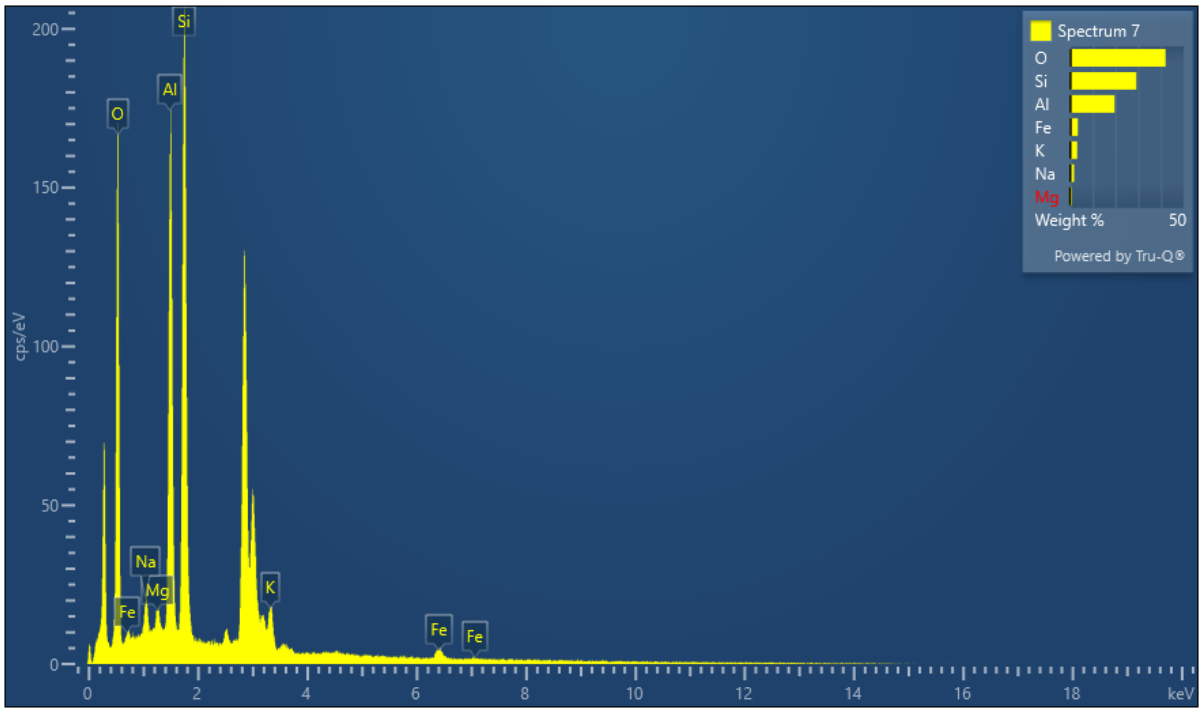

Spectrum 7

Element	Signal Type	Line	Apparent Concentration	k Ratio	Wt%	Wt% Sigma	Standard Name	Factory Standard	Standardization Date
O	EDS	K series	9.81	0.03303	42.06	0.32	SiO2	Yes	
Na	EDS	K series	0.43	0.00182	1.78	0.11	Albite	Yes	
Mg	EDS	K series	0.17	0.00115	0.86	0.09	MgO	Yes	
Al	EDS	K series	4.14	0.02975	19.61	0.19	Al2O3	Yes	
Si	EDS	K series	5.22	0.04137	29.14	0.24	SiO2	Yes	
K	EDS	K series	0.63	0.00533	3.12	0.15	KBr	Yes	
Fe	EDS	K series	0.58	0.00584	3.43	0.27	Fe	Yes	
Total					100.00				

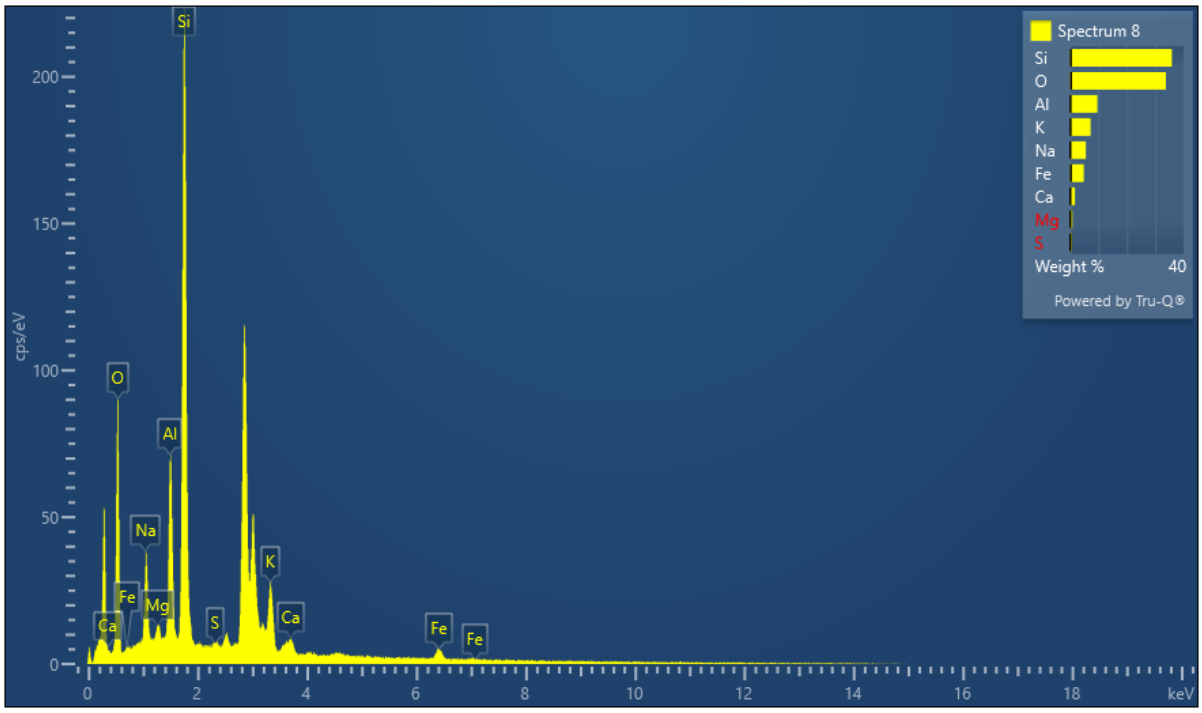

Spectrum 8

Element	Signal Type	Line	Apparent Concentration	k Ratio	Wt%	Wt% Sigma	Standard Name	Factory Standard	Standardization Date
O	EDS	K series	5.24	0.01764	33.78	0.34	SiO2	Yes	
Na	EDS	K series	1.11	0.00467	5.55	0.14	Albite	Yes	
Mg	EDS	K series	0.13	0.00087	0.84	0.09	MgO	Yes	
Al	EDS	K series	1.61	0.01160	9.61	0.15	Al2O3	Yes	
Si	EDS	K series	5.70	0.04517	35.83	0.28	SiO2	Yes	
S	EDS	K series	0.08	0.00068	0.57	0.10	FeS2	Yes	
K	EDS	K series	1.20	0.01019	7.24	0.18	KBr	Yes	
Ca	EDS	K series	0.28	0.00253	1.75	0.14	Wollastonite	Yes	
Fe	EDS	K series	0.68	0.00679	4.83	0.30	Fe	Yes	
Total					100.00				

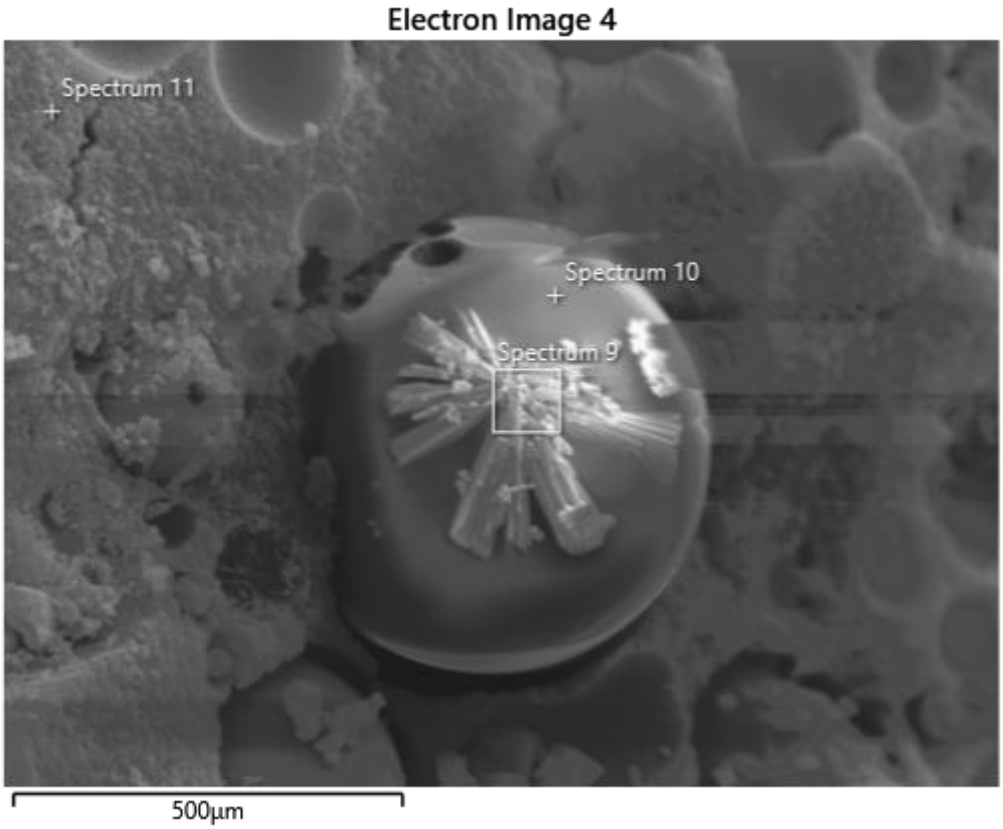

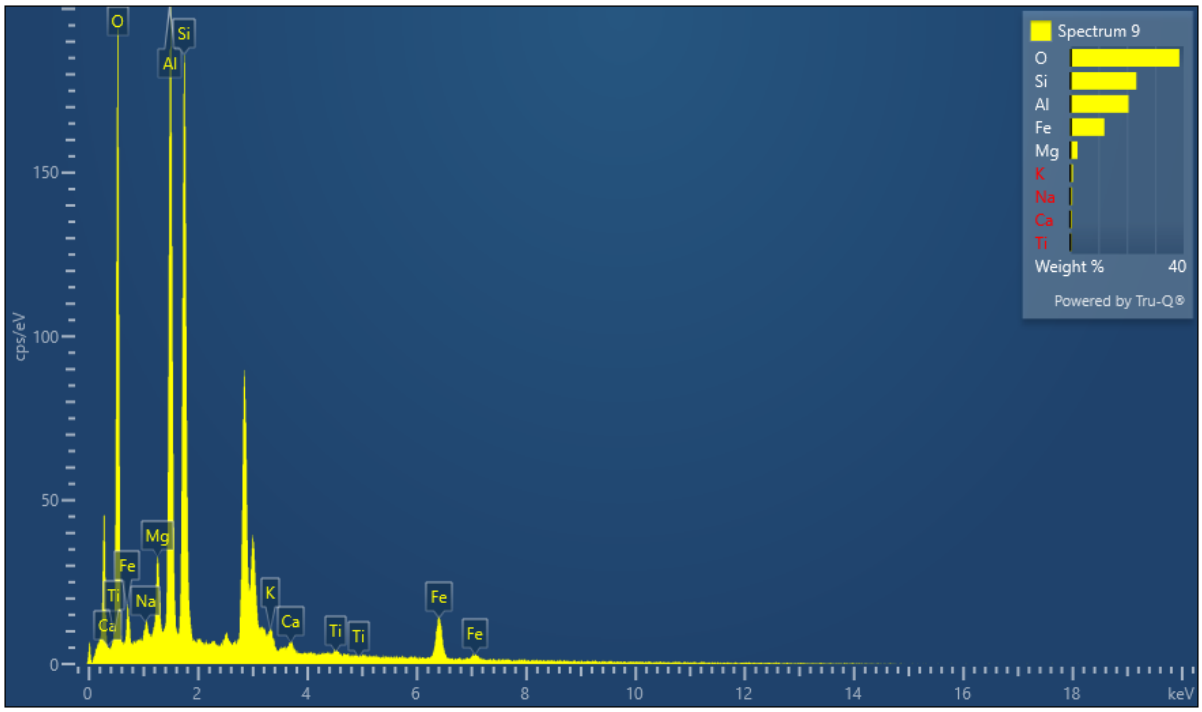

Spectrum 9									
Element	Signal Type	Line	Apparent Concentration	k Ratio	Wt%	Wt% Sigma	Standard Name	Factory Standard	Standardization Date

O	EDS	K series	11.37	0.03827	38.47	0.29	SiO2	Yes	
Na	EDS	K series	0.19	0.00082	0.76	0.09	Albite	Yes	
Mg	EDS	K series	0.58	0.00386	2.63	0.09	MgO	Yes	
Al	EDS	K series	4.79	0.03441	20.57	0.18	Al2O3	Yes	
Si	EDS	K series	4.71	0.03730	23.32	0.20	SiO2	Yes	
K	EDS	K series	0.24	0.00203	0.99	0.10	KBr	Yes	
Ca	EDS	K series	0.17	0.00156	0.72	0.09	Wollastonite	Yes	
Ti	EDS	K series	0.09	0.00092	0.45	0.11	Ti	Yes	
Fe	EDS	K series	2.48	0.02480	12.09	0.28	Fe	Yes	
Total					100.00				

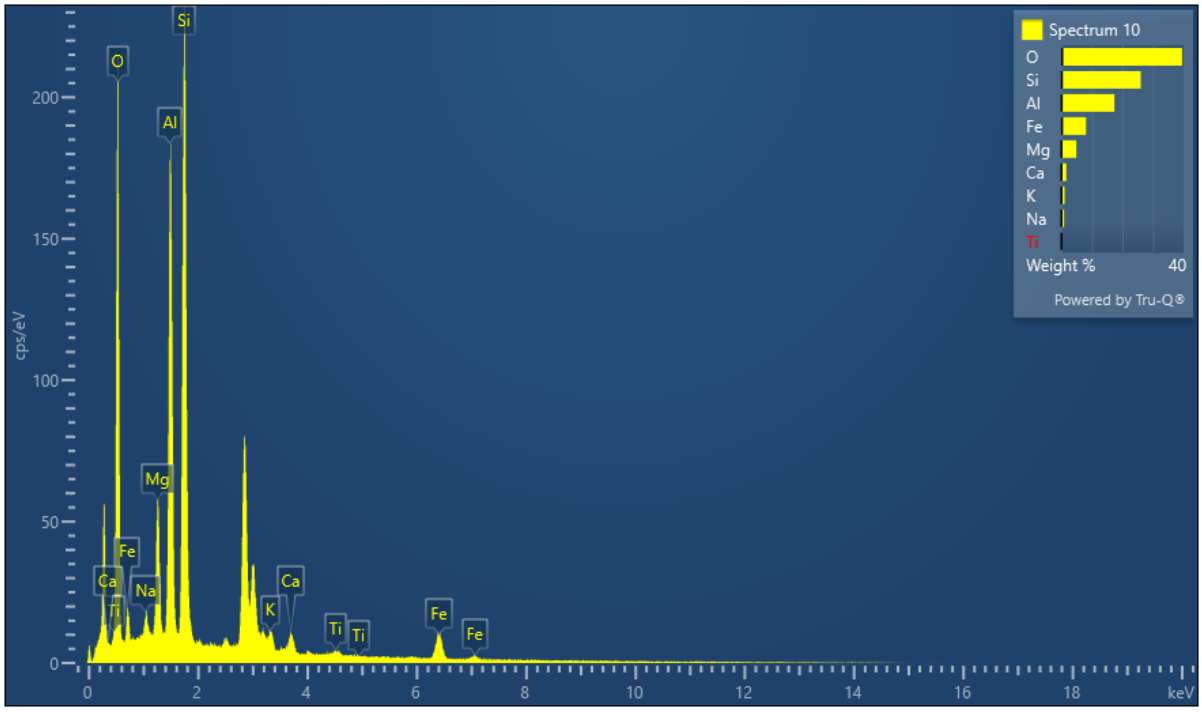

Spectrum 10

Element	Signal Type	Line	Apparent Concentration	k Ratio	Wt%	Wt% Sigma	Standard Name	Factory Standard	Standardization Date
O	EDS	K series	12.08	0.04065	39.46	0.29	SiO2	Yes	
Na	EDS	K series	0.27	0.00114	0.92	0.09	Albite	Yes	
Mg	EDS	K series	1.24	0.00819	4.94	0.10	MgO	Yes	
Al	EDS	K series	4.40	0.03162	17.40	0.16	Al2O3	Yes	
Si	EDS	K series	5.86	0.04642	25.97	0.20	SiO2	Yes	
K	EDS	K series	0.29	0.00246	1.11	0.10	KBr	Yes	
Ca	EDS	K series	0.43	0.00381	1.63	0.09	Wollastonite	Yes	
Ti	EDS	K series	0.10	0.00100	0.45	0.11	Ti	Yes	
Fe	EDS	K series	1.80	0.01801	8.12	0.25	Fe	Yes	
Total					100.00				

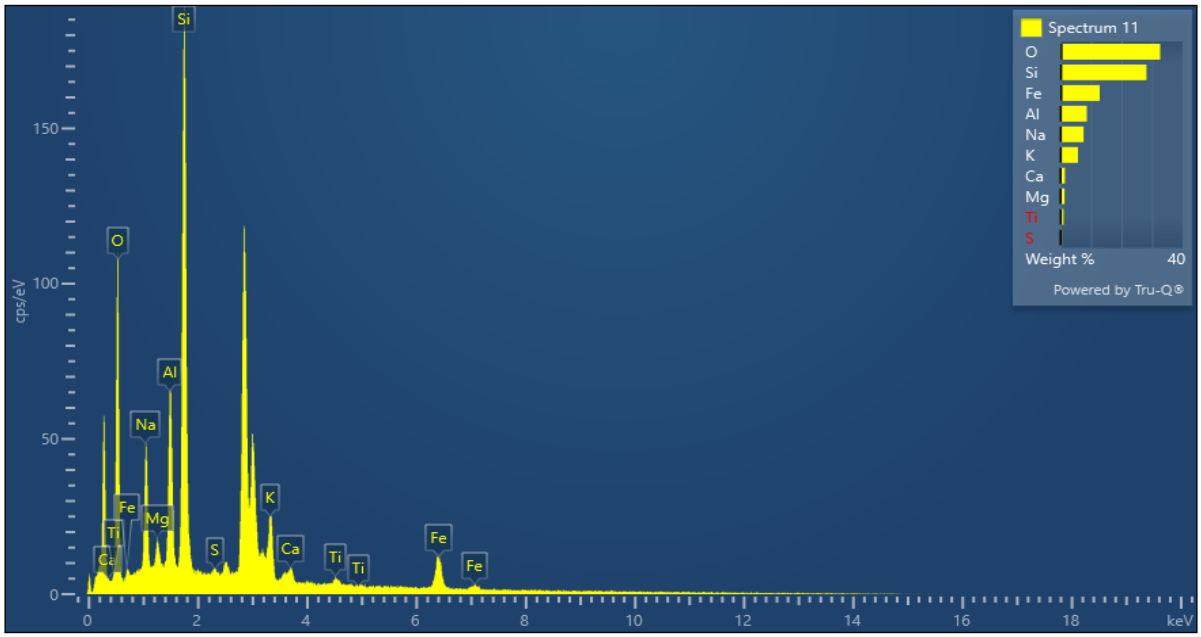

Spectrum 11

Element	Signal Type	Line	Apparent Concentration	k Ratio	Wt%	Wt% Sigma	Standard Name	Factory Standard	Standardization Date
O	EDS	K series	6.21	0.02089	32.63	0.35	SiO2	Yes	
Na	EDS	K series	1.51	0.00636	7.62	0.16	Albite	Yes	
Mg	EDS	K series	0.21	0.00140	1.35	0.10	MgO	Yes	
Al	EDS	K series	1.48	0.01061	8.63	0.15	Al2O3	Yes	
Si	EDS	K series	4.76	0.03771	28.14	0.25	SiO2	Yes	
S	EDS	K series	0.08	0.00069	0.50	0.09	FeS2	Yes	
K	EDS	K series	1.09	0.00921	5.75	0.16	KBr	Yes	
Ca	EDS	K series	0.27	0.00246	1.48	0.12	Wollastonite	Yes	
Ti	EDS	K series	0.16	0.00160	1.02	0.15	Ti	Yes	
Fe	EDS	K series	2.04	0.02043	12.86	0.34	Fe	Yes	
Total					100.00				

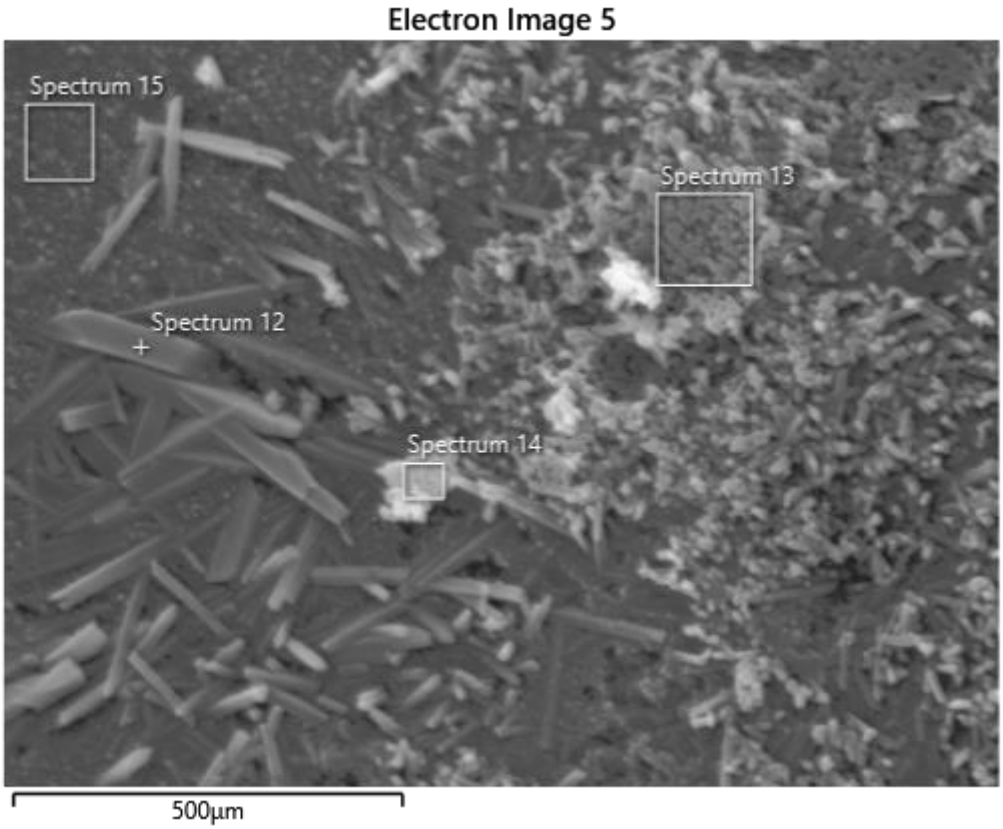

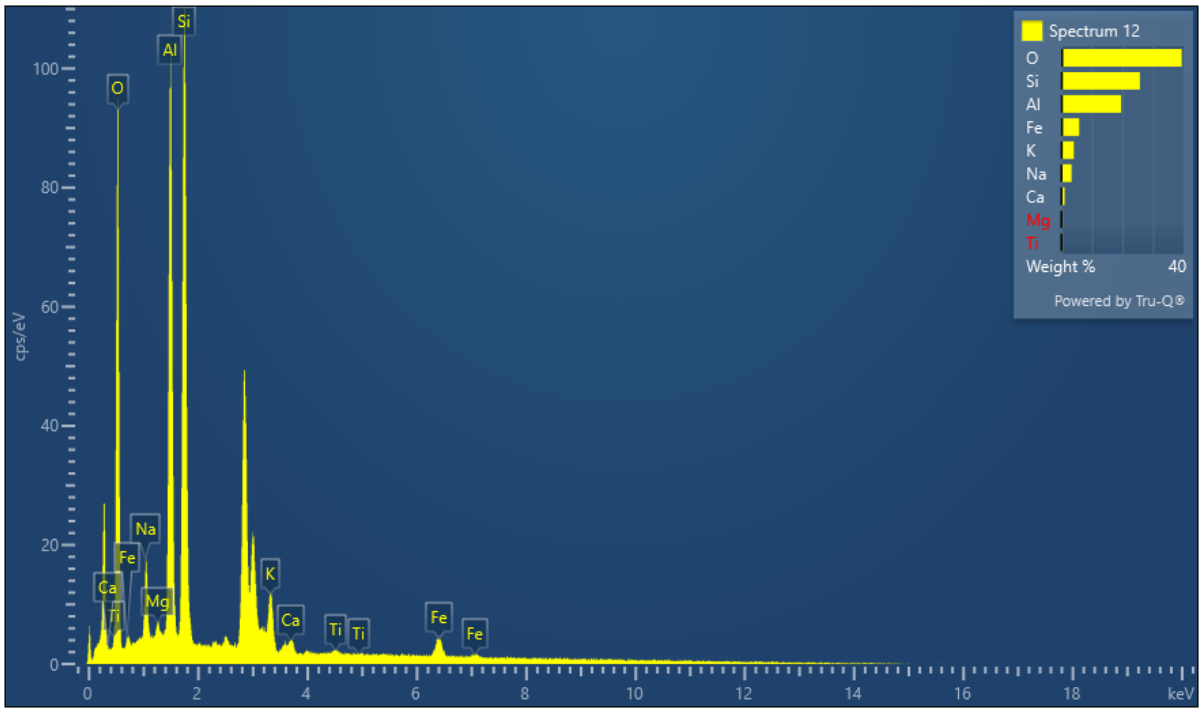

Spectrum 12									
Element	Signal Type	Line	Apparent Concentration	k Ratio	Wt%	Wt% Sigma	Standard Name	Factory Standard	Standardization Date

O	EDS	K series	5.34	0.01796	39.39	0.31	SiO2	Yes	
Na	EDS	K series	0.48	0.00204	3.37	0.11	Albite	Yes	
Mg	EDS	K series	0.06	0.00037	0.48	0.07	MgO	Yes	
Al	EDS	K series	2.45	0.01762	19.52	0.18	Al2O3	Yes	
Si	EDS	K series	2.78	0.02204	25.73	0.22	SiO2	Yes	
K	EDS	K series	0.51	0.00431	4.08	0.13	KBr	Yes	
Ca	EDS	K series	0.13	0.00119	1.08	0.10	Wollastonite	Yes	
Ti	EDS	K series	0.05	0.00049	0.47	0.12	Ti	Yes	
Fe	EDS	K series	0.62	0.00617	5.87	0.28	Fe	Yes	
Total					100.00				

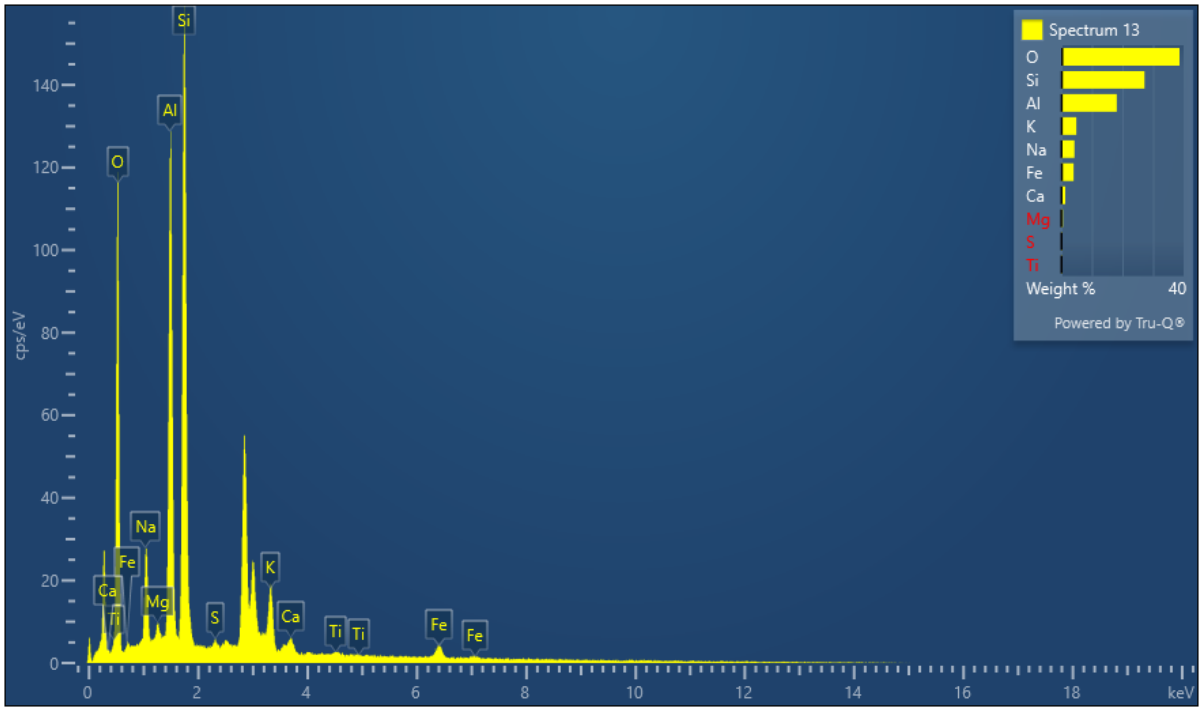

Spectrum 13									
Element	Signal Type	Line	Apparent Concentration	k Ratio	Wt%	Wt% Sigma	Standard Name	Factory Standard	Standardization Date
O	EDS	K series	6.73	0.02265	38.66	0.29	SiO2	Yes	
Na	EDS	K series	0.86	0.00365	4.34	0.11	Albite	Yes	
Mg	EDS	K series	0.09	0.00058	0.55	0.07	MgO	Yes	
Al	EDS	K series	3.09	0.02218	18.16	0.16	Al2O3	Yes	
Si	EDS	K series	4.02	0.03189	27.23	0.21	SiO2	Yes	
S	EDS	K series	0.06	0.00052	0.43	0.07	FeS2	Yes	
K	EDS	K series	0.82	0.00699	4.93	0.13	KBr	Yes	
Ca	EDS	K series	0.21	0.00192	1.31	0.10	Wollastonite	Yes	
Ti	EDS	K series	0.05	0.00048	0.34	0.11	Ti	Yes	
Fe	EDS	K series	0.57	0.00571	4.05	0.23	Fe	Yes	
Total					100.00				

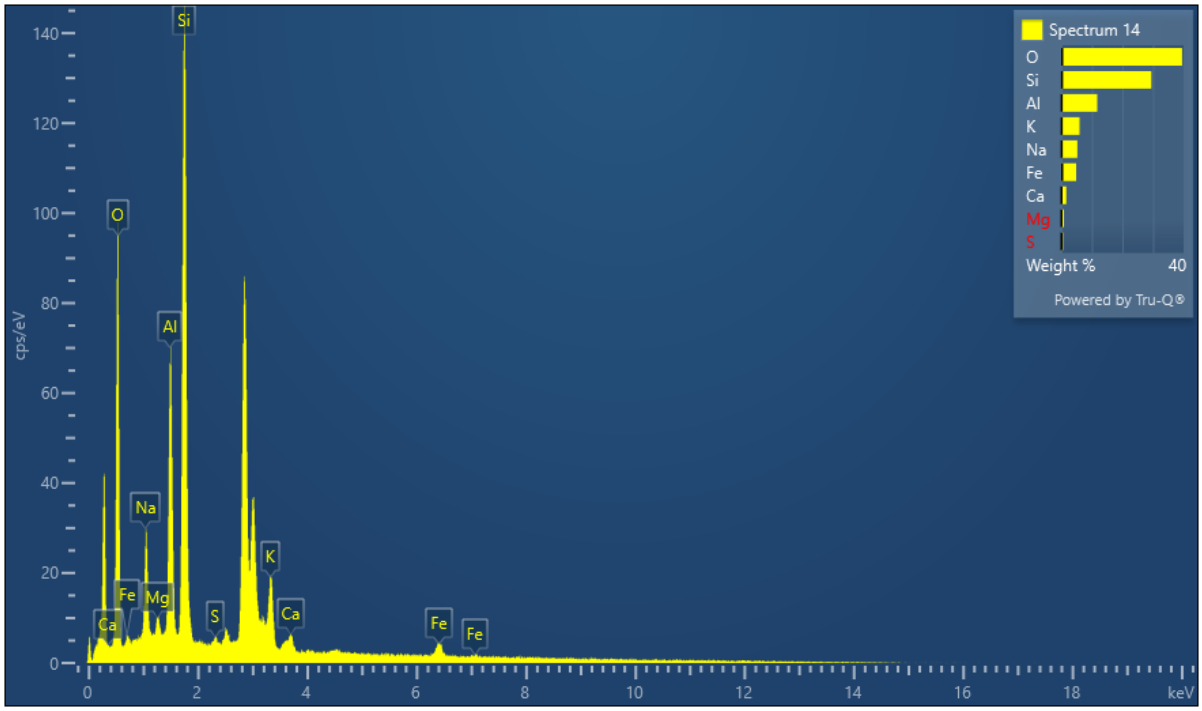

Spectrum 14

Element	Signal Type	Line	Apparent Concentration	k Ratio	Wt%	Wt% Sigma	Standard Name	Factory Standard	Standardization Date
O	EDS	K series	5.57	0.01874	39.48	0.33	SiO2	Yes	
Na	EDS	K series	0.84	0.00353	5.29	0.14	Albite	Yes	
Mg	EDS	K series	0.11	0.00072	0.86	0.09	MgO	Yes	
Al	EDS	K series	1.60	0.01147	11.78	0.16	Al2O3	Yes	
Si	EDS	K series	3.73	0.02952	29.45	0.25	SiO2	Yes	
S	EDS	K series	0.07	0.00061	0.61	0.09	FeS2	Yes	
K	EDS	K series	0.83	0.00699	6.00	0.16	KBr	Yes	
Ca	EDS	K series	0.22	0.00195	1.63	0.12	Wollastonite	Yes	

Fe	EDS	K series	0.57	0.00566	4.90	0.30	Fe	Yes	
Total					100.00				

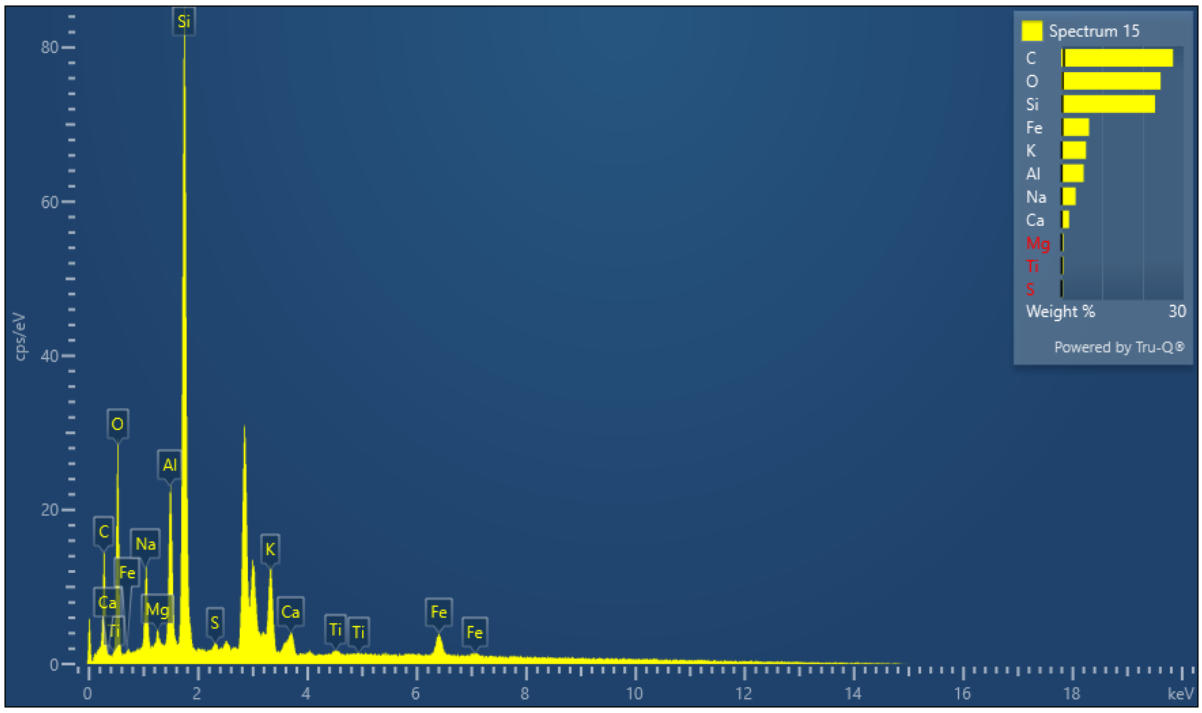

Spectrum 15

Element	Signal Type	Line	Apparent Concentration	k Ratio	Wt%	Wt% Sigma	Standard Name	Factory Standard	Standardization Date
C	EDS	K series	0.46	0.00462	27.42	0.64	C Vit	Yes	
O	EDS	K series	1.65	0.00555	24.37	0.37	SiO2	Yes	
Na	EDS	K series	0.39	0.00163	3.52	0.09	Albite	Yes	
Mg	EDS	K series	0.05	0.00031	0.53	0.05	MgO	Yes	
Al	EDS	K series	0.52	0.00377	5.48	0.10	Al2O3	Yes	
Si	EDS	K series	2.17	0.01720	22.99	0.26	SiO2	Yes	

S	EDS	K series	0.03	0.00029	0.39	0.06	FeS2	Yes	
K	EDS	K series	0.59	0.00503	6.08	0.13	KBr	Yes	
Ca	EDS	K series	0.18	0.00159	1.89	0.09	Wollastonite	Yes	
Ti	EDS	K series	0.04	0.00040	0.51	0.11	Ti	Yes	
Fe	EDS	K series	0.54	0.00541	6.83	0.27	Fe	Yes	
Total					100.00				